Aerospace Vehicle Simulation

MANCHESTER 1824

The University of Manchester

Aerospace Vehicle Simulation

Individual Project 2009-2010 Final Report

Adrian R. G. Harwood, MEng (Hons)

Tutor: Dr I Dupère
Supervisor: Dr D Diston

21st April 2010

Summary

Flight simulation is a specialised application of a broad range of engineering subject matter. This project seeks to develop a knowledge of the subject through three key investigative and practical work packages:

1. The project briefly explores historical progression in flight simulation and examines its role in engineering programmes past and present. Flight simulator and flight model development is considered from early, simple, fixed-based systems to the more complex and more advanced systems of the present day through a wide-ranging literature review.

2. The project drives acquisition of the skills and techniques required to model the behaviour of flight vehicles and documents the application of the acquired knowledge to the development of mathematical and mechanical sub-models. A variety of approaches are researched and practiced to demonstrate understanding of the subject matter.

3. The project promotes current flight simulation technology and allows demonstration of model limitations through the interrogation of current models within the capabilities of faculty facilities.

The project develops a mathematical aircraft representation which is developed into both a software solution and a physical model. The mathematical representation is compiled and simulated in both non-real-time and real-time, and the physical model visualised in 3-dimensions. Current University flight simulation capabilities are analysed through flight testing and research and the limitations discussed. The project documents the acquisition of the knowledge and experience necessary to construct a more detailed machine in the future.

This report is lovingly dedicated to all my family for your unending, greatly appreciated support and patience.

Adrian

CONTENTS

Symbol	Definition
$[\mathrm{A}, \mathrm{B}, \mathrm{C}, \mathrm{D}]$	State Space matrices
AR	Wing Aspect Ratio
a	Temperature Gradient (Figure 4.4). Speed of Sound. Real Component of Complex Number. 6-Series Aerofoil Meanline Parameter.
a_1	Tailplane Lift Curve Slope
a_2	Elevator Lift Curve Slope
b	Wing Span
c	Landing Gear Damping Coefficient
$\bar{\bar{c}}, \tilde{c}$	Mean Aerodynamic Chord
C	Specific Fuel Consumption
C_{D_T}	Tailplane Drag Coefficient
C_{L_T}	Tailplane Lift Coefficient
C_D	Drag Coefficient
C_{D0}	Profile Drag Coefficient
C_L	Lift Coefficient
C_{L0}	Zero Angle of Attack Lift Coefficient
$C_{L\alpha}$	Lift Curve Slope
$C_{M^1/_4}$	Quarter Chord Pitching Moment Coefficient
d	Landing Gear Distance from Centre of Gravity
D	Drag Force
D_f	Fuselage Drag
D_t	Tailplane Drag
D_w	Wing Drag
e	Oswald Efficiency Factor
F	Frictional Force
g	Acceleration Due to Gravity
g_0	Sea Level Acceleration Due to Gravity
h	Altitude
I_x	Mass Moment of Inertia in Roll
I_{xz}	Product Mass Moment of Inertia about X and Z Axes
I_y	Mass Moment of Inertia in Pitch
I_z	Mass Moment of Inertia in Yaw
k	Lift Induced Drag Factor. Landing Gear Stiffness.
K_n	Controls Fixed Static Margin
l_t	Tail Arm Measured Between Tailplane and Wing Quarter Chords
L	Lift Force. Lift Force per Unit Length.
L_t	Tailplane Lift Force
L_w	Wing Lift Force
m	Mass
m_q	Concise Derivative of Pitching Moment with respect to Pitch Rate Perturbation
m_u	Concise Derivative of Pitching Moment with respect to Horizontal Velocity Perturbation
m_w	Concise Derivative of Pitching Moment with respect to Vertical Velocity Perturbation
m_η	Concise Derivative of Pitching Moment with respect to Elevator Angle Perturbation
m_θ	Concise Derivative of Pitching Moment with respect to Pitch Angle Perturbation
M	Mach Number

M_0	Pitching Moment
M_∞	Free Stream Mach Number Figure 4.30.
$\widehat{M}_{\dot{w}}, M_{\dot{w}}$	Dimensional, Non-Dimensional Derivative of Pitching Moment with respect to Vertical Acceleration
$\widehat{M}_q, M_q$	Dimensional, Non-Dimensional Derivative of Pitching Moment with respect to Pitch Rate Perturbation
$\widehat{M}_u, M_u$	Dimensional, Non-Dimensional Derivative of Pitching Moment with respect to Horizontal Velocity Perturbation
$\widehat{M}_\eta, M_\eta$	Dimensional, Non-Dimensional Derivative of Pitching Moment with respect to Elevator Angle Perturbation
$\widehat{M}_\tau, M_\tau$	Dimensional, Non-Dimensional Derivative of Pitching Moment with respect to Thrust Perturbation
n	Number of Wavelengths
p	Pressure. Total Pressure Figure 4.11.
p_0	Seal Level Pressure
p_∞	Freestream Static Pressure Figure 4.11.
q	Pitch Rate Perturbation
r_0	Cylinder Radius Figure 4.11.
R	Molar Gas Constant. Ground Reaction Force.
R_E	Average Radius of the Earth
Re	Reynolds Number
S	Reference Area
S_T	Tailplane Area
S_w	Wing Area
t	Time
T	Temperature. Thrust Figure 4.48. Period Time.
T_0	Sea Level Temperature
u	X Velocity Component. Horizontal Velocity Perturbation.
$\dot{u}$	Horizontal Acceleration Perturbation
U	Freestream Velocity Figure 4.11
U_e	Trimmed Equilibrium Horizontal Velocity
v	Y Velocity Component
V	Generic Velocity
$[\mathrm{V}]$	Eigenvector Matrix
V_0	Initial Velocity
V_1	Decision Speed
V_∞	Freestream Velocity
$\bar{V}_t$	Volume Tail Coefficient
V_X	Horizontal Freestream Component
V_Z	Vertical Freestream Component
V_c	Cruise Velocity
w	Vertical Velocity Perturbation
$\dot{w}$	Vertical Acceleration Perturbation
$\dot{w}_z$	Net Fluid Element Rotation about the Z Axis
W	Weight
W_e	Trimmed Equilibrium Vertical Velocity
x	Horizontal Displacement. Generic Distance.
$\dot{x}$	Horizontal Velocity
$\ddot{x}$	Horizontal Acceleration
x_q	Concise Derivative of Horizontal Displacement with respect to Pitch Rate Perturbation
x_u	Concise Derivative of Horizontal Displacement with respect to Horizontal Velocity Perturbation
x_w	Concise Derivative of Horizontal Displacement with respect to Vertical Velocity Perturbation

x_η	Concise Derivative of Horizontal Displacement with respect to Elevator Angle Perturbation
x_θ	Concise Derivative of Horizontal Displacement with respect to Pitch Angle Perturbation
X	Horizontal Axis
X_0	Horizontal Datum Axis
$\hat{X}_{\dot{w}}, X_{\dot{w}}$	Dimensional, Non-Dimensional Derivative of Horizontal Displacement with respect to Vertical Acceleration
$\hat{X}_q, X_q$	Dimensional, Non-Dimensional Derivative of Horizontal Displacement with respect to Pitch Rate Perturbation
$\hat{X}_u, X_u$	Dimensional, Non-Dimensional Derivative of Horizontal Displacement with respect to Horizontal Velocity Perturbation
$\hat{X}_\eta, X_\eta$	Dimensional, Non-Dimensional Derivative of Horizontal Displacement with respect to Elevator Angle Perturbation
$\hat{X}_\tau, X_\tau$	Dimensional, Non-Dimensional Derivative of Horizontal Displacement with respect to Thrust Perturbation
Y	Perpendicular Axis
Y_0	Perpendicular Datum Axis
z	Vertical Displacement
$\dot{z}$	Vertical Velocity
$\ddot{z}$	Vertical Acceleration
z_q	Concise Derivative of Vertical Displacement with respect to Pitch Rate Perturbation
z_u	Concise Derivative of Vertical Displacement with respect to Horizontal Velocity Perturbation
z_w	Concise Derivative of Vertical Displacement with respect to Vertical Velocity Perturbation
z_η	Concise Derivative of Vertical Displacement with respect to Elevator Angle Perturbation
z_θ	Concise Derivative of Vertical Displacement with respect to Pitch Angle Perturbation
Z	Vertical Axis
Z_0	Vertical Datum Axis
$\hat{Z}_{\dot{w}}, Z_{\dot{w}}$	Dimensional, Non-Dimensional Derivative of Vertical Displacement with respect to Vertical Acceleration
$\hat{Z}_q, Z_q$	Dimensional, Non-Dimensional Derivative of Vertical Displacement with respect to Pitch Rate Perturbation
$\hat{Z}_u, Z_u$	Dimensional, Non-Dimensional Derivative of Vertical Displacement with respect to Horizontal Velocity Perturbation
$\hat{Z}_\eta, Z_\eta$	Dimensional, Non-Dimensional Derivative of Vertical Displacement with respect to Elevator Angle Perturbation
$\hat{Z}_\tau, Z_\tau$	Dimensional, Non-Dimensional Derivative of Vertical Displacement with respect to Thrust Perturbation

Greek Letters

α	Angle of Attack
α_T	Angle of Attack at the Tail
β	Quadratic Discriminant
γ	Ratio of Specific Heats
Γ	Circulation
δ	Logarithmic Decrement
ε	Downwash Angle
ζ	Damping Ratio
η	Elevator Angle Perturbation
θ	Pitch Angle Perturbation

θ_e	Trimmed Equilibrium Pitch Angle
λ	Temperature Gradient
$[\Lambda]$	Eigenvalue Matrix
μ	Dynamic Viscosity. Freestream Vector Inclination. Coefficient of Friction.
ρ	Density
ρ_0	Sea Level Density
τ	Thrust.
ψ	Yaw Angle Perturbation
ω	Rotational Velocity. Natural Frequency.
ω_d	Damped Natural Frequency
ω_p	Natural Frequency of the Phugoid Mode
ϕ	Bank Angle

Abbreviation	Definition
2-D	Two-Dimension(-s)(-al)
A320	Airbus A320-200
BFL	Balanced Field Length
BRE	Breguet Range Equation
CAS	Calibrated Airspeed
CG	Centre of Gravity
COM	Communication
CPU	Central Processing Unit
DOF	Degree of Freedom
FAA	Federal Aviation Administration
FDD	Floppy Disk Drive
HIL	Hardware In The Loop
I/O	Input/Output
IAS	Indicated Airspeed
ILS	Instrument Landing System
ISA	International Standard Atmosphere
JAR	Joint Aviation Requirement
LTI	Linear Time Invariant
MAC	Mean Aerodynamic Chord
MACE	Mechanical, Aerospace and Civil Engineering
MLW	Maximum Landing Weight
MTOW	Maximum Take-Off Weight
NACA	National Advisory Committee for Aeronautics
OEI	One Engine Inoperative
OEW	Operating Empty Weight
OOP	Object-Oriented Programming
PAY	Payload
PC	Personal Computer
PID	Probability Impact Diagram. Proportional Integral Derivative
Q&A	Questions and Answers
RMS	Root Means Square
RT	Real-Time
RTW	Real-Time Workshop
SAR	Specific Air Range
SDK	Software Developers' Kit
SFC	Specific Fuel Consumption
SSLT	Static Sea Level Thrust
TAS	True Airspeed
TET	Task Execution Time
TO	Take-Off

TOW	Take-Off Weight
TSFC	Thrust Specific Fuel Consumption
V&V	Verification and Validation
VGA	Video Graphics Array
VR	Virtual Reality

Application	Description
XFoil	Version 6.9 by Mark Drehla (MIT). Available under the General Public License, XFoil is a Fortran based program for the basic analysis of subsonic aerofoils.
MATLAB	Version 7.9 by The Mathworks Inc. MATLAB is a language for technical computing and integrates computation, visualisation, and programming in an environment accessible through the associated MATLAB application.
Simulink	Version 7.4 by The Mathworks Inc. Simulink is a graphical, building block-based system modelling tool with the capability to simulate and analyse behaviour of dynamic systems.
DesignFoil	Version 6.32 by DreeseCODE Software LLC. DesignFoil is a powerful visual tool for rapid construction, full preliminary analysis, and export of subsonic aerofoils and associated data.

1 INTRODUCTION

Flight simulation is a discipline that has been in existence since the development of aircraft. Its value throughout history can be recognised in its use in aerospace research and development. Flight simulators as machines allow design options to be tested without the obvious time, cost and safety risks incurred from building and potentially destroying numerous prototypes. In more recent years additional benefits have been seen from the use of flight simulators in studying areas of abnormal operation of aircraft in regions such as deep stall, rare but dangerous weather scenarios and other environmental phenomena as well as the use of simulators for air crash investigation and pilot training. Commercial and military organisations alike agree that there is still a number of advantages that have not yet been fully exploited and regulatory bodies such as the Federal Aviation Administration (FAA) are examining the possibility of allowing 'Total Simulation' where pilot training would be 100% simulation based (Scans & Barns, 1979).
The history of the flight simulator is well documented (Rolfe & Staples, 1986) and began with the use of containers representative of aircraft of the time mounted either above or on the ground. The vehicle was large enough to house a human occupant. Control surfaces and interfaces between them and the pilot were present. Aircraft response to human demand was limited and physically only brushed the surface of the production of the illusion of flight. These early systems were seen more as a means of entertainment but investment was increased due to interest cultivated by the onset of war when pilot training became a requirement. By the mid 1940s computers were being employed to solve equations of motion and relate these solutions to much more intricate motion systems. It should not be forgotten that the ability to express the behaviour of an aircraft in terms of a system of equations existed long before any computer was invented capable of solving them rapidly enough to allow a representation of flight. Although flight simulators have existed for some time, it took until the 1960s before any advantages were truly realised.
Even present machines are still considered an approximation of the real vehicle even though they possess cockpits that mimic their counterparts down to finest detail and equation solutions are orders of magnitude more accurate than the first computer based machines.
Although the form and complexity of the flight simulator has changed with time the general requirement has always been the same: the creation of a dynamic representation of the behaviour of an aircraft with an option of virtual reality for the user. In order to meet the fundamental requirement, the flight vehicle, its environment and associated systems are represented mathematically by a number of equations and physically by appropriate hardware. Solution of the equations by means of an iterative process produces a response which forms the basis for the simulator's behaviour. In the absence of a suitable model, the simulator becomes either inaccurate (as with early mathematical simulations) or inert (as with the entertainment vehicles).
Rolfe & Staples go on to admit that elements of the real-life task being modelled by the simulation have to be distorted in order to allow a valid solution to the aim of the simulation as physically not all criteria can be met by an imitation.

Review of the literature provided advice on construction of a mathematical model: specifically the importance of holding the purpose of the model at the forefront of any development to ensure suitable scope and avoidance of unnecessary detail. For a project with a limited scope due to time constraints, this is acutely relevant. Other, more philosophical literature on the subject of systems modelling (Shannon, 1975) stress that models should be designed to produce answers to questions rather than to imitate real systems exactly. This can be achieved by including only those aspects of the system relevant to the objectives – this philosophy in particular was adopted when developing the models and simulations of the project (4 Flight Simulation Modelling). The solution of the simulation can be deemed practical when it is of adequate accuracy – although application specific steady-state and transient responses need to be of an accuracy within the bounds of the desired solution – achieved in real-time. Defined as one which the calculation of a

system's behaviour in one second is achieved in a second or less of computing time, a real-time simulation is an extension of the project which is investigated later in the project.

The flight simulation capabilities of the School of Mechanical, Aerospace and Civil Engineering (MACE) at Manchester University currently include a Merlin Flight Simulator with both hardware and software components, complete with a parametric specification of the Airbus A320, developed in 2003. The information flow through the Merlin system (Figure 1.1) provides an insight into the opportunities offered from a mathematical perspective for investigation of existing simulations.

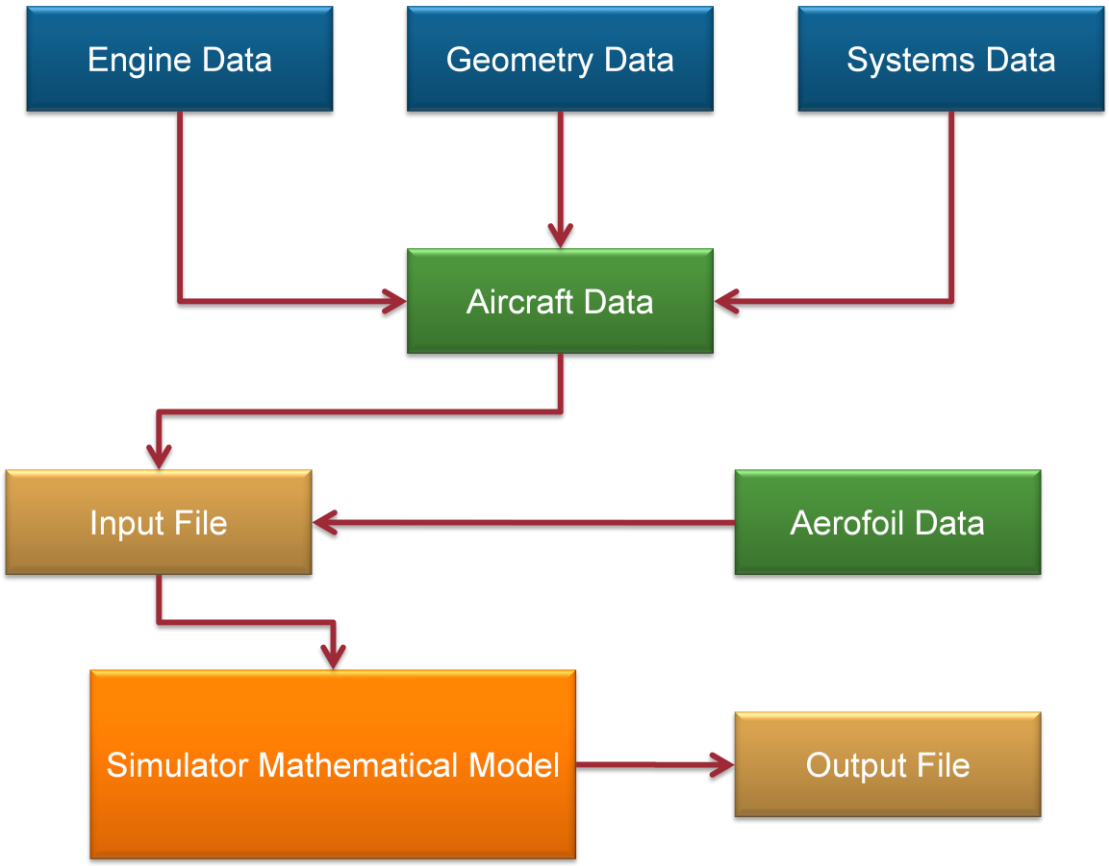

FIGURE 1.1: INFORMATION FLOW THROUGH MACE FLIGHT SIMULATOR

The input file and output file are accessible and it is suspected that these are central to some appropriate work packages.
In order to ensure a broad but suitable range of material is studied, the flight simulator as a machine requires dissection with the intent of the interpretation driving any proposed areas of study. Figure 1.2 shows the architectural impression used to formulate the work package content of the project proposal presented in the Interim Report. This proposal is duplicated in the next section for information.

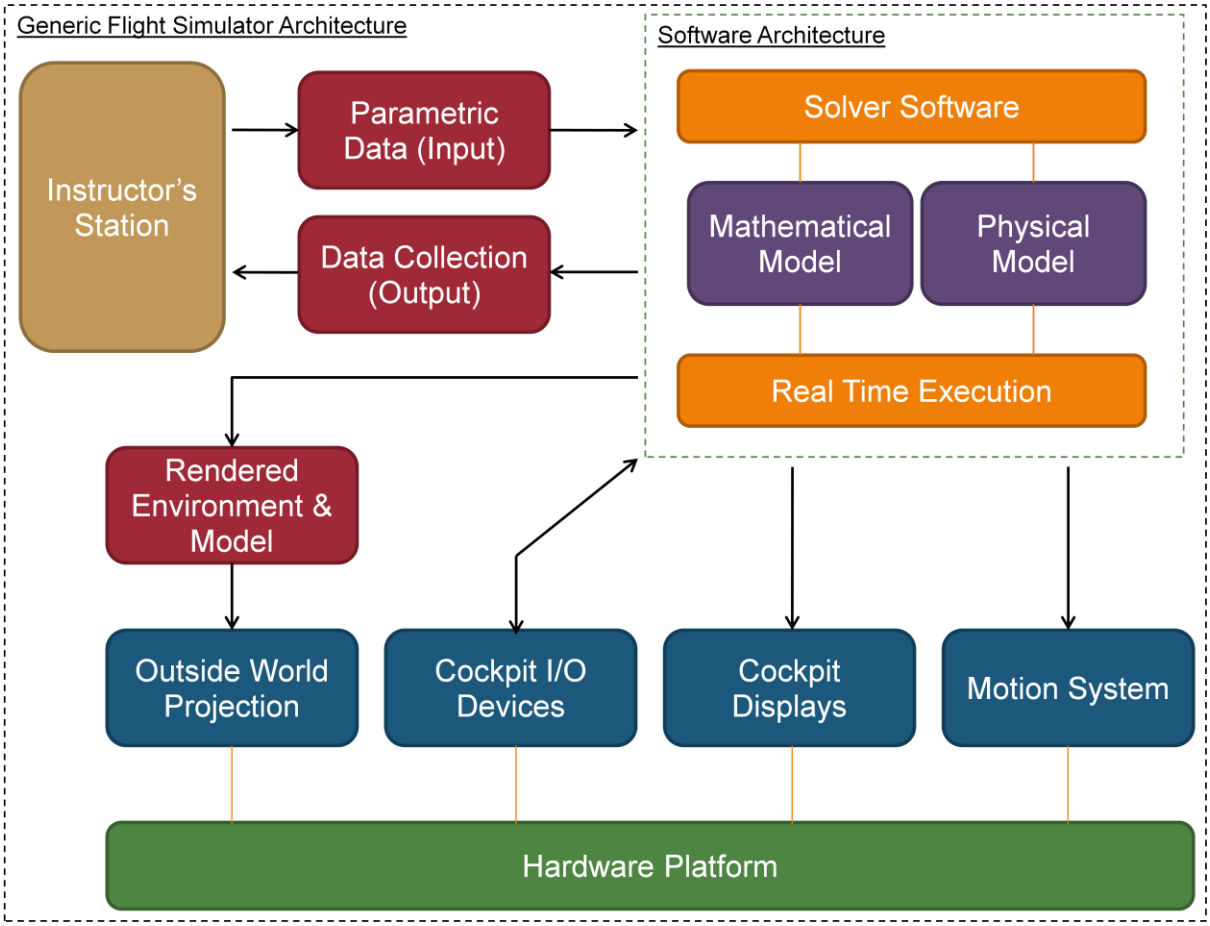

FIGURE 1.2: GENERIC FLIGHT SIMULATOR ARCHITECTURE

Time constraints make it impractical to cover all the material available in the field of flight simulation in great detail but the agreed comprise is to gradually restrict the breadth to encourage depth.

2 PROPOSAL

Understanding the project requirements is a key aspect in the project life-cycle. Although to ensure continued quality and breadth of material the project scope is initially large and definition fluid, there are common elements to any project within the chosen academic field that can be defined. The content of this section was produced through an iterative process considering all stakeholders and is in line with the context set out in the Introduction and in particular Figure 1.2.
The material under the following headings was adapted from a proposal which was drafted in the early stages of the project after consideration of possible outcomes. The draft was reviewed by the project supervisor and a project sponsor and reworked. The proposal identified project requirements for both leading parties involved, the school of MACE at the University of Manchester and the author, and agreed key tasks required to achieve the objectives.

2.1 PROJECT AIMS & DELIVERABLES

- To analyse the current A320 model on the School's simulator for fidelity.
- Design improvements for existing A320 model, post analysis where necessary.
- Investigate and demonstrate understanding of the theoretical field of Flight Dynamics with suitable practical application.
- Investigate and develop modelling solutions through exploration of the capabilities of industry standard software.
- Present findings in the form of a poster and attend a Q&A session on the project content and related material. (24/03/2010)
- Deliver Interim and Final Reports documenting all aspects of work undertaken. (18/12/2009 & 23/04/2010)

2.2 LEARNING OUTCOMES

- To be familiar with aircraft performance parameters and make decisions on their relevance to a variety of specific applications.
- To explore a method for flight dynamic model verification and validation (an integral part of aircraft development programmes.)
- To develop data mining skills through literature reviews.
- To develop communication and informational skills in report writing and presentation delivery.
- To learn project management techniques through planning, control and risk management.
- To gain a firm understanding of flight dynamics and related knowledge areas and develop an appreciation of their roles in the mathematical modelling of flight.
- To appreciate and manage the inevitable challenges of accurately modelling vehicle flight.
- To cultivate cognitive skills such as critical thinking and decision making by working on a multi-disciplinary, unbound problem within boundaries and certain constraints.
- To develop an appreciation of skills required to solve engineering problems.
- To become familiar with product research and development activities
- To be educated on technology and software tools in current use in the field of interest

2.3 KEY TASKS

In order to realise the deliverables and objectives set out in the previous section it was necessary to brainstorm a list key tasks required to drive a work breakdown structure. These tasks take into account knowledge at the time. Any reassessment of the activities is described in 3.2 Project Control Activities.

- Generate a list of behavioural, physical and performance criteria for the A320 aircraft to form the basis of model validation
    - Based criteria on data made available from MACE simulator download and parameters used to specify model behaviour
- Populate expected performance criteria by calculation and research
    - Use estimation techniques (Jenkinson, Simpkin, & Rhodes, 1999)
- Define a test programme to test the listed performance criteria for the current A320 model
    - Based on defined techniques (Filippone, 2006)
- Test model on simulator downloading data to be used to compare with criteria
    - Interrogation of the current parameter model using supplied software will assist data collection
- Arrive at a conclusion on the accuracy of the parameter model based on performance criteria and model parameters
    - 3rd party evidence supplied from literature review(Jackson, Munson, & Peacock, 2008) to aid validation
- Identify potential limitations of simulator mathematical model
- Suggest improvements for the current model
    - Update model using supplied software upgrades
    - Attempt more accurate modelling of more intricate behavioural elements
    - Include aerofoil model using data taken from wind tunnel testing
- Perform work to improve model and retest to prove if applicable
- Develop unique flight simulator solution using Simulink as a means of practical investigation into the subject matter
    - Various other flight simulators available with which to compare development (Berndt) and (Swedish Defence Research Agency)
- Explore possibilities of developing flight vehicle model further, documenting assumptions and rationale
    - Explore other software tools available to perform flight simulation functions
- Potential to breakdown real systems at a flight simulation level
    - Use modelling techniques and notations such as Systems Modelling Language (Weilkiens, 2008)
- After completion revisit the project objectives to see if the project was successful in the final report.

3 PROJECT MANAGEMENT ACTIVITIES

3.1 INTIAL PLANNING ACTIVITIES

Having established the key tasks and project deliverables, planning commences. Initial considerations include resource requirements and availability and the influence of other projects on schedule. Once resources are defined for project use, work packages are identified from the key tasks and disassembled into sub-tasks as means of scheduling work. Imposed milestones by the project supervisor include set dates for report delivery and presentation. Finally, in order to schedule work with a reasonable degree of confidence in the achievability of the deliverables, an element of realism and risk is introduced into the scheduling.

3.1.1 RESOURCE AVAILABILITY

Initial resources required are recognised and preliminary assessment of likely availability performed with the intention of the resulting information feeding into the risk management process. A resource scheduling and availability study is performed through analysis of resource types (Figure 3.1) and the current weekly calendar (Figure 3.2) to produce a basis on which to generate a work breakdown for the project.

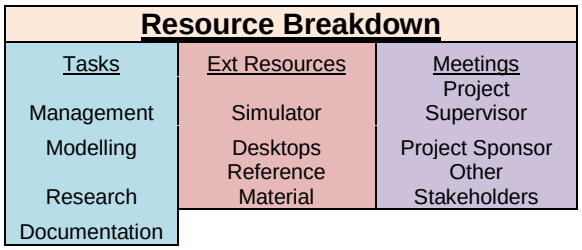

FIGURE 3.1: RESOURCE TYPING

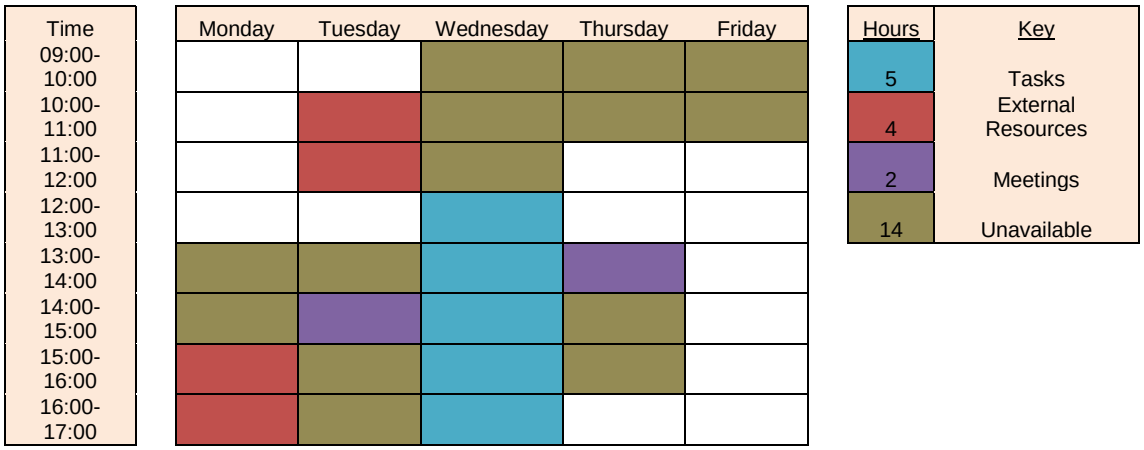

FIGURE 3.2: RESOURCE SCHEDULING

Awareness of resource interdependency is considered critical in the assessment of availability as well as the level of control. Figure 3.3 summarises the conclusions drawn from the exercise including a scoring system to highlight those resources whose availability will require continuous management.

Resource Dependency					
Resource	Variability	Usage	Availability	Score	Comments
Management	M	H	MH	6	Desktop Availability, Reference Material and Stakeholder Review
Modelling	H	H	HH	9	Requires Desktop Availability, Research Prerequisite
Research	M	M	MM	4	Reference Material Availability
Documentation	M	H	MH	6	Desktop Availability, Reference Material and Stakeholder Review
Simulator	M	L	ML	2	Requires Supervision and Training, Stakeholder Consultation
Desktops	H	H	HH	9	Key Resource, Dependency Uncontrollable and Variable
Reference Material	L	M	LM	2	Resource Availability Under 3rd Party Control
Project Supervisor	H	H	HH	9	Availability Limited, Scheduling Required
Project Sponsor	L	M	LM	2	Availability Limited, Scheduling Required
Other Stakeholders	H	L	HL	3	Demand is Low, Availability Restricted

FIGURE 3.3: RESOURCE DEPENDENCY ANALYSIS

3.1.2 WORK BREAKDOWN

Consideration of methods to realise activities defined in 2.3 Key Tasks requires integration of all available information. A general brief is available for a project of this nature with some definition of the content of deliverables (School of MACE, 2009). Key tasks are populated with activities at a lower level of consideration and internal milestones agreed. The packages of work are then arranged and scheduled based on this information, resourcing and deliverable specifications mentioned in the proposal.

For the purposes of planning, a 7.5 hours per day working week calendar is adopted and it is assumed that the demand for time spent per week on the project amounted to 8 hours as is aligned with School policy. The scheduling of the tasks identified in early issues of the work breakdown structure (Appendix A.1) is driven through a fixed work estimation method; the number of hours predicted for completion of the task is held in the plan and assuming 20% of resource available time is allocated to the project, incorporating all immovable deadlines, the scheduling calculations are performed.

Due to the variability of the project and the potential for unforeseen slippage from numerous sources, the initial plan reflects a slightly pessimistic estimate of work and a conservative approach to planned activities. Baseline assignment and tracking is employed throughout the project to allow monitoring of progress.

3.1.3 RISK MANAGEMENT

Based on the latest project information including resources and scheduling, risks may be identified. In order to ensure success of a project, risk needs to be carefully managed. The risk assessment found in (Appendix B.1) analyses the initial risks identified at the planning stage and suggests mitigation strategies as appropriate. Having obtained an impression of the initial risk, subsequent reviews allow residual risk to be obtained throughout the life-cycle. Probability-Impact Diagrams (PIDs) for the initial risk assessment and mitigation are provided in (Figure 3.4).

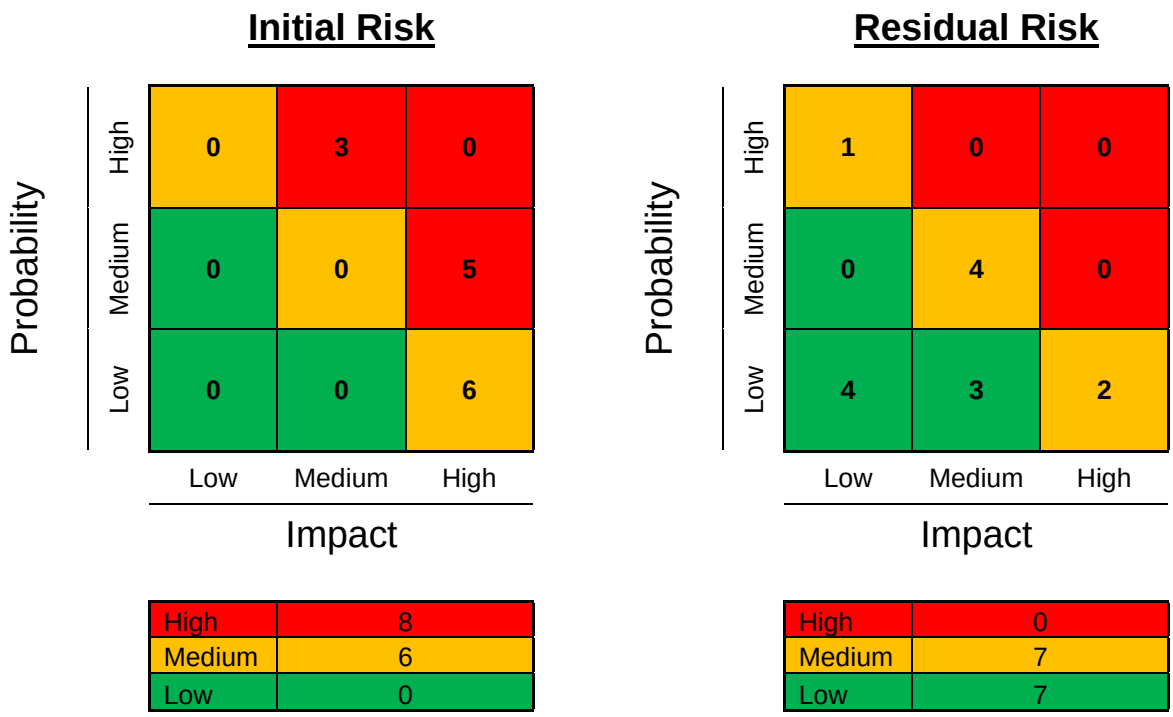

FIGURE 3.4: PIDS FOR INITIAL RISK ASSESSMENT

3.2 PROJECT CONTROL ACTIVITIES

In order to maintain relevance of the project management tools and to allow continuous control of the project, the project management tool kit needs continuous review. Due to the forecast of a potential scope reduction based on the current work break down structure, it was necessary to re-plan and consequently re-baseline the project plan. As suggested in the project Interim Report, this significant re-planning activity, undertaken in December 2009, not only provided the option to exploit opportunities presented by the project work up to that date but also to acknowledge and integrate changes in the working calendar due to the beginning of a new semester. Furthermore, information was received regarding the planned absence of the Flight Simulator – an activity critical resource – and the January Exam period was announced which removed human resource for approximately a 4 week period adding delays to the project which without suitable mitigation strategies could result in time overruns.

3.2.1 RESOURCE AVAILABILITY UPDATE

With the change in calendar and the knowledge of Flight Simulator unavailability, the resource schedule Figure 3.2 requires revising. The new work breakdown structure proposed by the Christmas re-planning event introduces no new resources in order to minimise the global impact to the project which in turn simplifies the task somewhat. The calendar is modified for the 1st and 2nd Quarter of 2010 to produce the modified weekly resource usage schedule of Figure 3.5.

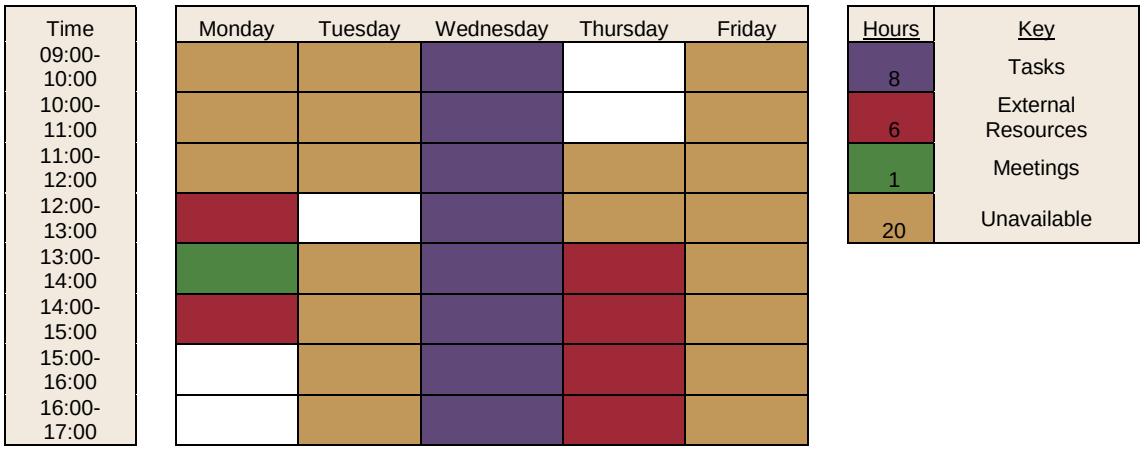

FIGURE 3.5: MODIFIED RESOURCE SCHEDULE

The change in calendar served to increase human resource unavailability but this was counteracted by the increase in immovable time for project activities. This in turn increased human resource focus by reducing the slack time available (white areas in Figure 3.2 and Figure 3.5) previously used for 'off-plan' exploration of the subject matter.

3.2.2 WORK & SCHEDULE UPDATE

The re-planning of the project served to expand the mathematical modelling area of the project, developing a broader skill set and understanding through consideration of a wider variety of material. In addition, the parametric model improvement work package was shelved in favour of a thorough parameter specification and model performance assessment. The alterations were sufficiently minor as to allow sustained validity of the original proposal. Before implementation, the proposed plan modifications were discussed through the project Interim report with the project supervisor.
The modified work breakdown structure, contained in Appendix A.2, was passed and implemented effective 21st December 2009. The rescheduling of work also served to bring the projected end date of the project back to several days before the immovable deadline. From a

risk perspective this is more controllable and allows for further slippage. On implementation of the plan, the project baseline was recorded. As a result, not only was the plan capable of driving work on a weekly basis, but also allowed the monitoring of progress relative to this fixed baseline. The completed project Tracking Gantt with baseline and actual recorded data can be found in Appendix A.3.

3.2.3 RISK REVIEW

Additional knowledge acquired over the project life-cycle as well as the impact of the internal re-planning event, required analysis through the risk management process to ensure the project remained controlled and ultimately successful. The updated risk register may be reviewed in Appendix B.2 with the corresponding PIDs shown in Figure 3.6.

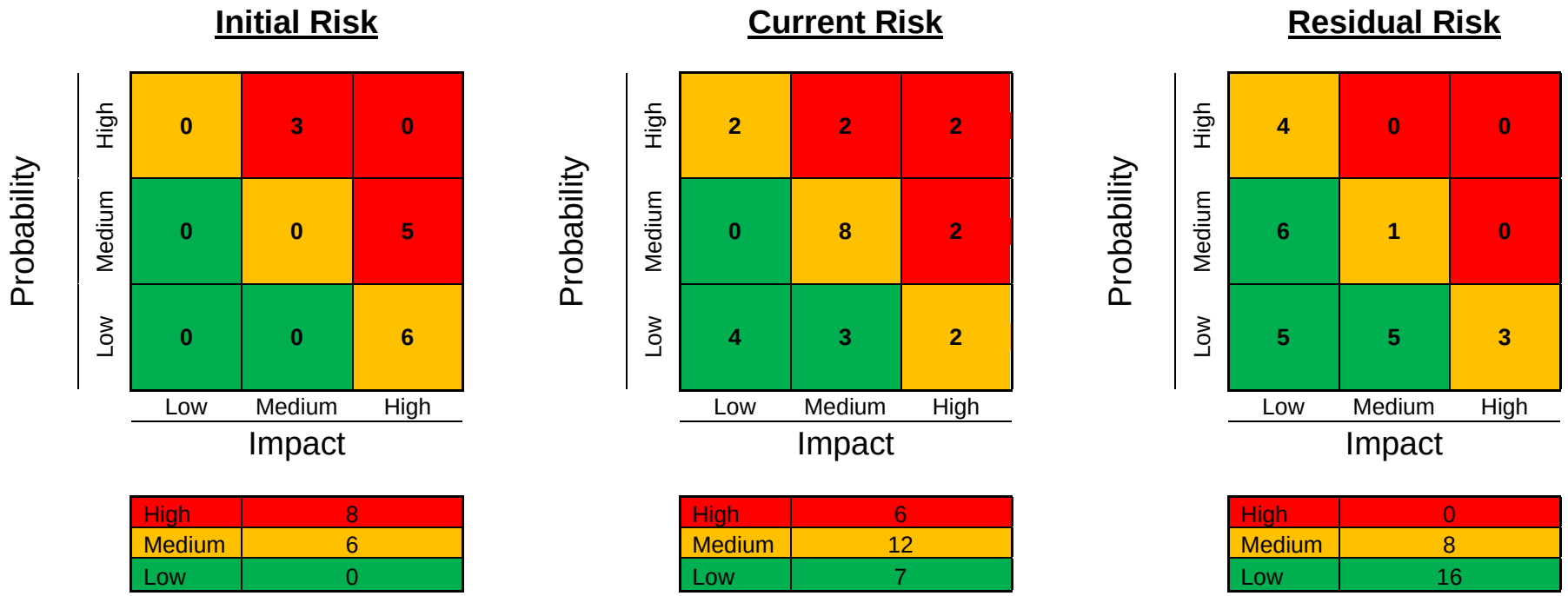

FIGURE 3.6: QUARTER 1 RISK REVIEW PIDS

The project risk assessment is expressed in terms of risk histogram in Appendix B.3.

4 FLIGHT SIMULATION MODELLING

The project commences with the development of a functional flight simulation in a number of different forms. The learning of the modelling tasks simultaneously builds on and aids the parametric specification and simulation analysis later.

4.1 BACKGROUND TO SIMULINK

Simulink is a graphical modelling tool based on the MATLAB language. A Simulink model consists of functional blocks arranged in a workspace and linked together using connectors that serve as a means to route data of various types from sources to sinks.
Solutions to modelled equations are obtained by running simulations over a specified time interval; numerical solvers obtain solutions of the functional block diagram over this time period. Simulink comes with a number of prefabricated blocks that for specific inputs calculate output without the need for the user to model the mathematics in detail. These are packaged in the tool into topical groups called blocksets. In addition, there are a number of toolboxes which contain specialised blocks to allow realisation of particular capabilities based on the Simulink interface.

4.2 MATHEMATICAL MODEL DEVELOPMENT

As part of any investigation into flight simulation, it is important to understand the fundamental element to any flight simulator: the mathematical model. Figure 4.1 adapted from (Rolfe & Staples, 1986) displays graphically the contributions to a flight simulation mathematical model.

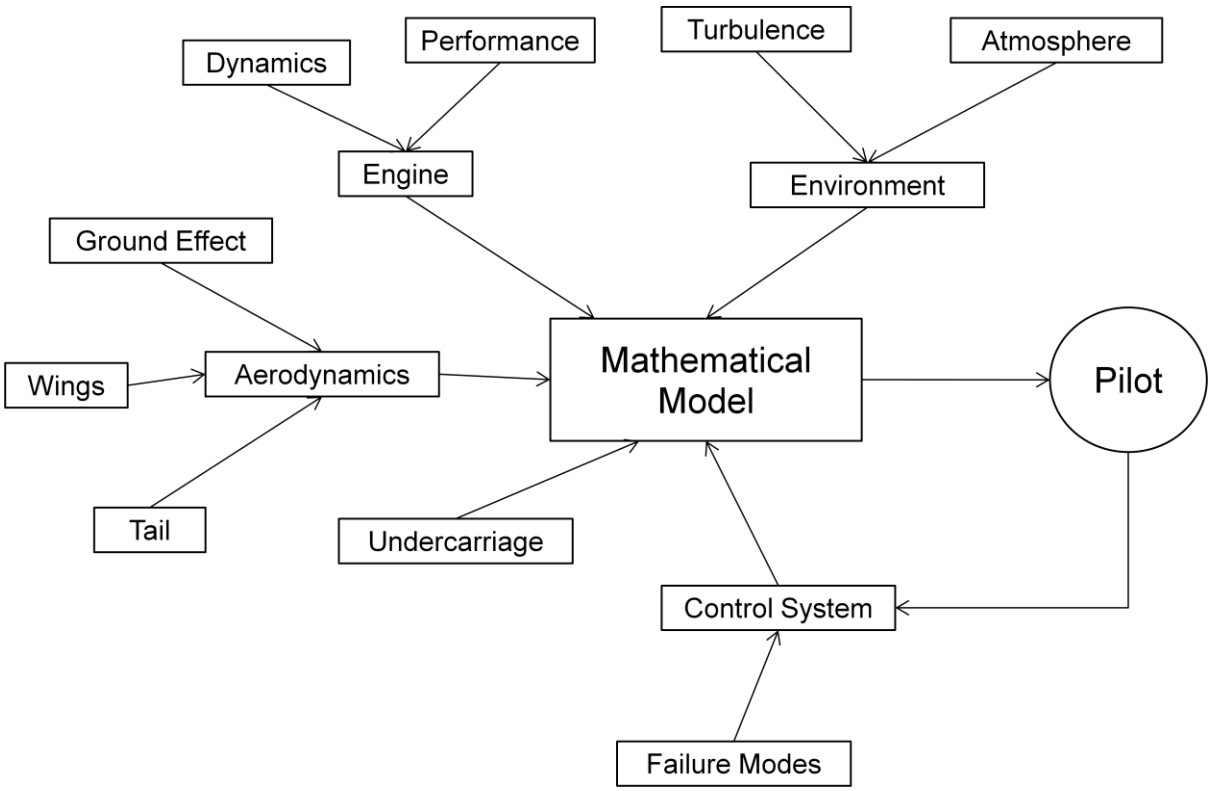

FIGURE 4.1: CONTRIBUTIONS TO THE MATHEMATICAL MODEL OF A FLIGHT SIMULATOR

In order to secure an insight into each of the contributory areas summarised in Figure 4.1, development of an initial functional model is undertaken. Simulink was chosen as the preferred tool due to its visual nature and solver suitability.

4.2.1 INITIAL STEPS

The ultimate goal of any flight simulation model is to accurately reproduce the dynamic behaviour of a real flight vehicle. This includes calculation of the 6 degrees of freedom (DOFs) of a flying body – Rotation and Translation with respect to 3 axes. However, it was necessary to break the problem down into various areas of model functionality and to build-up the areas from simple, heavily approximated representations to detailed functions that resemble reality more closely. The functional areas identified in Figure 4.2 differ from those in Figure 4.1 by how the functions have been packaged but essentially, the breakdown contains similar information and this can be seen as a limited interpretation of the earlier model.

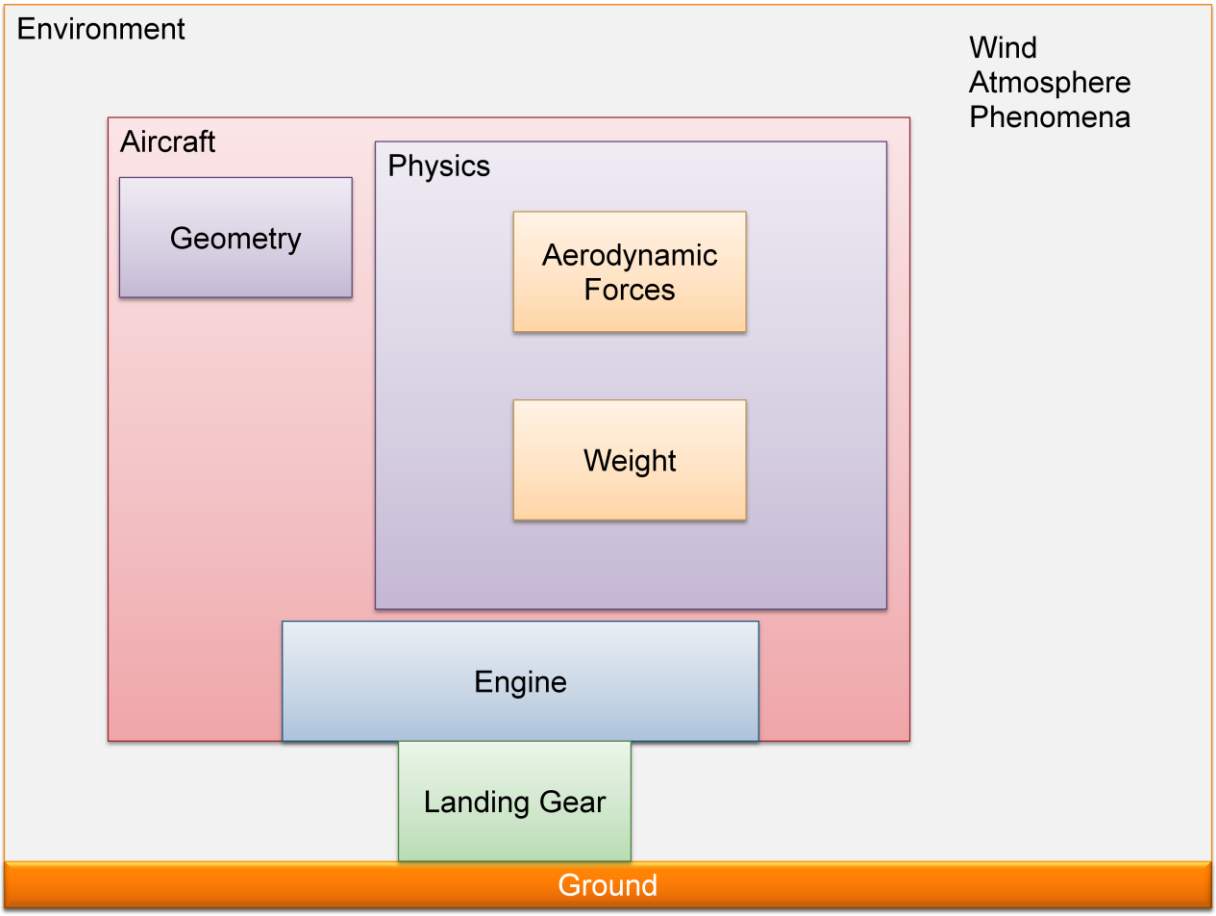

FIGURE 4.2: INTERPRETED FLIGHT SIMULATION MODEL

4.2.1.1 TWO DIMENSIONAL AXES DEFINITION

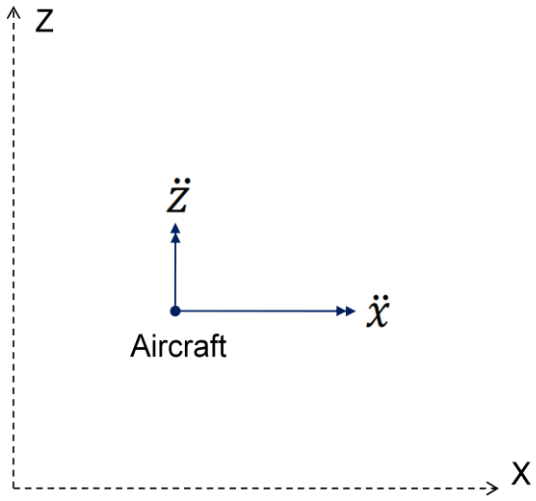

FIGURE 4.3: DEFINITION OF 2D AXIS FOR INITIAL PROBLEM

4.2.1.2 INITIAL CONDITIONS

Initial conditions for the simulation were introduced as the aircraft being stationary at an arbitrary origin (0,0) in an (X, Z) Cartesian plane – Z axis upwards is positive. Velocity and Acceleration quantities in the X and Z directions are denoted the standard notation $\dot{x}, \ddot{x}, \dot{z}, \ddot{z}$. (All descriptive properties of the aircraft and the environment will set by the simulation at the initial time step).

4.2.2 INITIAL MODEL

4.2.2.1 ENVIRONMENT

From Figure 4.2, the logical place to start development is to accurately model the environment in which the vehicle will be functioning; in this case, the atmosphere. The interaction between the vehicle and the environment is reflected in the aerodynamic forces on the vehicle which characterise all aspects of its motion. Mathematically, these forces depend on a number of atmospheric quantities.

As a starting point for the simulation, the atmosphere can be assumed to mimic the International Standard Atmosphere (ISA). Quantities which will be of interest are Pressure, Density, Temperature and potentially the Speed of Sound at the range of altitudes at which the vehicle will fly. The troposphere and lower stratosphere is the likely location of operations, therefore the variation of the quantities of interest will only be considered in these regions. The troposphere transitions to the lower stratosphere at a point known as the tropopause. This is assumed to be at a height of 11 km above sea level. Heights above the lower stratosphere are of no interest as it is not expected that aircraft will encroach on this region of the atmosphere.

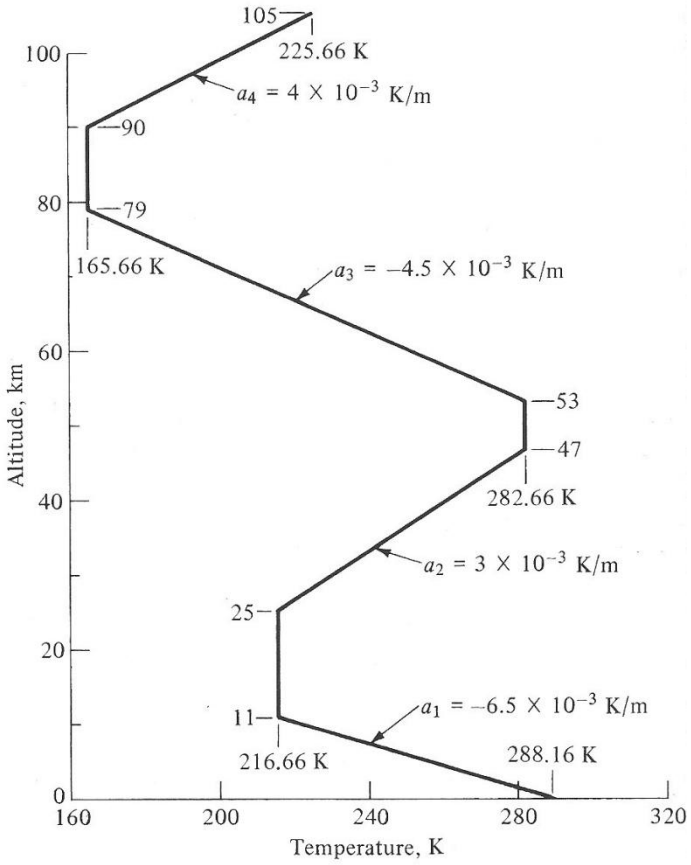

FIGURE 4.4: TEMPERATURE VARIATION IN THE STANDARD ATMOSPHERE

To initialise calculations of atmospheric parameters at a given altitude, the temperature needs to be known. The temperature profile for the standard atmosphere (Figure 4.4 – adapted from (Anderson, 2005) where a here is the temperature gradient) is considered to obtain the local temperature using Equation 4.1 and the remaining parameters calculated using Equation 4.2 to Equation 4.4 – alternative notation to literature has been used for long-term consistency.

$$T = T_0 - \lambda h$$

EQUATION 4.1: TEMPERATURE EQUATION

$$p = p_0 \left(\frac{T}{T_0}\right)^{-g_0/\lambda R}$$

EQUATION 4.2: PRESSURE EQUATION

$$\rho = \rho_0 \left(\frac{T}{T_0}\right)^{-\left[\left(g_0/\lambda R\right)+1\right]}$$

EQUATION 4.3: DENSITY EQUATION

$$a = \sqrt{\gamma R T}$$

EQUATION 4.4: SPEED OF SOUND EQUATION

The nomenclature for Equation 4.1 to Equation 4.4 is defined in Table 4.1.

T	Local Temperature
T_0	Sea Level Temperature
λ	Temperature Gradient
h	Height Above Sea Level
g_0	Acceleration Due to Gravity at Sea Level
p	Local Pressure
p_0	Sea Level Pressure
ρ	Local Density
ρ_0	Sea Level Density
R	Molar Gas Constant
a	Speed of Sound
γ	Ratio of Specific Heats

TABLE 4.1: DEFINITION OF NOMENCLATURE

The atmospheric calculations were then modelled in Simulink and enclosed in a subsystem. All atmospheric parameters were written to memory stores with a view of reuse by future subsystems. The ISA subsystem computed atmospheric parameters for a sinusoidal climb and descent profile. The output shown in Figure 4.5 was verified by manual calculation.
As further elements are introduced in the model, the atmospheric parameters may be best stored in a lookup table which would improve simulation efficiency.

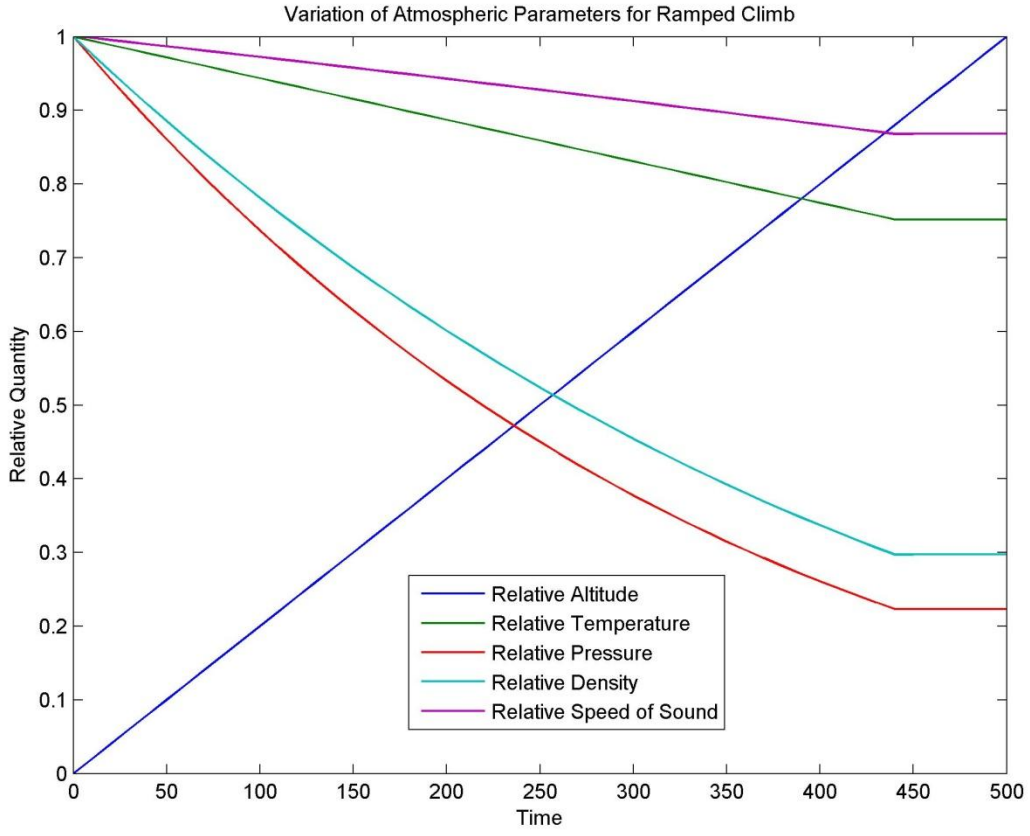

FIGURE 4.5: ATMOSPHERIC READOUTS FROM MODEL

4.2.2.2 POINT ELEMENT MODEL

Having successfully produced an accurate atmospheric model, the introduction of a basic element within the environment to interact with the atmosphere is the next logical step. In the case of this being an aircraft, if the DOFs are initially restricted to translation in the vertical (Z) and horizontal (X) planes then the vehicle can be reduced to Figure 4.6.

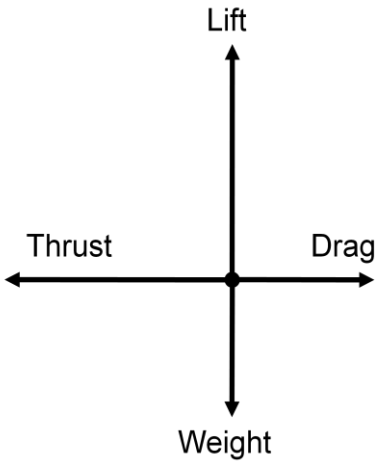

FIGURE 4.6: 2-DOF FOUR FORCE INTERACTION

The four forces summarised in Figure 4.6 need now to be modelled individually and the effect of atmospheric variation on these forces examined.

4.2.2.3 MASS REDUCTION WITH TIME

The weight force is simply the mass of the vehicle multiplied by the acceleration due to gravity (g = 9.81 m/s^2). However, in reality, as the fuel onboard is burnt, the mass reduces. If a linear relationship of fuel burnt to thrust is assumed then a mass reduction profile can be modelled.

4.2.2.4 AERODYNAMIC FORCES

Drag and Lift forces for aircraft are dependent on a number of variable parameters. However, in terms of the dimensionless coefficients, the lift and drag can be represented by Equation 4.5 and Equation 4.6 below where ρ is the local density, S_w is the wing area, C_L is the lift coefficient and V_∞ is the free stream velocity which for the purposes of the model at this stage can be considered to be equal to the forward (X) velocity:

$$Lift = \frac{1}{2}\rho S_w C_L {V_\infty}^2$$

EQUATION 4.5: EXPRESSION FOR THE LIFT COEFFICIENT

$$Drag = \frac{1}{2}\rho S_w C_D {V_\infty}^2$$

EQUATION 4.6: EXPRESSION FOR THE DRAG COEFFICIENT

The use of these equations carries a number of assumptions. The lift coefficient will in fact vary with amongst other things, angle of attack and the deployment of high lift devices. As the point model of the aircraft has neither the ability to pitch nor any inclusion of high systems, the lift coefficient is assumed to be a constant average lift coefficient for a flight cycle.
The density is already a product of the atmospheric model and hence the situation simplifies to the lift and drag forces being a function of density and velocity squared. More accurate modelling of lift and drag will be attempted later on the model development.

4.2.2.5 FOUR FORCE INTERACTION

The four forces obtained from the 2-D point model of the aircraft in Figure 4.6 interact with each other to produce the motion of the body. In the absence of changes in thrust angle, wing angle of attack, presence of wind, and aircraft pitch, the forces on the point body can be considered perpendicular. Using Newton's second law of motion in two dimensions two equations of motion can be produced (Equation 4.7 and Equation 4.8). Solution of the equations of motion should allow determination of vertical and horizontal speeds as well as vertical (altitude) and horizontal displacements as a result of the four force system.

$$L - W = \frac{d(m\dot{z})}{dt}$$

EQUATION 4.7: VERTICAL 1-D EQUATION OF MOTION

$$\tau - D = \frac{d(m\dot{x})}{dt}$$

EQUATION 4.8: HORIZONTAL 1-D EQUATION OF MOTION

4.2.2.6 X-VELOCITY CALCULATION

Initially, functionality needed to be introduced into the model to allow calculation of drag and lift forces for more than just a constant speed. Newton's 2nd Law of Motion in the horizontal direction yields the one dimensional relationship shown above (Equation 4.8). If it is assumed that for now that Mass m is constant and Thrust τ does not vary with speed the one dimensional equation of motion rearranges to Equation 4.9 (below). Drag itself is a function of velocity (Equation 4.6) and hence the solution is not easily obtained manually. Continuous integration of the assembled function coupled with an under-relaxed solution method (solver strategies will be discussed at a later date), allows solution of the equation.

$$\int \frac{1}{m}(\tau - D)dt = \dot{x}$$

EQUATION 4.9: X-MOMENTUM EQUATION TO BE SOLVED FOR VELOCITY

Solution of the problem for variable mass, variable altitude, with variable speed yields profiles as shown in Figure 4.7. Examination of the peak values allow conclusions to be drawn on the model's current accuracy. It can be predicted that the peak velocity will be higher than expected due to the absence of the limiting factor of transonic drag rise. Modelling of this phenomenon is not attempted in this project but would be a suitable pursuit in continuation of this work.

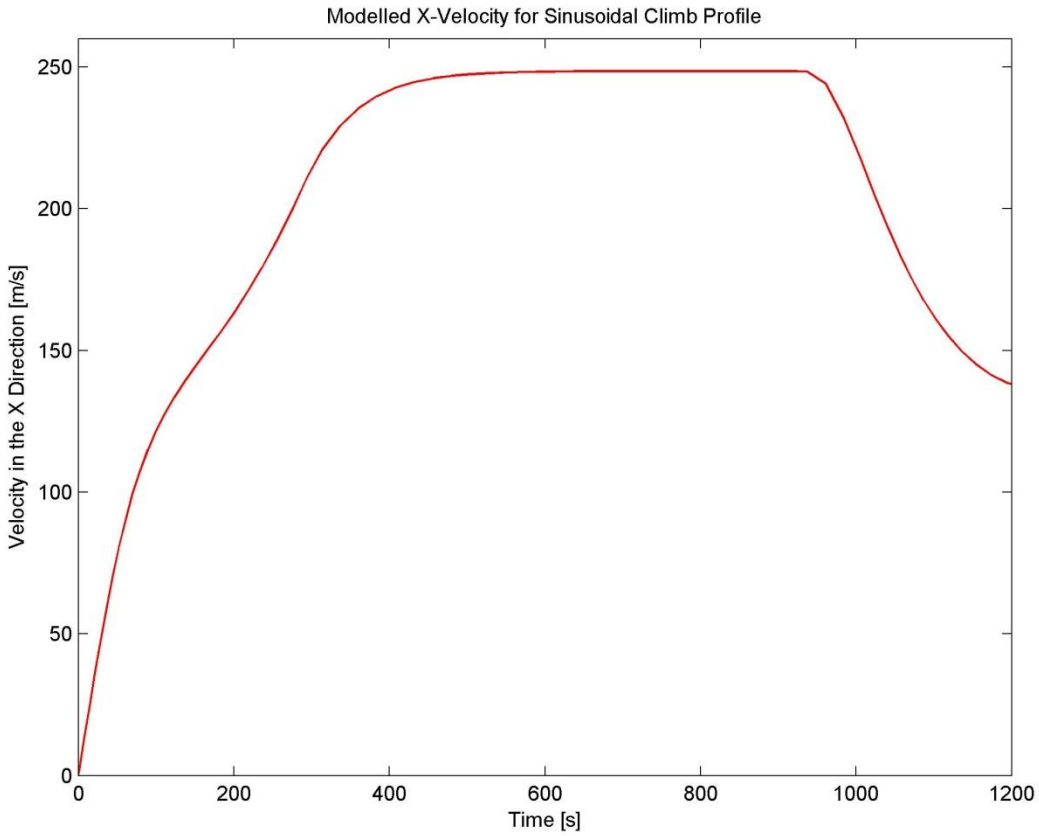

FIGURE 4.7: MODELLED VELOCITY VARIATION

4.2.2.7 Z-VELOCITY CALCULATION

As with the horizontal equation of motion, the equation for vertical motion is solved using continuous integration over time in Simulink. Having integrated the calculated vertical displacement to replace the previous climb and descent profile of previous model versions, the results demonstrated a discontinuity early on in the simulation. Investigation concluded that the lack of vertical boundary conditions resulted in the point aircraft descending into negative values of altitude while the lift was sufficiently small to prevent flight. Consider vertical equilibrium when on the ground (Figure 4.8):

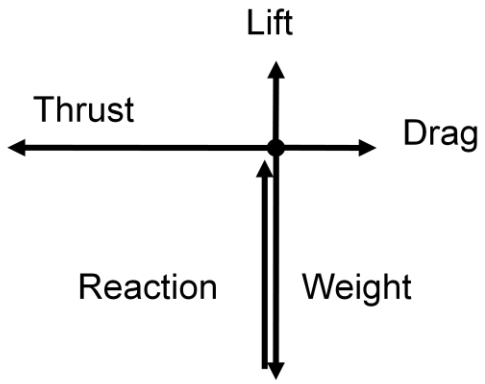

FIGURE 4.8: ON GROUND SCENARIO POINT MODEL

Resolving vertically:

Lift + Reaction = Weight

As the lift increases with velocity, the reaction will decrease until the point of lift off when the reaction will equal zero and the lift will equal the weight. In order to effectively apply this boundary condition, a logical operator was used to govern the influence of a ground reaction and its magnitude. The simulation was run using very low thrust inputs to ensure a ground run, and results showed that the condition was satisfactory applied.
Subsequently, the condition had to be considered of the lift reducing in flight to the point that the aircraft would descend. It would not be desirable for the reaction logic to allow a reaction force to be generated in this scenario. Hence, additional logic to ascertain weight on wheels by means of examination of the vertical position was incorporated and linked to the existing logic. Further testing concluded that this condition was integrated successfully.

At this stage the model allows climb to excessive altitudes and does not provide an appropriate limit to the flight envelope. This is likely due to the incorrect representation of lift and drag and the exclusion of key aspects including angle of attack, lift curve relationships and elevator effectiveness. These issues will be addressed in Lift Modelling activities by the addition of another degree of freedom as indicated by the plan (Appendix A).

4.2.2.8 THRUST MODELLING

Thrust is currently a constant value set to allow aircraft acceleration. In reality, thrust is a quantity which at the engine level is a function of a complex set of environmental and engine variables. At a more black box level, thrust is an output quantity from a pilot set input and there are characteristics that govern the response of the engine to pilot demand. A transfer function (Murphy, 1957) can be used to model the response curve of a typical engine. The resulting model is an approximation only with engine control steady-state accuracy, settling time, and overshoot all estimated within what is considered sensible bounds.

4.2.3 MODEL WITH ADDED COMPLEXITY

4.2.3.1 IMPROVED THRUST MODELLING

In order to improve the modelling of the engine with minimal complexity (as intended by the preliminary work of 2009), a transfer function (Equation 4.10) was derived empirically from a combination of experience and regulatory requirements for an engine control system response (EASA, 2007) and used to model the pilot-thrust-response interface. The regulatory documents require a response to input within 1 [s] and achievement of 95% thrust from 15% in under 5 [s]. In addition, settling time, overshoot and steady state accuracy are to be kept within suitable limits as agreed by the authorities. *Note: $\tau(s)$ is the thrust reponse in the Laplacian ('s') domain and $P(s)$ is the pilot or throttle lever input function in the Laplacian domain.*

$$\tau(s) = \frac{2}{s^2 + 3s + 2} P(s)$$

EQUATION 4.10: ENGINE RESPONSE TRANSFER FUNCTION

The response of the modelled control system (Figure 4.9) in addition to a table of performance parameters (Table 4.2) is published below.

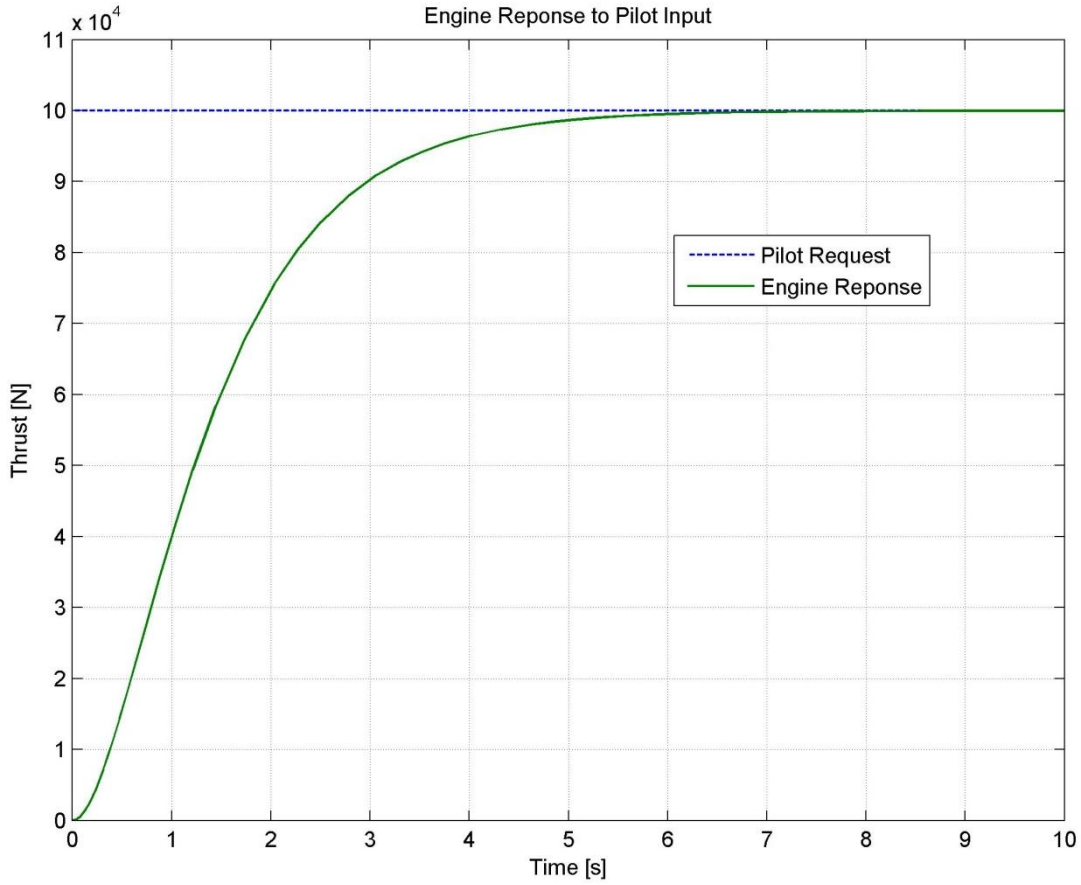

FIGURE 4.9: ENGINE RESPONSE CURVE

Response Property	Value
Overshoot	0 [%]
Settling Time (+/- 1% error band)	5.3 [s]
Initial Response Time (1% change)	0.12 [s]
Steady State Error	0 [%]
15% to 95% Acceleration Time	3.27 [s]

TABLE 4.2: ENGINE RESPONSE DATA

In reality, the control system is a far more complicated affair including an array of sensor inputs, air data and aircraft interfaces to provide situational awareness such that this information, coupled with the known over-specification of the necessary aircraft thrust rating, rarely results in 100% of the pilot requested thrust setting being allowed by the control system in a standard operating scenario. Furthermore, the accuracy of the model is dependent only on specified mathematical parameters and does not include any anomalous behaviour introduced when involving mechanical components.

Further thrust-related phenomena include the variation in thrust (due to mass flow variation) with atmospheric parameters (influenced by altitude) and velocity. No attempt has been made to model this variation in Simulink but related data was located in various books (Shevell, 1989) and an empirical relationship is incorporated into a software solution in (4.3 Simulation Software) from this published data.

4.2.3.2 LIFT MODELLING

So far, the lift force in the simulation model has been calculated using the initial model equation (Equation 4.5). However, it has been assumed to this point that the angle of attack remains fixed and hence the need for lift curve slope data that would otherwise dictate the lift coefficient has been unnecessary. This being the case, the variation of lift force can be attributed to speed and density changes (in the absence of high lift devices which may be responsible for changing the planform area – the area of a geometric shape projected vertically onto the ground). As the aircraft climbs, the density decreases. On crossing the tropopause, the density becomes a constant. Therefore, in the lower stratosphere, the lift will only vary with speed. As drag increases with speed only since there is currently no coupling between lift and drag (addressed in 4.2.3.3 Drag Modelling), and thrust is constant, it is expected that horizontally the aircraft will reach a state of equilibrium. This being the case, it is expected that the speed will also tend to a constant resulting in the lift above the tropopause (the atmospheric boundary between the troposphere and stratosphere) tending to a constant value; there will be no limiting factor to the aircraft's ability to climb. In order to address this error, the modelling of lift needs to be advanced.

4.2.3.2.1 LIFT AROUND AN AEROFOIL

The following is a brief summary of lifting theory assuming prior familiarity of fluid and solid governing equations, notations and principles. Detailed literature on the subject is widely available (Katz & Plotkin, 2001).

Lift originates from the presence of rotation of the constituent fluid elements within a flow. This rotation is a result of the viscosity of the fluid. Considering a three dimensional fluid element in a rotational flow simplified to two dimensions for visualisation (Figure 4.10), velocity gradients across the fluid element are induced by the viscous forces acting tangentially to the centre of gravity of the fluid element at its boundaries to neighbouring elements. These gradients result in a net rotational velocity $\dot{w}_z$ of the fluid element around an axis perpendicular to both X and Y axes (as indicated in the figure below) is given by Equation 4.11. Similarly the principle may be applied to calculate the rotation of the fluid element about the remaining two axes.

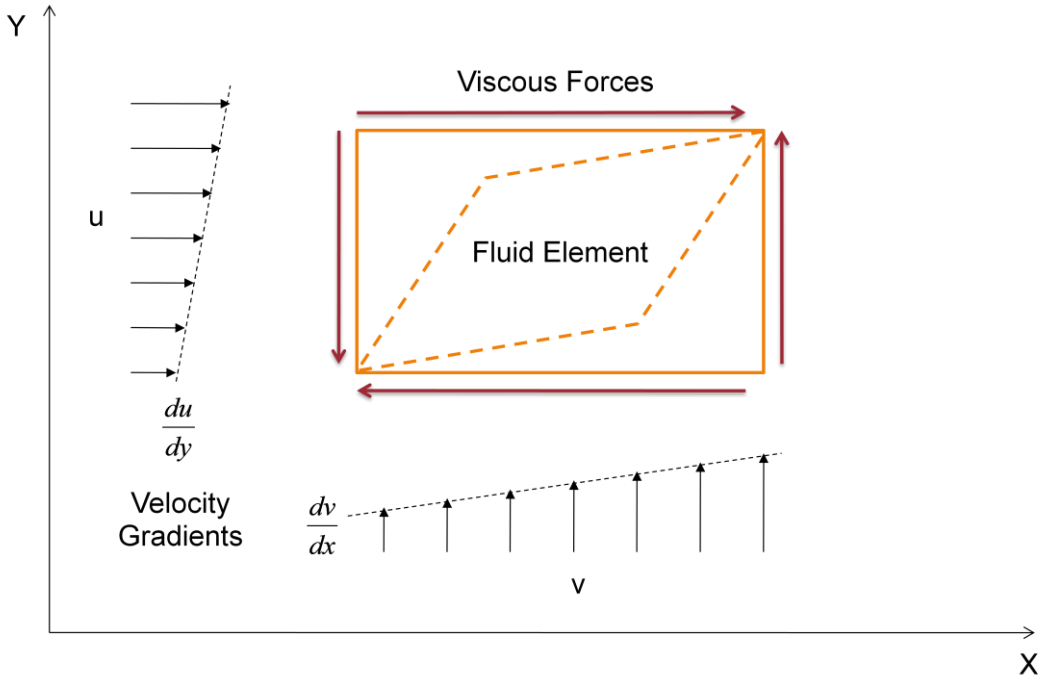

FIGURE 4.10: FLUID ELEMENT DEFORMATION AND ROTATION

$$\dot{w}_z = \frac{dv}{dx} - \frac{du}{dy}$$

EQUATION 4.11: NET ROTATION OF FLUID ELEMENT ABOUT THE Z-AXIS DUE TO VELOCITY GRADIENTS

The concept of flow circulation is defined as the summation of the net rotation of the fluid, derived from the constituent fluid elements, around a closed path within the fluid. In terms of a simple example, if a cylinder is placed in a uniform flow (Figure 4.11) and is rotated with a surface velocity $u = r_0\omega$, in the absence of flow separation, the velocity of the flow at a given point on the cylinder surface is the tangential velocity of the flow plus u. This sets up the equiavalence of a scenario where a stationary cylinder is placed in a rotating flow. The flow clearly has circulation around a path located around the cylinder surface.

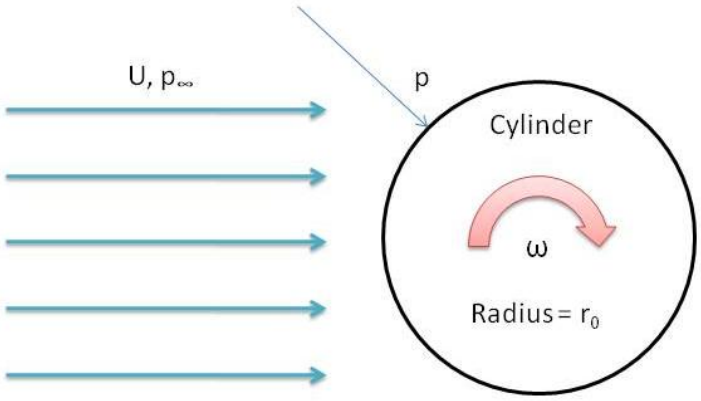

FIGURE 4.11: ROTATING CYLINDER IN A UNIFORM FLOW

Using Bernoulli's equation for incompressible, adiabatic flow, and neglecting changes in potential energy, an expression for the surface pressure difference $(p - p_\infty)$ at any location with respect to the flow static pressure can be obtained. This pressure distribution over the cylinder surface comes about due to the variation of local velocity due to the circulation of the flow and results in a net force on the cylinder. This pressure distribution and can be integrated over the cylinder surface and resolved in the vertical direction to obtain an expression for this Lift force L per unit length in terms of the flow density ρ and velocity U and the net circulation Γ around the cylinder (Equation 4.12).

$$L = \rho U \Gamma$$

EQUATION 4.12: THE KUTTA-JOUKOWSKI EQUATION

The purpose of the derivation of lift in the context of the project is a means of demonstrating the complexity of the phenomenon and illustrates the impracticality of modelling it from first principles. The previous theory can be applied to a stationary wing due to presence of circulation around the wing. This circulation is the result of a 'bound vortex' setup around the wing surface in opposition to the 'starting vortex' when flow first begins to pass over the wing. This starting vortex is formed at the trailing edge of the wing section due to the flow initially trying to flow round the trailing edge from the bottom surface to the top surface. This bottom to top motion, encouraged by the presence a stagnation point (local flow velocity = 0) at the sharpened trailing edge, is forced downstream due to the flow velocity and attempts to draw the upper surface flow with it. In effect, it is this drawing action that induces the bound vortex circulation, in turn responsible for generating the lift force.

When simulating lift, in favour of derivation from these first principles, models may make use of the characteristic curves of particular aerofoil sections which exist through testing or numerical calculation. These curves illustrate the variation of dimensionless quantities of Lift, Drag and

Pitching Moment about the leading edge with angle of attack for a particular aerofoil section. Examples of these curves (Nakayama & Boucher, 1999) show in particular that for the aerofoil section under consideration, the lift increases approximately linearly with angle of attack up to a point, thereafter the flow on the suction side of the wing becomes detached and the wing stalls. This stall induces large amounts of drag but also prevents effective maintenance of the bound vortex and lift falls off. These curves are applicable for given flow conditions described by the Reynolds Number and the Mach number. It is expected that an increase in Reynolds Number will increase the lift curve slope (Anderson, 2005). The capture of all behaviour can only be attempted due to the huge scope of flow conditions allowable within a flight envelope.

4.2.3.2.2 MODELLING LIFT

The current A320 E1 Excalibur (see 5.1.1 Background to Excalibur) model on the simulator requires an input file to provide data on how the aerofoil coefficients vary with angle of attack – defined as the angle between the wing chord line and the free stream velocity vector. From this data the relationship between the lift coefficient (C_L) and the angle of attack (α) can be plotted as shown in Figure 4.12, the linear portion being represented by the familiar relationship in Equation 4.13 where C_{L0} is the lift coefficient at zero angle of attack – nonzero for cambered aerofoils, and $C_{L\alpha}$ is the lift curve slope and α is the angle of attack given in radians.

$$C_L = C_{L0} + C_{L\alpha}\alpha$$

EQUATION 4.13: LIFT COEFFICIENT IN TERMS OF ANGLE OF ATTACK

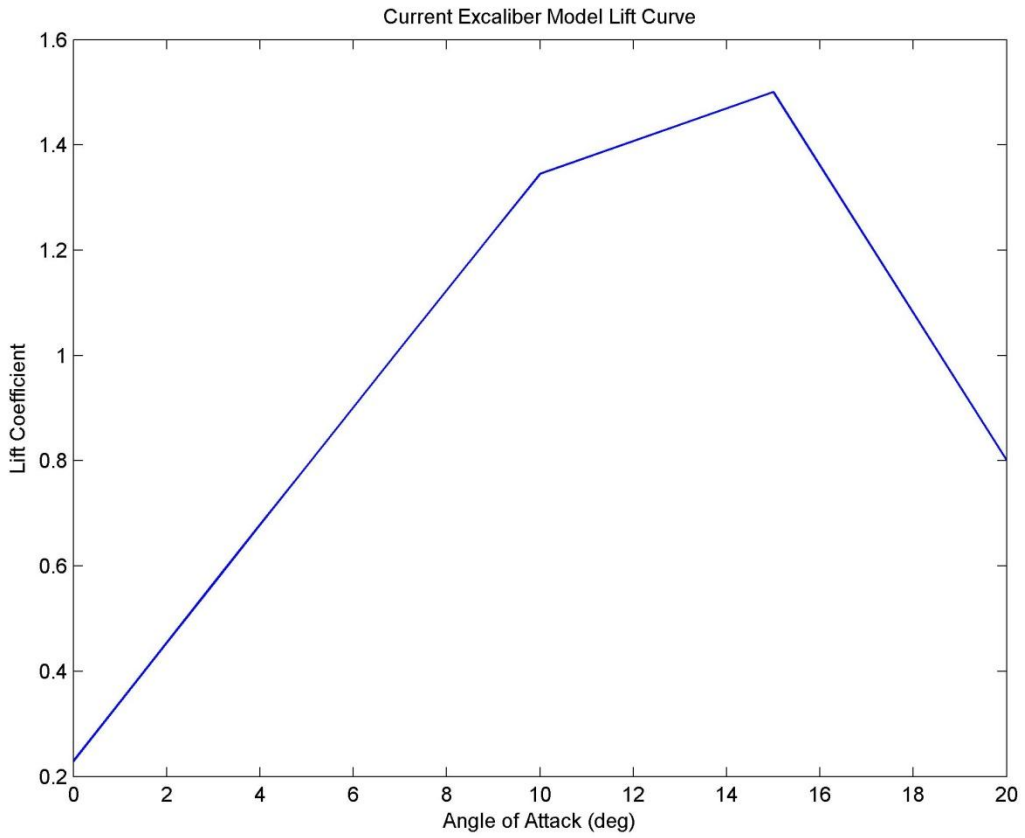

FIGURE 4.12: CURRENT E1 MODEL LIFT CURVE DATA

The history of this data is unavailable and hence if obtained from experimental or theoretical derivation, the values of key parameters were unclear. For example, the pressure distribution over an aerofoil will vary with Mach number (M) and Reynolds Number (Re) and the values for the lift coefficient will vary with reference lengths and areas. As a means of analysing the data in the E1 model (5.2 Existing Model Specification & Simulation Analysis) and to develop a set of data or calculation that will be used by the Simulink model, it was necessary to research methods of obtaining this data for a known aerofoil.
Initially a web-based program (Childs, 2006) was discovered, which exported a text file containing X and Y coordinates of a specified 4-digit NACA aerofoil (see Appendix C). The text file was then read by the commercially available program XFoil (see Nomenclature for description) which imported the coordinates and generated a 2-dimensional wing section. The software could then be used to obtain the pressure distribution over the surface of the aerofoil for specified values of α, M and Re. Alternatively a suitable manual calculation could be performed (Houghton and Carpenter, 1960). Documentation of both these methods follows.

4.2.3.2.2.1 PROGRAMMING BASED DATA GENERATION

It was hypothesised that if multiple C_L against α curves could be obtained for a variety of Re then it is possible to use the data obtained to select a lift coefficient that correctly corresponds to the lift at any time in the simulation.

XFoil represents the aerofoil through a non-linear distribution of individual panels and numerically integrates a system of equations to produce a pressure distribution function over the aerofoil geometry. This function is then integrated over the surface to calculate the resultant lift distribution.
XFoil operates using a number of assumptions. All reference areas and length are unity; the wing is of unit width with chord equal to 1.0. Density is assumed to 1.0 also and the flow is compressible. The program has the capability to perform both viscous and inviscid calculations.

Having generated the current E1 model's NACA 2412 wing section in the tool, simulations were run to obtain the lift coefficient amongst other parameters for the specified conditions. Numerous data sets were obtained for $0 \leq \alpha \leq 90$ degrees and for $0 \leq M \leq 0.9$ for the corresponding sea level Reynolds numbers ($\mu = 1.827 \times 10^{-5}$ Pa s).
During post processing, the data can be corrected by introducing the chord as being the graphically calculated 3.36 [m] and the reference area being the wing area 122.4 [m²] (see 5.2.2 Verification & Validation Activities*).*
Data was limited when using a viscous setup for Mach numbers in excess of 0.35 due to compressibility effects where software calculations become invalid. However data was available for a full range of Mach numbers and flow conditions for an inviscid setup. Figure 4.13 compares data from both setups for Mach number 0.3 and sea level conditions.
Considering the expected cruise velocity of the A320 (high-subsonic), compressibility effects, the beginnings of drag divergence and transonic flow phenomena all need to be incorporated into the data calculation. This is likely to be beyond the scope of the software. Furthermore, the wing section itself is likely to undergo design changes as a result of the changes in flow conditions meaning an alternative to the NACA 2412 ought to improve the realism of the model (5.4.1.1 Wing Section Redesign).

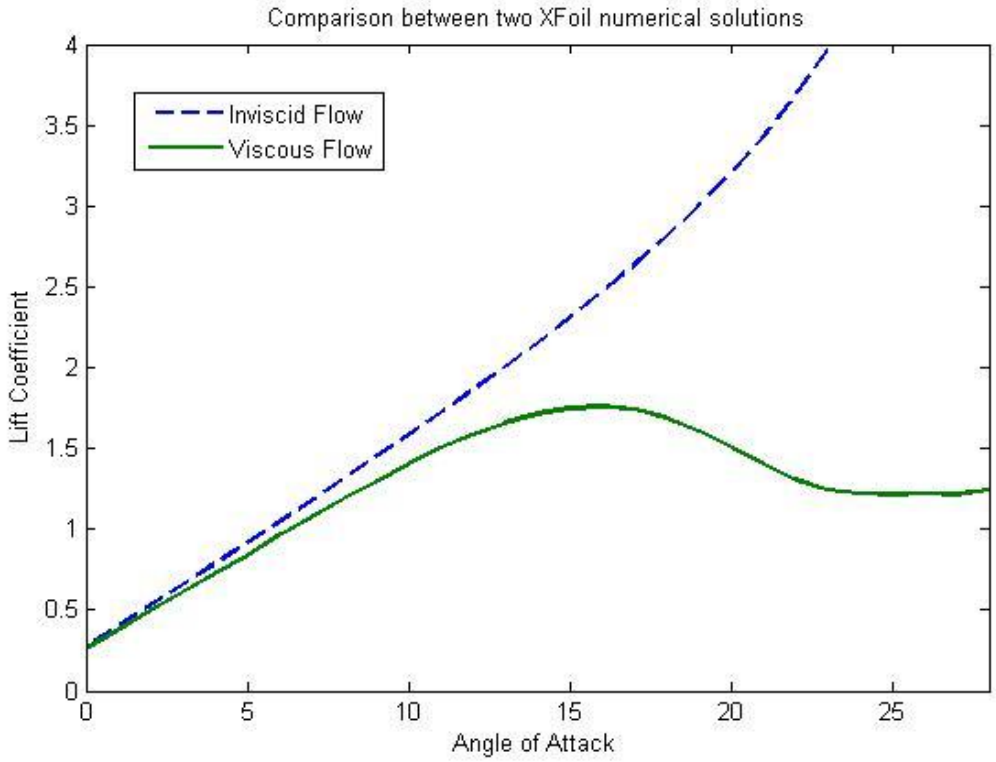

FIGURE 4.13: COMPARISON OF NUMERICAL DATA FOR INVISCID AND VISCOUS SETUPS

4.2.3.2.2.2 THEORETICAL CALCULATION METHOD

A theoretical method (Houghton & Carpenter, 2003) is derived based on thin aerofoil theory whereby for any 4-digit NACA aerofoil section, the lift coefficient and moment coefficient about the quarter chord location can be calculated for a specified angle of attack.
Using the prescribed method, a MATLAB function (verified by hand) was written to return C_L and $C_{M^1/_4}$ for any NACA 4-digit wing section for any value of α (Appendix C.2).
Although thin aerofoil theory was used, Houghton and Carpenter go on to say: "The predictions of thin aerofoil theory [have been] compared with accurate numerical solutions and experimental data…[and] are in satisfactory agreement with the accurate numerical results".

4.2.3.2.2.3 COMPARISON OF METHODS

The simulation data for both viscous and inviscid calculations showed an increase in gradient of the lines with Mach number and a higher overall value than the theoretical values calculated (Figure 4.14 and Figure 4.15).

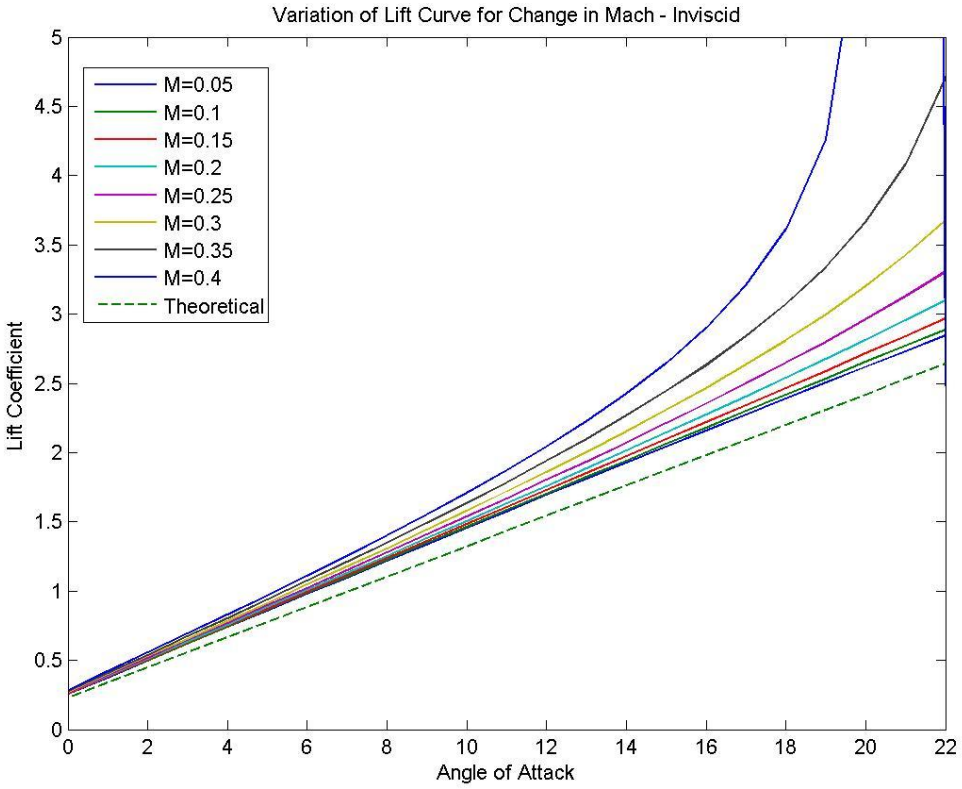

FIGURE 4.14: LIFT CURVE SLOPE (INVISCID SETUP) FOR CHANGE IN MACH NUMBER

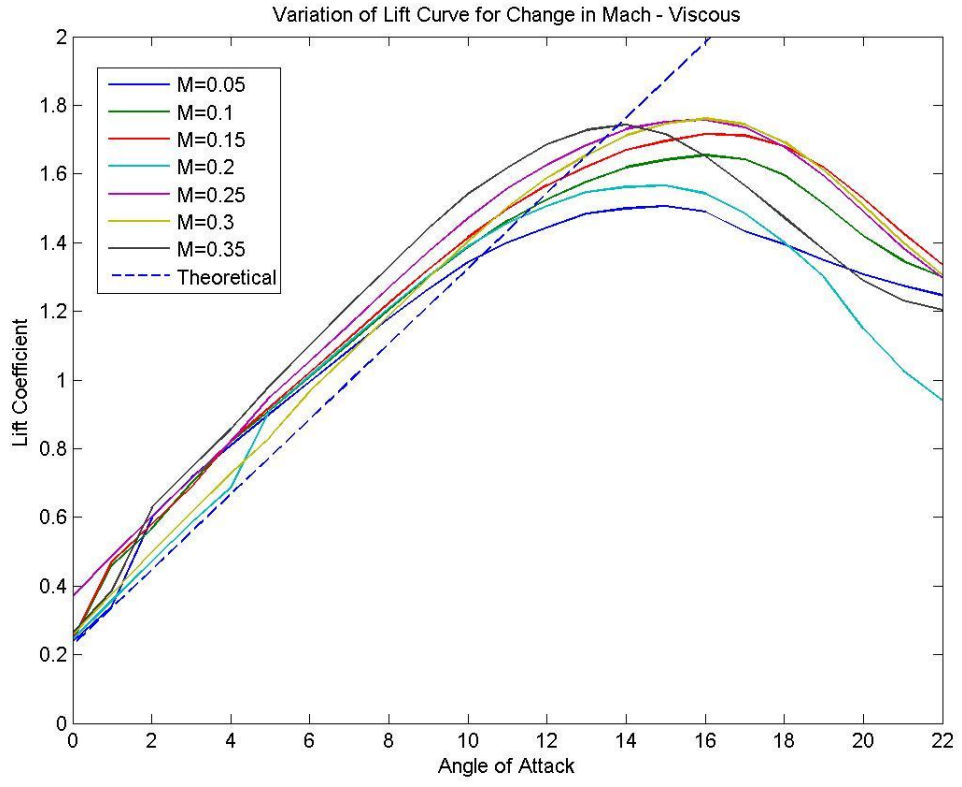

FIGURE 4.15: LIFT CURVE SLOPE (VISCOUS SETUP) FOR CHANGE IN MACH NUMBER

Behaviour of the simulated curves at Mach numbers greater than 0.35 were erratic. In the range displayed in Figure 4.14 and Figure 4.15 the flow is slow enough to be considered incompressible. At greater Mach numbers compressibility effects, amongst other phenomena associated with higher speeds, start to impact on the characteristics. Suitability of the wing section for higher subsonic Mach numbers is discussed in 5.4 Validation Summary.
The purpose of these experiments was to obtain lift curve slope data to be used in the simulation. However, as multiple sources of lift curve data have been acquired, it is first necessary to select an appropriate source. Figure 4.16 compares the lift curve data from simulation, theoretical and existing model sources. Due to there being a limit of accurate simulation data, the result of the selection is likely to exclude compressibility effects.

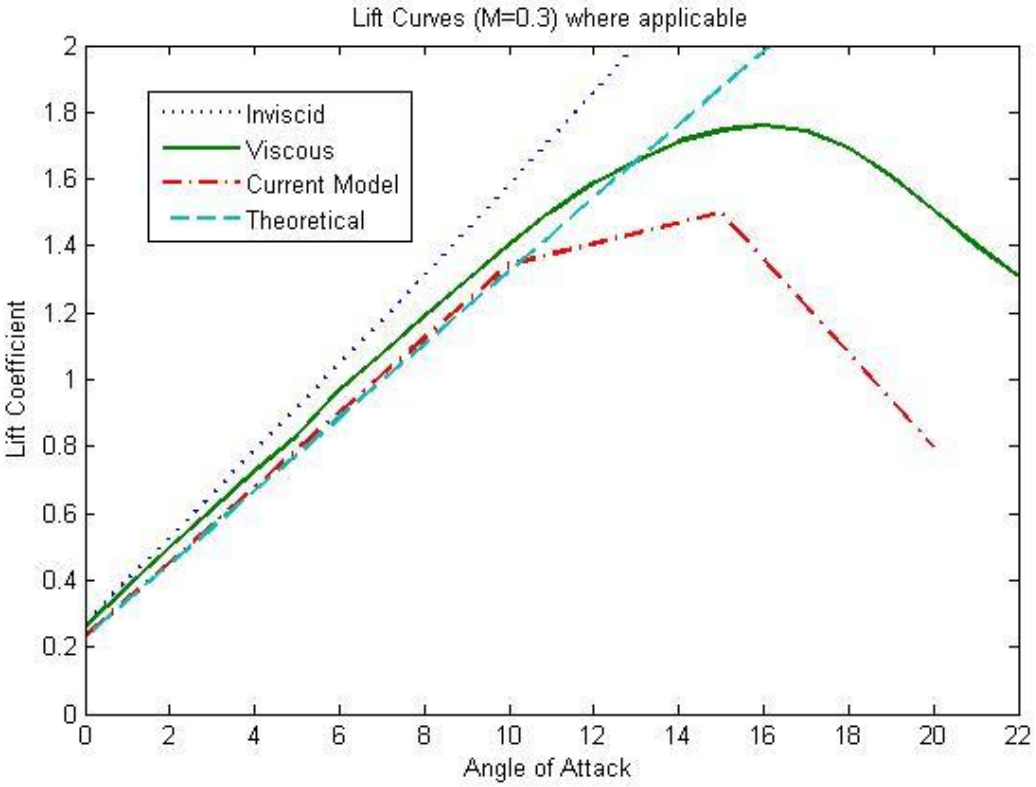

FIGURE 4.16: AVAILABLE LIFT CURVE DATA

The viscous curve data has built in stall characteristics, something which would be difficult to estimate without wind tunnel testing ordinarily. However, assuming the viscous curve set is chosen as a suitable data set for the simulation to refer to, this still leaves the problem of taking data from the correct curve within the set. Reynolds Number is a function of density (ρ), free stream velocity (Mach number) and dynamic viscosity of air (μ) which itself varies with temperature (altitude). Both density and viscosity vary with altitude, essentially due to the change in temperature. It was hypothesised that a function to relate the lift coefficient to the variable of the Reynolds number for a specific angle of attack would allow accurate values of C_L to be obtained across the data set during the simulation. If the basic curve at Mach = 0.05 was used as a baseline, the function to select a lift coefficient from the other curves in the set would be of the form in Equation 4.14.

$$C_L = C_{L_{M=0.05}} + f(Re, M)$$

EQUATION 4.14: LIFT CURVE ADAPTATION HYPOTHESIS

At this stage of model development, the activity of adding a Mach number correction function is postponed as the complexity of the model is still being deliberately limited but could be potentially achieved using a two-dimensional look-up table as in Table 4.3 with the data for the range of Mach numbers being calculated based on a polynomial fitted through the data available from the earlier numerical simulation.

Angle of Attack (deg)	*f(Re,M)* 1	*f(Re,M)* 2	*f(Re,M)* 3	*f(Re,M)* 4	*f(Re,M)* 5	*f(Re,M)* 6	*f(Re,M)* 7	*f(Re,M)* 8	Etc…
0	…	…	…	…	…	…	…	…	…
1	…	…	…	…	…	…	…	…	…
2	…	…	…	…	…	…	…	…	…
3	…	…	…	…	…	…	…	…	…
4	…	…	…	…	…	…	…	…	…
Etc…	…	…	…	…	…	…	…	…	…

TABLE 4.3: POTENTIAL TWO-DIMENSIONAL LOOKUP TABLE FORMAT

Presently, mirroring of the curve $M = 0.3$ for positive angles of attack allows a full set of data for $-90 \leq \alpha \leq +90$ to be assembled and a lookup table block used in the model to allow the selection of the correct lift coefficient corresponding to the input angle of attack. This was integrated into the model as shown in Figure 4.17. The use of a lookup correction was required to allow larger than zero references to matrix locations for negative angles of attack. Built into the lookup block is a rounding facility to address continuous input of α.

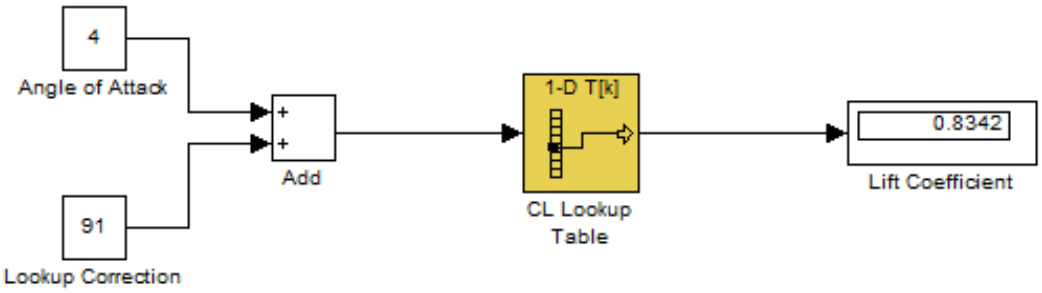

FIGURE 4.17: LIFT COEFFICIENT LOOKUP MODEL

This more realistic behaviour of lift serves to address the lift calculation errors identified at the beginning of this section through addition of the angle-of-attack-controlled lift force; the lift coefficient may become a limiting factor over the climb as well as the previously established atmospheric parameter of density.

The inclusion of a more accurate approach to lift modelling introduces an additional degree of freedom to the model – that is rotation about a horizontal axis fixed to the aircraft. Currently the axis system used has been simplified to assume that inclination of the aircraft to the free stream and inclination of the aircraft to the ground horizontal are the same quantity. In reality this is not the case as is discussed later in 4.2.3.4 Modification of 2-D Equations of Motion.

Up to this point the modelling of drag has been approached from the same angle as lift. A constant drag coefficient was specified and then the drag force was computed from this value using Equation 4.6. However, this is not an accurate representation. Drag throughout a flight will vary in a similar fashion to lift due to dependence between the two. In addition there are a host of other phenomena that influence drag throughout a flight cycle. In the spirit of reducing model complexity, essential elements will be tackled only.

At subsonic velocities drag has two components: profile drag and induced drag. The profile drag component is due to the skin friction generated through viscous shear stress over the surfaces and is dependent on the geometry of the body and the local Reynolds number, and the induced drag is the related to the lift generation. Equation 4.15 represents the composition of the total drag coefficient.

$$C_D = C_{D_0} + kC_L{}^2$$

EQUATION 4.15: SUBSONIC DRAG EQUATION

Realistically the profile drag coefficient ought to be composed of the drag coefficients of the individual components of the aircraft including, tailplane, wing, engine, and fuselage. For this simulation the total profile drag (C_{D0}) will be estimated from literature on similar aircraft as equal to 0.04 (Filippone, 2006).

The induced drag factor (k) is given by: $k = {}^{1}/_{\pi eAR}$ where AR is the aspect ratio and e is the Oswald efficiency factor. This latter quantity is related to the spanwise lift distribution. When $e = 1$ the lift distribution is considered to be elliptical. For the A320, $e = 0.85$ is a suitable estimate and the aspect ratio is known to be 9.5 (Jackson, Munson, & Peacock, 2008). This produces an induced drag factor of 0.0394.

Once the wing stalls the drag increases rapidly. There is limited literature available that mathematically deals with the drag coefficient after stall. The simulation method employed to cater for this extrapolates data taken from (Nakayama & Boucher, 1999) and increases the profile lift contribution on the approach to stall (Angle of Attack = 14-18 degrees Figure 4.16) and after stall using an empirical exponential function. Figure 4.18 compares the modelled drag to the current E1 model data.

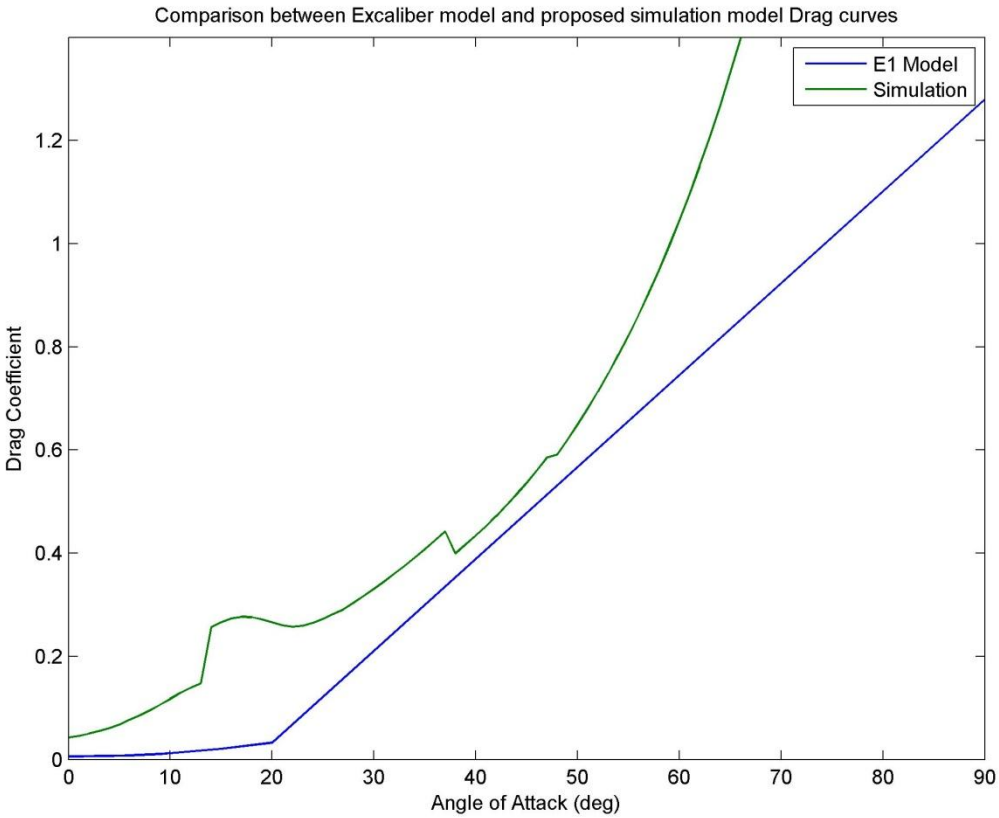

FIGURE 4.18: MODELLED DRAG TO E1 DRAG COMPARISON

Inclusion of post-stall drag required the development of a Simulink block-based logic switch. The development of this custom sub-system proved useful for future modelling and minor upgrades to previous work and is worthy of reference at this time (Figure 4.19).

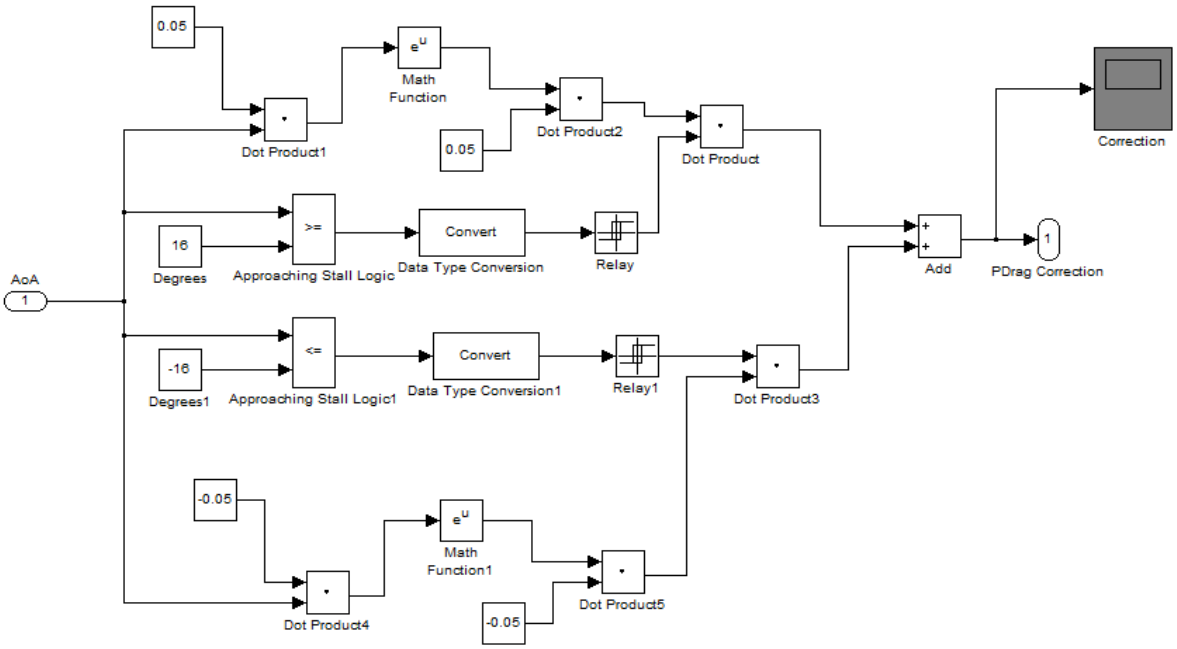

FIGURE 4.19: POST-STALL DRAG TRIGGER

As mentioned in previous sections, there is an additional degree of freedom introduced to the model due to advances in modelling techniques. Due to the inclusion of angle of attack (α) in calculations, the aircraft needs to be allowed to rotate in the XZ plane. This impacts the 2-D Equations of Motion by requiring resolution of forces. Figure 4.20 shows how these changes come about.

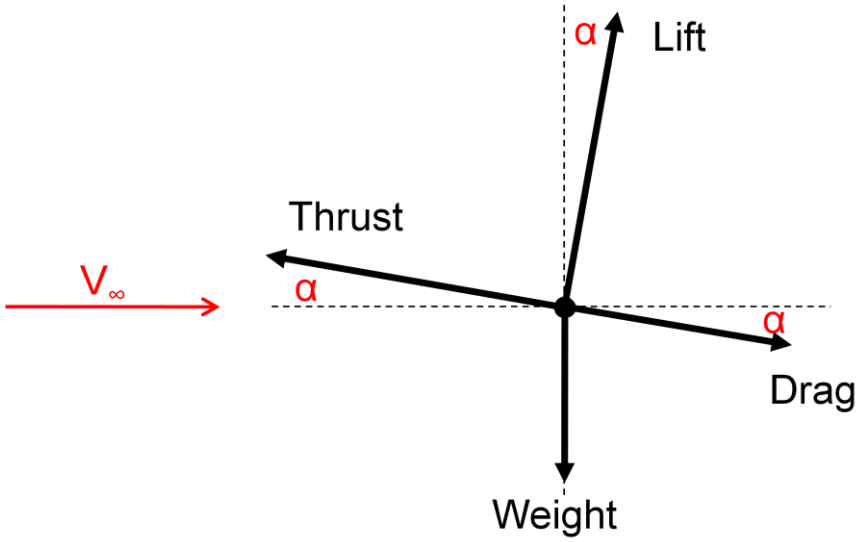

FIGURE 4.20: INCLUSION OF ANGLE OF ATTACK IN POINT MASS MODEL

However, further consideration of the problem clarifies that this illustration is only valid for when the aircraft rotation is equal to the angle of attack. This situation would occur in a scenario where the aircraft has rotated on the ground and potentially at cruise or top of climb where the free stream velocity remains parallel to the global axes (defined in 4.2.1.1 Two Dimensional Axes Definition), but not when there is a vertical velocity component (V_z). In this case, the free stream velocity vector will be inclined by an angle μ to the horizontal global axis as in Figure 4.21.

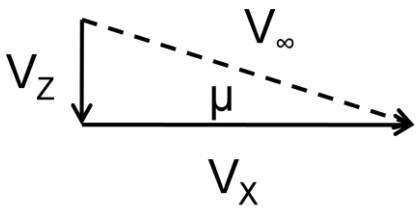

FIGURE 4.21: FREESTREAM VELOCITY VECTOR DEFINITION

If the rotation of the aircraft (pitch angle) is denoted θ, the four force diagram is more accurately represented as in Figure 4.22.

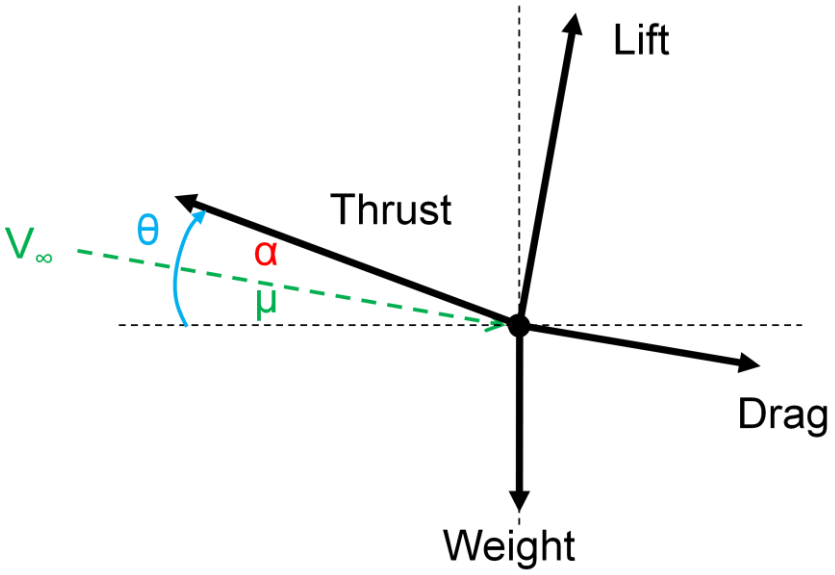

FIGURE 4.22: REVISED FOUR FORCE POINT MASS DEFINITION

Using Figure 4.22 to resolve the forces vertically and horizontally, the new equations of motion with respect to the global axes read:

$$Tcos(\theta) - Lsin(\mu) - Dcos(\mu) = \frac{d(m\dot{x})}{dt}$$

EQUATION 4.16: REVISED EQUATION OF MOTION X DIRECTION

$$Lcos(\mu) + Tsin(\theta) - W - Dsin(\mu) = \frac{d(m\dot{z})}{dt}$$

EQUATION 4.17: REVISED EQUATION OF MOTION Z DIRECTION

A block diagram is now constructed to solve these equations.

The modification of the equations of motion allows the aircraft to return to ground under certain scenarios. Previous model configurations involving a discrete switching mechanism for a static ground reaction (4.2.2.7 Z-Velocity Calculation) had not catered for this dynamic scenario and hence the contact could not be handled adequately. It was decided that a simple landing gear subsystem should be included to prevent the inevitable conclusion of the ground failing to stop the aircraft's descent.

If the landing gear is assumed to compose of the standard oleo-pneumatic mechanism (Conway, 1958), it can be modelled as a mass, spring, dashpot system as shown in Figure 4.23. Ignoring any horizontal interaction, the one-dimensional forces produced by the spring and the dashpot will then be fed into the vertical equation of motion. This assumes, when at simulation initialisation, the lift is zero and the vertical forces consist only of the initial weight. The stiffness constant (k) and the damping coefficient (c) need to be defined for the system. The value of k must be sufficiently high enough to prevent significant deflection of the landing gear at the simulation start-up and the value of c appropriate for the expected transient characteristics of the oscillation.

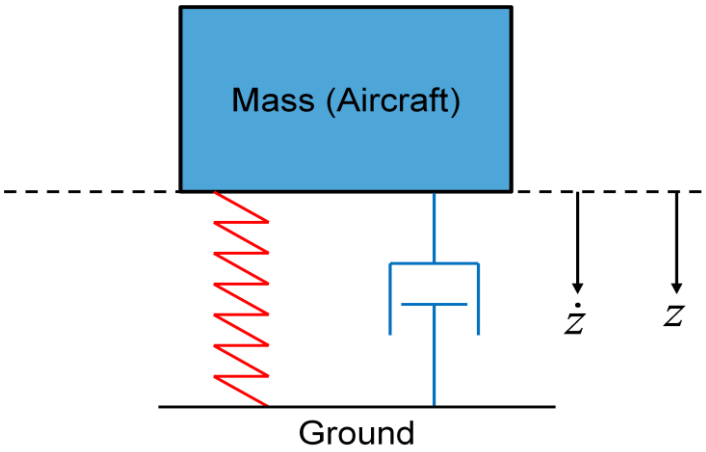

FIGURE 4.23: REVISED LANDING GEAR MODEL

This system is implemented by retaining the existing switching system and incorporating the solutions to the vertical equation of motion (velocity and position) into the sub-model. The tuning of the stiffness and damping properties of the landing gear model in the absence of data for expected landing gear behaviour is an empirical process, the stability of the response of the landing gear and the maximum or steady state displacement being the key driving factors for suitability of parameters. However, an alternative would be to solve the equation of motion for the landing gear system to produce suitable values of stiffness and damping. Using Newton's 2nd Law of motion, and recognising that the force due to damping is proportional to the velocity and the force due to the stiffness is proportional to the displacement, the free equation of motion can be assembled (Equation 4.18).

$$m\ddot{z}(t) + c\dot{z}(t) + kz(t) = 0$$

EQUATION 4.18: SINGLE DOF LANDING GEAR FREE EQUATION OF MOTION

The solution to the above second order ordinary differential equation (ODE) may be of three distinct forms depending on the damping and stiffness coefficient combination. Specifically, the range of possible values for the characteristic equation (Equation 4.19) depends on the nature of the discriminant.

$$\beta_{1,2} = -\frac{c}{2m} \pm \sqrt{\left(\frac{c}{2m}\right)^2 - \frac{k}{m}}$$

EQUATION 4.19: CHARACTERISTIC EQUATION OF THE 2ND ORDER ODE

With reference to existing parameter models (Project Airbus) typical damping ratios ζ, defined in Equation 4.20, lie between 0.6 and 0.95. For an estimated typical or desired vertical static displacement, the stiffness k of the landing gear can be approximated by considering the equilibrium for vertical forces. Using this stiffness and an appropriate value of ζ in the typical range, the damping coefficient c can be obtained.

$$\zeta = \frac{c}{2m}\sqrt{\frac{m}{k}}$$

EQUATION 4.20: DAMPING RATIO DEFINITION

Damping ratios less than 1 indicate a 'lightly damped' system and generate an oscillatory response of the general form as in Equation 4.21 in terms of the damping ratio ζ, two constants specific to the initial conditions and the circular damped natural frequency of the system oscillation $\omega_d = \sqrt{\frac{k}{m}(1-\zeta^2)}$.

$$z(t) = e^{-\zeta t\sqrt{\frac{k}{m}}}[C_1 sin(\omega_d t) + C_2 cos(\omega_d t)]$$

EQUATION 4.21: LIGHTLY DAMPED GENERAL SOLUTION OF LANDING GEAR MODEL

Extending the theory further, for the initial condition corresponding to displacement of the aircraft from the static equilibrium position when resting on its landing gear (the default condition at the simulation start-up), the lightly damped response can be visualised from simulation scopes as shown in Figure 4.24.

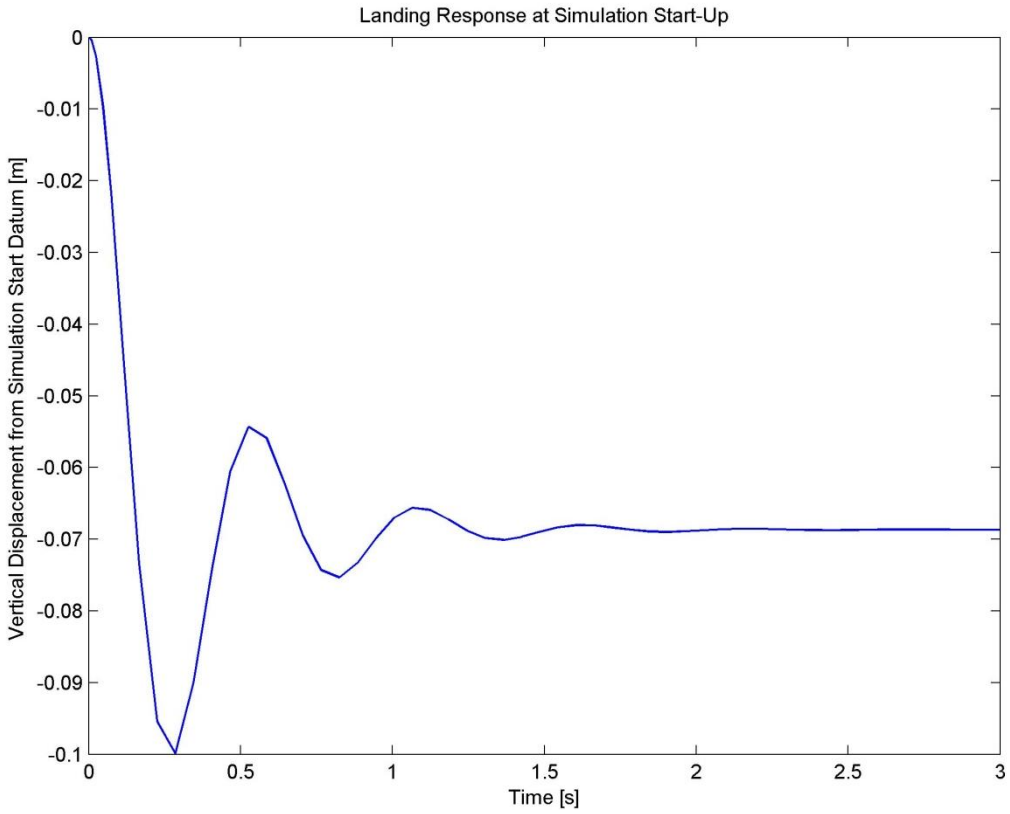

FIGURE 4.24: 1-DOF MODEL LANDING GEAR RESPONSE PLOT

The representation of the landing can be further refined through broadening of the model to include more than one landing gear strut and wheel. In the two-dimensional case of current interest, the tricycle configuration of two main gear struts and a nose gear strut lends itself to the 2-DOF approximation shown in Figure 4.25 as the appropriate extension of Figure 4.23.

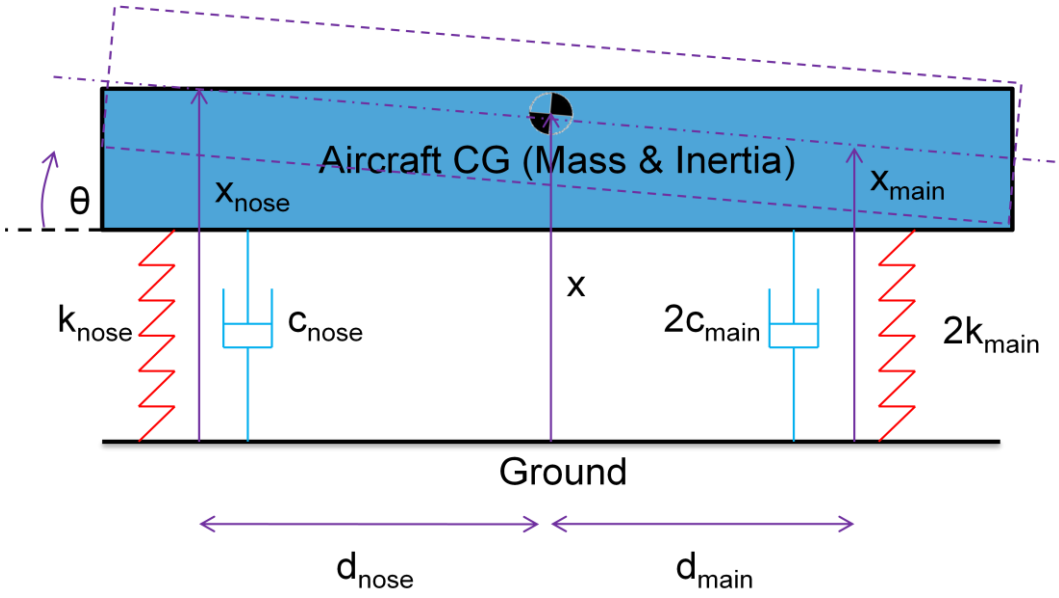

FIGURE 4.25: 2-DOF LANDING GEAR MODEL

Solution of the problem requires solution of the equations of motion (Equation 4.22). The degrees of freedom of the system include the familiar bouncing motion as well as the pitching motion due to the relative motion between the two spring-dashpot systems.

$$\begin{bmatrix} m & 0 \\ 0 & I \end{bmatrix} \begin{Bmatrix} \ddot{x} \\ \ddot{\theta} \end{Bmatrix} + \begin{bmatrix} (c_{nose} + 2c_{main}) & (c_{main}d_{main} - 2c_{nose}d_{nose}) \\ (c_{main}d_{main} - 2c_{nose}d_{nose}) & \left(c_{nose}d_{nose}^2 + 2c_{main}d_{main}^2\right) \end{bmatrix} \begin{Bmatrix} \dot{x} \\ \dot{\theta} \end{Bmatrix} + \begin{bmatrix} (k_{nose} + 2k_{main}) & (k_{main}d_{main} - 2k_{nose}d_{nose}) \\ (k_{main}d_{main} - 2k_{nose}d_{nose}) & \left(k_{nose}d_{nose}^2 + 2k_{main}d_{main}^2\right) \end{bmatrix} \begin{Bmatrix} x \\ \theta \end{Bmatrix} = \begin{Bmatrix} 0 \\ 0 \end{Bmatrix}$$

EQUATION 4.22: 2-DOF LANDING GEAR MODEL EQUATIONS OF MOTION

Finally, the inclusion of frictional rolling resistance adds to the realism of the aircraft ground interface definition. The rolling resistance of the aircraft on the ground may be modelled as a single frictional force acting on the point mass, parallel to the ground in the opposite direction of motion. Its magnitude is dependent on a constant and the reaction by the ground on the object due to vertical load. It can be expressed by the familiar Coulomb friction relationship in Equation 4.23. Typical values of the coefficient of friction μ are available in literature (Filippone, 2006) a selection of which are provided in Table 4.4.

$$F = \mu R$$

EQUATION 4.23: COULOMB FRICTIONAL RELATIONSHIP

Runway Condition	Coefficient of Friction μ
Dry Concrete/Asphalt	0.02
Hard Turf and Gravel	0.04
Short and Dry Grass	0.05
Long Grass	0.10

TABLE 4.4: TYPICAL VALUES FOR THE COEFFICIENT OF FRICTION

4.2.3.6 SOLVER AND MODEL CONSTRUCTION MODIFICATIONS

As the model develops, it is essential to digest what requirements the user has of the solution software, what it can offer and how the user may aid the satisfaction of the requirements (Dabney & Harman, 2001). Adhering to a Simulink best practice when using data store blocks where values are written to a memory location once calculated and read from the memory location when required needs the consideration of solver behaviour. It ought to be remembered that although the use of graphical interface negates the need for raw coding by the user, the inevitable compilation of the model for solution is in fact where software is written and hence Simulink models are susceptible to the same numerical issues encountered in software construction. Consideration needs to be given to the order in which the calculations are performed for a segregated solver strategy in order to ensure the calculation is using the correct or latest value of a particular parameter. If a data store is read from before it is written to in a particular time step, it can cause inaccuracies (large residuals), convergence issues or instabilities during the solution process. In order to reduce the impact of such events, signals will be read once and written once if possible (assuming the chosen solver attempts to solve the model equations simultaneously within a time-step) with the intermediate values being routed from one subsystem to another. Model elements such as continuous functions, for complex scenarios can be temperamental and care must taken to manage options appropriately. A great deal of time can be and has been spent in ensuring a level of stability in the model to a degree that allows the presentation of a credible solution.

Various solver configurations and in particular methods of numerical integration are offered by the Simulink software. In general, solvers are characterised by the specification of initial and maximum step sizes for the numerical integration and the relative and absolute tolerances of the size of the residuals. The residual is a measure of the imbalance between the known side of an equation and the side calculated using the approximate solution. Tolerances specify the allowable magnitude of the residual and allow control of the number of iterations required by the solver to obtain a solution for a particular step. Consequently a degree of control over the computational load and computation time can be exercised by the user. In addition, the specification of step sizes serves as a means to control the rate of examination of the system performance allowing capture of fast dynamics. A system with both fast and slow dynamics is known as a stiff system, an example of which is considered later (5.3 Longitudinal Stability Case Study).

As a means of developing an understanding of different solution methods, the application of different methods of modelling integration was explored as solution errors over the model life-cycle are generally traced to this operation in particular.
Simulink offers two distinct blocks that provide integration capability. They include continuous and discrete numerical integrators. A discrete system is one which can be represented by difference equations that operate on an input of pulsed (or discretely supplied) data. Discrete integration therefore uses the values of the pulses in order to compute the integral as the area under a curve as given by a finite number of rectangles or trapezoids depending on the configuration specified. A continuous system is one which can be represented by differential equations with continuous integrators using algorithms appropriate to handling continuous functions. Discrete integration can be applied to a continuous signal but requires sampling of the signal to form the necessary discrete input.
Equations in the time domain can be represented in other domains to an intermediate step to solution. Currently, the software integrates the continuous equations by means of mapping the time domain equations to the Laplacian or S-domain using Laplace Transforms. Discrete integration makes use of Z-Transforms. The details of solution mathematics are available in a number of books (Banks, 1986). In order to visualise the affects of a change in integration technique, a small study was setup. The results of the integration of a sine wave using two fixed step discrete integrations and continuous integration are shown in Figure 4.26. As is clear from the plots, the accuracy of the function varies with configuration. The magnitude of the error is directly proportional to the rate of change of the input or in other words the slope of the input

curve. In addition, the overall residual is lower for a smaller time step as is expected by the increased number of calculations for over a particular duration. Finally, the final errors of the functions are essentially out of phase. As the function is periodic, the error is not steady state but there is a visible intersection of the error lines. This phase shift may be related to the step size and is likely to become more pronounced with time due to an accumulation with error. Therefore, for practical application, the relative residuals as well as the change in residual over time may be factored into the choice of solver.

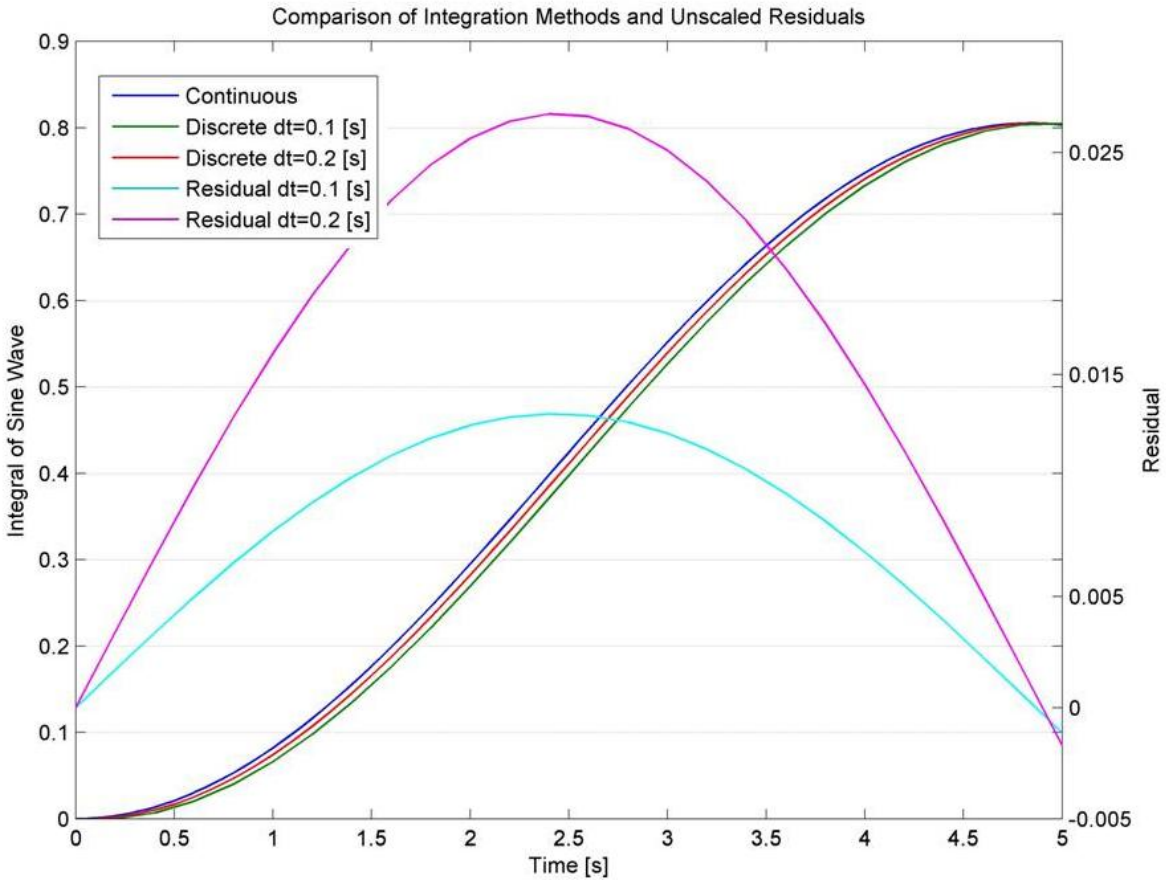

FIGURE 4.26: COMPARISON OF INTEGRATION METHODS

Solver configurations offered by Simulink include both variable step and fixed step solvers. The merits of these two methods can be discussed at length but essentially depends on application. Variable step solvers adjust subsequent time steps based on a fixed residual; if the current answer is too accurate, the time step is increase and vice-versa, which can have computational speed and loading advantages. Knowledge of the system dynamics is necessary to ensure capture by specified time steps in using a fixed step solver and care must be taken when using discrete integrators with a specified sample rate. Rate transition blocks serve to adjust the sampling of data between blocks at the expense of computational efficiency. However, this is unnecessary as long as the discrete integration sample time is a integer multiple of the solver step size – a technique used in the development of the current model.

Finally, there is the issue of algebraic loops introduced through the modelling technique. This is of particular interest when attempting Real-Time execution (see 4.4 Real-Time Flight Simulation Model) as there is currently no facility available to handle algebraic loops without model modification prior to the application build. Algebraic loops are constructed where one block requires the input of itself or a dependent block. Resolution of loops may involve the inclusion of a memory block, which delays the transfer of data until the next time step, or a redesign of the model. Memory blocks may introduce issues with accuracy and convergence due to the out-of-step behaviour they introduce.

The work on the development of the mathematical model is concluded with the production of a series of plots describing the behaviour of the model for two given scenarios. The scenarios chosen for visualisation of the behaviour is dependent on the envelope of validity of the model. Considering the model behaviour during simulations covering take-off, climb and cruise segments, the applicability of the model as well as some impacts of the modelling approximations can be deduced. Two fundamental measurements that provide an insight into the solution are altitude and speed and will be used as primary indicators in the data plots.

The take-off run of an aircraft normally requires the addition of a pitch input to induce a climb in an acceptable time frame from brake-release at the beginning of the runway. The mathematical model contains the rotational degree of freedom to allow such behaviour. Pitch is assumed to be the inclination of the aircraft with respect to the ground. This value is supplied to the model through a deliberate orientation signal 80 [s] into the simulation to simulate rotation on the runway.

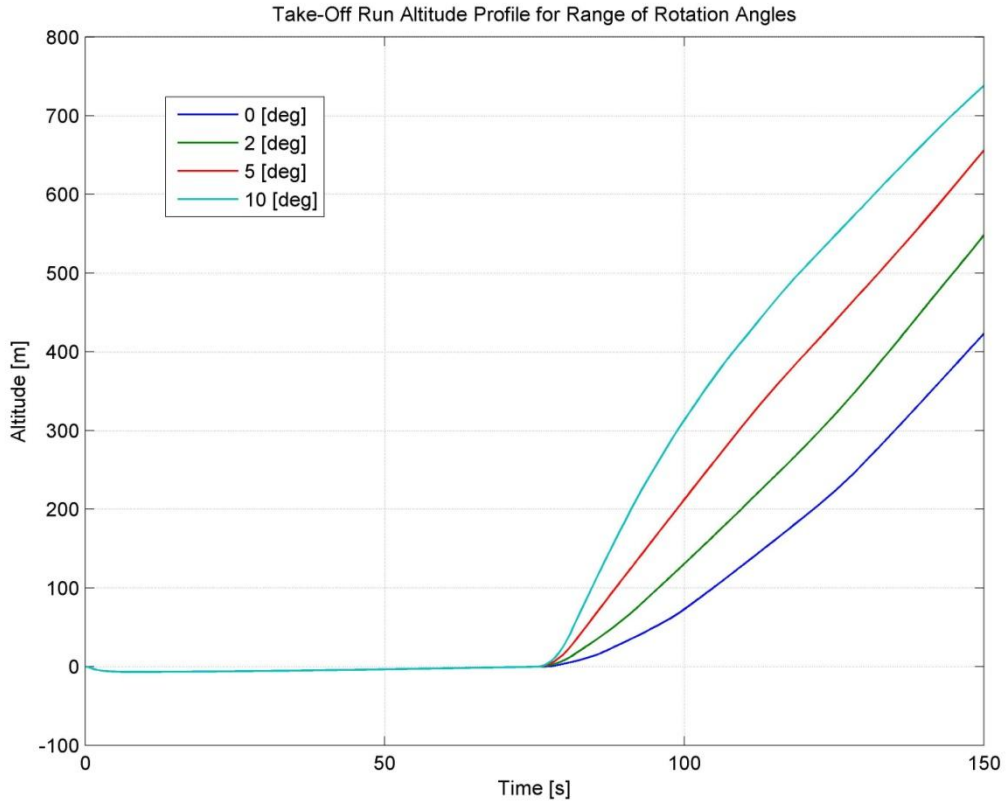

FIGURE 4.27: MATHEMATICAL SOLUTION ALTITUDE VARIATION DURING TAKE-OFF RUN

Examining the variation in altitude for the simulation Figure 4.27 it is possible to draw conclusions on the model behaviour. The first 80 seconds of the simulation correspond the time the aircraft is accelerating from rest along the runway. On initialisation the altitude falls below the zero datum as this is the process of the landing 'taking the weight' of the aircraft. As the speed increases Figure 4.28 as does the lift and a gradual increase in altitude in witnessed throughout the ground run back to the limiting case at an altitude equal to zero where the wheels are still in contact with the ground but the landing gear supports no load as the entire weight is balanced by the lift.
A pitch or rotation of the aircraft is introduced at a time equal to 80 [s]. And the variation in altitude response of the aircraft can be seen by the divergence of different lines on Figure 4.27 corresponding to a particular rotation magnitude. The initial climb angle, although dependent on the forward motion of the aircraft may be interpreted as being dependent only on the change in

altitude since the instantaneous velocity of all curves is the same at rotation. This climb angle varies intuitively with the magnitude of the pitching displacement. Subsequently the lines demonstrate a particular tendency; lower rotation angles induce a tendency of the aircraft to increase the rate of climb and with the opposite being also true. This may be explained in combination with Figure 4.28.

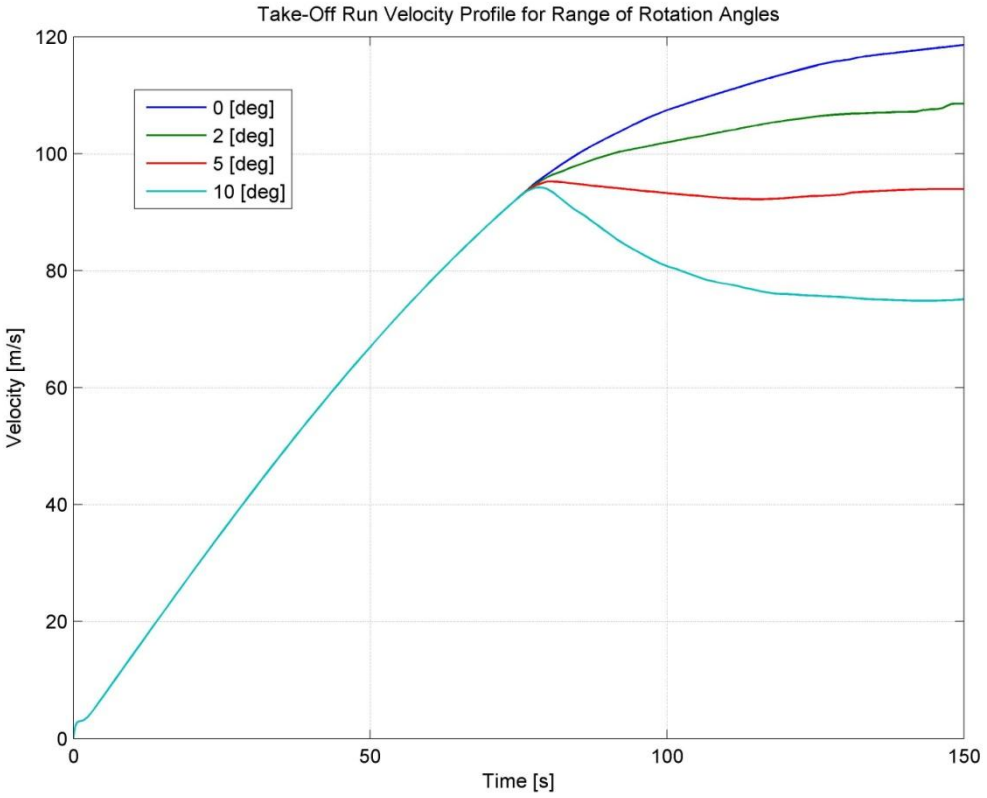

FIGURE 4.28: MATHEMATICAL SOLUTION VELOCITY VARIATION DURING TAKE-OFF RUN

Those models subjected to larger values of pitch, due to the equilibrium of forces governing the model (Figure 4.22) also incur a reduction in velocity due to the reduced thrust component in the horizontal direction. The magnitude of the velocity reduction is directly attributed to the magnitude of the thrust reduction which is trigonometrically linked to the rotation of the aircraft. Other than the deviation in rate of climb due to the velocity, there is also a contribution from both the change in angle of attack and the atmosphere model running in parallel. A lookup table constructed from aerofoil analysis generates a lift coefficient corresponding to a particular angle of attack. In addition, with altitude, the density decreases. As a result, due to the relationship given by Equation 4.5, the lift force magnitude as well as its direction (Figure 4.22) serves to alter the balance of forces in the vertical direction resulting in a change in the vertical velocity.

The take-off data need not be extrapolated for further analysis of the model and simulation. Lengthening of the simulation duration allows the climb profile to be visualised once again in terms of altitude and velocity (Figure 4.29).

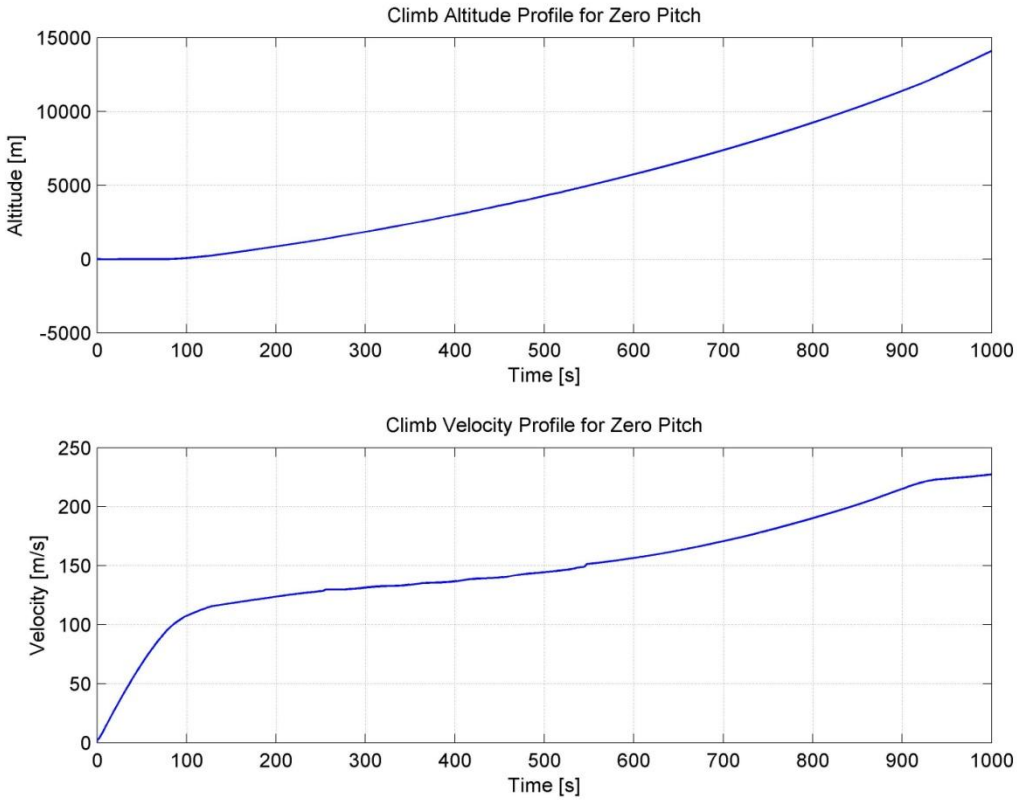

FIGURE 4.29: MATHEMATICAL SOLUTION ALTITUDE & VELOCITY DURING CLIMB

The acceleration of the aircraft throughout the climb stage is significantly more gradual than the take-off ground run due to the changes in density and angle of attack described above. The noteworthy elements of Figure 4.29 include the behaviour up to the tropopause (11,000 [m]) and the tendency of the aircraft over time. The atmosphere model incorporates the variation in thermodynamic parameters over between the ground and the tropopause. It assumed, incorrectly that all parameters thereafter remain constant. In reality, only temperature remains constant within the immediate region above the tropopause. However, the reduction in density with altitude appears to have a more pronounced effect on the velocity than the rate of climb. The reduction in density serves to increase the velocity at a rate faster than that encountered after approximately 920 [s] of the simulation where the density remains constant. This may be directly correlated with a decreasing rate of change of lift force and, as a consequence of the drag equation coupling, a decreasing the rate of change of drag force. Once the density has become fixed, changes in the lift and drag forces and, as a result of force resolution, net accelerating force become dependent on other variables.

Finally, the tendency of the simulation over a long period of time is not to obtain a trimmed equilibrium at a value of absolute ceiling as can be expected in reality, but to exponentially increase the rate of climb with time. The main contributory factor to this phenomenon is the decreasing mass profile. The reduction in the vertical weight component over time increases the rate of climb in accordance with elementary mechanics – Newton's 2nd Law to be precise. The result is that any limiting conditions achieved at the top of climb will be short lived. The mass will reduce in the ensuing moments and the vertical equilibrium will be lost causing a vertical acceleration. Furthermore, at a critical time equal to 3400 [s], the aircraft mass decreases to zero and the simulation becomes unstable due to unrestricted acceleration vertically. In reality, this scenario would not occur with the mass only decreasing to value equal to the empty weight plus payload. Also, the lack of fuel would result in a total loss of thrust, which would demand a speed reduction and a loss of lift. It is expected that this loss of lift would cause a pitching down of the aircraft and an induction into a long period phugoid oscillation at decreasing altitudes (for more on Phugoid motion see 5.3 Longitudinal Stability Case Study). This behavioural prediction highlights not only the inadequacies associated with thrust and fuel modelling but also the lack

of a complete definition of the pitching degree of freedom; in reality aircraft have a tailplane offset from the centre of gravity. The lift generated by this tailplane in addition to offsets of wing lift and thrust forces define the pitching moments about the centre of gravity (explored later in Figure 4.48).

4.2.3.8 FURTHER WORK

Although the mathematical modelling is far from comprehensive, due to time constraints and the project requirements instructing exploration of numerous areas of interest, development of this particular model now ceases. However, the research and development expertise accrued as part of this work feeds into later activities including the specification of other model variants and the construction of executable applications.
Within the scope of the current mathematical model it is possible to list a group of building blocks that ideally would form the next development step of the work. These building blocks include:

- The modelling of transonic phenomena including the lift and drag characteristics associated with high subsonic Mach numbers.
  This is a natural progression from the current work on lift and drag modelling with the potential to extend lookup tables to form multi-dimensional arrays from virtual wind tunnel testing simulation data for the aerofoil over a range of relevant Mach numbers. It is expected that drag divergence is witnessed towards the high subsonic speed range (Figure 4.30) due to the wave drag contribution from developing local supersonic pockets of flow over the surface of wing. Supercritical wing sections such as the NACA 6 Series are designed with flat upper surfaces and finite trailing edges to modify any shock systems induced by the flow speed transition – hence the use of data for this wing section for a more accurate representation of the A320 wing data in the parametric specification analysis (5.4.1.1 Wing Section Redesign). Moreover, high lift devices such as flaps may be easily included through modification of the lift and drag curves as appropriate (Rolfe & Staples, 1986) with triggers to allow retraction after take-off, improving the accuracy of climb profile graphs such as Figure 4.29.

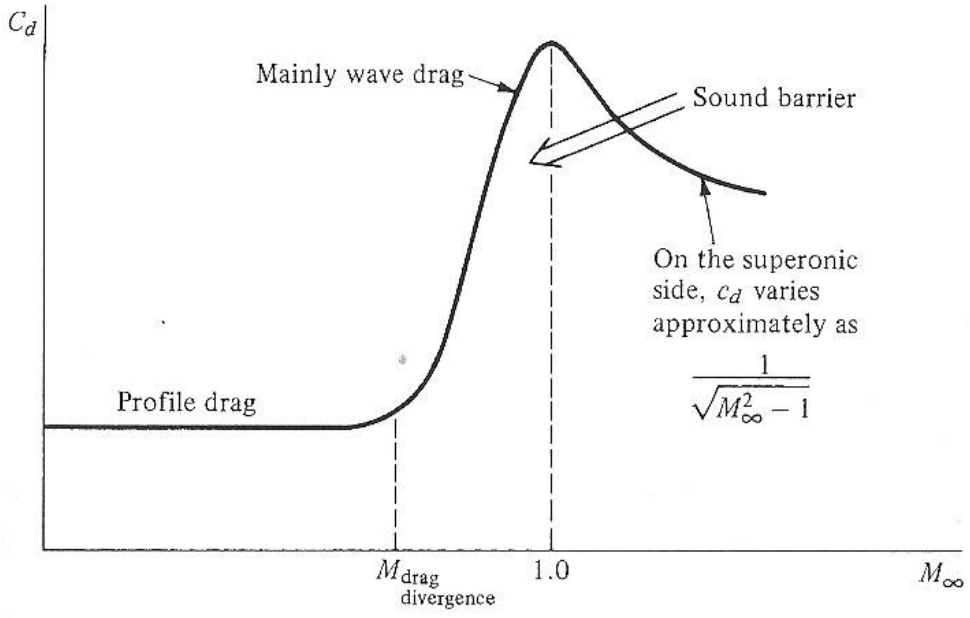

FIGURE 4.30: DRAG DIVERGENCE (ANDERSON, 2005)

- Further development of the engine sub-model.
  The engine currently is modelled at black box level and the intricacies associated with engine control have been reduced to a simple transfer function. Maintaining this level of abstraction, there are a number of phenomena in existence which affect the model output and hence the simulation result. Therefore, forgoing the complexity of modelling the engine at a level lower than the current black box, it is relevant to account for thrust lapse due to altitude and speed in addition to shock system and atmospheric influences on flight envelope limiting phenomena such as intake buzz and compressor surge (explained more in 5.4.3 Identified Simulation Limitations). Attempts to model thrust lapse in Simulink may be easier achieved with software code. This is included as part of the simulation software work later.

- Returning to the subject of lift and drag modelling, three dimensional correction factors for the coefficients would be a further refinement of the sub-models as well as the accompanying recognition of the induction of a trailing edge downwash field. Due to wing tip circulation the effective lift generated by a wing of finite span is less than the theoretical prediction for an aerofoil section of infinite span. Furthermore, the spiralling motion induces a small vertical velocity in the flow leaving the trailing edge which sets up a downwash field. Mathematically, Equation 4.24 represents the correction factor for the coefficients in terms of the flight Mach number M and inclusion of this observation can readily be achieved through building block addition. Downwash representation is more difficult and in simple cases can be merely a linearly relationship with angle of attack. However, the inclusion of downwash is only beneficial when the model includes a tailplane, as the angle of attack of this surface is the affected party.

$$C_{L,finite} = \frac{C_{L,infinite}}{\sqrt{1 - M^2}}$$

EQUATION 4.24: FINITE WING LIFT COEFFICIENT CORRECTION FACTOR

- Furthermore the model has no concept of control. In order for it to be a useful simulation tool, it requires the ability to accept user input and response accordingly. The model is currently of 3-DOF which allows control of pitch (and thrust) by the pilot or simulation user. Thrust control has already been represented using a transfer function which summarises the control characteristics of the parameter. Pitch, however, is still merely a mathematical function or constant. Ideally, if the model were extended to include a tailplane, as is technically more appropriate for a 3-DOF model, the control system related to the elevator displacement could be modelled using a transfer function to map the input to a relevant response variable. I suspect that prior to including this type of model, the approximation of the aircraft will require an expansion from the point element representation to something like that developed in 4.5 Physical Modelling of an Aircraft.

- Finally, retaining point element representation, the decoupled motion of the aircraft may be extended to incorporate the remaining degrees of freedom. This could be achieved through further resolution of forces in the basic equations. Alternatively, reconstruction of the model would be favourable, integrating all the current building blocks around a equation of motion subsystem (described in the next sub-section).

This is not an exhaustive list of additions but it recognised that the increased complexity of the model results in an increase in size and the potential for error. Hence, an integrated restructuring of the fundamental physics is necessary before any further modelling of the finer variations is attempted.

4.2.3.8.1 SIX DEGREE OF FREEDOM MODEL

The derivation of the equations of motion for an aircraft is developed in detail in literature (Cook, 1997) and summarised briefly in 5.3.1 Longitudinal Equations of Motion thereafter the set of equations in reduced to those applicable to work. Simulink contains a prefabricated toolbox, which contains sub-models incorporating the mathematics of flight and the basic behaviour of the environment. In order to develop a personal understanding of the theory behind the modelling procedure, these sub-models were ignored. However, the toolbox includes various sub-models of the equations of motion, atmosphere, gravity, wind, aerodynamic forces, engines etc. which may all be interfaced with minimal effort to produce a flight simulator. However, the knowledge of various dimensionless parameters is necessary and the input to such a model requires a substantially more complex estimation of aircraft data.

4.3 SIMULATION SOFTWARE

A key activity of flight modelling and simulation is the compilation of code for model solution. So far industry built-in numerical solvers have been employed to solve a model specified in Simulink blocks through a graphical interface. These solution methods are software algorithms that use sophisticated mathematical setups. As part of this project exploration has led to the use of both continuous and discrete numerical integration and variable and fixed time steps (4.2.3.6 Solver and Model Construction Modifications). An alternative to this approach is to specify the model in terms of a system of variables and governing equations using raw code. Activities undertaken in this sphere will be documented in this section with the final code being found in Appendix E.2.

4.3.1 BACKGROUND

Simulation software is an integral part of the simulation of real systems. The representation of functional relationships between components of a system is described in terms of software statements. Mathematically, these statements are usually equations and the process involved in generating system behaviour through solution of these equations is conducted using syntax and structure associated with the software environment particular to the language chosen for the expression of the system. The simulation software is consideration of modelling and simulation at a much lower level than the graphical user interface of Simulink and as a result allows much more customisation, optimisation and versatility, particularly when developing interaction between custom model elements or physical hardware – many existing flight simulators use a typical model which is solved using standard algorithms which incorporate custom code to handle interfaces between custom external hardware such as those mounted on the Hardware Platform in Figure 1.2.

4.3.2 DEVELOPMENT

In order to develop a software solution to the governing equations of a flight simulation model, it is necessary to first make explicit the limitations and assumptions implicit to the model. Upon selection of a scope and derivation of the model within the scope, a strategy for software implementation can be devised. In order to minimise the amount of new development required, the 3-DOF Simulink model developed in (4.2 Mathematical Model Development) will be reused for the purpose.
The chosen language is MATLAB due to its ability to manage array variables easily and the potential for post processing of data within the same software tool, although almost any language can be used for execution of the code. The equations set out by the aforementioned model are assembled into functional groups. The segregation of equations in the code is identified by the existing subsystem boundaries in the model and as a result the order of equation solution is selected based on minimising the volume of out-of-date information to be used in each case. In other words, as the code is executed on a line-by-line basis, for a given time step, the variable information available to the current equation for its solution consists of only the values of those variables which have already been determined in that time step. Where the variable value is unavailable, then information on that variable from the previous time step is used. This is likely to lead to inaccuracies in the solution and potentially stability and convergence issues. However, due to the segregated strategy employed for the software solution, this practice is necessary. The detrimental effects can therefore be minimised through a sensible choice of equation solution sequence.

Figure 4.31 summarises the agreed high level breakdown of an iterative software solution to a generic set of time-dependent equations of motion. This structure provides the framework for the specification of the code required to allow solution to the chosen model.

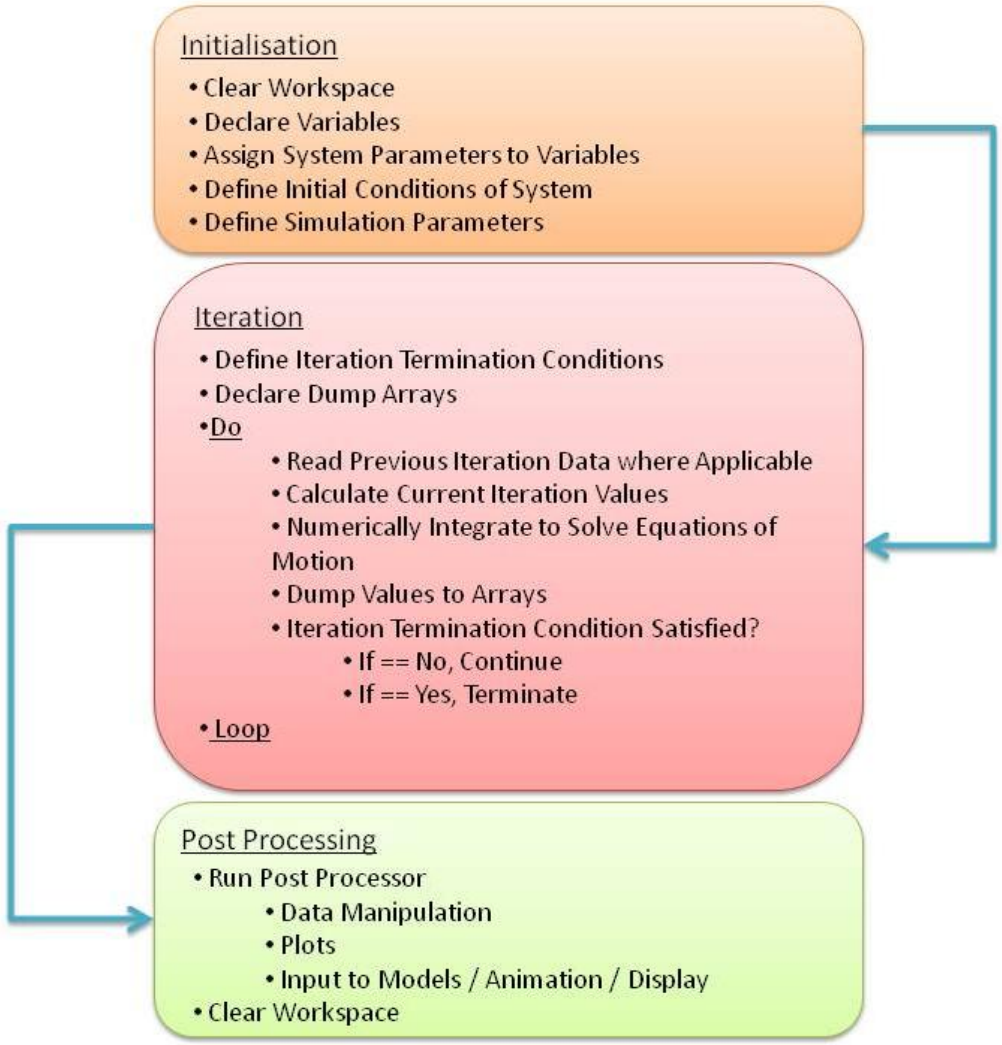

FIGURE 4.31: GENERIC SOFTWARE ARCHITECTURE

4.3.2.1 CODE CONSTRUCTION

The governing equations for the software (Appendix E.1) are collected from the development process of the source model with the exception of a gravity model and a thrust lapse model introduced for this simulation only. The gravity model uses Equation 4.25 to compute the instantaneous acceleration due to gravity (g) for an instantaneous altitude (z) based on the known constants of the sea level value (g_0) and the radius of the Earth (R_E). In reality the radius of the Earth has a range of values but for the purposes of the model, the planet is considered spherical and of mean radius. Derivation of the equation can be found in numerous reference books (Anderson, 2005).

$$g = g_0 \left(\frac{R_E}{z + R_E} \right)^2$$

EQUATION 4.25: GRAVITY MODEL GOVERNING EQUATION

The thrust lapse model is constructed through derivation of empirical relationships from published thrust lapse data (Shevell, 1989). The empirical formula (Equation 4.26) uses data acquired from a large turbofan designed c1970 and hence application to a modern product may be inaccurate. This is acknowledged, and is a limitation of the model. There is an effect on Specific Fuel Consumption (SFC) by the Mach number of the free stream flow which in turn

affects the thrust. An empirical relationship is available (Equation 4.27) but was omitted from the model due to the lack of an explicit, existing relationship between SFC and thrust.

Equation 4.26 is applicable when altitude in metres (h) is greater than 5000 [m]. Note $\tau_{h=SL}$ is the static thrust at sea level.

$$\tau_h = \tau_{h=SL} \times [0.45 - 0.17 \times 10^{-4}(h - 5000)]$$

EQUATION 4.26: EMPIRICAL THRUST LAPSE EQUATION

Equation 4.27 is applicable when Mach number (M) is greater than 0.3 but less than 0.85 and is used to manipulate the SFC in any thrust relationship to appropriately alter the engine performance.

$$SFC\ factor = 0.55 + \frac{0.25}{0.35(M - 0.3)}$$

EQUATION 4.27: EMPIRICAL SFC FACTOR EQUATION

The governing equations contain time-dependent equations of motion. The solution of time-dependent equations requires a discrete method of integration. 1st Order Euler Integration (Rectangular Integration) is of the form specified in Equation 4.28 and is used in this solution due to its simple coding and minimal requirement on computational resources. It requires a discrete time interval (dt), known as a time step, which is specified at initialisation. The size of time step is selected as 0.1 [s] as this is likely to produce data at a suitable rate and capture system dynamics with limited impact on system resources. Solution of the governing equations can be performed for each time step by setting the equations within an iterative loop whose exit condition is a parameter to be specified – normally the termination time of the simulation.

$$\varphi_{t=2} = \varphi_{t=1} + \dot{\varphi}_{t=2} dt$$

EQUATION 4.28: GENERIC FORM OF RECTANGULAR INTEGRATION

Having collected the governing equations it is apparent that due to the sequential nature of the software structure specified earlier not all data is available when required within a single time step to calculate certain variables. As a result, solutions can become stagnated in algebraic loops as illustrated by Figure 4.32. The red line in the figure indicates the requirement for a variable to be passed against the process flow – an impossibility due to the variable B1 being dependent on the result A1 of the calculation requiring B1. The dashed lines represent the modified information flow to break such loops. It is important to manage the problem by using the best data available to the software. This tends to be taken from the previous time step. This can give rise to problems of accuracy for parameters with large rates of change.

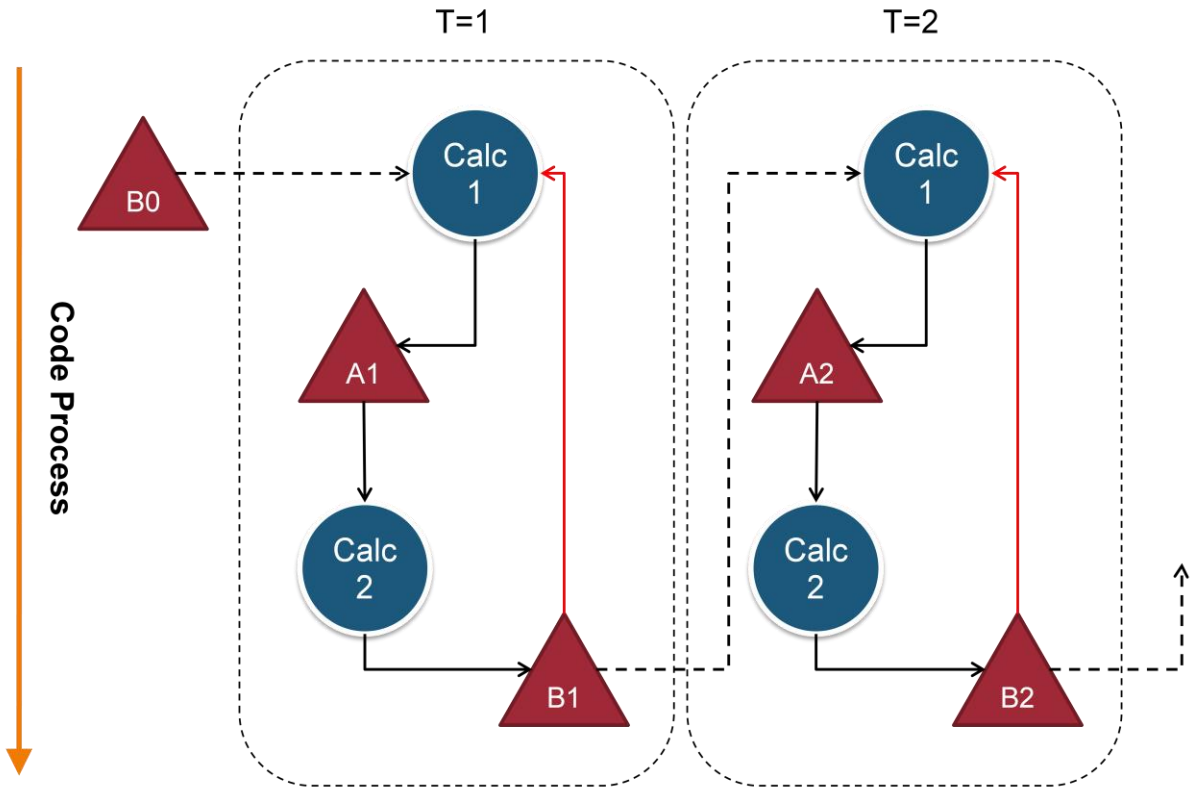

FIGURE 4.32: VARIABLE FLOW ILLUSTRATION

The code tackles the problem of data availability by using specified initial conditions to complete the equation for the first time step. Each potential algebraic loop requires an initial condition and hence an initial condition cell is added to the code structure. Finally, a code cell is written to process the post-iteration data and display relevant parameters.

Some programming best practices are integrated into the coding process. These include a cell programming philosophy to allow easier debugging and navigation, the use of comments to describe parameters, units, and cell content and the preallocation of array variables to prevent growing of variables within the iteration loop – a known cause of slower execution. Another practice which is impractical from a post processing perspective but would allow minimal use of memory locations would be to limit the size of the variables to two elements – one storing the current variable value and one storing the value from the previous iteration as these are the only two values required for computation within a given time step. This exercise would require additional routines to be written to handle the variable management and although memory allocation would be reduced, there may be additional demands on computational resources.

4.3.2.2 MODEL ELEMENT ADAPTATION

In the main, most subsystems in the model were mapped directly to software expressions. However, in two particular cases, adjustments to either the system parameters or the calculation procedure were required to address some unacceptable oscillations in the solution.

The landing gear model was originally modelled as a logic switch coupled to a displacement- and velocity-linked function which was controlled through stiffness and damping constants. These parameters were tuned for realism in the static displacement when using the mathematical model in Simulink. They were not however optimised for use with a discrete, 1st Order solver as defined by the custom software build although the equations of motion are essentially the same. Minor changes to the gear parameters saw an improvement in the realism (based on research values of landing gear stiffness) of landing gear displacement on initialisation of the simulation and improvement in the response.

The calculation of lift coefficient within the source model was performed by obtaining an Angle of Attack through calculation followed by use of a one-dimensional lookup table containing simulated aerofoil data to select the appropriate value for the lift coefficient. Due to the requirement for a discrete input to the table, actual values for angle of attack were rounded to the nearest integer value. This resulted in the potential for sudden oscillations in the value of lift for minimal changes in angle of attack if the change caused rounding alternately up and down as illustrated by the trace in angle of attack for the first 200 [s] of execution (Figure 4.33). In order to remove these oscillations in the software solution, the calculation procedure for lift coefficient was altered. The technique of using a lookup table of values was removed in favour of calculation of the lift coefficient from the average value of the lift curve slope and the value of the lift coefficient at zero angle of attack. These two values were combined into a linear function allowing with a lift curve slope of 0.115 [/deg] which is comparable to the 2-D idealised value (Houghton & Carpenter, 2003) of 1.110 [/deg]. The result of this modification not only removed unrealistic oscillations (Figure 4.34) but also the ability for the aerofoil to stall at large angles of attack – a feature built in to the lookup table data. As a result, in order for the simulation to be valid, angles of attack must remain within the stall limits. Furthermore, the presence of the oscillations in the lift force resulted in spikes in the equations of motion which affected the overall solution accordingly as is evident on the graphs from the difference in the average values of the two functions.
Finally the increase in drag after stall, initially modelled in Simulink as a triggered contribution to the drag coefficient, was removed during the migration. Validity of the simulation is assured in the absence of this function by maintaining the angle of attack within aerofoil stall limits.

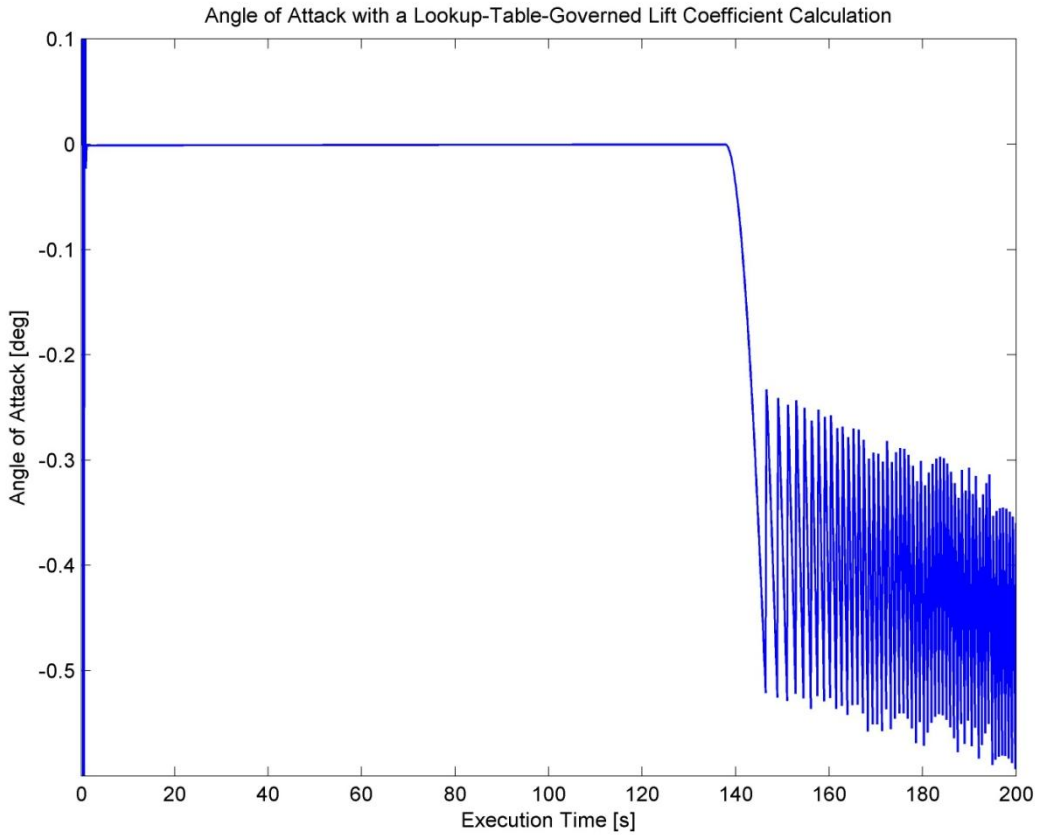

FIGURE 4.33: ANGLE OF ATTACK PLOT FOR LOOKUP TABLE CALCULATION FOR LIFT COEFFICIENT

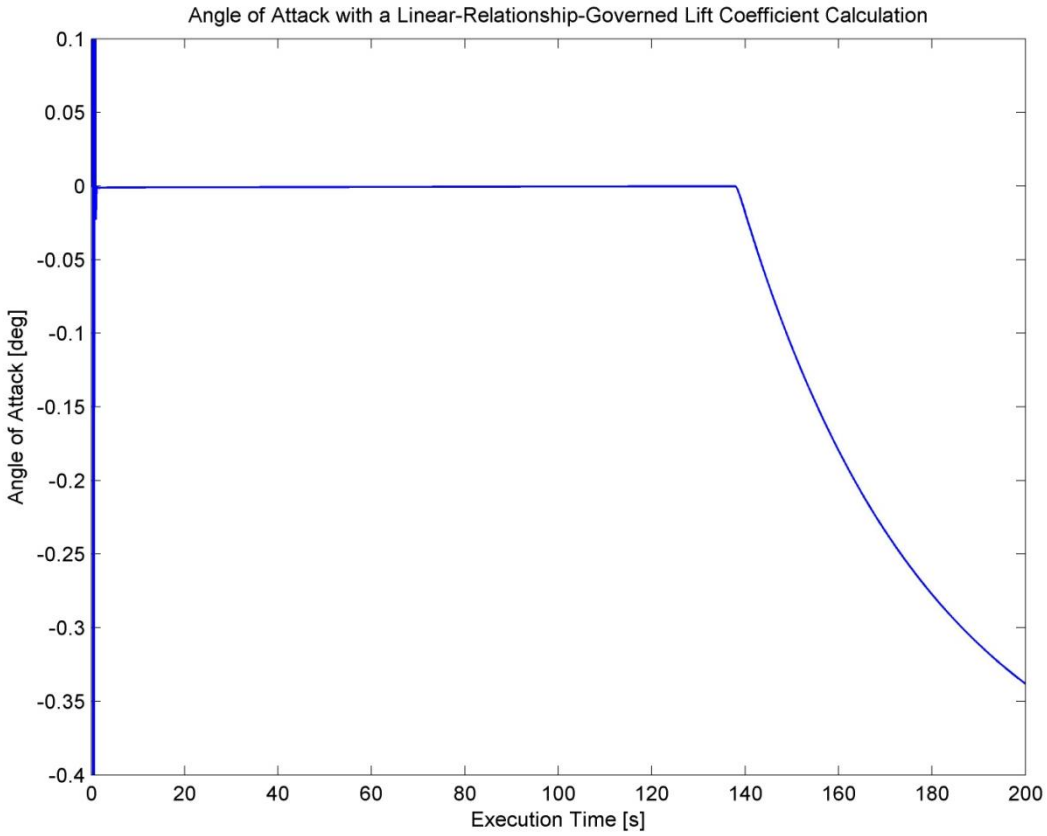

FIGURE 4.34: ANGLE OF ATTACK PLOT FOR LINEAR RELATIONSHIP CALCULATION FOR LIFT COEFFICIENT

4.3.2.3 SOLUTIONS

Completion of the software coding allows execution and post processing of the data. Amongst the scenarios to be analysed using the software are examination of model behaviour during scenarios identical to those defined for the mathematical model. Due to the similarities in the governing logic behind the two models explanation of behaviour in these scenarios is restricted to examination of any differences between the two sets of data as general behaviour has already been discussed (4.2.3.7 Mathematical Solutions).

Figure 4.35 traces the take-off performance as calculated by the Simulink mathematical model and the software specification.

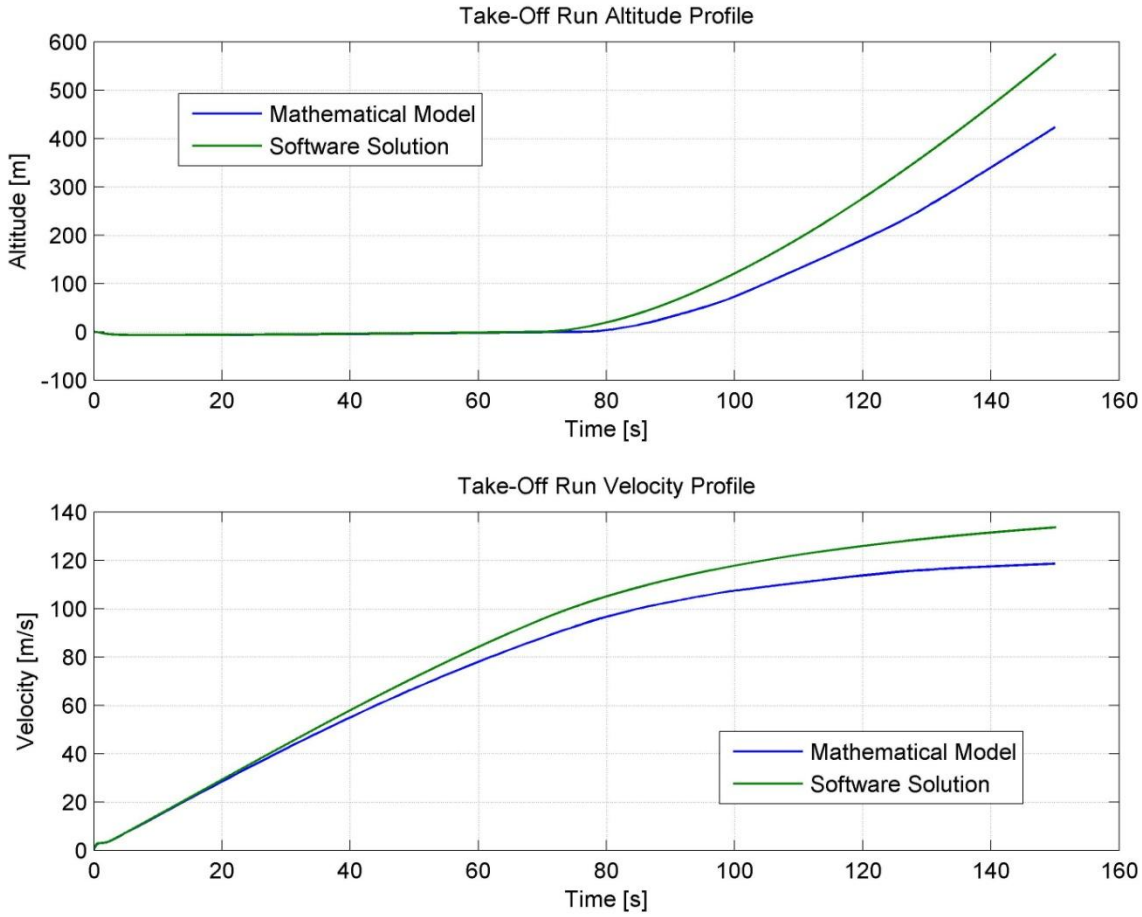

FIGURE 4.35: TAKE-OFF PERFORMANCE OF MATHEMATICAL MODEL AND SOFTWARE SOLUTIONS

Divergence in the data can fundamentally be attributed to the variation of velocity over the simulation duration. Considering purely the ground run of the aircraft, the acceleration performance of the software model is noticeably better than that of the mathematical model. However, the lift off speed of the aircraft is approximately the same. Therefore, the software model departs the ground earlier than the mathematical Simulink model. Due to the increased velocity, the lift force is greater, resulting in a faster rate of climb towards the end of the simulation. Explanations for the divergence include the three primary differences between the model definitions:

- The lift coefficient determination within the mathematical model is performed using a lookup table of data whereas the software simulation uses a linear relationship to represent the lift coefficient variation with angle of attack. As a result, although the linear relationship fits the same data, there are marginal discrepancies between the two values due to interpolation. Furthermore, any discrepancies are magnified by the drag equation which is dependent on the square of the lift coefficient. The magnified discrepancies in the drag coefficient and hence drag force may be the cause of the differences in velocity.

- The software model contains a number of additional functions, not previously included in the mathematical model. These are documented in 4.3.2.1 Code Construction. One such addition is the reduction in the acceleration due to gravity with an increase in altitude. This reduction impacts the weight of the aircraft and hence the vertical forces. The faster rate of climb may be attributed to the difference in weight values.

- Finally, the method of integration used for the software solution is primitive and of a lesser accuracy than the Simulink solver used to simulate the mathematical model. Integration studies (4.2.3.6 Solver and Model Construction Modifications) have visualised errors and there is a suggestion that these inaccuracies could cause a divergence in the calculated values of velocity from the true value.

In reality, the cause of discrepancies may well be a combination of the above plus additional factors.

Further investigation of the effect of the sampling rate (simulation time step) on the software solution yields some interesting results (Figure 4.36).

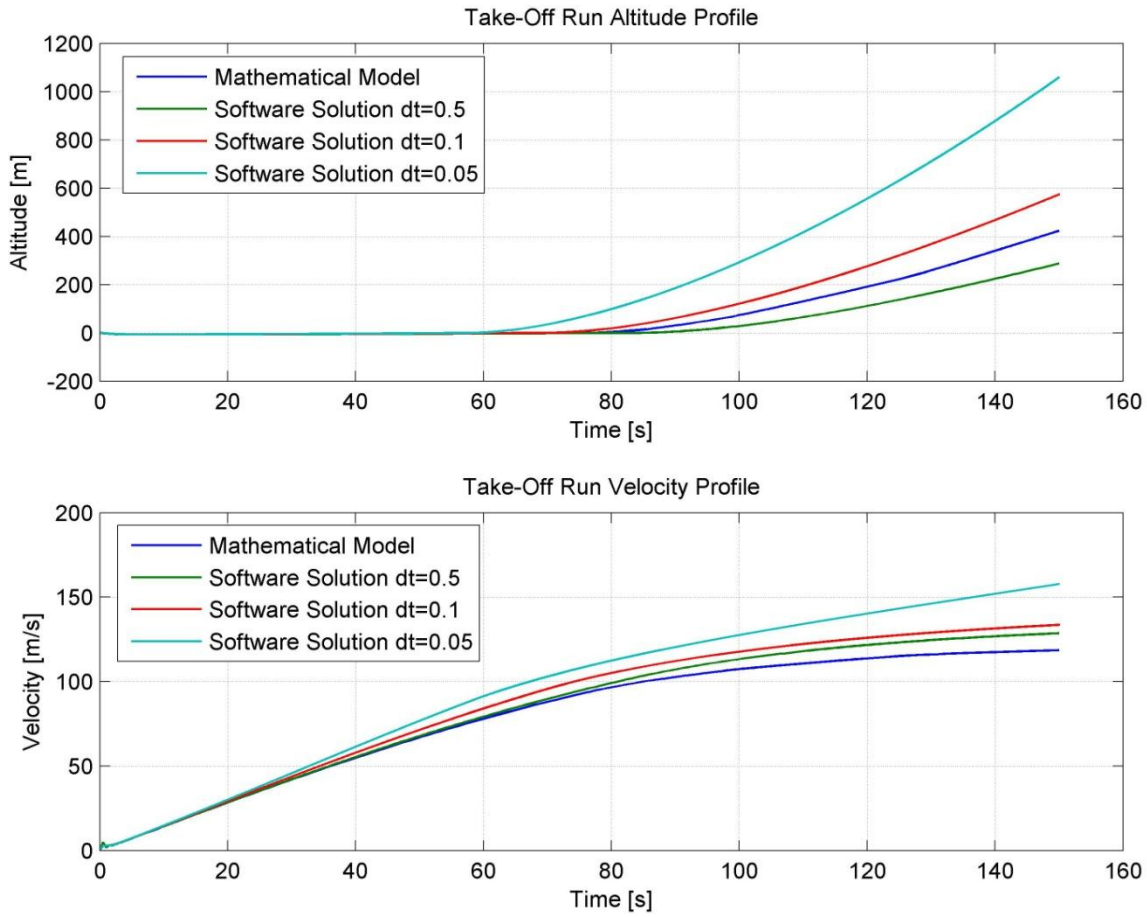

FIGURE 4.36: VARIATION IN SOFTWARE SOLUTION WITH TIME STEP

It is known from the nature of rectangular integration (Equation 4.28) that the time step is fundamentally linked to the solution of the model. Many other parameters calculated in the software depend on the output from the integration and hence most parameters are essentially driven by the output of the integration. The wholesale effect on the output of the software is therefore impacted by any change in the time step. Physically an increase in the time step means that the approximation of under curve area as a rectangle becomes less and less accurate. The magnitude of the residual error therefore increases. Examination of Figure 4.36 suggests that the converged solution is in fact further from the mathematical solution that previously thought. Unfortunately, there is no further time allocated to investigate this phenomenon thoroughly but there is certainly an area of work identifiable.
Despite these revelations, the conclusion may still be drawn that the software solution responds in a manner that is consistent with expected behaviour and is a successful representation of a 3-DOF aircraft model.

4.3.3 FURTHER WORK

The software code sets up and solves equations relating to the mathematical modelling of gravity, atmosphere, and point mass behaviour. It is acknowledged that it remains an approximation of real scenario and additional time could be spent to increase the applicability of the simulation results. Many further model elements have been discussed in 4.2.3.8 Further Work that could be representation mathematically and solved as part of the code execution. Software specific improvements can be made however. They may include an attempt at rearranging the governing equations into a series of matrix systems. Although the performance of the solving code will not be affected in the short term, as the software becomes more complex and the arrays of information become larger, the efficiency of the computation will increase greatly in comparison to the segregated method currently in use. This is primarily due to the optimisation of MATLAB for solving matrix systems; for the time it takes to perform multiple line calculations, one matrix calculation of all lines can be completed. One particular method of rearrangement could include representing the 3-DOF in terms of state variables through conversion to a state space format (5.3.2 State Space Representation).
Finally, the method of integration used is a simple first order (Euler) rectangular approximation. Physically, this method approximates the area under the curve representing the integrand as a series of rectangles of a height dictated by the simulation time step. This integration is the link between one time step in the iterative solution and the next; the output of the integration drives the update of the software values for the next time step. For relatively large time steps, rectangular integration provides only a limited degree of accuracy. More accurate integration methods include the selection of Newton-Cotes methods such as the Trapezoidal Rule or Simpson's Rule which rely on polynomial fitting (Whittaker & Robinson, 1944). Increased algorithm complexity demands more from the software, which can have negative consequences in terms of computing and coding time.

4.4 REAL-TIME FLIGHT SIMULATION MODEL

The simulation of models to this point has been in a non-Real-Time sense. That is to say the duration over which the solution process takes place is less, sometimes significantly than the specified start to finish duration over which the model behaviour is considered. For instance, if the simulation duration is specified to be 100 seconds, the computer hardware solves the model behaviour over this duration but will complete the solution in a something similar to a tenth of the time depending on solver configurations including step sizes and tolerances and available processing resources of the computer. An element of flight simulation (as discussed in the Introduction) is to portray the illusion of real flight to the user. Expanding the focus of the models currently employed, disregarding the absence of human interaction, an essential element of the solution is missing in order to achieve this illusion – Real-Time visualisation of the model solution.
The material which follows, documents the investigation into a particular means of Real Time simulation including the background of the model configuration, processing and execution.

4.4.1 INTRODUCTION TO XPC TARGET

MATLAB and Simulink, as software tools, form merely the core of a suite of available functional toolboxes which can allow the realisation of more advanced or bespoke capabilities. The simulation in Real-Time of Simulink models requires both the Real-Time Workshop toolbox along with additional components to allow the building and deployment of a Real-Time executable model. One particular toolbox, defined as a "solution for prototyping, testing, and deploying real-time systems using a host PC [Personal Computer] and a separate target PC"(The Mathworks Inc., 2004) is the xPC Target capability. So far, models have formed the basis for non-Real-Time simulations. The xPC Target capability allows configuration of the model for functions including Real-Time execution, Hardware-in-the-Loop (HIL) testing and Real-Time parameter tuning. For the purposes of this project, scope will be restricted to examining the process required for Real-Time deployment and monitoring of the model.

The basic process involved (Figure 4.37) in producing a Real-Time model using xPC Target is use Real-Time Workshop (RTW) along with a 3rd Party Visual C or C++ Compiler to build a Visual C executable version (target application) of a Simulink model generated in MATLAB on the 'Host PC'. This executable is downloaded via a hardware link to a 'Target PC' which itself runs the xPC Target Kernel, started from a xPC Target Loader introduced via a boot disk. The model is executed in Real-Time on the Target PC and monitored through a MATLAB/Simulink interface running on the Host PC.
A Kernel also referred to as a 'nucleus' is a fundamental element of an operating system and is defined in a variety of ways in most books on operating system design and concepts (Silberschatz & Galvin, 1994). *All sources agree that the Kernel is the lowest level software component available to a computer operating system. It forms a bridge between the computer hardware and the application software. In the context of an xPC Target operation, the xPC Target Kernel is specifically designed to allow use of the computer hardware in a way beneficial to the Real-Time execution of the xPC Target applications. The target applications themselves are built from the model with a set of intrinsic commands interpreted by the bespoke Kernel.*

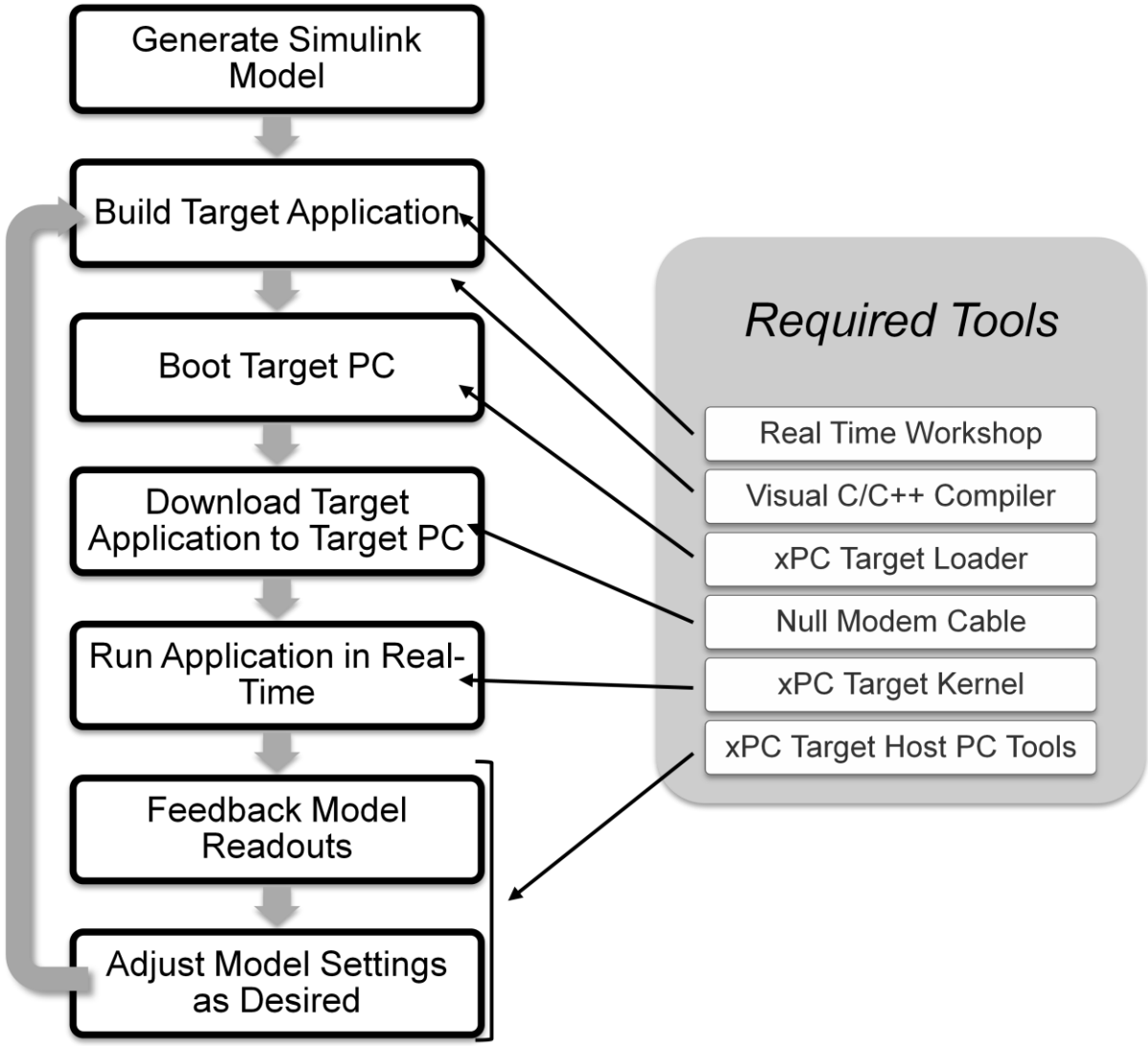

FIGURE 4.37: XPC TARGET BASIC PROCESS

As previously alluded to the hardware requirements for the xPC Target process are essentially a pair of personal computers with keyboards, displays and 3 ¼ inch Floppy Disk Drives (FDDs) which also possess a serial (COM1/2) port for communication using a cross-over serial cable – also referred to as a Null Modem Cable. Specifically this is a cable whose pins are connected in a way that allows direct communication between like ports. Due to the limited space and hardware available for the investigation into the xPC Target capability, certain concessions were made with the hardware setup including the use of a single monitor. The exact hardware configuration is described by Figure 4.38.

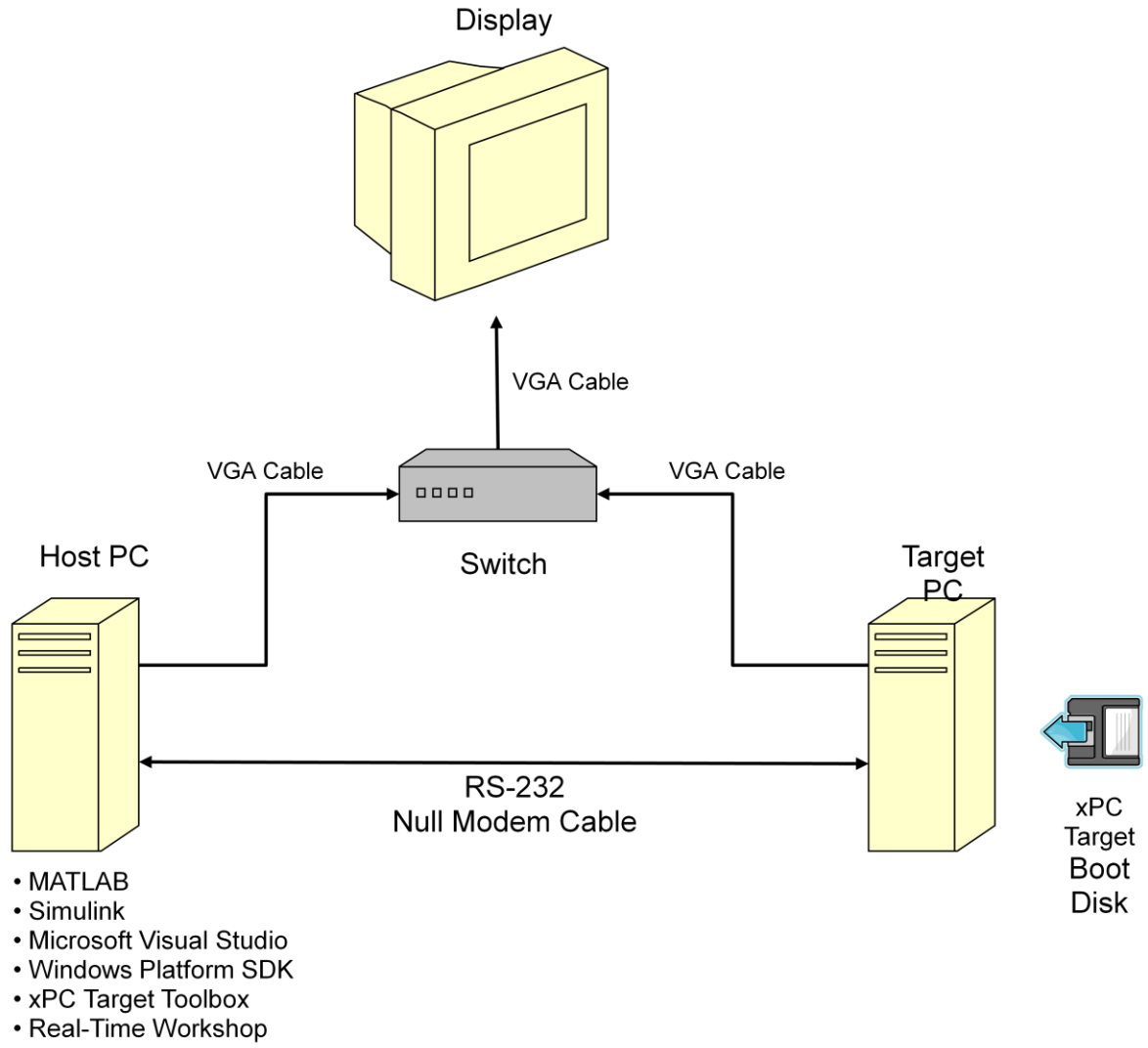

FIGURE 4.38: XPC TARGET CONFIGURATION

The software necessary to realise xPC Target consisted of MATLAB and Simulink residing on the Host PC, in addition to the RTW and xPC Target toolboxes and a Visual C/C++ Compiler. The software combination is instrumental in the success of the task, hence details of the software used in the setup can be found in (Appendix F.1). It should be noted that in addition to those software component referred to be Figure 4.38 it is assumed that the Host PC possesses an Operating System and both PCs possess a Basic Input/Output System (BIOS) to allow recognition of hardware.

Due to minor incompatibilities between software packages, a significant amount of troubleshooting was required in order to attain functionality. Certain exercises included setting environmental variables in the operating system using the MATLAB function 'setenv(<Name>,<Value>)' and the transfer of compiler source files from Software Developer Kits (SDKs) to reference libraries.

4.4.2 INITIAL DEVELOPMENTS

Initially, having procured the necessary hardware and software, in order to develop a familiarity with the xPC Target capability preliminary information (The Mathworks Inc., 2004) was examined and principles applied to a simple model. The model featured an step input signal followed by a double integrating feedback model and is represented in Simulink block diagram form as shown in Figure 4.39 (alternatively this may be represented as a transfer function).

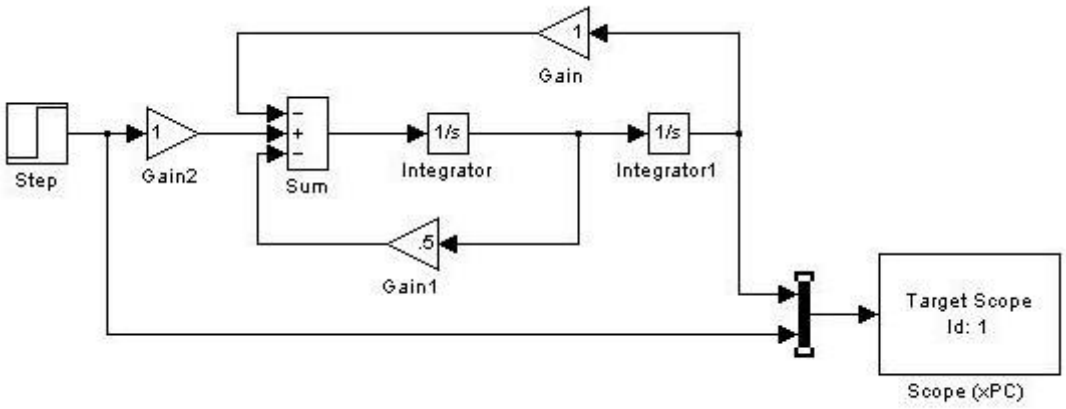

FIGURE 4.39: XPC TARGET STEP MODEL

It should be noted, that the model is constructed in a form that is equivalent to a non-Real-Time Simulink model but with one notable exception: The use of a scope block from the xPC Target toolbox, configured to allow visualisation of the input signals during Real-Time execution. The block is identified as Scope (xPC) of identification number '1' and type 'Target Scope'. This information implies that the scope is to be loaded by the Target PC Kernel and displayed on the Target PC during the simulation.

A degree of configuration was required before the model could be built into the target application. Firstly, the solver used is by default, a variable-step numerical integration algorithm 'ODE45 Dormand-Prince'. RTW supports the generation of code for fixed-step solvers only and hence the specification was changed to the more appropriate 'ODE4 Runga-Kutta'. It was then necessary to configure RTW to produce the correct type of application, that is to say one which is executable using the xPC Target Kernel on the Target PC. This was achieved through selection of the 'xpctarget.tlc' settings file which populated the RTW fields necessary for the appropriate operational behaviour. Finally, the local path of Visual C compiler is specified in the RTW settings.

The model was built into an application and automatically downloaded over the serial link to the Target PC. On completion of the process, MATLAB creates a software object representing the built application in the MATLAB environment. From the MATLAB command line, it is possible to access and edit all the properties of the target application object as is common to Object-Oriented Programming (OOP) languages.
The details of object-oriented programming languages will not be discussed here but literature is available (Budd, 1996) *on the subject.*
Specifically, due to the high latency of the serial connection, properties such as start and stop times and commands as well as sample rates were all specified through the MATLAB command line as opposed to the significantly slower alternative of using a Graphical User Interface (GUI) as a means of interacting with the Target PC.

The xPC Target Scope loaded on the Target PC functions in a similar fashion to an oscilloscope; data is collected at the sample rate of the model and displayed once a predetermined buffer capacity has been reached. In order to assign the buffer size it was necessary to create an object in the MATLAB environment and map the scope to object (<ScopeObjectName>=<TargetApplicationObject.getscope(<ScopeID>)). The buffer size property (<ScopeObject>.NumSamples) was then specified to allow a single refresh of the scope on the Target PC on termination of the execution.
The sample time of the model is equivalent to the step size of the integration and although a faster sampling rate (shorter sampling time) improves the ability of the solver to capture the short period dynamics of the system, due to latency of the serial connection, it also increases the chance of overloading the Central Processing Unit (CPU) of the Target PC.

After the Target PC has received the target application, the model is initialised and any target scopes loaded into the Target PC environment. The Target PC loader displays a graphical readout of its own (Appendix F.2). A critical region of the Target PC display is located in the upper left corner, a photograph of which is shown in Figure 4.40. The details provided include the name of the loaded application, memory available on the Target PC, application execution mode (Real-Time – 'RT', single-tasking – 'single'), which signals the application is recording for output to the MATLAB environment (time – 't', task execution time – 'tet'), the designated stop time of the simulation in seconds, the specified sample time in seconds, the average time taken to execute an operation in seconds (dependant on the capabilities of the Target PC hardware and finally the current time in the Real-Time execution of the application.

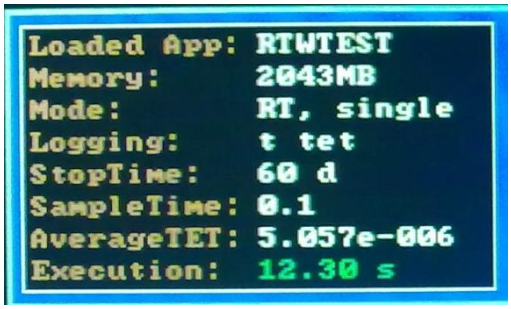

FIGURE 4.40: TARGET PC LOADER DISPLAY

On completion of the execution the scope displays the signals on the Target PC display. Figure 4.41 and Figure 4.42 compare the non-Real-Time Simulink scope output and the Real-Time xPC scope output respectively. Results are consistent with the successful execution of the model in Real-Time using the xPC Target capability.

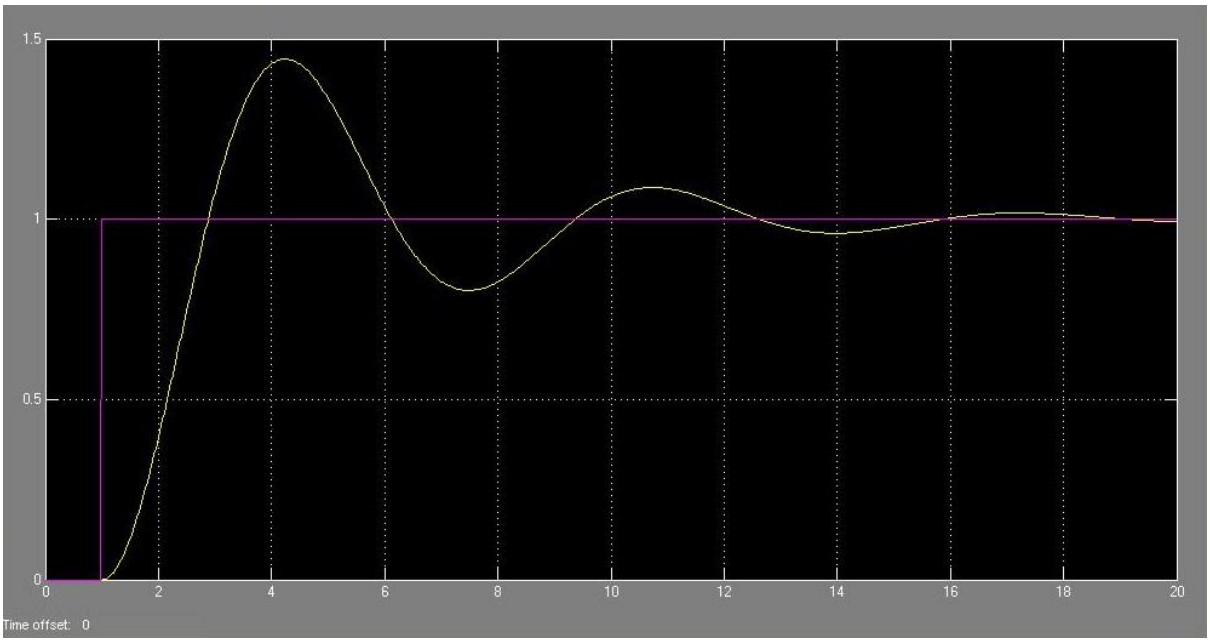

FIGURE 4.41: NON-REAL-TIME SIMULINK SCOPE TRACE FOR STEP MODEL

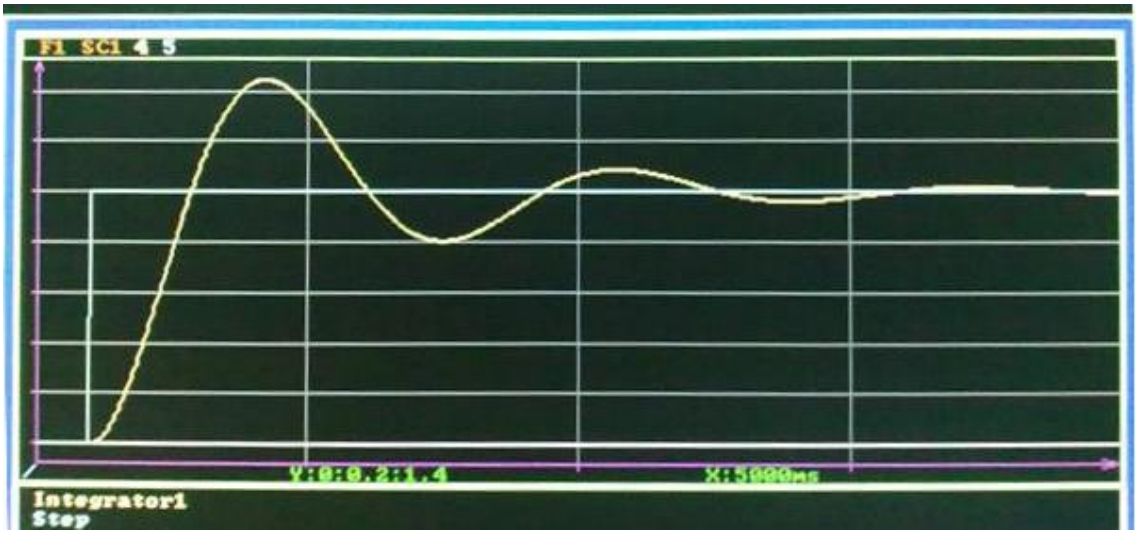

FIGURE 4.42: REAL-TIME TARGET PC SCOPE TRACE FOR STEP MODEL

4.4.3 FLIGHT SIMULATION APPLICATION

Having developed a general understanding of the xPC Target capability, in order to realise the benefit in a flight simulation context, a suitable model was selected and modified to produce results necessary to demonstrate successful application.

A 2-DOF Simulink model, built as part of the modelling activity of (4.2 Mathematical Model Development), was selected for the xPC application. The limitations of the model were known and were acknowledged by limiting the simulation time to a take-off run only, terminating at the time approximately corresponding to lift off. Beyond this point in a flight cycle the approximations used in formulating the subsystem equations would degrade the model accuracy to the extent that results would be far from reality. Due to the desire for Real-Time execution, a model of short duration is more appropriate than one which requires lengthy execution as in order to obtain results from the model, the full duration of the simulation must be endured. In addition, it is advised (The Mathworks Inc., 2003) that the speed of Real-Time models – specifically the Task Execution Time (TET) – may be increased through the inclusion of look up tables in the model block diagram. As a result, the look up table used for lift coefficient was replaced by an embedded MATLAB function block containing explicit code to perform a lift curve calculation through reuse of the code from the development of the software solution to the equations of motion documented in (4.3 Simulation Software). The addition of xPC target scopes configured to display the increase of velocity and lift during the Take-Off run as well as one configured to display the landing gear displacement (equivalent to aircraft displacement for the model) completes the model adaptations for the xPC Target application (Appendix F.3).

Prior to the build of the target application, mathematically the model is required to be free of algebraic loops as indicated by a Real-Time Workshop diagnostic (see background contained in 4.2.3.6 Solver and Model Construction Modifications). The xPC Target build settings were applied as before and the application built and downloaded to the target PC. The temporary addition of a Simulink scope block to the model allowed non-Real-Time simulation data to be obtained for comparison (Figure 4.43).

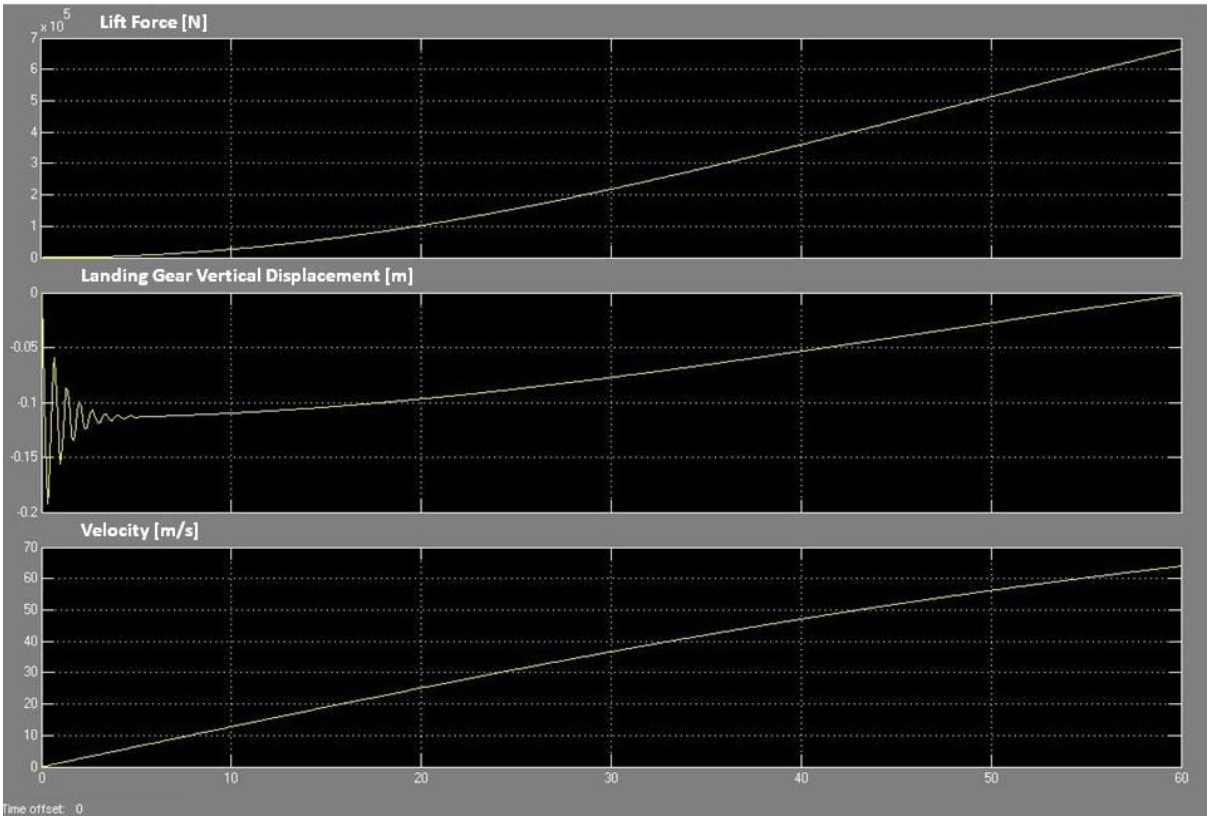

FIGURE 4.43: NON-REAL-TIME TRACE FOR FLIGHT SIMULATION MODEL

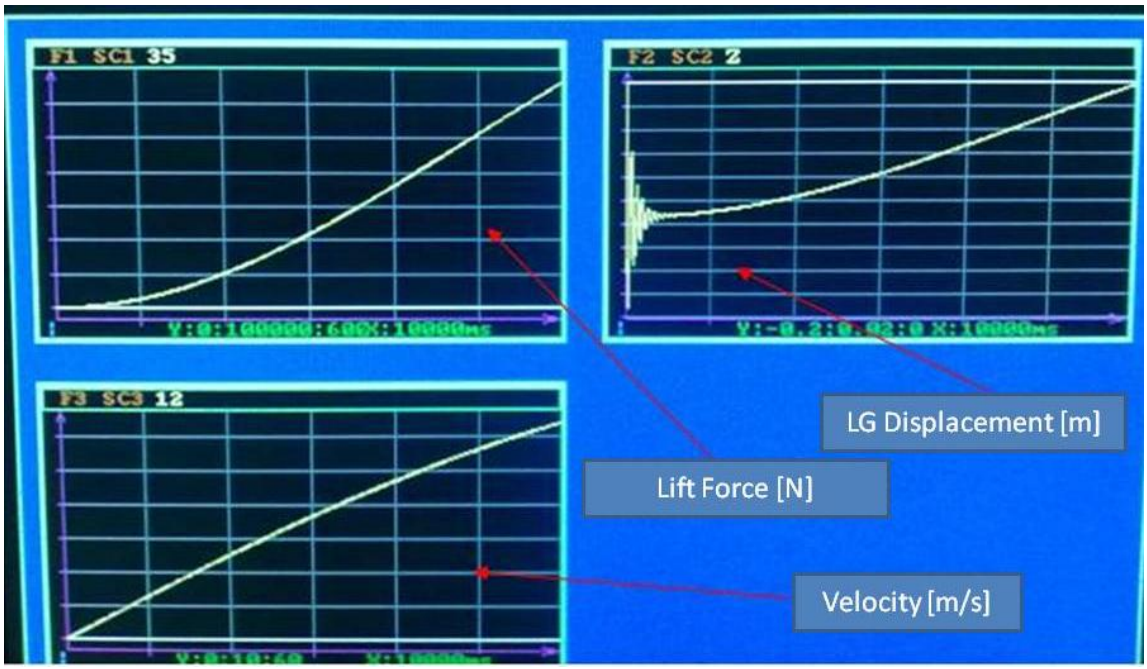

FIGURE 4.44: REAL-TIME TRACE FOR FLIGHT SIMULATION MODEL

The success of the simulation is evident from the inspection of the non-Real-Time and Real-Time traces (Figure 4.43 and Figure 4.44).

The mechanics associated with the nature of the solutions given by this simulation are covered in earlier material on the modelling process, specifically for the landing gear response 4.2.3.5 Landing Gear Model.

4.4.4 OTHER FEATURES

The ability of the xPC Target function to run a simulation in Real-Time does not realise its full potential. It also possesses the ability to allow both the active modification of target application properties and the communication during execution of the target application with external hardware through an input/output (I/O) interface through the inclusion in the model of specific xPC blocks.
The use of these capabilities particularly in combination allows both the tuning of simulation or model parameters whilst the simulation is running and also allows the inclusion of external hardware into the model architecture for the benefit of returning the response due to a real and not approximated model component – known as Hardware-In-The-Loop (HIL). In terms of the application of such features within the flight simulation sphere, if it were dictated that the hardware is to be a simulator motion platform or cockpit hardware including switches or flight control equipment, the Real-Time simulation is allowed to respond to the input from the external hardware through tuning block properties or signals. Such an example can be summarised as in Figure 4.45. Due to time constraints the Hardware-In-The-Loop capability will not be explored but is an example of an effective tool for the construction of an interactive flight simulation.

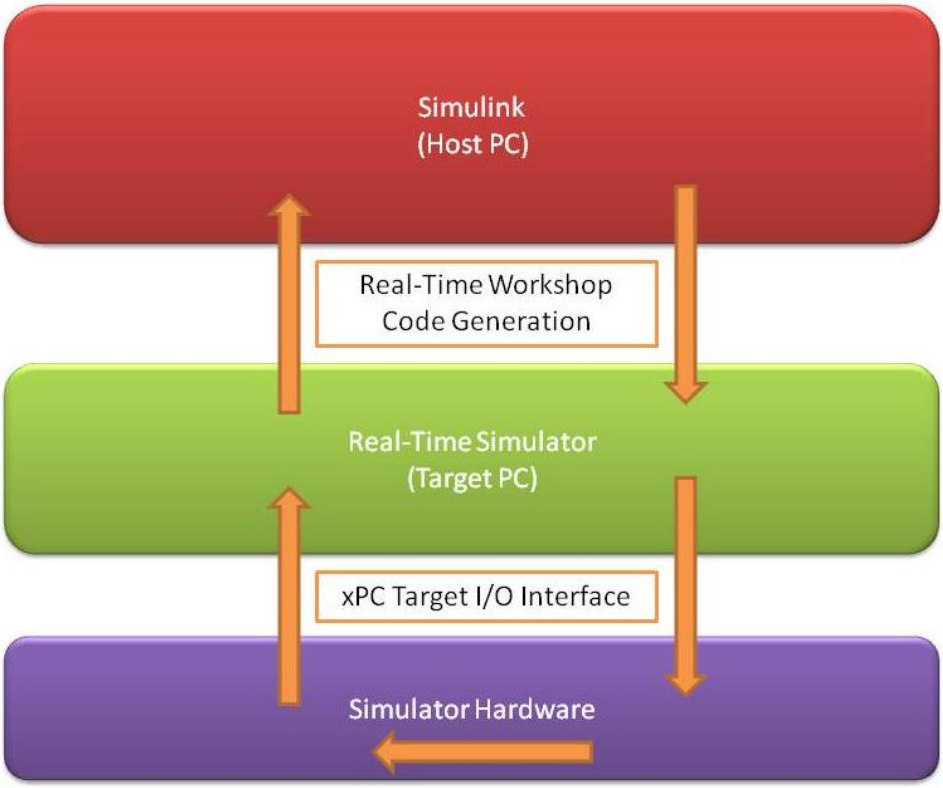

FIGURE 4.45: HARDWARE-IN-THE-LOOP FOR XPC TARGET PLATFORM

4.5 PHYSICAL MODELLING OF AN AIRCRAFT

In the previous two sections, the modelling solution has been based on a number of equations derived from existing and well documented physical relationships. These equations were modified to maintain applicability to the developing model and represented in terms of block diagrams in order to allow continuous solution and output in Simulink. Currently no attention has been paid to the nuances of individual components that have been disguised through functional grouping or approximation. Complimentary to this functional approach to the modelling process is the concept of physical modelling whereby components forming the system (an aircraft in this case) are studied individually at a lower level of abstraction. The modelling of the components considers component properties including mass and mass moment of inertia, and recognises their impact on the solution. Interactions between components and general behaviour are also captured through definition of component interfaces.
However, as is the case with all models a degree of approximation is required within limits imposed by the desired outcome of simulation utilising the physical model. In the context of this project, it is required to limit development through assignment of model goals. A physical model is then produced to meet the requirements necessary to achieve the goals and simulations run to verify model success.

4.5.1 INTRODUCTION TO SIMMECHANICS

SimMechanics is a toolbox supplied with the MATLAB software tool which is designed for the physical modelling and simulation of rigid body machines and mechanisms through implementation of Newtonian mechanics. The selection of this particular toolbox for an aerospace application introduces initial approximations including the restriction of mechanical components to rigid body motion – a continuous representation of a flexible wing cannot be accurately assumed to be a rigid body due to the realistic observation that a wing bends under loading, aerodynamic or otherwise (Dingle, 2004).
The SimMechanics toolbox allows visualisation of the model through representation of model elements as blocks displayed in a Simulink workspace. All models contain specifications of the environmental conditions and global coordinate systems, with rigid bodies and joints being represented by customisable blocks. Integration of standard Simulink functionality provides a wide range of physical modelling capabilities.

4.5.2 PHYSICAL MODEL DEVELOPMENT

For the purposes of this brief investigation into a physical model of an aircraft for flight simulation purposes, in keeping with project limitations the model will be restricted to 3-DOF – that is to say the aircraft (body) is permitted translation in the horizontal-vertical plane and rotation about a perpendicular axis as illustrated by Figure 4.46.

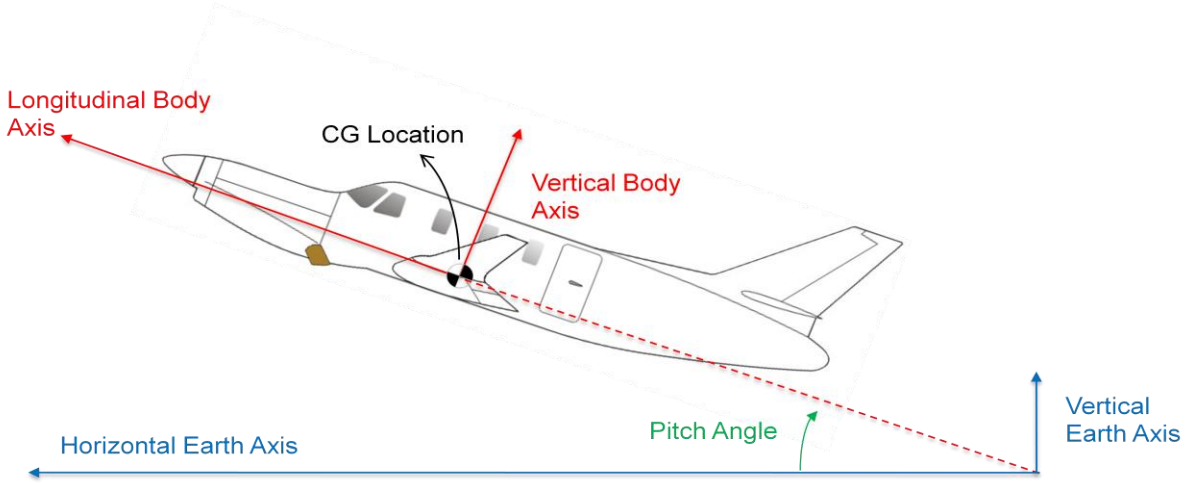

FIGURE 4.46: AXIS DEFINITION FOR PHYSICAL MODEL

The goal of the physical model is to provide suitable output data representative of aircraft behaviour due to variations in the aerodynamic forces for longitudinal disturbances. The problem is approached by determining which independent components of the aircraft will impact the aerodynamic behaviour in this scenario and then defining bodies with associated properties, relative positions, orientations and degrees of freedom in addition to the forces acting upon them.

Using this principle, the aircraft is modelled as a fuselage with two wing panels and a tailplane – consisting of two separate horizontal surfaces – attached using joints preventing relative motion referred to as weld joints. The inclusion of the tail fin is not necessary for this model due to the restriction of the motion to a plane decoupled from the plane of influence of the fin.

The introduction of these rigid bodies requires the specification of both the location and orientation of each body with respect to the global (Earth) coordinate system either directly or through specification of locations relative to a body whose location in the global coordinate system is known. It can be useful to specify extra points (nodes) on the body for the purposes of force application or body visualisation (see 4.5.3 Physical Simulation & Visualisation).

The body node locations and orientations for the developing model are specified using row vectors of values $[x\ y\ z]$ positions and, $[Euler-X, Euler-Y, Euler-Z]$ angles corresponding to translational and angular displacements in the chosen coordinate system. Potential locations of these geometric nodes in the X-Y plane are labelled in Figure 4.47.

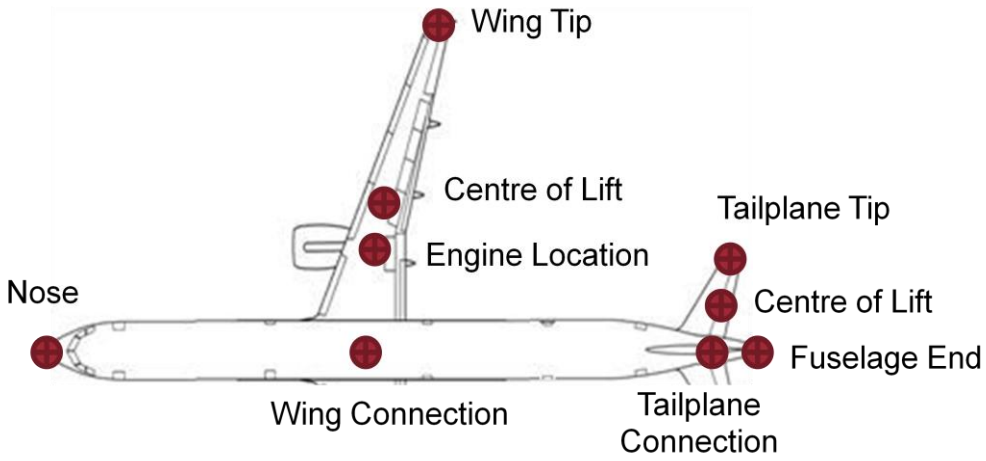

FIGURE 4.47: POTENTIAL NODE LOCATIONS

Due to the large number of nodes, their positions, orientations and body property specification is a complex task to undertake with a substantial scope for error. It is a best practice to record the

data for the model elements in term of variables in the MATLAB environment. The model is then configured to reference the variables during initialisation. Specification of model properties using a MATLAB script (m-file) allows ease of modification and calculation traceability (Appendix G.1).

The first step in constructing the model is to define the machine environment (including the gravity vector) and a fixed global coordinate system. The degrees of freedom of the model are restricted by the use of a planar joint block. This block allows translation along two axes and rotation about the third of those bodies connected between its ports. Adding initial conditions at this joint allows specification of the aircraft cruise conditions for simulation initialisation. Working from a datum defined at the aircraft nose, the fuselage, wings and horizontal stabilisers are added sequentially. The orientations such as wing dihedral and positions of key locations such as the aerodynamic centre are defined relative to an appropriate coordinate system which in some cases is not the global system but defined by an adjoining body. The choice of relative coordinate system depends purely on the ease of calculation for the required values in each potential reference frame. Properties such as mass and inertia are inherited from the full fuel parametric specification data (Appendix M.1). However, this parametric data is specific to the aircraft as a whole. In order to migrate the information to the physical model these values are assigned to the fuselage and the wings and stabilisers reduced to massless and hence inertia-less bodies. Although this is an unrealistic simplification, it remains a valid approximation for the limited degrees of freedom as relative motion between the bodies is disabled through welded joints, any forces applied to the massless bodies are essentially applied to the fuselage.
Having established the body assembly, sensors and actuators are added to allow the application of forces to the aircraft. One of the main strengths of SimMechanics is its ability to manage the interaction of force through built-in functions during simulation without the need for consideration of these interactions in any user scripting. In other words, during model construction, the only specification required is that of the force calculation. How the model responds to the combination of these forces is a complexity taken away from the user and is a key advantage over the functional model (4.2 Mathematical Model Development) or the software simulation (4.3 Simulation Software). The forces are specified using user-defined software functions for convenience, which reference data defined by the initialisation script. Wing forces consist of a thrust force in addition to aerodynamic drag and lift. The horizontal stabilisers are subjected to drag and lift only and the fuselage to a drag force. Once more, gross simplification is evident although the potential for development of the model to a more realistic representation is aided by the versatility of these user-defined software functions embedded in the model.

The thrust force can be modelled in a number of ways depending on the desired outcome of model simulations. The use of a fixed value for each engine is appropriate for the current model as simulations designed to demonstrate a response to a longitudinal disturbance are expected to encounter speeds and altitudes over only a narrow range. Changes in these quantities adversely affect the thrust output of an engine (discussed in 4.3 Simulation Software). This also accounts for the lack of an atmospheric model that would update the density in particular for the scenario. An alternative, considering the need to start simulating from a trimmed equilibrium condition, would be to control the thrust based on the instantaneous speed. A proportional integral derivative (PID) controller, accompanied by a desired cruise speed, in tandem with a signal saturation configured for a maximum available thrust setting is a method of controlling this aspect. However, dynamically, a speed decrease is essential for perpetuation of the oscillatory response expected from the simulated disturbance, an element which would be impeded by a control loop.

The fuselage drag force is simplified to a sinusoidal variation with fuselage angle of attack from a minimum to maximum value. Rationale for this approximation assumes that drag is a minimum when the cross sectional area of the fuselage exposed to incoming flow is at a minimum – when the longitudinal axis of the body is parallel to the flow direction. This function requires the knowledge of forward and vertical velocity components with respect the body's local coordinate system. The angle of attack may then be calculated by taking the inverse tangent of the ratio

between the two. The fuselage drag force is assumed to act through the body centre of gravity in a direction parallel to the flow.

Aerodynamic Lift and Drag forces are assumed to act at the quarter chord location of the wing or horizontal stabiliser. For a subsonic design, this assumption is generally acceptable. In general, cambered aerofoils also have a pitching moment as well as a lift force. For the purposes of simplicity, the horizontal stabiliser will be assumed to be symmetric. Both lift and pitching moment can be governed by linear relationships up to a specific maximum in terms of their corresponding dimensionless quantities and the drag equation is a function of the lift coefficient (Equation 4.15). It is necessary to consider the equilibrium of the aircraft when specifying these forces; the wing and tailplane geometry and positions are specified by researched aircraft data (Appendix M.1) or graphical estimates, therefore for this approximate model, aerodynamic data is the only remaining factor controlling the trim conditions. Lift and drag coefficient variation with angle of attack is required in particular which is a function of the aerofoil section geometry. Establishment of the trimmed equilibrium condition of the aircraft is possible through consideration of the longitudinal force and moment distribution (Figure 4.48) where lift, drag, weight and thrust are given the symbols L, D, W, T.

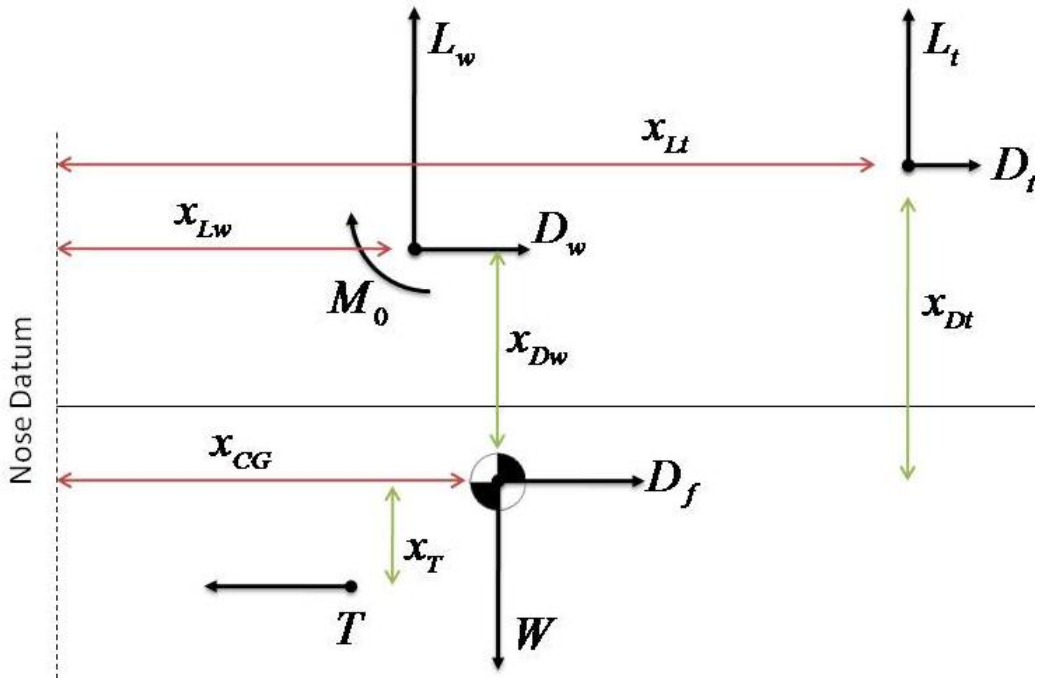

FIGURE 4.48: LONGITUDINAL FORCE AND MOMENT EXAMINATION

The aerofoil section for the main wing is taken to be a NACA 6-series with lift curve slope and drag equation data inherited from the parametric improvements (Appendix M.2). The governing equations therefore simplify to equilibrium represented by Equation 4.29 to Equation 4.31 where the horizontal stabiliser lift and drag in addition to the cruise thrust are the only unknowns. Equation 4.29 is in fact an alternative perhaps simplified form of the simple longitudinal static stability equation given in Appendix J.1. For given a given cruise speed and atmospheric density, these equations are solved simultaneously to determine the tail drag followed by the tail lift and thrust setting. These lift and drag values are back-fitted to lift curve slope and drag equations for the stabiliser, taking into account any aerodynamic surface setting angles. *It is worth noting at this point that the incoming flow to tailplane is considered to be at the same angle of attack as that approaching the main wing. In reality, the presence of the wing ahead of the tailplane induces a deflection of the flow known as downwash which effectively reduces the angle of attack seen by the horizontal stabiliser. The quantification of this phenomenon is ignored for this model.*

$$M_0 + Tx_T + L_w(x_{CG} - x_{Lw}) + D_w x_{Dw} + D_t x_{Dt} = L_t(x_{Lt} - x_{CG})$$

EQUATION 4.29: ROTATIONAL EQUILIBRIUM EQUATION

$$T = D_f + D_w + D_t$$

EQUATION 4.30: HORIZONTAL FORCE EQUILIBRIUM EQUATION

$$L_w + L_t = W$$

EQUATION 4.31: VERTICAL FORCE EQUILIBRIUM EQUATION

4.5.3 PHYSICAL SIMULATION & VISUALISATION

Having established the model construction and the equilibrium initial condition, a unit pitch input is added to the aircraft model on commencement of the simulation. The visualisation of physical model's response to this initial disturbance can be seen over two different time scales in Figure 4.49 and Figure 4.50. The expected short period and phugoid modes of oscillation are apparent with the dynamic stability being proven in Figure 4.50 by the decay of the oscillatory amplitude with time. The longitudinal case study examines this response in more detail (5.3 Longitudinal Stability Case Study).

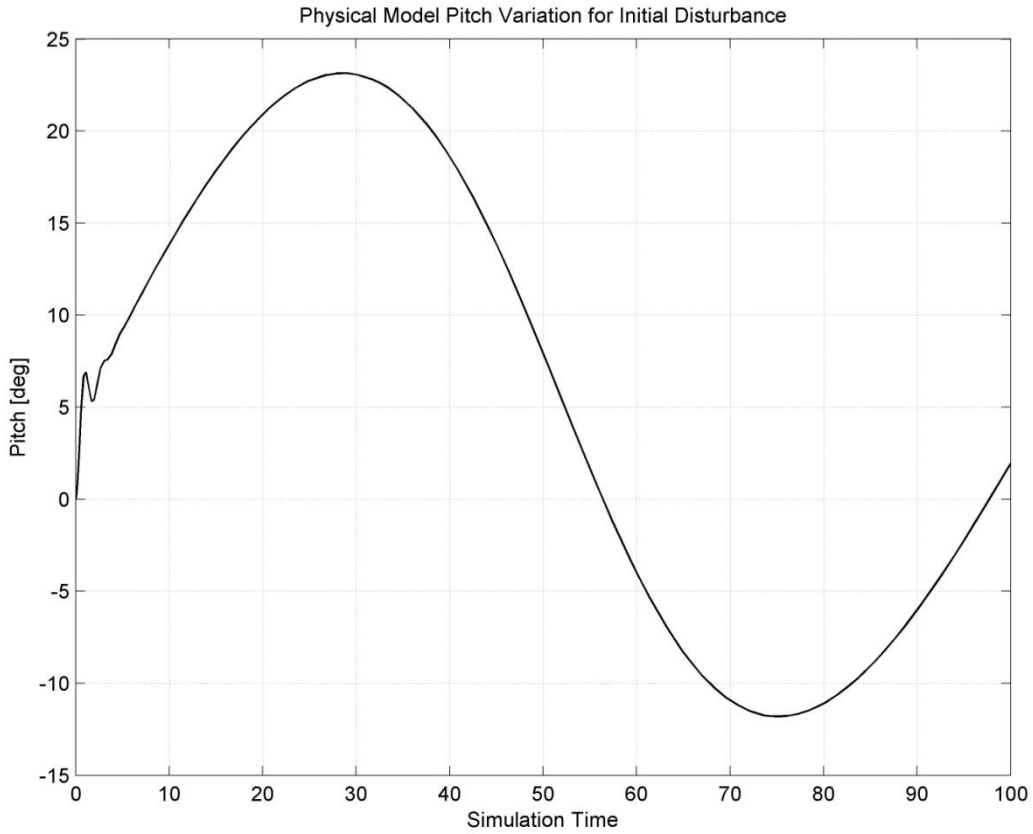

FIGURE 4.49: SHORT PERIOD AND PHUGOID PHYSICAL MODEL MODES

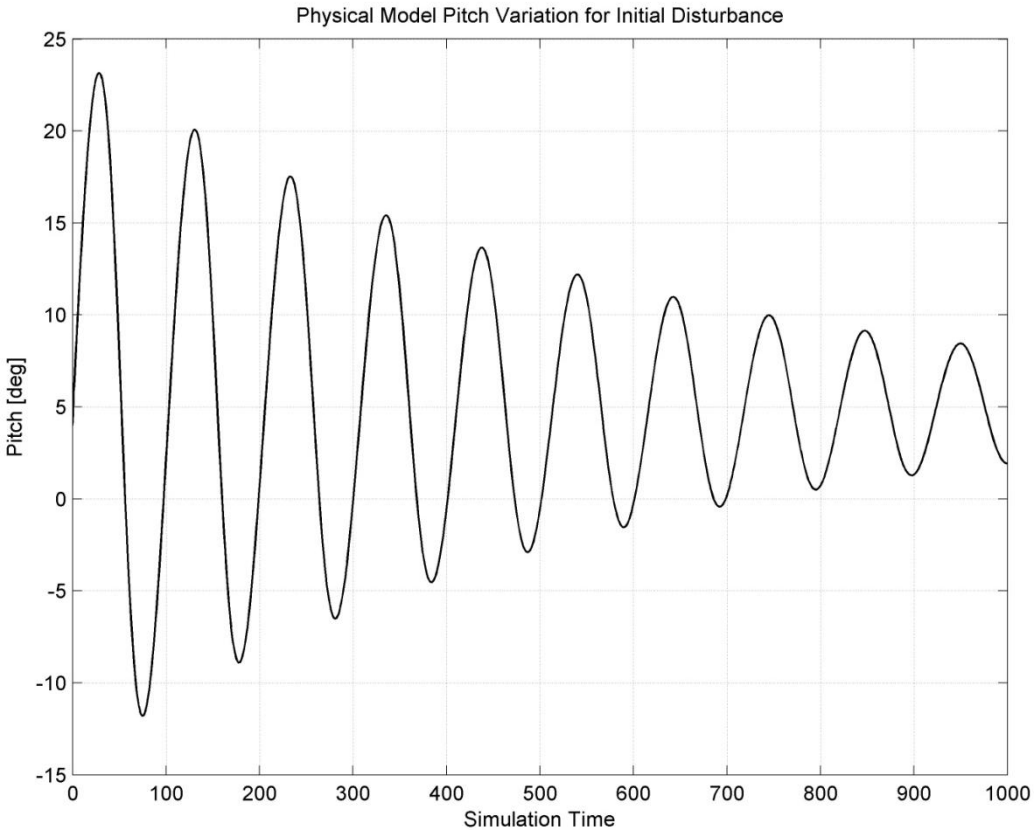

FIGURE 4.50: PHYSICAL MODEL PHUGOID MODE DECAY

Visualisation of the response has been shown graphically through the plotting of output parameters which is useful for analysis but in terms of producing a realistic impression of flight to the user of such a flight simulation model it is a relatively unappealing. SimMechanics as a toolbox allows a more elegant albeit primitive method of model visualisation through a 'machine view'. Based on the node locations, orientations and connections and mass and inertia properties specified during model construction the coordinate systems of the physical components are linked by approximating a body with equivalent mass and inertia of the real-life component. The representative body may be either an equivalent ellipsoid (Figure 4.51) or a convex hull (Figure 4.52). The animation of these machines is possible during simulation and a facility exists for capture of the animation in the form of a compressed video file.

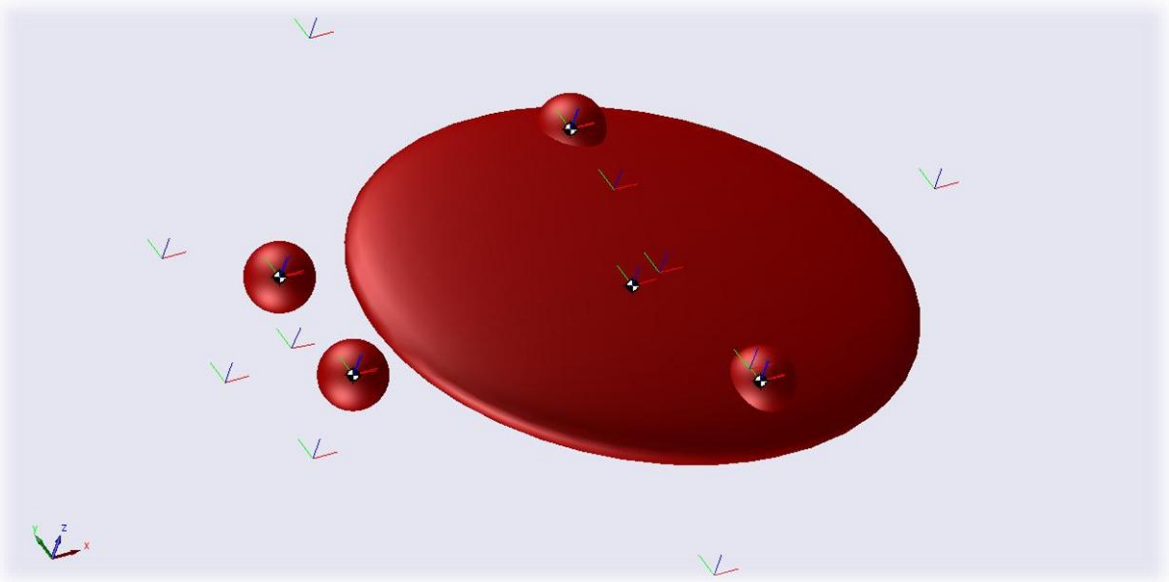

FIGURE 4.51: EQUIVALENT ELLIPSOID MACHINE VISUALISATION

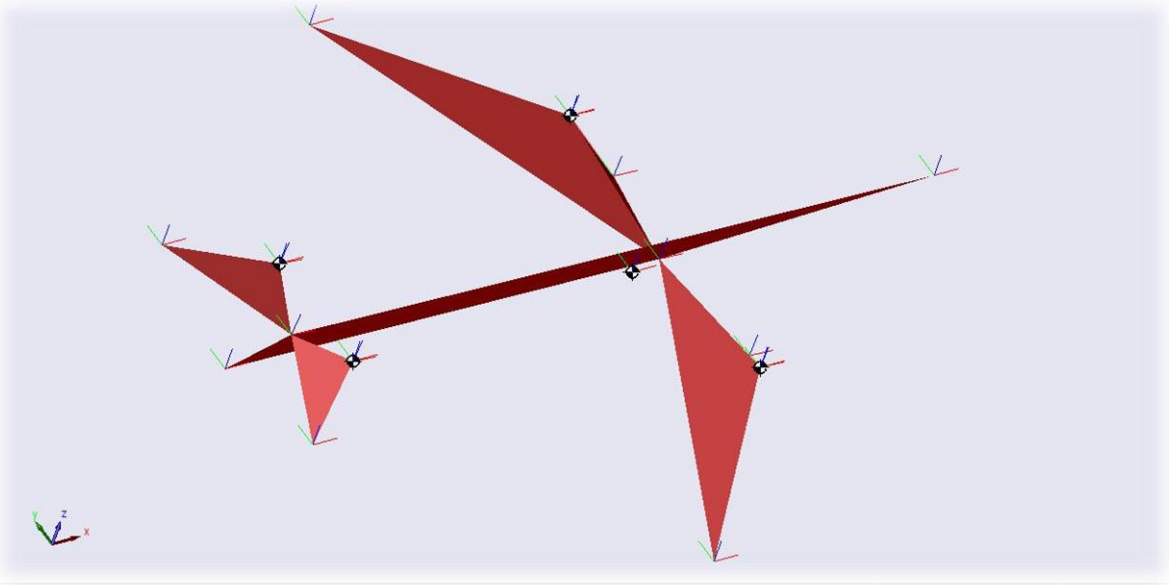

FIGURE 4.52: CONVEX HULL MACHINE VISUALISATION

Furthermore, through body or joint sensor blocks integrated into the model block diagram, information on the position and orientation of the physical machine can be output from the model simulation in a convenient format to animate a graphically-rendered, inert object. This is achieved using the functionality provided by MATLAB's Virtual Reality (VR) Toolbox. The position and orientation data is routed to a VR Sink block on a Simulink diagram. This block initialises a virtual world and the rendered object within it. During the simulation, the object can be seen to be animated with movements corresponding to physical model output.
Although no investigation takes place here into the potential of virtual reality, it is apparent that this capability is a stepping stone to full realisation of the key visual element of flight simulation desired by the user as described in the next sub-section.

4.5.4 FURTHER WORK

The VR capability, in addition to those facilities mentioned in the previous sub-section, also allows the control of camera configurations including user viewpoints. Although not an area of focus for this project, visualisation mechanisms are a fundamental requirement for flight simulators as a training aid (FAA, 1995). The development of a VR environment along with the animation of a model within the environment allows the freedom to view the scene from any angle defined by the user. This is an effective method of visualisation, particularly when the viewpoint is moved to a location that is equivalent to location of the eye of the pilot. In order to achieve this, the complication of an appropriate reference location along with run-time position and orientation increments needs to be overcome.
Developing this idea further, the establishment of the spatial orientation of the aircraft allows the establishment of a line of sight drawn between the pilot and any arbitrary reference point in the three dimensional world within the expected visible field of the pilot. The application of this for the display of visualisation images as a means of projecting the external world to the simulator pilot is explored from a theoretical standpoint in literature (Diston, 2.5 Line of Sight, 2009).

Maintaining the theme of flight simulation hardware, there are resources available to relate output data similar to the output from the physical model to motion platforms. In particular there are 3-DOF applications in existence which, with some customisation, could be used to experiment with generating the appropriate motion of a platform driven by the model cues provided by the simulation of the physical model (BFF Design Limited, 2008).

Further detail may also be added to the model through expansion of the degrees of freedom allowed by re-specification of the joint between the machine and the fixed datum but this complicates the modelling of the forces as with further developments of the mathematical model discussed earlier. Further improvements to the modelling detail, specific to a physical model, is to include flexible behaviour of the mechanical components by replacing the welded joints between the wing and fuselage for example and to distribute the mass and inertia more accurately between machine elements. In addition, the software functions that govern the forces are far from precise and may be revised for an improved approximation. In particular, the resolution of forces and the incorporation of more complex phenomena similar to those referred to in 4.2.3.8 Further Work.

4.6 DEVELOPMENT SUMMARY

In reality, although the modelling tasks have been documented sequentially, the engineering development was in fact conducted in parallel. This concurrent approach, relied on a degree of resource sharing between ‘development threads’ and included an interface with the validation activities discussed in the next section. Figure 4.53 provides a visual summary in order to demonstrate the interrelated nature of the tasks undertaken as well as the benefit of the concurrent development.

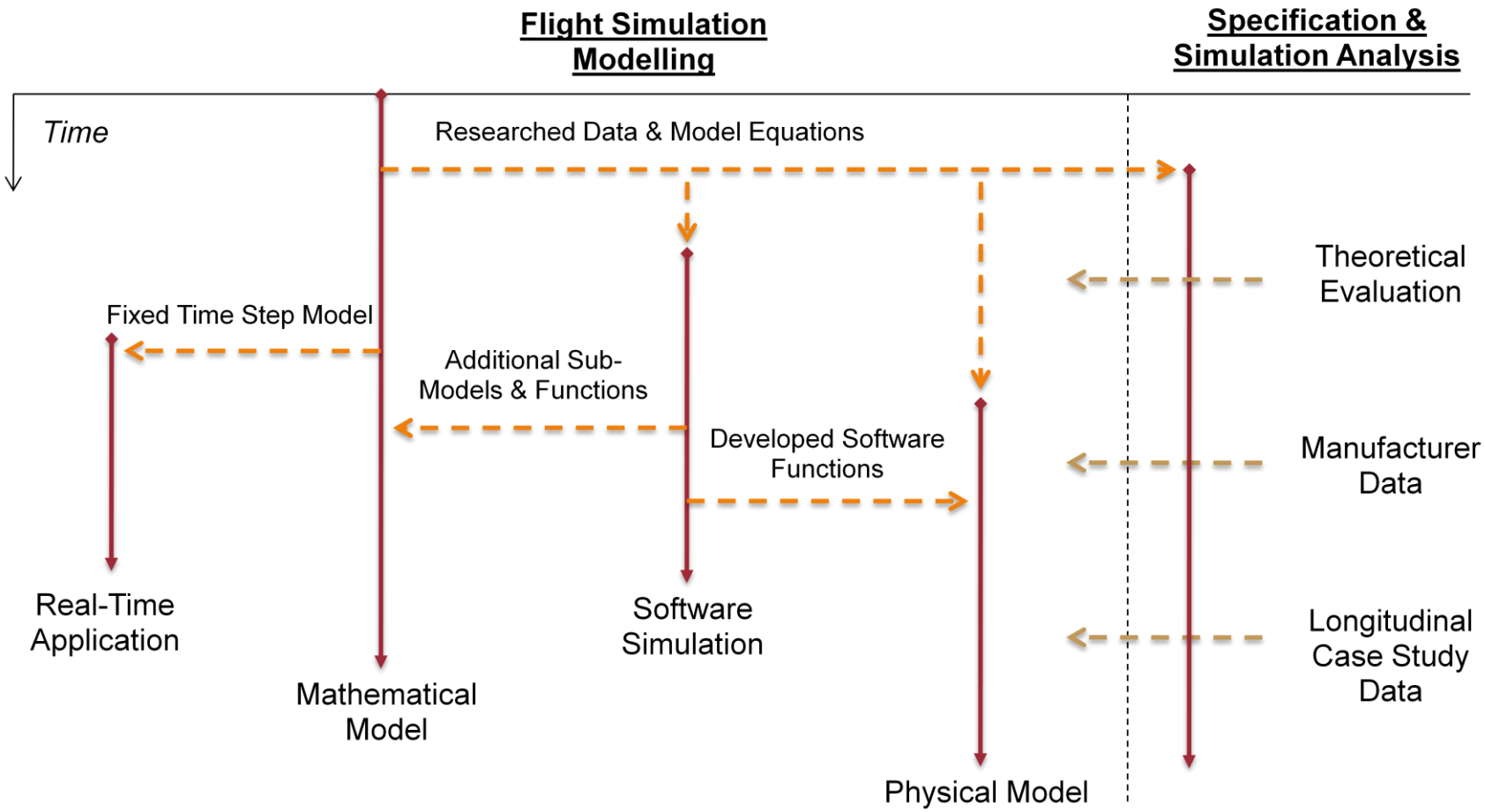

FIGURE 4.53: DEPENDABILITY TIMELINE

5 PARAMETRIC SPECIFICATION & SIMULATION ANALYSIS

The flight simulation capability of the university comprises a mathematical model. The model has been developed by the company Merlin, the manufacturer of the simulator. A critical aspect of modelling as an activity is the combined process of verification and validation. Verification "confirms that the internal structure of a model is correct and that its constituent parts are mutually consistent" where as validation "confirms that the external behaviour is credible and that it satisfies the user requirements" (Diston, 1.4 Models, 2009). As the structure of the simulator mathematical model is not visible to the user, direct verification is not something which is possible. However, the output of the simulator can be measured and compared to real world expected data in order to validate the model both parametrically and empirically.

In line with the project plan, it is necessary to develop an understanding of current flight simulation technologies including the resources available to the University with respect to the current field of investigation. This exercise serves a number of purposes. Firstly, it enables the formation of an impression of the nature of flight simulation industry standards based on analysis of input files and output data associated with the University's resources. Secondly, the research necessary to validate the input file to the simulator can be transferred to the modelling spine of the project to allow the production of models which accurately represent the real-life counterpart. Finally, as alluded to above, through a set of bespoke test flights, the performance of existing aircraft specifications and simulator core functionality can be assessed in terms of accuracy and suitability. Ultimately, the flight simulator and consequently the developed models will all be validated against manufacturer data for the project aircraft.

5.1 PARAMETRIC SPECIFICATION INVESTIGATION INTRODUCTION

The flight simulation capabilities of the University have been discussed prior to this introduction and Figure 1.1 summarises the overall structure of the technology available, highlighting the need for a parametric specification for a given aircraft which serves as an input to a generic mathematical model at the flight simulator core. Initially, this work package is associated with the analysis of one particular example of this parametric model specification, drawing conclusions to assess the University's current capabilities, to understand their limitations and to suggest ways of improving the resources through the formulation and testing of a new parametric specification.

As alluded to previously, the definition of a parametric specification in the current context is a repository of specified quantities, which themselves form the defining elements required to transform the generic flight model into a representation of a particular aircraft. This is achieved through compilation of the data into a file which provides input to the mathematical process used to solve the equations, now customised by the parametric data, relating to flight of the aircraft.

5.1.1 BACKGROUND TO EXCALIBUR

The University facilities provide a bespoke software tool known as Excalibur ('E1') with a number of available functions. Essentially this Windows-compatible software tool is the link between the simulator mathematical model and the user, providing a graphical interface to allow configuration, monitoring and control of simulator parameters and functions. One particular operation of the tool is a form-based editor of the parameter model definition (input) file. The forms allow an accessible and comprehensive method of specification of model properties. An example of the user interface is shown in Figure 5.1, and although a degree of understanding of nomenclature is required, it is an effective means of model definition.
The tool compiles a specification from the specified values and caches the data for direct supply to the simulator core mathematical model on initialisation of the simulation. In addition, E1 provides a portable data file through an export function containing feedback from the simulation

software and hardware including a plethora of calculated values and statuses from the position of flap and gear switches to the fundamental accelerations and velocities associated with the equations of motion. A comprehensive list of exported values can be found in Appendix K.1.

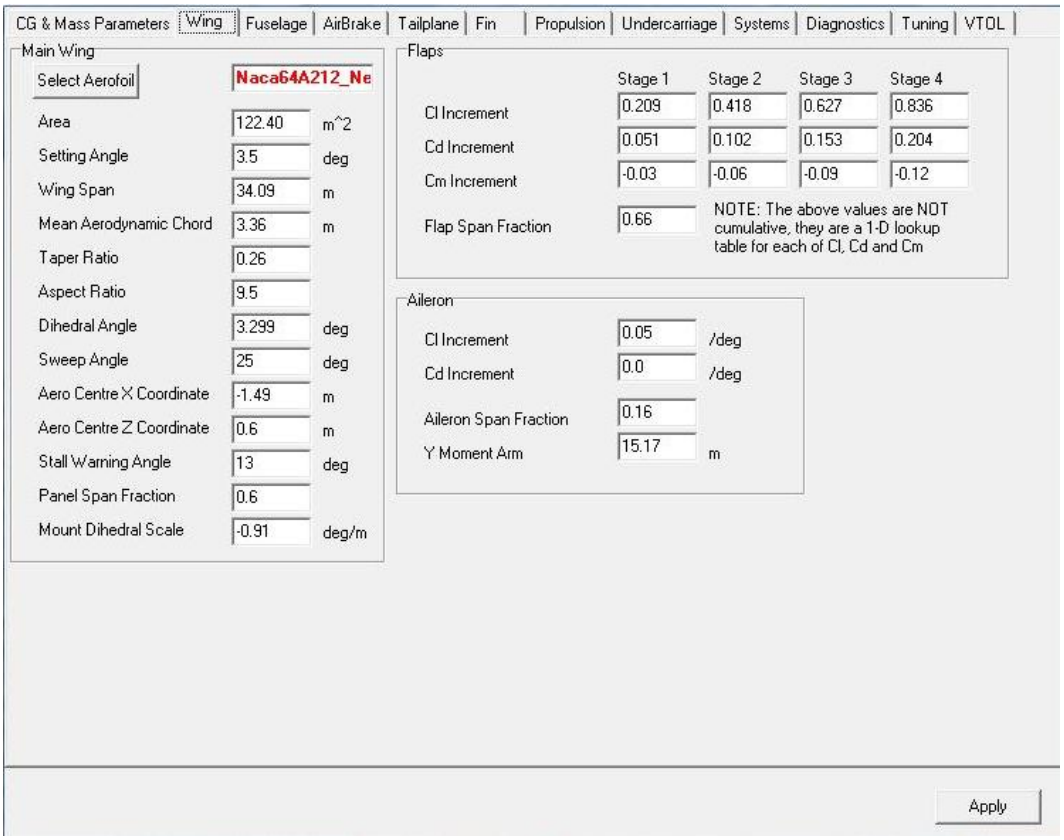

FIGURE 5.1: FORM-BASED MODEL EDITOR

In addition, when specifying initial conditions for a simulation, the linearised nature of the software results in automatic calculation and assignment of control settings including thrust and trim values for maintenance of the specified altitude, directions and speeds. The use of this capability becomes a factor in reducing the time required for flight test procedures (5.2.3 Flight Test Programme).

5.1.1.1 EXCALIBUR MODEL DEFINITION

The E1 model editor requires two primary groups of information; the geometrical, aerodynamic and mechanical properties of the fuselage, engines, surfaces and systems along with the specification of lift, drag and pitching moment coefficients with respect to angle of attack. The latter is contained within a separate data file which is chosen during the definition activity (see Figure 5.1) – Exhaustive definition of the variation of coefficient with angle of attack is unnecessary due to the ability of the simulation software to interpolate between specified values. However, in the interests of behavioural accuracy, any new files generated contain data specified every 1 degree increment in angle of attack for both small angles and throughout stall to increase granularity and capture the variation at these locations (see 5.4.1.1 Wing Section Redesign).

5.2 EXISTING MODEL SPECIFICATION & SIMULATION ANALYSIS

As a vehicle for the critical assessment and improvement of University resources, the project plan demands the analysis of the existing Airbus A320 model defined to the aforementioned E1 standard. It is hypothesised prior to work commencing on the study that sources of inadequacies of the facilities, recognisable as unexpected or unrealistic simulator output, could be attributed to both the use of incorrect or inaccurate parameters during model specification or through loss of mathematical fidelity during approximation processes within the model and associated solution software. In order to dispute or endorse the proposition, it is necessary to both assess the input data as well as the output data. Improvements suggested are implemented, to an extent governed by the complexity of the task, to produce an alternative specification summarised later in this section.

5.2.1 TASK DEFINITION

In order to gather knowledge on suitable criteria on which to judge the existing A320 parametric specification, it is necessary to ascertain what obtainable data existed on the aircraft and how this related to readily extractable data in the model specification. Input files and output files related to the model and its simulation results are sourced and inspected. The appropriate data selected consists of a list of all the input parameters to the model specification as displayed by the editor (Appendix K.2). In order to allow verification and validation (V&V) of these values, appropriate information is assembled in a detailed review of literature available on the aircraft. To ensure an informed decision, a range of sources and means of research are considered. These include manufacturer data as well as reference annuals or 3rd party parametric specifications. Furthermore, specialist estimation software as well as a number of other scientific techniques are necessary (see 5.2.2 Verification & Validation Activities) as depicted by Figure 5.2.

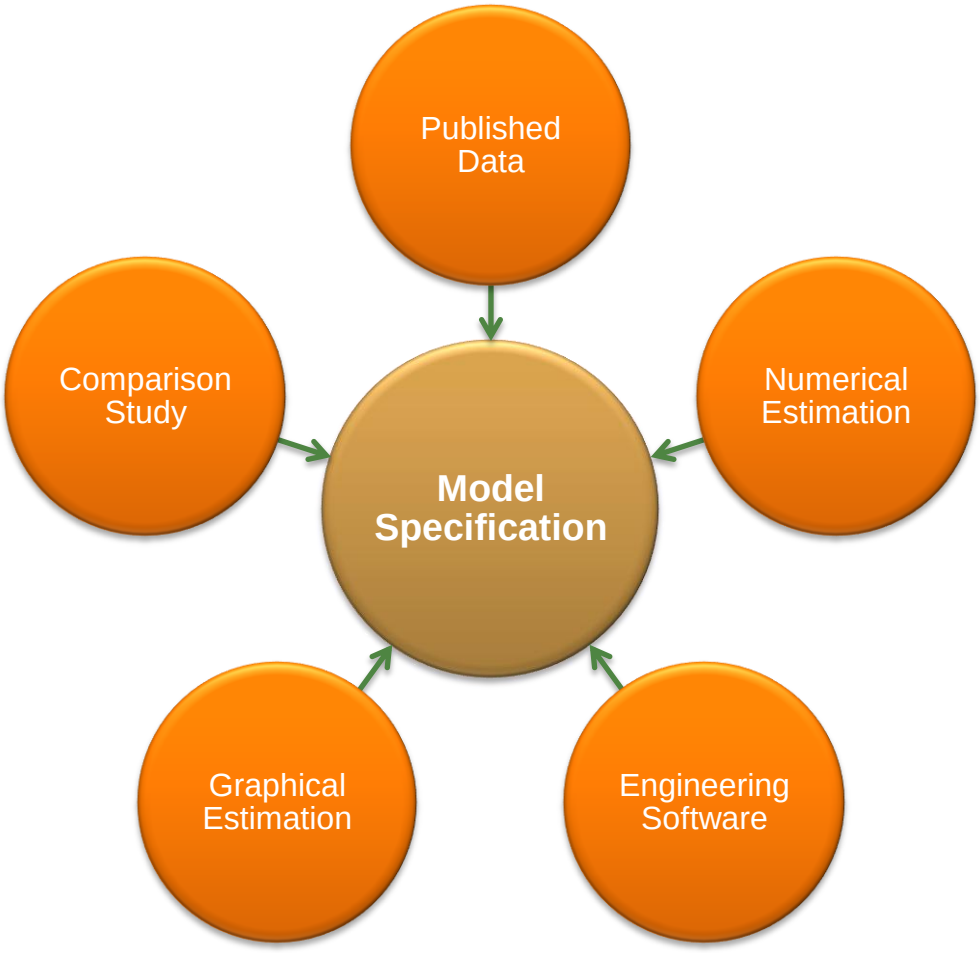

FIGURE 5.2: MODEL SPECIFICATION V&V ACTIVITIES

The availability of technical specifications for aircraft varies depending on the aircraft manufacturer and the aircraft's purpose. Data can be biased in undesirable senses. From the point of view of a manufacturer of a commercial aircraft such as the Airbus A320, information that is of use to customers and the enthusiast is readily available including data such as range, seating configurations and wheel base (Airbus, 2009). From a technical standpoint, when precise recreation or comparison is required, this information is of limited value. In order to analyse an existing parametric specification for accuracy, information needs to collected that includes data that either directly corresponds to a model specification quantity or else can be manipulated to obtain the quantity. A recommended resource (Jackson, Munson, & Peacock, 2008) for information of this nature is consulted and data used in combination with approximate design equations (Jenkinson, Simpkin, & Rhodes, 1999) in order to obtain the necessary parameters. Also, 3rd party flight dynamics models, specifically a Microsoft Flight Simulator A320-200 model (Project Airbus) is interrogated through manual and interpretative inspection of the associated data files compiled from a wider range of sources and non-experts. This range of material adds strength to the assessment.

5.2.1.1 PERFORMANCE CRITERIA

Further to the verification of model input data, the simulation output data lends itself to the calculation of performance, handling and stability criteria. Additional research is undertaken (Filippone, 2006) in order to generate a list of performance criteria for the aircraft. The expected values for these criteria are not necessarily something that is made public by manufacturers, particularly if it is proprietary or commercially sensitive. However, it is possible to assume sensible limits for the value through formal enquiries (FAA, 2009). The assessment of performance criteria takes into account not only the specification of the model but the accuracy

of solution of the problem. The capabilities of the mathematical model within the simulator therefore can be assessed using this particular method.

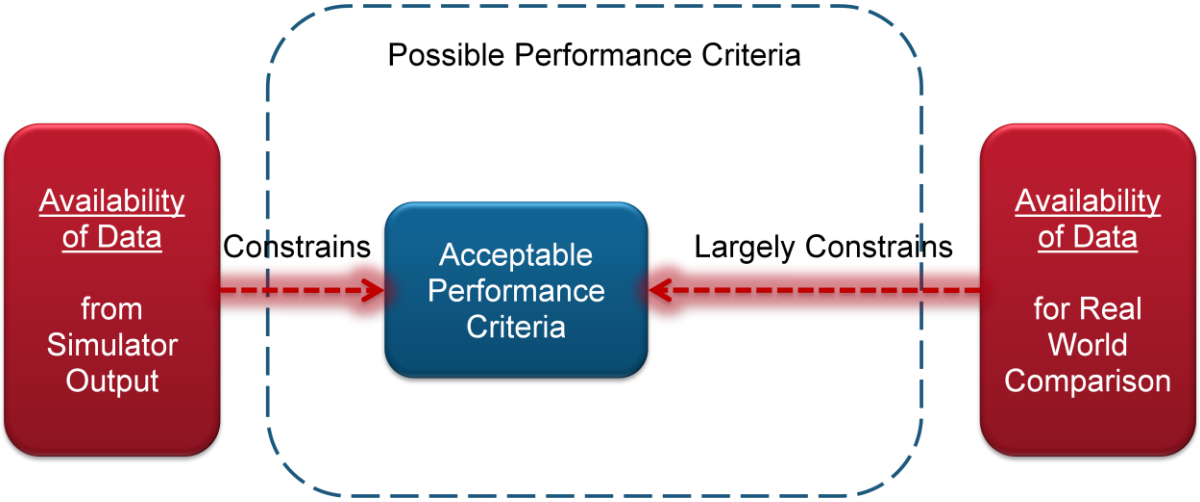

FIGURE 5.3: PERFORMANCE CRITERIA SELECTION CONSTRAINTS

The list of performance criteria to be agreed for the validation of the existing model depends greatly on the quantities obtainable from the simulation results and the data available from comparison as shown by Figure 5.3 . The definition process results in a list of criteria that satisfy both conditions through consultation of a list of exported quantities (Appendix K.1) followed by a review of available literature on the subject. Those items that are agreed include:

- Payload-Range Diagram
  Range is a key weight-driven performance criterion for a passenger aircraft and commercial data is available for the A320. Considering the equilibrium of forces at cruise it is possible to observe that weight along with the size of the fuel tanks will be the primary factors influencing the range; lift will directly have to balance the weight and for a given aircraft with a given cruise lift coefficient, at a constant altitude, the lift is dependent only on speed, which is in turn depends on thrust, which in turn impacts the rate of fuel consumption and hence time allowed in flight. However, the payload-range diagram requires three different ranges to be established: the ferry range, maximum economic range and maximum payload range (see Figure 5.4). Definition of validation procedures will follow later.

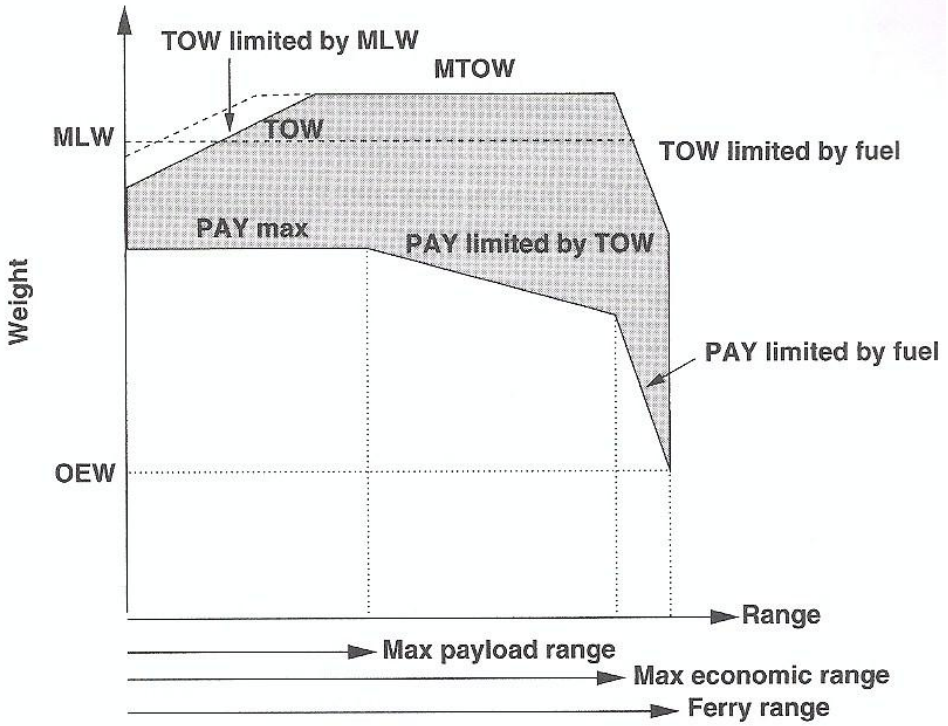

FIGURE 5.4: TYPICAL PAYLOAD RANGE DIAGRAM FOR COMMERCIAL AIRCRAFT (FILIPPONE, 2006)

- Wing Loading
  Defined as the gross weight divided by the wing area, the wing loading is a decreasing quantity with flight duration due to the mass and hence weight reduction due to fuel burn. It may also be seen as an indication of aerodynamic efficiency, a low wing loading being the preferable value due to the structural benefits associated with lower peak loading. It carries the assumption that the entire weight of the aircraft rests on the wing planform area and neglects contributions from the tailplane.

- Landing Speed
  Found in aircraft flight manuals, the range of speeds at which the aircraft is expected to land depends on the high lift devices in use and the weight at the time of approach. The Maximum Landing Weight (MLW) is an upper limit governed by the maximum wing bending moment.

- Lift Curve Slope
  Although this can be viewed as a design rather than performance aspect of an aircraft, the location and nature of stall ought to be investigated. In a simulation context, inaccuracies may be introduced by the use of approximations, linearisation of equations or omission of the three-dimensional effects, inappropriate aerofoil section data or Mach number influence on lift curve slope.

- Maximum Lift Coefficient
  Within the model, this is likely to be a direct combination of the behaviour of the lift curve slope and the high lift devices. However, tail and fuselage lift contributions are built in to the parametric design and the resulting lift coefficient will in fact dictate the landing speed.

- Drag Polar
  The drag polar is a parabolic graph of lift coefficient against drag coefficient. Having constructed the polar, the maximum lift over drag ratio can be found graphically from the

maximum gradient.

- Maximum Static Thrust
  This is generally classified as the maximum static thrust at sea level (taking into account thrust variation with both speed and altitude) and is a quantity used to define the maximum thrust to weight ratio of the aircraft amongst other engine performance parameters.

- Specific Thrust
  Also known as the thrust to weight ratio, this dimensionless performance parameter provides an indication of the thrust available. Typical values for subsonic aircraft vary between 0.2 and 0.4 (Filippone, 2006).

- Specific Impulse
  Specific Fuel Consumption (SFC) relates the rate at which fuel is burnt to the weight of the engine. This measure is of little use for comparing jet engine performance as values tend to lie in a very narrow range (Filippone, 2006). However, if combined with the thrust output of the engine more meaningful parameters can be derived. One of these is the Specific Impulse of the engine. This is defined as the ratio between Thrust and SFC and represents the time that an engine could operate by burning the amount of fuel of weight equal to its thrust. In real terms, this can be seen as a judge of overall engine efficiency and in terms of the simulation model would depend on the complexity of the thrust modelling for its accuracy.

- Flight Envelope
  Aircraft flight envelopes are represented in terms of altitude and speed. Limits exist that restrict the aircrafts ability to operate within a range of speeds and altitudes (Figure 5.5). The nature of these limits may require information or complex models that are not currently available to the simulation software when performing calculations based on the parametric specification. Investigation into the capability of the simulator at these boundaries should yield a definitive answer to the query.

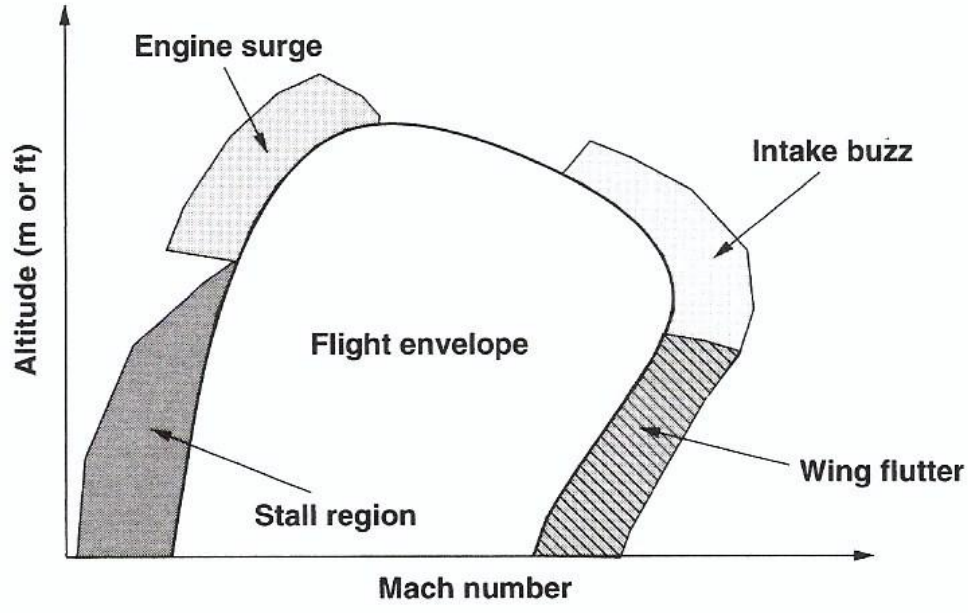

FIGURE 5.5: GENERIC FLIGHT ENVELOPE AND THE LIMITING PHENOMENA (FILIPPONE, 2006)

- Absolute Ceiling
  Arguably this is derived from the flight envelope, however, for a commercial aircraft, the absolute ceiling – defined as the point at which the aircraft can no-longer climb due to thrust and lift limitations (vertical speed = 0) – is of little use as a performance parameter. This is due to the upper limit to the envelope defined in manufacturer information being attributed a 'service ceiling' normally defined by the limit of the ability of the cabin pressurisation system to ensure a comfortable atmosphere within the cabin.

- Thrust variation with Mach and Altitude
  Due to changes in density and pressure at the engine intake that arise from changes in altitude and speed, thrust will vary throughout the flight envelope from the static sea level value. Specifically the thrust will decrease with increases in altitude and speed. The magnitude of such variation defines the performance of the engine. The effects are more pronounced, however, for a piston engine than the jet engine of an A320.

- Stall Speed
  The stall speed is an important definition for both safety and operational reasons but in the context of the project it is useful in comparison with reality to ensure that modelling of high lift devices and lift is performed to a level that will produce results comparable to those expected for the aircraft.

- Take-Off Distance, Landing Distance, Associated Profiles and Balanced Field Length
  The determination of behaviour of the aircraft near the ground is critical to operational performance. For a model to accurately represent its real-life counterpart, particularly for determination of instructional material such as braking distances, procedures for missed approaches and aborted take-offs, the performance of the model in simulation of certain events is required. Within a specified environmental model, the parametric data can be used to define the performance of the aircraft on the ground.
  The balanced field length can be determined from the condition that the distance to continue a takeoff following failure of an engine at some critical speed is equal to the distance required to abort it. It represents the worst case scenario, since failure at a speed less than the critical speed requires less distance to abort, whilst failure at a speed higher than the critical speed requires less distance to continue the takeoff. When these two distances are equal, the length is said to be 'balanced' as shown by Figure 5.6 adapted from (Mair & Birdsall, 1996) where the term One Engine Inoperative is represented by the acronym OEI. It should be noted that the take-off distance for continued take-off OEI may indeed be greater than the runway length available for small values of decision speed.
  In addition, the definition of distance required for a continued Take-Off with OEI can be found in the Airworthiness Specifications (EASA, 2003).

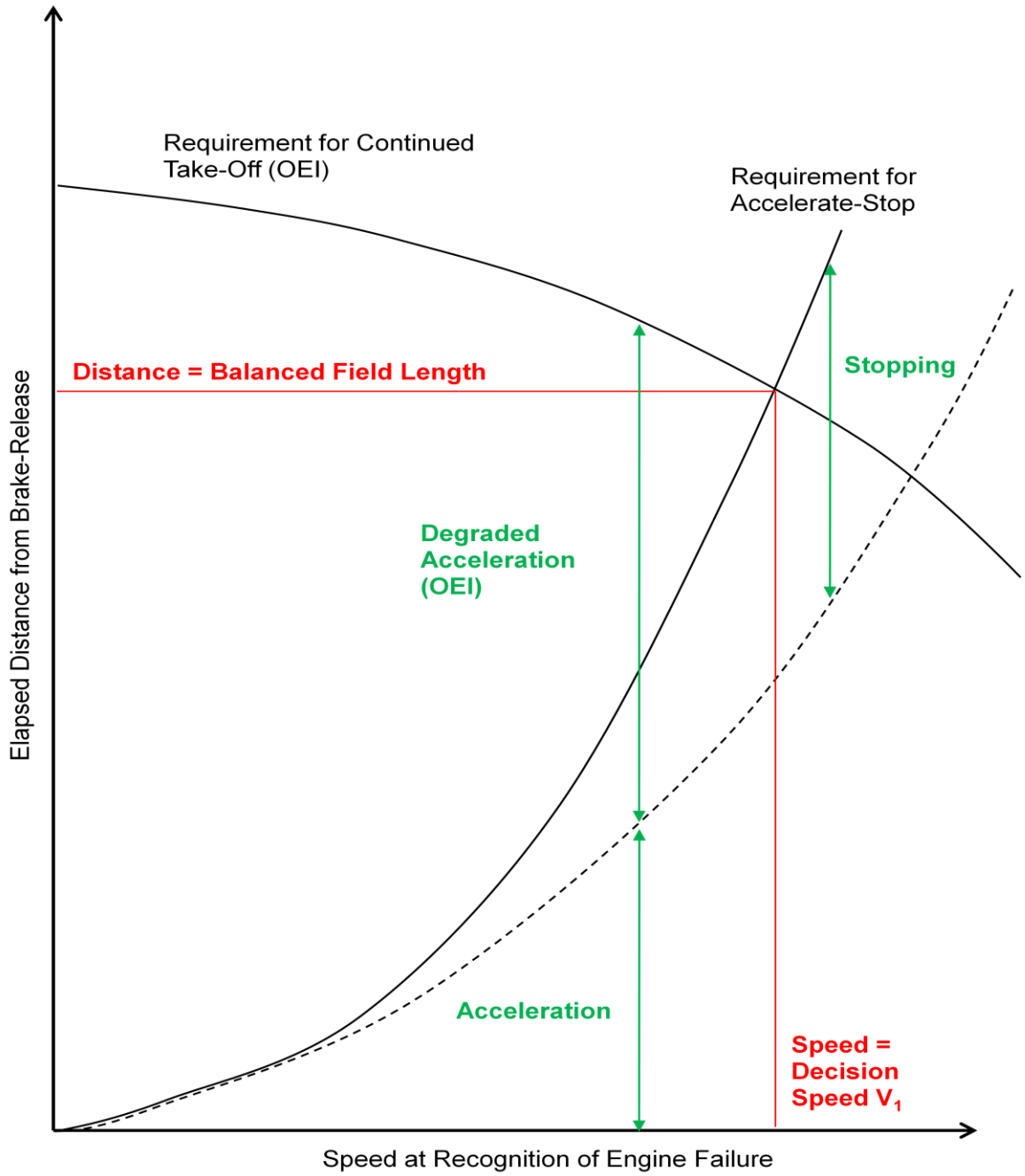

FIGURE 5.6: GRAPHICAL DETERMINATION OF DECISION SPEED (V1) AND BALANCED FIELD LENGTH

- Fastest Climb
  The maximum rate of climb of an aircraft is related primarily to the imbalance of vertical forces on the aircraft and will influence the time to ceiling of the aircraft. In reality, the ability for commercial aircraft to climb quickly has operational benefits in terms of the amount of fuel used for climb but may be limited by the rate of change of this quantity which would induce large vertical loads on passengers and crew and may therefore be provided in manufacturer information as the Maximum Allowable Rate of Climb.

- Specific Air Range and Specific Endurance
  Specific Air Range (SAR) is a measurement of the change in range for the incremental change of aircraft weight to fuel burn having the units [m/kg] and is a useful quantity for comparing aircraft operational performance. However, it varies with altitude and Mach

number amongst other things and is of increased value when combined with a fixed velocity (usually the cruise speed) to obtain the flight time per unit of fuel mass burned or Specific Endurance.
Incidentally, the current record for non-refuelled flight is the flight of the Global Flyer in 2005 taking 67 hours, 1 minute to cover 19,894 [nm]. The aircraft was a single-seat, turbo-fan powered machine with a lift to drag ratio estimated at 37.(Filippone, 2006)

- Longitudinal Stability
  In addition to the aforementioned performance criteria, the analysis of the longitudinal response of the aircraft to an abrupt disturbance is investigated in an effort to examine the flight dynamics of the A320 model. Although data for real-world comparison is unlikely to be available, a realistic solution space can be estimated and potentially simulator accuracy as well as Simulink model fidelity assessed. (See 5.3 Longitudinal Stability Case Study).

5.2.2 VERIFICATION & VALIDATION ACTIVITIES

The verification and validation activities require two distinct packages of work to be performed: The inspection of model input data, including aerofoil coefficient variation, and the calculation and validation of performance criteria as set out earlier. Taking each model specification parameter in turn, the value is justified through research or calculation. However, specific tools are required for certain parameters. In some cases small experiments or simulations are run to obtain the necessary data.
The use of 3rd party flight dynamics models presents numerous difficulties. Initially the data files require decompilation, a process hindered by the lack of suitable freeware available to perform the task. Once decompiled, the data is presented in a format which requires a degree of deciphering. Coupled with the absence of units for each quantity, the lack of a specified reference location complicates matters more. Some further deduction resolves a number of these issues but the problem associated with the lack of units remains. The challenge is circumnavigated by comparing the magnitude of the parameter to similar parameters in the file for which a data range was known through experience.
Several parameters require information which is related to the position of aircraft properties with respect to a geometrical datum. Using projected drawings (Appendix L) these parameters can be determined, having first computed the scale of the drawing set. An example is the calculation of the Mean Aerodynamic Chord (MAC). The graphical method employed for the calculation of this property of the wing uses a top-down drawing of the aircraft. Referring to Figure 5.7, the MAC is determined using a widely documented method (Raymer, 1992) of extending the tip chord by twice the root chord ($C1$) – considered as being inside the fuselage – and the root chord by twice the tip chord ($C2$) as shown. Joining the diagonal ends of the extended chords produces two lines which intersect. The location of intersection corresponds to the spanwise location of the MAC. The chord of the wing at this point is equal to the length of the MAC. The location of the aerodynamic centre can be assumed to be at the quarter chord location of the MAC (Houghton & Carpenter, 2003) and the CG limits at approximately 15% and 35% (Project Airbus) with the typical value being at 26% of the MAC (Airbus). Admittedly these are vague values but in general the approximation is known to hold.

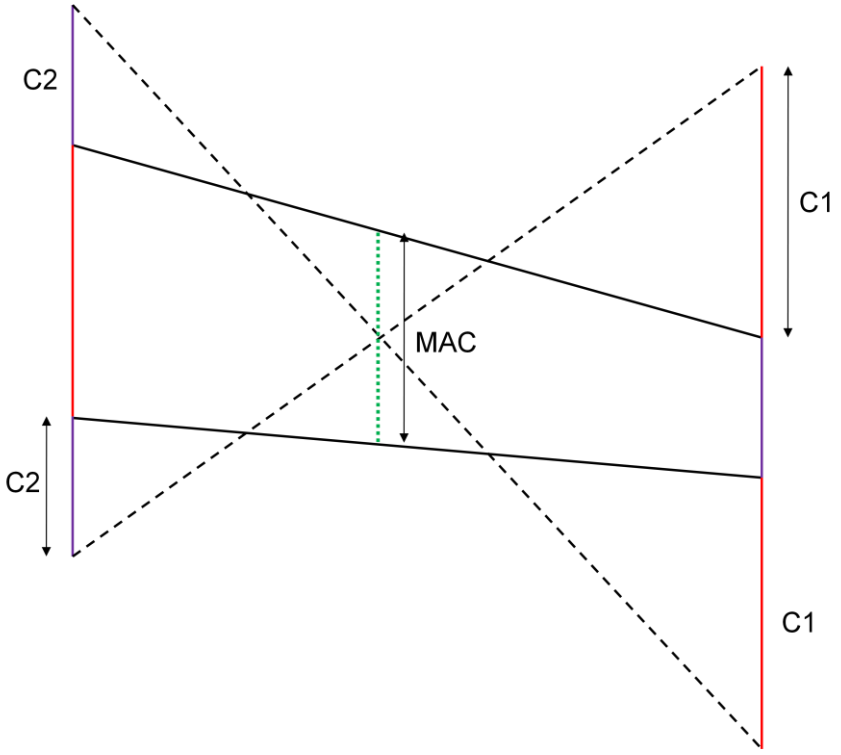

FIGURE 5.7: GRAPHICAL DETERMINATION OF THE MEAN AERODYNAMIC CHORD

Further estimates include the use of empirical formulae. In particular for the variation of thrust with both altitude and Mach number (see the equations of 4.3.2.1 Code Construction).
Obtaining the drag coefficients for the fuselage and landing gear requires approximation of the component to a simpler geometrical shape which is then either cross referenced with known drag coefficients for the geometry or else opened up to obtain a wetted area estimate for use with an average skin friction coefficient determined from experimental procedures documented in literature of viscous flow (White, Viscous Fluid Flow, 2006).
The Design Foil software is available (see Nomenclature) to estimate the more complex parameters related to aerofoil shapes and control surface deflections. Specifying the coordinates of the desired aerofoil and the angle of attack, the software generated data on the lift, drag and pitching coefficients which in turn is used as a means of verifying the aerofoil data specified by the existing model input file. In addition, with the aid of fitting polynomials through data and extrapolating, lift and drag increments for high lift devices is estimated.
Appendix M holds the completed input file analysis. For each parameter, rationale was provided for the decision amongst other notes regarding the method of approximation. As part of improvement suggestion and delivery, the estimated values for the parameters can be amalgamated into a single model specification. Where this has been done, the chosen value is highlighted. Decisions on parameter selection in cases where two or more values from the researched sources exist is driven by majority vote or perceived source reliability.

5.2.3 FLIGHT TEST PROGRAMME

Validation of several of performance criteria requires a process more complex than data mining and estimation. Although estimates for this small set of criteria could be obtained through solution of approximated equations of motion, a more interactive approach with the mathematical solution is seen as a more effective alternative which also serves to provide insight into the limitations of the simulator software. Examples of those performance criteria which require flight test include the response to longitudinal disturbances and investigation into the boundaries of the flight envelope.
The natures of the tests are tailored to ensure output of the appropriate data for the specific performance parameter. Table 5.1 summarises the test definitions for the selected performance

elements (the ID number refers to the global set of performance criteria defined later in Table 5.3) and is accompanied by rationale designed to explain the logic behind the deduction of the test procedures and the designed use of the data acquired.

ID	Performance Element	Description of Test	Rationale
1	Payload-Range Chart	1. Climb Out to 30,000 [ft], trimmed flight at 300 [kts IAS]. 2. Fly for 2 Minutes straight and level for data capture. 3. Repeat for two other specific weight configurations.	In order to construct a payload range chart, the limits of the payload range envelope need establishing. These limits are given at specific conditions of weight equal to or less than the maximum take-off weight (MTOW). Predetermined parametric model specifications (see Appendix H.2) specify the fuel and payload fractions of the total aircraft weight applicable to these limits and are used to collect data related to the aircraft mass reduction over time during a cruise phase established at a typical speed and altitude. (In reality, in lieu of the total mass, the 'fuel state' recorded in the simulator output file is used in the ensuing calculations – the fuel state refers to the percentage of fuel in the tanks relative to the simulation starting value). A linear relationship is calculated for the data captured and extrapolated to the specific weight condition of zero fuel. The endurance (maximum flight time before zero fuel) obtained from this method is then multiplied by the average speed throughout the test to arrive at an estimated range value. A suitable alternative method involves the use of the Breguet Range Equation for the extrapolation which more accurately incorporates a exponential decay of mass with time (see 5.4.2 Performance Criteria).
3	Landing Speed	1. TO @ MLW and circle for landing. 2. ILS approach - speed and flight path may vary. 3. Repeat for 2 other weights <MLW.	In order to generate data that is comparable to data obtained from A320 flight manuals, the test allows data capture for landing scenarios over a range of distinct weight configurations below the Maximum Landing Weight. The approaches used during the test are expected to vary considerably due to the lack of an autopilot or a trained pilot able to closely recreate behaviour for each of the test runs. Due to this, there are several restrictions on the use the data obtained. The touchdown speed will be taken from the time of contact of the main gear with the runway having no further flight recognised thereafter – a 'bounced' landing being a sign of an approach speed above that of the recommended value.

11	Altitude vs. Airspeed Flight Envelope	1. Climb Out to ceiling for maximum thrust. 2. Trim at ceiling and increase thrust to terminal velocity. 3. Reduce speed and maintain altitude until stall. 4. Descend to 10,000 [ft] and repeat step 2 and 3. 5. Descend to 5,000 [ft] and repeat steps 2 and 3. 6. Repeat for 2 other weight configurations.	Establishing the altitude and speed governed flight envelope requires knowledge of the operational limits of the aircraft. The boundaries of the envelope are probed by accelerating to the maximum possible speed and decelerating to stall for a number of different altitudes including the upper limit of absolute ceiling. The data obtained is analysed for limiting values and these values are linked using a polynomial fit to establish the boundary of the model. In reality, this locus is governed by structural, material and physical laws in addition to aerodynamic and mechanical forces and provides insight into limitations of the simulation software (see 5.4.3 Identified Simulation Limitations)
14	TO Distance	1. Perform TO run controls free, TO flap configuration at MTOW. 2. Repeat for one or more stages of flaps.	Within the parametric specification, the effect of high lift devices is incorporated into the simulation through specification of dimensionless increments in the lift, drag and pitching moment of the aircraft wing due to the stage of device deployment. The effects are visualised through the data acquired from this simulation and compared to estimated or researched flight manual values for the given weight.
15	Balanced Field Length	1. Execute TO run again at MTOW but abort at decision speed V1. 2. Repeat for one or more decision speeds. 3. Repeat previous steps but continue Take-Off OEI.	As indicated by Figure 5.6 the balanced field length requires knowledge of the intersection between two plots related to distances from the brake-release to either the location of aircraft stop after an aborted take-off or the clearance of a 35 [ft] screen(FAA, 2009) with a continued take-off OEI, for a range of decision speeds. The test uses decision speeds within a realistic range below the expected lift off velocity as trial values and performs the necessary take-off run procedures to obtain data for the scenario. From the simulator data obtained, the distances covered by the aircraft can be calculated for each case and a polynomial of suitable degree fitted through the data. The resulting polynomial equations or alternatively the graphical intersection of the plots can be used to determine both the critical decision speed and the balanced field length.

17	Fastest Climb	1. TO and climb out at maximum possible rate @ MTOW with flaps and gear retracted. 2. Repeat for zero payload, minimum fuel.	The maximum rate of climb is governed by such properties as the excess thrust available and wing performance characteristics. However, the maximum value of climb (or vertical) speed can be influenced by an energy exchange process whereby the kinetic energy of the aircraft can be rapidly used to gain a swift increase in potential energy through, for example, a sudden nose-up pitching motion and a resulting increase in altitude – known as a zoom climb. The test takes these possibilities into account by finding the maximum sustained rate of climb up to stall and considers the effect of weight on the value, if necessary extrapolating current data to predict a potential maximum.
19	Specific Air Range	1. Climb Out to 30,000 [ft], trimmed flight at 300 [kts IAS]. 2. Fly for 2 Minutes straight and level for data capture. 3. Repeat for 2 other weight configurations. 4. Repeat for 2 other cruise speeds.	The specific air range is calculated in a similar fashion to the ranges required for construction of the payload range chart but instead of using a typical cruise speed, the cruise speed and weight configurations are varied within suitable ranges to locate an optimum value. A polynomial fit through range data, determined using either a linear or exponential extrapolation, is the method of choice.
22	Longitudinal Stability - Phugoid/Short Period	1. Climb Out and trim at 5,000 [ft] in straight and level flight. 2. Insert Control Input and release controls. 3. Repeat for 2 other weight configurations.	Particular focus is paid to the aircraft response to a longitudinal disturbance later in this section (5.3 Longitudinal Stability Case Study). Data obtained from a pitching disturbance is used to illustrate aircraft damped oscillatory response graphically. However, factors including the aircraft weight and the type of control system in use allow further investigation. Comparison with a theoretical estimate is the ideal validation method through the construction and solution of the associated Eigenvalue problem or Transfer Function definition.

TABLE 5.1: SUMMARY OF INDIVIDUAL FLIGHT TESTS

Due to the occasional requirement of test repetition for a particular variable, operationally it is sensible to reuse a model with an appropriate specification. Purely from a project management perspective, the time allocated to a flight simulation test programme is already rationed and the availability of the equipment limited. It is therefore also necessary to compress the duration of the tests through combination. Tests are grouped based on the models and conditions required, and the stage of the flight cycle on which the test is centred. A revised schedule can be found in Appendix H.1, with the model definitions specified in Appendix H.2. The tests are, in reality, shorter still as the user of the simulator has the ability through Excalibur to set the initial conditions of the simulation. That is, take-off and climb, necessary for real-life test flights, is not necessary for a similar simulation. Instead, the altitude and speeds are specified and the simulation initialised from this point.

Having completed the test programme to plan for the existing A320 specification at the centre of the assessment activities, any remaining time allocated to simulation is spent formulating and testing a model specification formulated using the estimated parameters. The specification of this model is discussed in (5.4 Validation Summary). Due to time constraints related to resource availability, selected flight tests only were completed.

5.3 LONGITUDINAL STABILITY CASE STUDY

One particular performance criteria defined in the bulleted list in the previous section is that of the response of the aircraft in the horizontal-vertical plane due to an in-plane rotational disturbance from the trimmed equilibrium condition. The trimmed equilibrium condition is defined as the fixed attitude (or orientation) and configuration of the aircraft (including control surface deflections) that allows the aircraft to maintain steady, straight and level flight. The upset of this condition is referred to as a disturbance or perturbation. In this study, the disturbance is manifested as a pitch disturbance due to an elevator input.

The axis system required to generate the theoretical prediction of this behaviour in terms of the perturbation variables (zero before the perturbation) for this scenario is defined by Figure 5.8 where $u, \dot{u}$ are the axial body perturbation velocity and acceleration, $w, \dot{w}$ are the vertical body perturbation velocity and acceleration, θ, q are the body pitch angle and rate and η is the elevator deflection from the trim position. This system is based on the right-hand Euler coordinate system (Appendix I) which defines the aircraft attitude in three-dimensional space with respect to a fixed datum. The orientation is given in terms of the Euler angles which when applied to the displaced aircraft in strict sequence allow the aircraft to realign with the datum. A third set of axes in addition to the fixed datum or Earth Axes and fixed Body or Aircraft Axes used for Euler computation is known as the Wind Axes. These axes are attached to the free stream airflow and are generally used for computation of aerodynamic force vectors. Although not officially defined, the axis systems used in (4.2 Mathematical Model Development) mimic those stated here. Transformation between axes systems can be derived, although if the axis system in use is identical to one formally defined in literature, many transformations already exist (Cook, 1997) without the need for derivation.

The response of the aircraft is in fact a combination of two unique pitching oscillations (or modes). These are termed the ‘short period’ and ‘phugoid’. The short period mode is quick to manifest itself and quick to dissipate with a frequency in the range 1 [rad/s] to 10 [rad/s] (Cook, 1997) and is a stabilising reaction from the tailplane due to a disturbance (static stability). The forward speed of the aircraft is approximately constant during the oscillation due to the short time period of the oscillation preventing any significant effects caused by the aircraft inertia or momentum. The phugoid mode in comparison is only lightly damped with a much longer period; frequencies are typically between 0.1 [rad/s] and 1 [rad/s] (Cook, 1997). For a ‘pitch up’ disturbance, the velocity of the aircraft is likely to be reduced. As a result, for constant incidence, the definition of lift (Equation 4.5) suggests that the lift will decrease. This causes an imbalance in the vertical equilibrium of the aircraft and the aircraft begins to lose height as the nose falls. The speed increases with the downward acceleration hence increasing the lift once more. This forces an increase in pitch of the aircraft due to the increased contribution to rotational forces by the lift. The momentum of the aircraft as it now climbs forces an overshoot of the previous trimmed equilibrium height. This climb also serves to reduce the speed and hence lift of the aircraft which in turn causes a gradual downward pitch. The aircraft then begins to descend and the cycle begins again. With time however, for a dynamically stable aircraft, the energy dissipation due to drag reduces the peaks of the oscillation and eventually the phugoid mode dies out. Insufficient drag or excessive thrust characteristics can lead to the mode becoming dynamically unstable; the oscillations get larger with time.

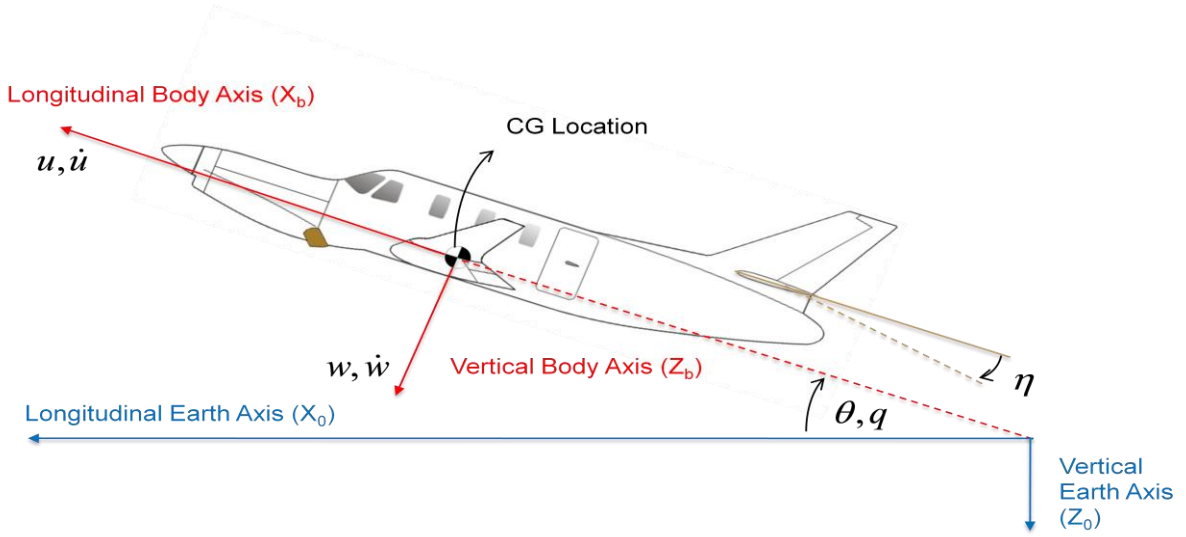

FIGURE 5.8: LONGITUDINAL PERTURBATION AXIS DEFINITION

This longitudinal case study requires the construction and solution of the relevant reduced set of equations of motion for the aircraft for specific initial conditions.

5.3.1 LONGITUDINAL EQUATIONS OF MOTION

Using classical mechanics – Newton's 2nd Law of Motion – in both a translational ($Force = Mass \times Acceleration$) and rotational ($Moment = Inertia \times Angular\ Acceleration$) sense, the equations of motion for a 6 degree of freedom aircraft of symmetric airframe and of uniform mass distribution may be assembled by considering the influence of all disturbing forces on the aircraft (Cook, 1997). Linearisation of these equations is achieved by considering small perturbations about the trim condition. The forces and moments given on one side of the equations of motion are in fact a summary of forces from a number of different sources. Those forces and moments attributed to aerodynamics are approximated in most literature to be a function of only the perturbation magnitude and the aerodynamic force derivatives. Further restrictions are imposed by considering only a first order approximation mathematically. As a result, in order to obtain the aerodynamic force and moment fluctuations due to a disturbance, the estimation or derivation of these derivatives (known as aerodynamic stability derivatives) is required (Appendix J.2). In a similar fashion, the disturbing forces and moments due to a control deflection, since dependent on aerodynamic behaviour also, are quantified using aerodynamic control derivatives. The effects of weight, thrust forces and atmospheric disturbances may also be included in the mathematical summary of the disturbing (or disturbed) forces.
A decoupled set of equations, driven only by the relevant forces and moments influencing the plane of interest for longitudinal motion, are given by (Equation 5.1) for level flight and implicitly suggest the zero value of coupled aerodynamic derivatives. In other words, aircraft roll due to aileron deflection has no effect on the longitudinal motion of the aircraft in a purely aerodynamic sense. *Note: The notation used for the equations of motion is summarised in* Nomenclature *section*.

$$
\begin{aligned}
m\dot{u} - \hat{X}_u u - \hat{X}_{\dot{w}}\dot{w} - \hat{X}_q q + mg\theta &= \hat{X}_\eta \eta + \hat{X}_\tau \tau \\
-\hat{Z}_u u + \left(m - \hat{Z}_{\dot{w}}\right)\dot{w} - \left(\hat{Z}_q + mU_e\right)q &= \hat{Z}_\eta \eta + \hat{Z}_\tau \tau \\
-\hat{M}_u u - \hat{M}_{\dot{w}}\dot{w} - \hat{M}_w w + I_y \dot{q} - \hat{M}_q q &= \hat{M}_\eta \eta + \hat{M}_\tau \tau
\end{aligned}
$$

EQUATION 5.1: LONGITUDINAL EQUATIONS OF MOTION

Further to the representation given by Equation 5.1, the coefficients may be converted to a non-dimensional form by division or multiplication by an appropriate expression usually involving the trim speed, density and a reference area or length.

5.3.2 STATE SPACE REPRESENTATION

For small perturbations, an aircraft is an example of a linear dynamic system. The instantaneous motion or 'state' of a linear dynamic system can be described by a set of variables known as 'state variables'. The number of state variables depends on the number of degrees of freedom of the system. The motion of the system therefore, may be summarised in a multidimensional vector known as the 'state space'. Identifying the state variables of the longitudinal system as u, w, q, θ and assigning these also as output variables of the state space the equations of motion (Equation 5.1) may be represented in the form below (Equation 5.2).

$$[M]\{\dot{x}(t)\} = [A]\{x(t)\} + [B]\{u(t)\}$$

EQUATION 5.2: STATE SPACE REPRESENTATION OF LONGITUDINAL EQUATIONS OF MOTION

Where:

$$\{x(t)\} = \begin{bmatrix} u \\ w \\ q \\ \theta \end{bmatrix}, \{\dot{x}(t)\} = \begin{bmatrix} \dot{u} \\ \dot{w} \\ \dot{q} \\ \dot{\theta} \end{bmatrix}, \{u(t)\} = \begin{bmatrix} \eta \\ \tau \end{bmatrix},$$

$$[M] = \begin{bmatrix} m & -\hat{X}_{\dot{w}} & 0 & 0 \\ 0 & \left(m - \hat{Z}_{\dot{w}}\right) & 0 & 0 \\ 0 & -\hat{M}_{\dot{w}} & I_y & 0 \\ 0 & 0 & 0 & 1 \end{bmatrix}, [A] = \begin{bmatrix} \hat{X}_u & \hat{X}_w & \left(\hat{X}_q - mW_e\right) & -mg\cos\theta_e \\ \hat{Z}_u & \hat{Z}_w & \left(\hat{Z}_q - mU_e\right) & -mg\sin\theta_e \\ \hat{M}_u & \hat{M}_w & \hat{M}_q & 0 \\ 0 & 0 & 1 & 0 \end{bmatrix}, [B] = \begin{bmatrix} \hat{X}_\eta & \hat{X}_\tau \\ \hat{Z}_\eta & \hat{Z}_\tau \\ \hat{M}_\eta & \hat{M}_\tau \\ 0 & 0 \end{bmatrix}$$

5.3.3 EQUATION SOLUTION

5.3.3.1 LAPLACE TRANSFORM METHOD

There are a number of ways in which the equations of motion may be solved. The most commonly used to date is the classical control theory approach of taking Laplace transforms of the time-domain system (Equation 5.2) and rearranging to represent the Laplacian output $\{x(s)\}$ in terms of a transfer function for given Laplacian input $\{u(s)\}$. The response can then be visualised in the s-domain to allow classical stability analysis of the response. As this project has significant computing power available, this technique is implicit and responses are in fact visualised in the time domain through a versatile MATLAB Control System Toolbox tool known as the Linear Time-Invariant (LTI) viewer.

Although these built-in software algorithms allow convenient performance of what otherwise would be a laborious by-hand procedure, they also disguise the theory behind them. Rearrangement of the time-domain equations transformed to the s-domain derives a set of transfer functions as has been previously stated. The denominators of the transfer functions are a fourth order, common characteristic equation of the aircraft response. The numerator serves a means of adapting the response according to the nature of the particular state variable. The characteristic equation may be factorised into two unique, quadratic equations. Each quadratic equation represents a particular mode of oscillation in the aircraft longitudinal response to disturbance (the short period and phugoid oscillations). Furthermore, each quadratic may alternatively be represented by a damped harmonic motion equation (Equation 5.3) where the mode-specific damping ratio and undamped natural frequency are given by ζ and ω respectively.

$$s^2 + 2\zeta\omega + \omega^2$$

EQUATION 5.3: DAMPED HARMONIC MOTION CHARACTERISTIC EQUATION

5.3.3.2 EIGENVALUE PROBLEM METHOD

Solution of the characteristic quadratic equations in the denominator of the transfer functions generated in the previous method produces two pairs of complex conjugate roots – one pair for each mode of oscillation. These roots correspond to the eigenvalues of the state space matrix $[A]$. The corresponding eigenvectors may be used in conjunction with the eigenvalues to obtain time-domain responses for the system thus.

Given a matrix of eigenvectors $[V]$ and a diagonal matrix of eigenvalues $[\Lambda]$ an eigenfunction of the form $Ve^{\Lambda t}$ may be defined for each mode for each of the state variables. Since the eigenvalues are complex (this is true for a dynamically stable response) they are of the form $\Lambda = a + jb$. Recalling the identity $e^{j\pi t} = cos\pi t + jsin\pi t$, the function may be rearranged into the set of time domain response functions of the form $Ve^{at}(cosbt + jsinbt)$ which corresponds to the harmonic response of $Ve^{\zeta\omega t}(cos\omega t + jsin\omega t)$. As with the transfer function solution, the basic response characteristic is fixed (by the state matrix eigenvalues or transfer function denominator) but with each response being adapted to fit the variable (by the state matrix eigenvectors or transfer function numerator).

5.3.3.3 SOLUTION CONSTRUCTION

Before any processing of results can be performed, the state space equations and subsequently the LTI model for solution by the MATLAB software need constructing. In order to use Equation 5.2, the state space matrices need computing from data available for the Airbus A320. Assuming a rearranged, non-dimensional form of the equations of motion in state space form for a elevator input and constant thrust (given by Equation 5.4), the non-dimensional coefficients in the $[A']$ and $[B']$ are calculated using a combination of reverse engineering of the equations (Cook, 1997) and published techniques (Appendix J.3). *Note: All parameters used for the computation for the matrices are inherited from first the model specification used in the longitudinal flight tests (5.2.3* Flight Test Programme*), then the research of the parametric specification data and development of the mathematical and physical models in other sections of this report unless stated otherwise.*

$$\{\dot{x}(t)\} = [A']\{x(t)\} + [B']\{\eta(t)\} \Longrightarrow \begin{bmatrix} \dot{u} \\ \dot{w} \\ \dot{q} \\ \dot{\theta} \end{bmatrix} = \begin{bmatrix} x_u & x_w & x_q & x_\theta \\ z_u & z_w & z_q & z_\theta \\ m_u & m_w & m_q & m_\theta \\ 0 & 0 & 1 & 0 \end{bmatrix} \begin{bmatrix} u \\ w \\ q \\ \theta \end{bmatrix} + \begin{bmatrix} x_\eta \\ w_\eta \\ m_\eta \\ 0 \end{bmatrix} \eta$$

EQUATION 5.4: NON-DIMENSIONAL STATE SPACE LONGITUDINAL EQUATIONS OF MOTION

When calculating the coefficients of the matrices in Equation 5.4, two key points are worth mentioning: Firstly, a number of aerodynamic quantities used in the computation are assumed to be equal to zero (ESDU, 2003). In particular, for a jet engine, any variation of thrust with speed, although finite, is minimal in comparison to the aerodynamic forces and hence for simplicity, the quantity $\frac{d\tau}{dV}$ is considered to be negligible. Also, the variation of lift curve slope with speed over a small range of subsonic Mach numbers can also be considered to be of minimal importance and hence due to their dependence on this variation, all the quantities $\frac{\partial C_L}{\partial V}$, $\frac{\partial C_D}{\partial V}$ and $\frac{\partial C_m}{\partial V}$ may be considered to be zero.

Secondly, it is necessary to undertake some further research as although there is much data available already due to previous project activities, for this exercise several parameters are as yet undefined, namely: the change in angle of attack at the tail due to the post-wing downwash field $\frac{\partial \varepsilon}{\partial \alpha}$ (can be estimated by comparing typical values for particular tail-wing combinations) and the drag equation of the tail. The latter quantity was required for construction of the physical model (4.5 Physical Modelling of an Aircraft) and was estimated from the simulated behaviour of a standard NACA 0012 aerofoil. For consistency, this data will be retained for this activity also, but it is acknowledged that there is little evidence to support the use of this aerofoil section for the purpose. It has been used, however, for lift curve slope data in the parametric specification

used in the flight test. In addition, the lift coefficient increment for a unit change in elevator deflection is required for the calculation of the corresponding control derivative and is imported from the parametric definition. The value used has been estimated from simulation in Design Foil of a simple flap (of geometry and position approximate to that of a graphical estimate of the A320 elevator and stabiliser – Appendix J.4) deflected at the trailing edge of the 0012 aerofoil.

The execution of a matrix assembly script (Appendix J.5) yields the following estimated state space for the A320 (Equation 5.5).

$$\begin{bmatrix} \dot{u} \\ \dot{w} \\ \dot{q} \\ \dot{\theta} \end{bmatrix} = \begin{bmatrix} -0.0027 & 0.1104 & 0 & -9.8100 \\ -0.2300 & -0.6626 & 183.7544 & 0 \\ 0.0008 & -0.0831 & -2.0019 & 0 \\ 0 & 0 & 1 & 0 \end{bmatrix} \begin{bmatrix} u \\ w \\ q \\ \theta \end{bmatrix} + \begin{bmatrix} 1.6841 \\ 35.0306 \\ 14.9499 \\ 0 \end{bmatrix} \eta$$

EQUATION 5.5: A320 STATE SPACE ESTIMATE

5.3.4 CASE STUDY CONCLUSIONS

The theory developed in this case study aids the verification of the parametric specification data. Specifically, the response to an elevator input for the alternative model specification was recorded as part of the flight test programme. This data is highlighted in particular as the information corresponds to a specification without dynamic actuators enabled (explanation available in 5.4.2 Performance Criteria Assessment Results). From the results plotted from solution of the state space equations, the frequency and damping of the two modes of oscillation can be calculated and compared with the corresponding values obtained for the flight test data. In this case, the state space representation was formulated using the initial conditions and model data from the alternative model flight test and it can therefore be predicted that the results will correlate closely with any exceptions being attributed to approximations made in either the derivative generation or the simulator mathematics.

Calculation of the frequencies and damping ratios is possible from simulation data by interrogating the data values to locate the peaks of oscillations. The time interval between these peaks is equal to the time taken for a complete cycle (or wavelength) referred to as the period of oscillation T. The period is then converted to an angular frequency ω in [rad/s] using Equation 5.6.

$$\omega = \frac{2\pi}{T}$$

EQUATION 5.6: ANGULAR FREQUENCY CONVERSION

In order to compute the damping ratio, a method known as logarithmic decrement is used (ESDU, 2009). The logarithmic decrement δ is expressed in terms of peak amplitude A a known number of wavelengths apart n as shown in Equation 5.7.

$$\delta = \frac{1}{n} \ln \left(\frac{A_1}{A_{1+n}} \right)$$

EQUATION 5.7: LOGARITHMIC DECREMENT

This decrement is then related to damping ratio by Equation 5.8.

$$\zeta = \frac{1}{\sqrt{1 + \left(\frac{2\pi}{\delta} \right)^2}}$$

EQUATION 5.8: RELATIONSHIP BETWEEN LOGARITHMIC DECREMENT AND DAMPING RATIO

Applying these methods to the flight test data, the frequency and damping ratios of the two modes of oscillation are obtained and compared to those calculated from the solution to the eigenvalues problem for the state space described earlier. The use of logarithmic decrement on the short period oscillation is difficult even with a relatively high rate of data capture for maximum resolution as the mode dies quickly. The data computed is from graphical extrapolation of the points and is highly subjective. Further investigation using data capture at the maximum possible rate would be a suitable method of increasing accuracy and credibility of the current results shown in Table 5.2. The experimental and theoretical results can be viewed in Appendix J.6 which also includes the transfer functions obtained from the use of the Laplacian Solution method also described earlier.

	Short Period		Phugoid	
Source	State Space Calculation	Parametric Specification & Simulator	State Space Calculation	Parametric Specification & Simulator
Frequency [rad/s]	3.8614	3.1416	0.1076	0.0722
Damping Ratio	0.3360	0.3623	0.0511	0.0510

TABLE 5.2: LONGITUNDINAL CASE STUDY RESULTS

Discrepancies between the values in Table 5.2 are evident. These may be attributed to a number of sources:

- The algorithm for calculation of the perturbation variables within the simulator is unknown to the user and may use methods which are more or less accurate than the state space method used for the theoretical calculation. A typical error may arise through neglecting the square of terms known to be relatively small in magnitude.
- The term 'perturbation' implies only small deviations from the trimmed condition and the validity of the state space equations depend on this condition being met. The pilot input used to excite the modes in the flight test involved displacement of the elevator through its maximum travel – far greater than what could be considered a small input. The effect of this on the mathematics within the simulator is not easy to obtain without further testing but potentially, any approximations used during the construction of the equations of motion may be classified as an oversimplification.
- At each stage of the calculation of the data given in Table 5.2, there is an element of error introduced through rounding of figures to a predetermined number of decimal places. This is of particular significance when performing calculations on an electronic calculator as opposed to the scripted calculations in MATLAB. However, this is only likely to account for minor errors.
- A source of error is certain to be attributed to the data capture and interpretation for the test flight on the simulator. Capture rates affect the resolution of data for a given time step and influence how close the peak data reading in the exported set is to the actual peak value of the simulation. In the case of the short period, the logging rate used for the flight test data allowed an acceptable calculation to be performed but a degree of interpolation in 'lumps' in the data variation with time was necessary. In particular, as the affect of the phugoid mode begins to make its presence felt towards the end of the short period mode, the short period data points tend to be 'dragged' with the mode phugoid oscillation making amplitude measurements from a common datum less accurate.

Although the above list may to some degree account for any misalignments between the values of frequency and damping ratio of the modes, the difference in values for the phugoid frequency is of sufficient magnitude as to warrant further investigation. In order to verify one calculation over the other, it necessary to consider a simplified estimate of the frequency; the equations of motion are reduced to containing only those terms which influence the phugoid dynamics. Such a 'reduced order model' is known as the Lanchester model and is valid, as stated in (Cook, 1997), when:

1. The aircraft is initially in steady level flight
2. The total energy of the aircraft remains constant
3. The incidence remains constant at its initial trim value
4. The thrust balances the drag
5. The motion is sufficiently slow that pitch rate effects may be ignored.

Using this method, for zero damping (as suggested by assumption number 2 above), the frequency of the phugoid ω_p may be approximated by Equation 5.9 where V_0 is the magnitude of the free stream flow.

$$\omega_p = \frac{g\sqrt{2}}{V_0}$$

EQUATION 5.9: THE LANCHESTER REDUCED ORDER MODEL APPROXIMATION OF PHUGOID FREQUENCY

The dependent parameters in Equation 5.9 are common to both calculations since for a zero initial angle of attack the free stream flow (measured on the wind axis) is equal to the aircraft forward speed (measured on the body axis). Using the reduced order approximation: $\omega_p = 0.0736$ [rad/s]. Comparing this frequency with the data provided in Table 5.2, it is clear that the simulator data yields a closer value. Reasons for the discrepancy in the state space therefore, may be related to the failure to include wing and tail setting angles which would affect the initial trim attitude, ultimately shifting the body axis system away from the wind axis system. This in turn would alter the free stream velocity for the same fixed body forward velocity as before. In order to increase the phugoid frequency, the free stream velocity would have to reduce. Any behaviour that contravenes the assumptions stated above may also suggest the inapplicability of the estimate and the cause of the error.

5.4 VALIDATION SUMMARY

The introduction to this assessment promises a method of simultaneously validating the simulator mathematical model, an A320 model specification fed into the simulator and the 3-DOF mathematical model developed as part of this project. In order to summarise this task for clarity, the relationships can be visualised as in Figure 5.9. The material which follows serves to share the results from the validation activities with a view of achieving this goal.

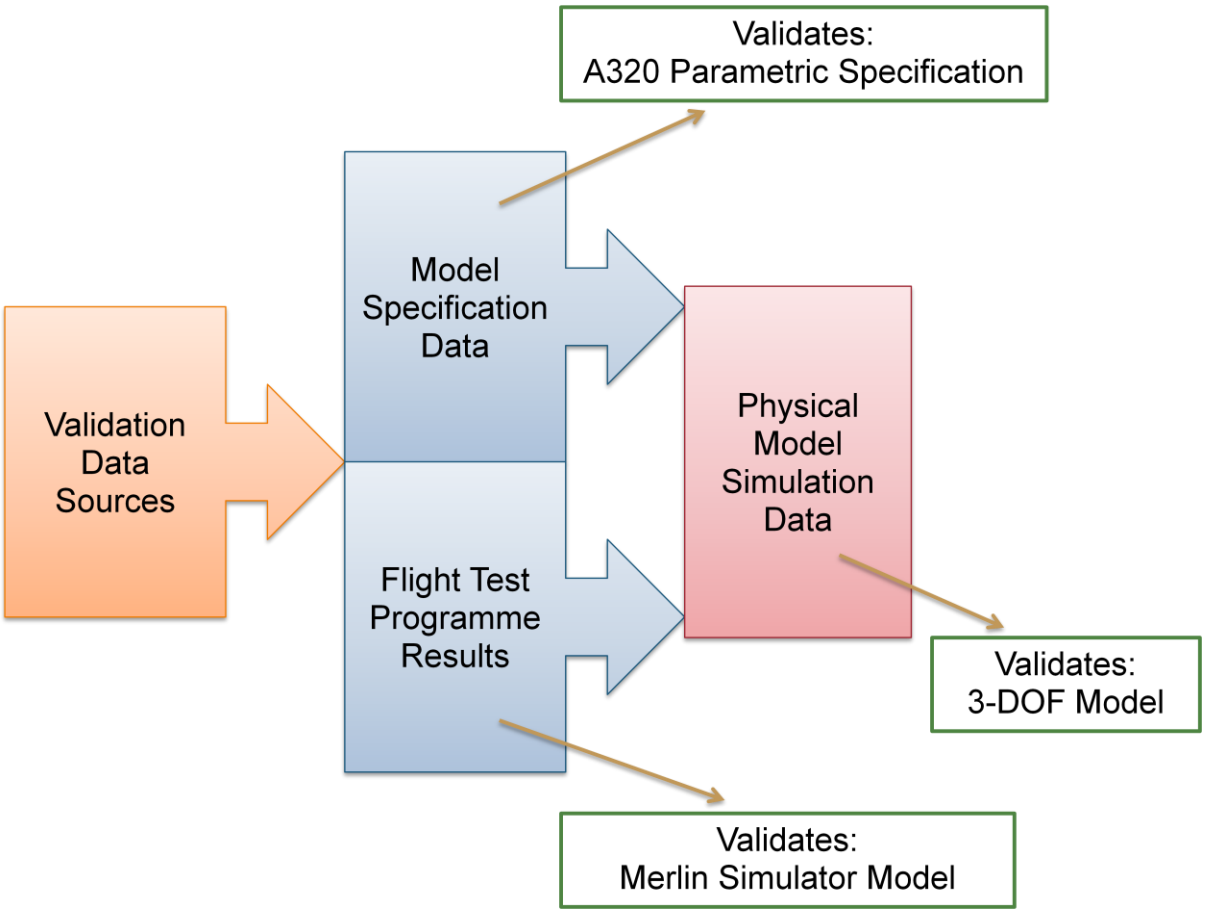

FIGURE 5.9: SUMMARY OF VALIDATION PROCESS

The validation process assesses only the 3-DOF physical model and not the other modelling outputs from earlier. Justification for doing this is provided in Figure 4.53; the mathematical and software areas of the modelling development served as building blocks for the physical model and hence assessment of the physical model is ultimately the validation of an external output as per its definition. Assessment of the other areas, in effect, is more of a verification activity as it would allow internal review of physical model elements.

5.4.1 MODEL SPECIFICATION ASSESSMENT RESULTS

The model specification of the model may be split into two distinct elements, namely the (aircraft) parametric specification data and the aerofoil specification data. These are combined to generate the input file to the Merlin simulator as indicated by Figure 1.1.
Initially, the assessment of the parametric specification allows a number of conclusions to be drawn based its suitability. In the main, the existing parameters appear to align with the real world or simulated data. However, there are some quantities whose assigned value is questionable. It is possible to categorise these assignments as follows:

A. Value appears to be a pure guess suggested by its limited numerical precision
B. Value is unchanged from the default value in the E1 tool
C. Value appears relatively inaccurate and method of estimation is unclear
D. Value appears to have been deliberately heavily approximated for convenience.

For instance, referring to the completed assessment found in Appendix M.1, parameter 126 is the main landing gear shock absorber stiffness. The value specified by the existing model is accurate to only two significant figures. Intuition suggests that this value has been determined through empirical testing of the simulation in terms of landing gear static displacement, the quantity on which this parameter has the largest effect. In fact, parameter 187 is a diagnostic output from the E1 editor which allows examination of this displacement. It can be speculated that this convenience in combination with a type A assignment (see above list) has resulted in the empirical fabrication of the parameter.
Some parameters demonstrate the lack of research into particular phenomena. This is evident through a type B assignment of parameter value. Parameters 114 to 122 inclusive hold multiplication factors designed to be superimposed on a 3 x 3 lookup matrix. The columns correspond to the variation in thrust with respect to density ratio and the rows variation in thrust with Mach number. In the case of the existing model, all elements of the matrix are equal to unity, which makes plain that the phenomenon has not been modelled. Although the effects of such variations may be minor for jet aircraft, if the facility exists for use by the modeller, failure to make use of it can be seen as lack of detail.
Type C assignments are uncommon but are likely to be the cause of the most severe cases of divergence from reality. For example, parameters 36 to 47 inclusive describe the change in the aerodynamic force behaviour of the wing through specification of increments of the dimensionless force quantities for a given stage of flap deployment. The data is assembled into a 3 x 4 lookup matrix. Due to the 'lookup nature', the increments should be implicitly cumulative incorporating all previous flap stage increments. Considering the data across all flap stages, it is clear that due to the repeated values beyond the second flap stage, stages three and four have no effect on the wing behaviour whatsoever. This is an unrealistic representation. The effect of flaps on the aerodynamic characteristics of the aircraft is significant and such a gross lack of realism should be visible during flight testing.
Finally, rife amongst parameters which have little effect on simulation performance, is the type D assignment. In the interests of time consumption and achieving an appropriate level detail, some parameters have been assumed to be equal to zero; an example being parameter 50. Simulations in Design Foil have shown that the drag increment due to a single degree deflection of the aileron is of an order of magnitude small enough for its effect to be neglected. Such an approximation is perfectly valid based on the perceived accuracy of the Merlin equipment. However, one instance of type D assignment does come under scrutiny. Parameter 142 holds a reference area from which logic assumes the proportional magnitude of the drag force generated by the landing gear is calculated. In the existing specification this parameter is assigned the value of zero. This suggests that the landing gear drag force is therefore also zero. This is an unacceptable conclusion and it is expected that landing gear drag is relatively significant and affects the landing speed amongst other quantities.

It is worth noting that there are several parameters that, in the absence of available data for comparison, are not analysed. Furthermore, those parameters that define spatial coordinates for the location of forces, components or references appear to be inaccurate. In fact this is not the case. The specification of these coordinates requires the position to be measured from an arbitrary datum. The datum is not defined explicitly; the mathematical model within the simulator requires only the knowledge of the relative positions of items in order to solve the system. Therefore, although defined at the top of the assessment, the datum chosen is likely to be different to that of the existing specification rendering any discrepancy meaningless. It is perhaps possible in hindsight to reverse engineer the model specification to deduce the original datum but added value from this exercise is likely to be limited.
Parameters 188 to 194 inclusive are referred to as tuning factors. As described in the

assessment, these are multiplication factors which alter the influence of certain aircraft movement on aerodynamic forces. It is unusual to find that the existing specification had these values set at anything other than 1. This suggests that when running a simulation based on the model described by that specification, the behaviour of the aircraft is modified from the calculated output through the inclusion of these non-unity tuning factors. The reason for the tuning capability is provided by the manufacturer as a means to demonstrate the influence of the corresponding aerodynamic behaviour on the aircraft performance. However, it may be speculated that these factors are included to counteract any inadequacies in either the simulator mathematical model or input file contents (both the parameter and aerofoil specifications). When specifying an alternative specification, the tuning factors are set to unity.

Finally, although care has been taken to source material from a variety of different locations, and simulations and estimates have been undertaken with provision to preserve accuracy where possible, there are still shortcomings in the verification activities and it is recognised that the assumptions made when estimating fundamental parameters such as centre of gravity and aerodynamic centre location (parameters 17, 18, 19, 31, 32, etc.) may introduce a divergence from reality and reduces the credibility of the model specification.

5.4.1.1 WING SECTION REDESIGN

In order to complete the input file to the simulator, the parametric specification is accompanied by a set of values which hold data points from curves relating the lift, drag and pitching moment coefficients to the angle of attack for a specific aerofoil section. Presently, the existing model specification uses an aerofoil data file constructed from estimates for the NACA 2412 4-digit section. The mathematical model reads the data file and either reads the coefficients for the appropriate angle of attack, or if the instantaneous angle of attack is outside the range of the data file, interpolates linearly between the nearest two specified values to arrive at the corresponding quantities. Implicit in this process are the assumptions that firstly the wing is of zero washout (twist from root to tip) and secondly, the aerofoil section is constant in the spanwise direction. These assumptions are amongst the limitations of the mathematical model as discussed in 5.4.3 Identified Simulation Limitations.

Picking up from 4.2.3.8 Further Work, the standard 4-digit aerofoil section is in appropriate for the expected transonic flight of the A320 (Mach numbers 0.7 – 1.2). Aircraft manufacturers pride themselves on the efficiency of wing design and will not release data concerned with the cross sectional geometry of the wing to the general public. As a result the exact data for the wing cannot be replicated. However, the assessment of the current data assumes the cross section is one of two typical NACA 6-series aerofoils. Data is collected through Design Foil simulations for the NACA 64-215 and the NACA 64A212 and compared with the curves plotted from the NACA 2412 data present in the existing specification. The range of angle of attack for the simulated data is of a finer granularity nearer the stall than the existing data in order to model the behaviour to a more accurate standard. The data is visualised in terms of individual plots in Appendix M.2.
However, the range of the appendix plots is restricted to +/- 20 degrees of incidence on the horizontal axis after which the aerofoil can be considered to be deep into stall. Behaviour beyond these values may either be left to the interpolation of the simulator software or else defined by the user through inclusion of a constant value for the coefficients within this range of incidence. In terms of simulation data, as the behaviour of an aerofoil in the stalled region is unpredictable, no calculation would be of use in obtaining the coefficients in deep stall. The existing specification handles post stall characteristics through a combination of the two, specifying apparently arbitrary data for the coefficients in this region and allowing interpolation to take place in between. Examples of these values are highlighted by rings in Figure 5.10 to Figure 5.12. As long as the aircraft is flown within expected bounds, this specification is likely to be adequate. There potentially may be a problem when the simulation takes the model into unexpected behavioural envelopes where the approximated and interpolated aerofoil characteristics are called upon unless justification of the irrational behaviour of the aerofoil in

these regions is stated.
Furthermore, simulated data agrees in the main with aerofoil data available in literature. (Anderson, 2005): Appendix D. The alternative model specification seeks to improve on the existing specification through use of the NACA 64A212 aerofoil data.

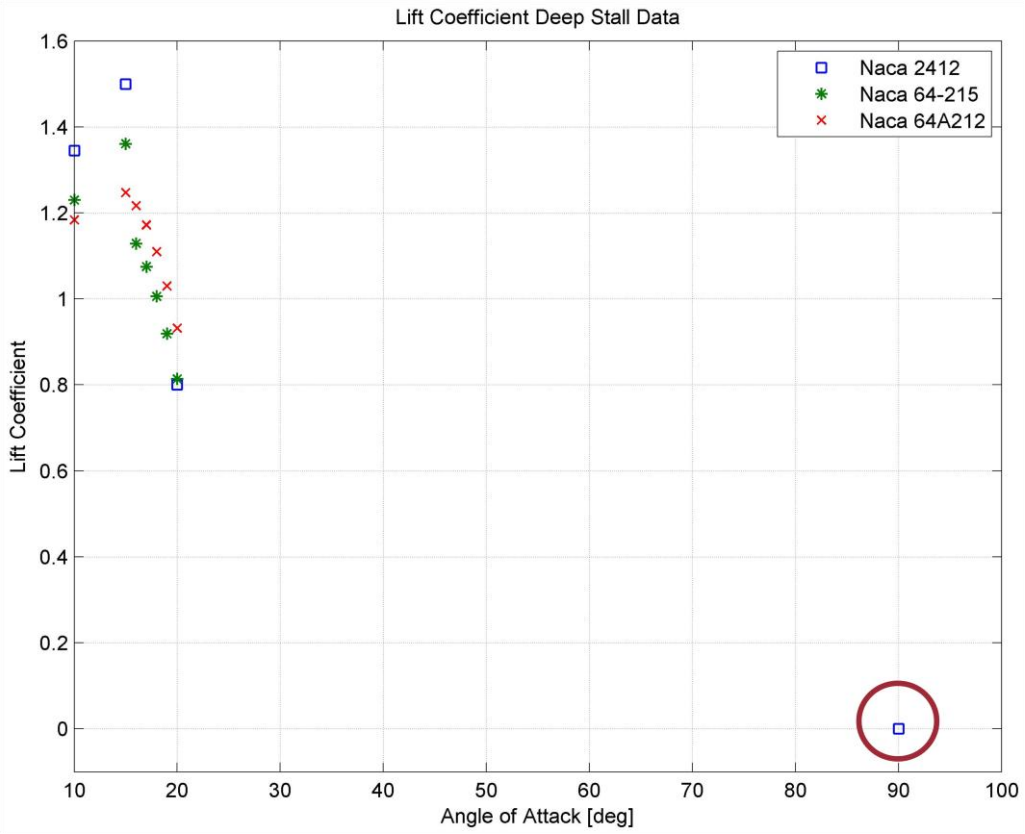

FIGURE 5.10: LIFT COEFFICIENT DEEP STALL PLOT

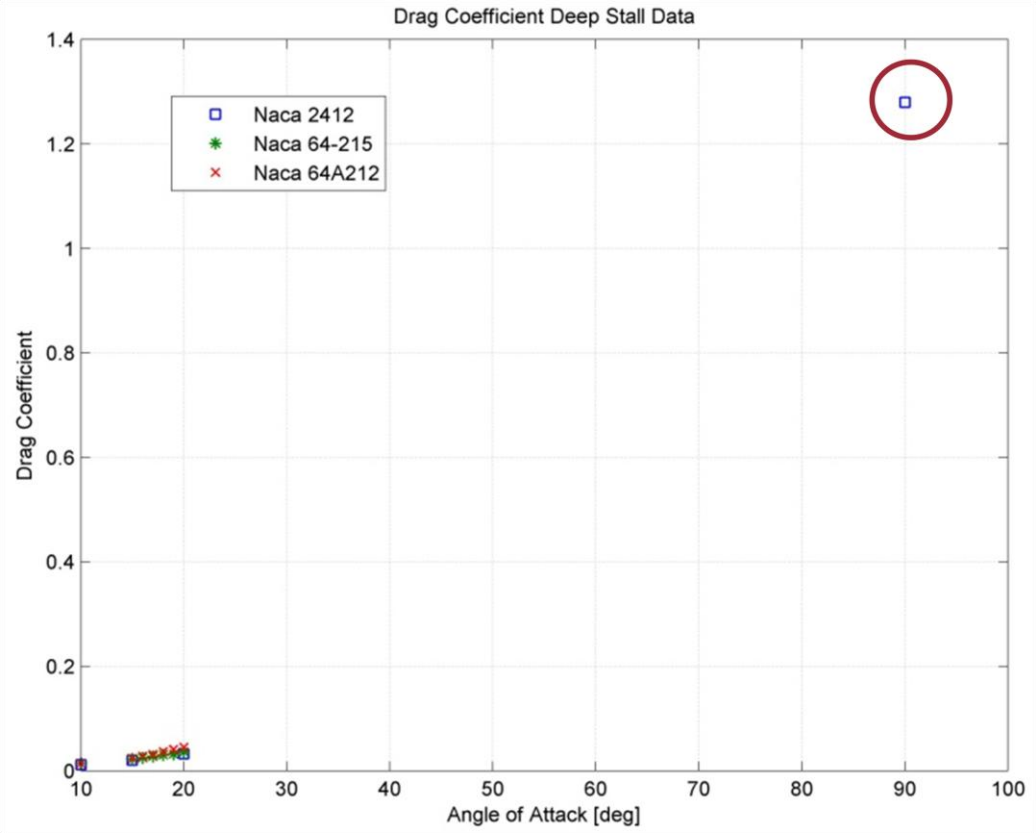

FIGURE 5.11: DRAG COEFFICIENT DEEP STALL PLOT

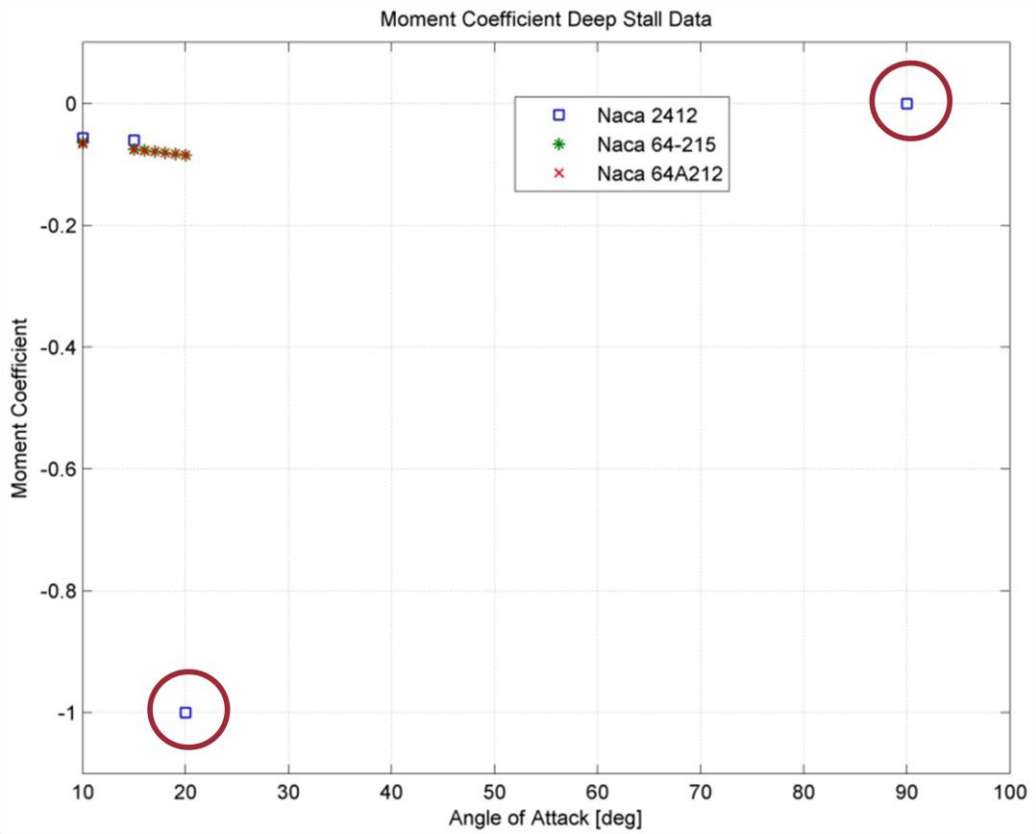

FIGURE 5.12: PITCHING MOMENT COEFFICIENT DEEP STALL PLOT

5.4.1.2 ALTERNATIVE SPECIFICATION

As a result of the work conducted as part of the assessment of the simulator input file, it is possible to use the data sourced for comparison to form an alternative specification for the A320. The precise nature of the specification is contained within the simulator input file assessment of Appendix M, with the NACA 65A212 being the aerofoil of choice for the definition. It should be remembered that this specification is merely a conglomeration of estimated values and has not undergone the degree of testing necessary to ensure a robust and functional definition for regular use on the simulator. The alternative specification has been used for a single flight test with a view of performing some preliminary comparison related to its stability and response as already discussed in the previous case study.

5.4.2 PERFORMANCE CRITERIA ASSESSMENT RESULTS

Using the flight test programme data collected for the existing model, it is possible to establish the nature of the criteria defined in 5.2.1.1 Performance Criteria. The analytical summary is shown in Table 5.3 with those criteria requiring further explanation being discussed in more detail in 5.4.2.1 Further Clarification. Time constraints do not allow detailed analysis of all encountered nuances in the data but general calculations and conclusions serve to provoke future work. The test identification number corresponds to the test flights defined in Appendix H.1.

It must be noted that the existing model suffers from a gross underestimate in fuel and payload capacity resulting in a Maximum Take-off weight far below that published by the manufacturer Airbus. As the test programme continues, these weight values are corrected using more appropriate magnitudes from the parametric assessment (Appendix M.1). This is done to preserve the relevance of the remaining test data and restricts the source of errors to aerodynamic inaccuracies with the weights being thereafter more closely in line with reality.

ID	Performance Element	Notes	Expected Result	Test	Method	Results / Conclusions
1	Payload-Range	Requires the knowledge of the elbows of the associated diagram. The Maximum Fuel and Payload exceed the Maximum Take-Off Weight (MTOW) as is predicted. Data capture for particular cruise configuration for 3 necessary weight conditions as specified by the model index Appendix H.2.	Estimation from the Airbus A320 Family Technical Appendices (Airbus, 2009) identify elbows as being at: 1,650 [nm] 3,000 [nm] 3,600 [nm]	A1 A2 A3	Extrapolate data to calculate the time to zero fuel. Use this endurance value to calculate range at constant speed. Repeat using the Breguet Range Equation.	Using a Linear Extrapolation / Range Equation calculation, the elbows are determined to be at: 1,401/1,593 [nm] 2,695/3,168 [nm] 2,639/3,233 [nm] The payload-range chart is plotted in 5.4.2.1 Further Clarification.
2	Wing Loading	The quantity assumes the weight rests entirely on the wing and is calculated by dividing the weight by the wing area.	Calculated from the Airbus Appendix: MTOW = 73,500 [kg] Area = 122.6 [m^2] Wing Loading = 5,881 [N/m^2]		Direct calculation from Model Specification data.	Considering both the existing specification and the alternative specification established after the parameter assessment: Existing = 3,687 [N/m^2] Alternative = 5,891 [N/m^2]
3	Landing Speed	In reality this value is calculated for a particular flap configuration and is the stall speed multiplied by some safety factor. The stall speed is calculated from the definition of lift coefficient for the limiting case of lift equal to weight and lift coefficient equal to the maximum available. Alternatively, data can be obtained from a landing run test.	Expected values can be established through consultation of a suitable pilot's handbook (Zagoren, 2009): Range of speeds corresponding to range of test weights are 56 [m/s] to 61 [m/s].	B1 B2 B3	Using the simulation data, the threshold crossing, touchdown and brake engage speeds may be calculated from the body speed sensors.	During the flight tests, the landing speeds varied due to lack of consistency between landing runs. The landing data is therefore not reliable enough to use as a basis for assessment. However, using the maximum lift coefficient given in line (5) of this table and a safety factor of 1.23 (Zagoren, 2009), the typical landing speed is calculated for the conditions identified in the notes of this row as being 56.0 [m/s]. Landing performance in general is discussed in 5.4.2.1 Further Clarification.

4	Lift Coefficient Variation with Incidence	Data is scarce however, the behaviour of the aerofoil is the primary driver of this performance factor and simulations of appropriate aerofoils provide some insight.	No data available for direct comparison.	Appropriate aerofoil selected based on known flight envelope of the aircraft and simulations run to obtain lift curve slope data.	The process required to generate the data overlaps with previous work on aerofoil data assessment and hence the results can be seen in Appendix M.2 with further information on the aerofoil selection found in 5.4.1.1 Wing Section Redesign.
5	Max Lift Coefficient	The maximum value of the lift coefficient can be found when considering the aircraft on the brink of stall with all high lift devices deployed. The assessment is limited as there will be a change in lift curve slope with Mach number which is not factored into most estimates.	Data is available which considers the effects on lift coefficients due to a variety of high lift device configurations. A range of expected values can therefore be produced: Generic Subsonic Airliner with a Single Slotted Flap & Slat = 2.9 (Anderson, 2005) A300-600 = 2.35 (Filippone, 2006)	Direct calculation from Model Specification data.	Considering both the existing specification and the alternative specification established after the parameter assessment: Existing = 2.9 Alternative = 2.1
6	Drag Polar	The drag polar can be used to find the maximum lift to drag ratio (glide ratio). See row (18) of this table.	Drag Polar tend to be aerofoil specific and hence data is not available for direct comparison.	Appropriate aerofoil selected based on known flight envelope of the aircraft and simulations run to obtain drag polar data.	The process required to generate the data overlaps with previous work on aerofoil data assessment and hence the results can be seen in Appendix M.2 with further information on the aerofoil selection found in 5.4.1.1 Wing Section Redesign.
7	Static Thrust		Airbus Appendix states Static Sea Level Thrust = 120,102 [N]	Direct calculation from Model Specification data.	Considering both the existing specification and the alternative specification established after the parameter assessment: Existing = 111,250 [N] Alternative = 106,000 [N]
8	Specific Thrust	This is calculated as the ratio of thrust to weight using the maximum thrust and weight values.	Airbus Appendix values of MTOW and Static Thrust for the V2500 give a specific thrust = 0.167.	Direct calculation from Model Specification data.	Considering both the existing specification and the alternative specification established after the parameter assessment:

					Existing = 0.247 Alternative = 0.147
9	Thrust Variation with Altitude & Mach Number	Complicated relationships that involve intake and engine component design. They also incorporate transonic phenomena and compressibility effects.	Empirical relationships can have already been obtained from data produced for legacy engines in 4.3.2.1 Code Construction. Data is not available for the V2500 engine specifically.		Direct examination of the model determines whether any variation has been modelled based on the entries in the input file (Appendix K.2). Empirical relationships can form an expected trend.	Existing model appears to contain no attempt at modelling the phenomena. The alternative specification uses the empirical relationships to add the functionality and its effects are visualised in 5.4.2.1 Further Clarification.
10	Specific Impulse	Calculated by dividing the static thrust by the Specific Fuel Consumption – the mass flow rate of fuel calculated from the common equivalent measure of Thrust Specific Fuel Consumption in [N/h of fuel burnt per N of thrust].	V2500 Engine Data gives the value of SFC to be 11.3 [kg/s] and using the static thrust the Specific Impulse = 10,630 [s].		Direct calculation from Model Specification data.	Considering both the existing specification and the alternative specification established after the parameter assessment: Existing = 10,626 [s] Alternative = 10,630 [s]
11	Altitude vs. Airspeed Flight Envelope	Other than aerodynamic limitations, the Flight Envelope is governed by an array of high speed and low speed thermodynamic and mechanical phenomena. More details are provided later.	A comprehensive description of the flight envelope boundaries for the A320 is not available. However, aircraft documentation should contain upper and lower limits for operating speeds. The flight envelope altitude ceiling can be established from the maximum operating altitude of the aircraft = 11,978 [m] (EASA, 2009) with the absolute ceiling being rarely disclosed.	E1 E2 E3	Test obtains data points at limits which can be joined with a polynomial to produce an approximate envelope. Expected envelopes for commercial aircraft can be compared to the data.	Flight envelope data processing takes place in 5.4.2.1 Further Clarification.
12	Absolute Ceiling	The absolute ceiling may be a parameter traded for the service ceiling as both are equally useful in	Figures tend to be available on the service ceiling of an aircraft (Rate of climb < 0.5 [m/s]) or on		The data will be analysed to find the altitude corresponding	This quantity is handled as part of the flight envelope activity on line (11) of this table.

		determining the simulation capability.	the operating ceiling defined by the cabin pressurisation system effectiveness. Realistically, these are the quantities of importance and will be used as a comparison.	to the appropriate rate of climb which defines the ceiling.	
13	Stall Speed	This can vary with altitude, weight, speed and high lift device configuration.	Data is widely available on the landing speed with full flap configuration at a range of weights (Zagoren, 2009). Therefore reverse engineering of the reference value by removing the 1.23 safety factor on the speed should produce a reasonable estimate of the stall speed for this scenario. For MTOW and Full Flaps, Stall speed = 60.2 [m/s].	As in line (3) of this table, stall speeds may be established for a particular weight configuration using direct examination of the model specification data.	Considering MTOW, Full Flap, maximum lift coefficients as in line (5) configuration, the stall speeds are obtained for the specifications: Existing = 45.6 [m/s] Alternative = 68.7 [m/s]. The significant difference in stall speed between the two specifications arises from the initial significant difference in the specified MTOW. The fuel capacity and payload of the existing specification is alarmingly low in comparison to researched data but action is taken to correct this as referred to in the introduction to this summary.
14	TO Distance	The Take-Off distance can be defined in numerous ways. Amongst the official definition given in the airworthiness regulations (FAA, 2009) known as the Take-Off Distance Required there is also the Take-Off Runway Required.	The Airbus Appendix provides a range of typical Take-off distances. However it is unclear which of the distances mentioned in the notes is applicable. In addition there is no configuration data or runway condition description. Take-off distances range between 1,290 [m] and 2,050 [m].	A1 A2 A3	Using the data collected for 'as early as possible take-off', the altitude variation with distance traversed along the runway can be obtained and the distance from brake release to the clearance of 35 [ft] screen (airworthiness definition) calculated.	For the test flights, take-off distance is calculated to be: Flaps Up = 1,429 [m] Flaps Stage One = 1,182 [m] Flaps Stage Two = 1,132 [m] These values seem quite low. Once again this may attributed to the under-specification of MTOW. The differences in the flap stages also correlate with a specification of flap aerodynamic influences for only the first stage. Therefore, the deployment of another stage, as is apparent from the results,

						makes little difference. A retest with a correct MTOW gives improved values between 2,845 [m] and 2,233 [m].
15	Balanced Field Length	Data of aborted take-off distances as well as the take-off distance required with one engine inoperative for a variety of speeds at which the failure occurs allows is required.	The critical speed (known as the decision speed 'V1' varies with flap configuration, weight, slope and other environmental factors. The flight manual data estimates a decision speed for MTOW of approximately 73 [m/s] = 142 [kts]. Balanced Field Length values for airliners are typically in the range 1500 [m] to 2500 [m] (Dassault Aviation, 2008).	C1 C2 C3	The data obtained from the tests should allow two lines to be plotted showing the variation of distance with decision speed. The intersection of the two lines yields a critical decision speed and a Balanced Field Length.	As with the tests for line (14) of this table, the models used contain a correction for the MTOW to ensure the validity of the remaining tests. Data processing is undertaken formally in 5.4.2.1 Further Clarification.
16	Conventional TO Diagram	Linked with ground performance criteria but is absorbed by take-off distance calculations.	Not Applicable			Not Applicable
17	Fastest Climb	With the flaps retracted, it is expected that this performance element should be directly related to the thrust, drag, lift and weight force equilibrium and energy exchange. The rate of climb should be the sustained rate before stall.	Typical rates of climb for commercial airliners are in the range 12 to 25 [m/s] (Filippone, 2006)	D1 D2 D3	Locate the maximum sustained value from the flight data and compare. The Root Mean Square (RMS) method (Weisstein, 2010) is used to obtain an average rate of sustained climb from the data although peak values are given also.	The climb rate expressed by the data is in fact oscillatory. This can be explained by similar logic to the phugoid behaviour discussed in the longitudinal case study; forced high rates of nose-up pitch reduces the speed and therefore lift, which causes the aircraft to pitch down until enough speed is gained to induce further climb. The range covers the variety of weight configurations used for the tests. Existing Peak Range = 18.7 [m/s] to 33.9 [m/s]. Existing RMS Range = 9.6 [m/s] to 22.3 [m/s].

						Testing the alternative specification for MTOW: Alternative Peak = 29.3 [m/s] Alternative RMS = 14.1 [m/s]. Differences between specifications are likely to be linked to the changes in thrust and drag modelling as indicated by the assessment in the appendix.
18	Glide Ratio	This can be obtained easily for aerofoils, but does not take into account the additional drag caused by the rest of the aircraft, not to mention the finite wing itself.	A320 glide ratio depends on the efficiency of the wing design, something which is not available for comparison. However, typical Subsonic Values = 15 to 20 (Filippone, 2006).		From the drag polar computed as part of line (6) of this table, if a tangent from the origin is drawn to the curve. The point of first contact yields the maximum gradient of the tangent which is equivalent to the maximum glide ratio.	Using model specification data to assemble an aircraft drag coefficient for flap and gear up configuration and dividing the lift coefficient by the estimate it is possible to compute a glide ratio. Ideally, in hindsight, a gliding simulation should have been performed to allow easier computation. Cumulative Model Data: Existing = 9.7 Alternative = 16.2
19	Specific Air Range (SAR)	This quantity is computed by dividing the cruise speed by the product of the Thrust and the Thrust Specific Fuel Consumption (TSFC in the units [kg/N.s]) – the amount of thrust for the equivalent weight of fuel burnt.	Although published values for TSFC and cruising speed exist, the cruising thrust of the A320 depends on the drag. In absence of a drag estimate the specific air range for given conditions cannot be computed. Typical published values for this performance measure for commercial airliners are between 6 [m/kg] and 17 [m/kg] at cruise (Filippone, 2006).	E1 E2 E3	For the specification TSFC, and simulated cruise and thrust conditions, a curve can be plotted to demonstrate the variation of SAR with cruise speed.	Differences in the values can only be attributed to the cruise conditions of thrust and speed as the model TSFC is already close to the manufacturer data. The plots are made in 5.4.2.1 Further Clarification.

20	Specific Endurance	The specific endurance considers a variety of cruise speeds by dividing the SAR by the appropriate speed.	The problems with sourcing data on endurance are similar to SAR but using the same source specific endurance values of between 0.03 [s/kg] to 0.08 [s/kg] are expected.		Using the data from line (19) of this table, the endurance curve may be computed.	Developed directly from the SAR, endurance is discussed in parallel in the section following this summary.
21	Landing Distance	Landing distance may be measured from a number of locations – the aircraft crossing the threshold of the runway, touchdown or the moment braking is applied. Also, braking mechanisms are normally a combination of reverse thrust, spoilers, and wheel braking, but with reverse thrust not being available in the simulator, the results may be inconsistent with published values.	The Airbus Appendix shows the variation of landing distance with gross weight. For the combinations used in the flight testing, the landing distances are expected to be within the range of 1,100 [m] to 1,250 [m].	B1 B2 B3	Due to the uncertainty of landing distance measurement, the landing performance will be examining from the instant the aircraft crosses the runway threshold up until the aircraft becomes stationary. Distances can be then be calculated from the data through examination of the plots.	The landing distance is incorporated into the landing performance analysis discussed in 5.4.2.1 Further Clarification.
22	Longitudinal Stability	Case study analysis of the Phugoid Short Period modes of oscillation.	The longitudinal theoretical data for the comparison is in fact a numerical estimate solved by software to assess the accuracy of the mathematical model in the simulator.	D1 D2 D3	There is an option to produce plots for all the perturbation variables for the longitudinal motion. In general, the pitch angle is a good visual indicator that the desired result is obtained.	Conclusions on the longitudinal performance were drawn in the previous case study.

TABLE 5.3: PERFORMANCE ASSESSMENT SUMMARY

5.4.2.1 FURTHER CLARIFICATION

As referred to in the performance summary (Table 5.3), some criteria require further discussion. Each criterion is grouped under an appropriate heading for clarity.

5.4.2.1.1 PAYLOAD RANGE

The linear extrapolation of the data relating to the fuel usage over time for the given cruise conditions allows the generation of first an endurance (flight time until the fuel quantity reaches zero) followed by a range when multiplying by a constant cruise speed. A polynomial fit was attempted in addition to the linear fit but results were unsatisfactory when comparing the polynomial relationship to the actual data. As a replacement, the Breguet Range Equation (BRE) (Equation 5.10) is used to produce another estimate. This is likely to be the most accurate as it is derived from the equilibrium conditions at cruise and captures changes with the decrease in mass.

$$R = \frac{V_c}{C}\frac{L}{D} ln\left(\frac{W_{cruise,start}}{W_{cruise,end}}\right)$$

EQUATION 5.10: BREGUET RANGE EQUATION FOR CRUISE SEGMENT

Equation 5.10 requires knowledge of the cruise velocity V_c, the SFC C, the glide ratio $\frac{L}{D}$ and the ratio of the weight at the start and end of the cruise segment.
There are sources of error in using the Breguet Range Equation. These arise from the fact that in the flight test, the simulation is initialised with fuel at full capacity and the range calculated up to the point of zero fuel. In reality, the equation should use initial and final mass values which take into account the other mission segments of a typical commercial flight (Figure 5.13 – adapted from (Raymer, 1992)). The range determined from the BRE may then be a more accurate value.

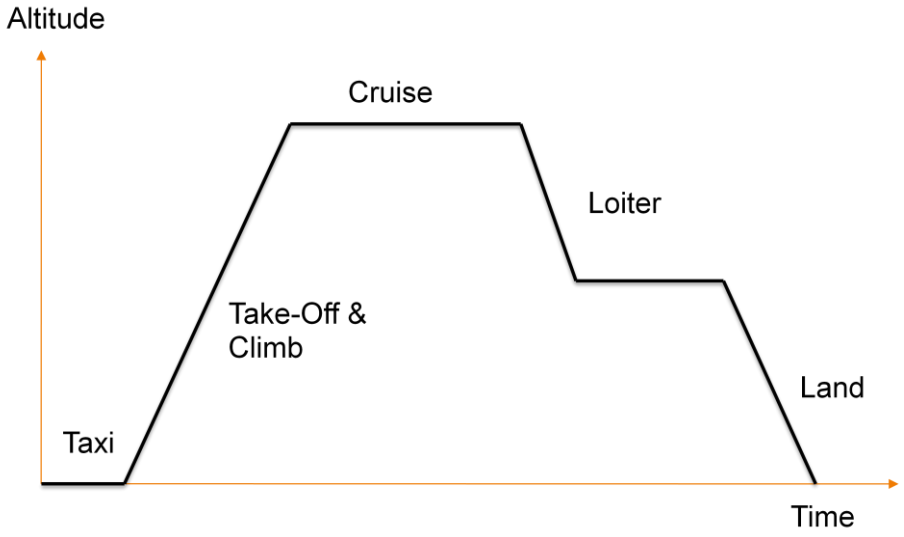

FIGURE 5.13: TYPICAL MISSION PROFILE FOR COMMERCIAL AIRCRAFT

It should be noted that the data from Airbus includes the assumption of a Joint Aviation Requirements (JAR) 3% flight profile. This corresponds to the contingency fuel the aircraft carries, particularly for the Loiter phase of the mission, as described by the Joint Aviation Authorities of Europe. JAR 3% means that this contingency is 3% of the mission fuel. The model weights identified from the model specifications, in combination with the processing code for the BRE (Appendix N.1) produces the ranges used to generate the payload range diagram shown in Figure 5.14.

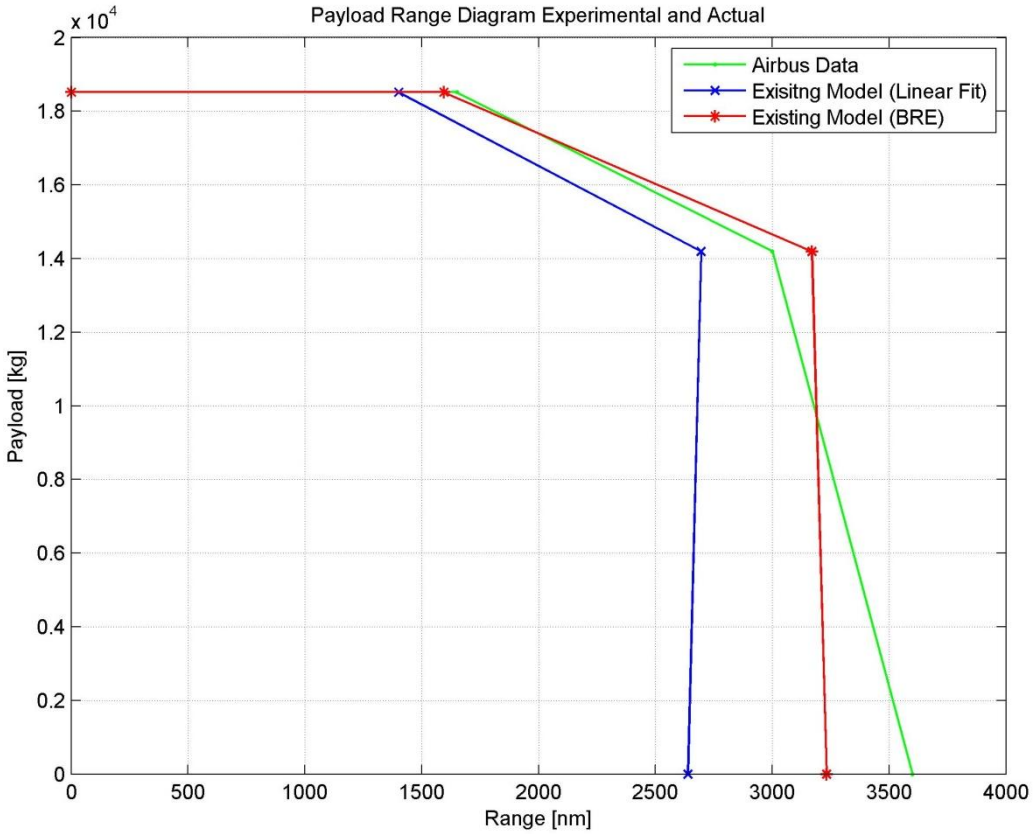

FIGURE 5.14: PAYLOAD-RANGE CHART CONSTRUCTED FROM FLIGHT TEST DATA

It appears as though in the main, the maximum payload range determined by the BRE is acceptable with minor errors being attributed to a misread from the technical appendices (Airbus, 2009). This is expected as the test model configuration makes use of the weights set out by the parameter assessment. The maximum economic range, however, shows some inaccuracy and the ferry range a larger degree of inaccuracy. Potentially, these inaccuracies may arise from the either flight conditions, including the cruise programme selected, or the way the simulator incorporates payload or models fuel burn.

Cruise programmes set out altitude and speed settings for the cruise segment. As the weight decreases, the pilot may maintain performance of the aircraft by climbing higher. The increase in altitude allows the use of less thrust and improves fuel economy. If the airbus ranges are computed for continuous or stepped climb profiles, it may explain the relatively low values for the simulation results as it was assumed the altitude and cruising speed remained constant throughout the cruise. However, the ferry range is calculated as being almost the same as the maximum economic range. It can therefore be concluded that the removal of just over 14,000 [kg] of payload makes little difference to the fuel consumption at a constant speed and altitude calculated by the simulation. This behaviour is corroborated by the data itself as the thrust setting for both scenarios are very similar. This appears to raise a concern about the drag and lift modelling which will be discussed later in 5.4.3 Identified Simulation Limitations.

5.4.2.1.2 LANDING PERFORMANCE

Admittedly the data recorded from the flight tests is below the standard required for a robust assessment. The lack of a pilot able to consistently repeat landing procedure has resulted in disagreeable trends in the data. Specifically, it is expected that landing speed should be higher for a higher weight due to the increased lift requirements for a given decent rate. Unfortunately, the simulation data demonstrates successful landings at speeds greater or less than the estimate values with no identifiable trend with aircraft weight. However, since the landings are successful, it can be concluded, assuming the crash trigger in the simulator is accurate, that the landing speed is appropriate for landing in the real aircraft.

The landing data does provide some interesting insight into the near-ground or on-ground behaviour of the aircraft. Using landing data restricted to consideration of the aircraft performance from the runway threshold to the simulation termination when the aircraft becomes stationary, the speed at the threshold and at touchdown may be found. In turn comparing the estimate of speed ranges to the expected values from Table 5.3 allows a reasonable assessment of the accuracy of the simulation. Furthermore, the distance measured from threshold crossing up to aircraft halting provides an indication of aircraft landing distance. Table 5.4 summarises the determined values.

Performance Aspect	Expected Range	Simulated Range (Runway Threshold Crossing)
Landing Speed [m/s]	56 to 61	56 to 65
Landing Distance [m]	1,100 to 1,250	607 to 1,026

TABLE 5.4: LANDING PERFORMANCE DATA

It is clear from Table 5.4 that although the landing speed appears in an acceptable range, the landing distance is lower than anticipated. In order to investigate this, the manipulation is taken a step further. A key portion of the landing distance is attributed to the distance required to slow the aircraft to a stop on the runway after touchdown. The deceleration performance of the aircraft over the runway length depends on the type of decelerating devices available to the pilot and the effectiveness of each of these devices. The simulator and model are restricted to allowing only spoilers and foot braking as methods of deceleration. The foot brake is controlled by a discrete switch and applies a constant braking force of a magnitude specified in the input file definition. In reality, foot braking magnitude varies and in a large number of aircraft is controlled by the amount of depression of the toe-end of the rudder pedals. The impact of this limited deceleration control on the landing distance is significant. Consider the change in velocity with the distance travelled by the aircraft from crossing the runway threshold (Figure 5.15). The spoilers are applied at approximately the touchdown location followed or preceded by the application of the brakes.

It is clear from the graph that the velocity variation can be divided into two distinct sections: The approximately linear section of the aircraft decelerating due to throttle back and ground contact and the more rapid deceleration section that can be attributed to brake application. *Note: The exact moment of brake application cannot be confirmed as the simulator data logger does not record a brake sensor.* It follows that a possible reason for the lower than expected landing distance is due to the higher than expected braking ability of the aircraft. This observation also serves to re-evaluate the braking specification as part of the parameter assessment results in Appendix M.1.

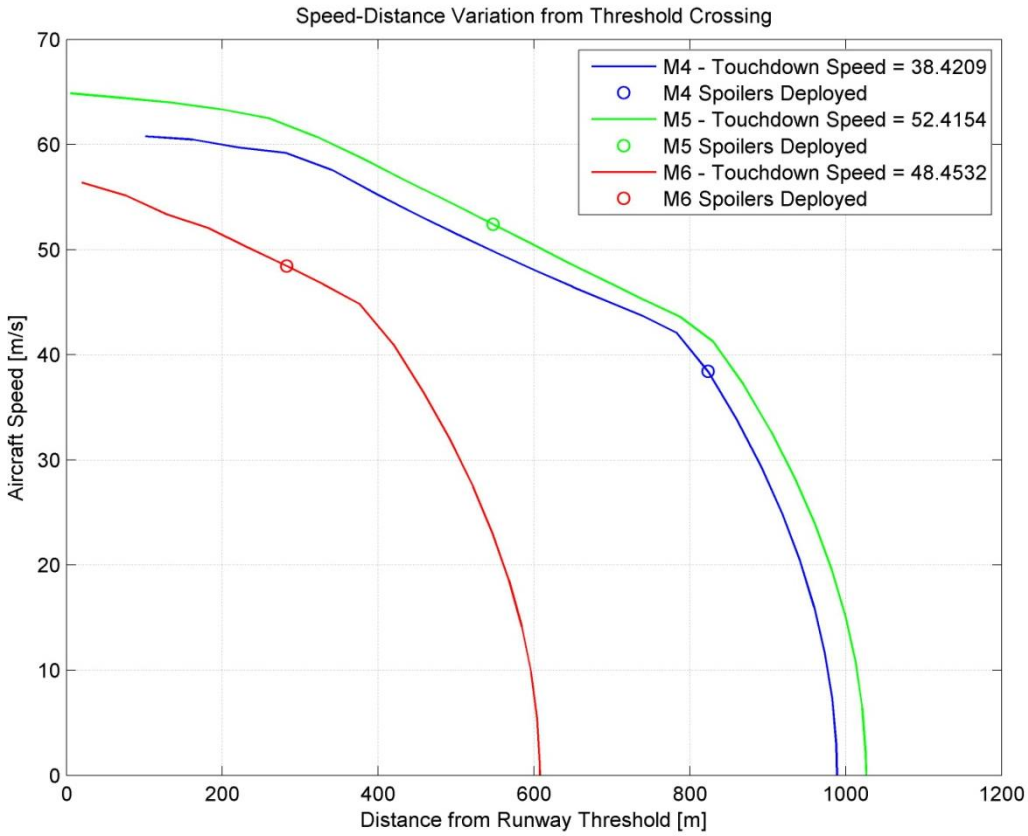

FIGURE 5.15: LANDING DECELERATION CONSIDERATION

5.4.2.1.3 THRUST VARIATION

The empirical variation in thrust with altitude and Mach number (mathematically expressed in Equation 4.26 and Equation 4.27) can be visualised as in the following figures. Equation 4.27 is reliant on a relationship between SFC and Thrust, the reason for its exclusion from the modelling work of earlier. However, the variation has been plotted by others, specifically for turbofan engines of a variety of bypass ratios (Figure 5.16). The thrust variation with altitude however is directly visualised from the empirical relationship (Figure 5.17).

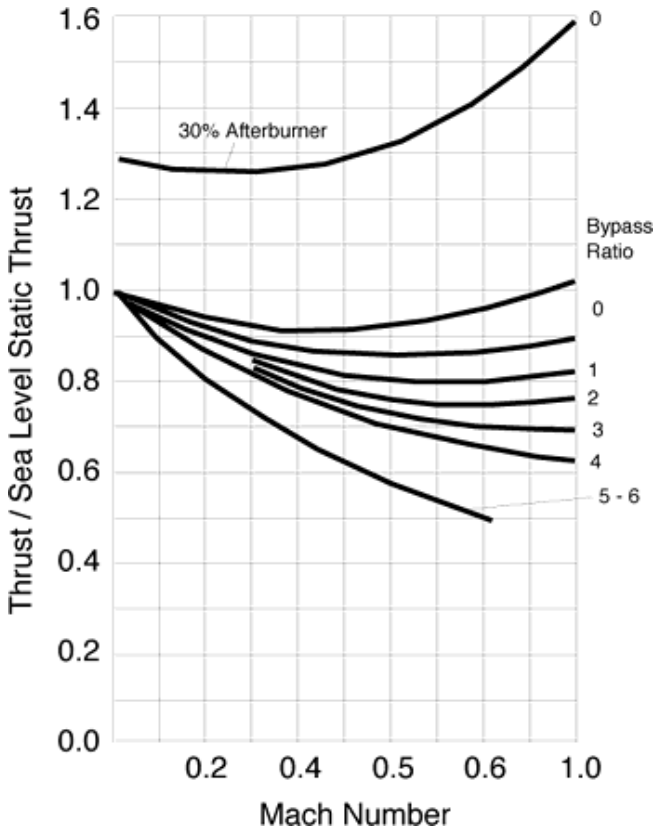

FIGURE 5.16: RELATIVE THRUST VARIATION WITH MACH NUMBER (KROO & SHEVELL, 2006)

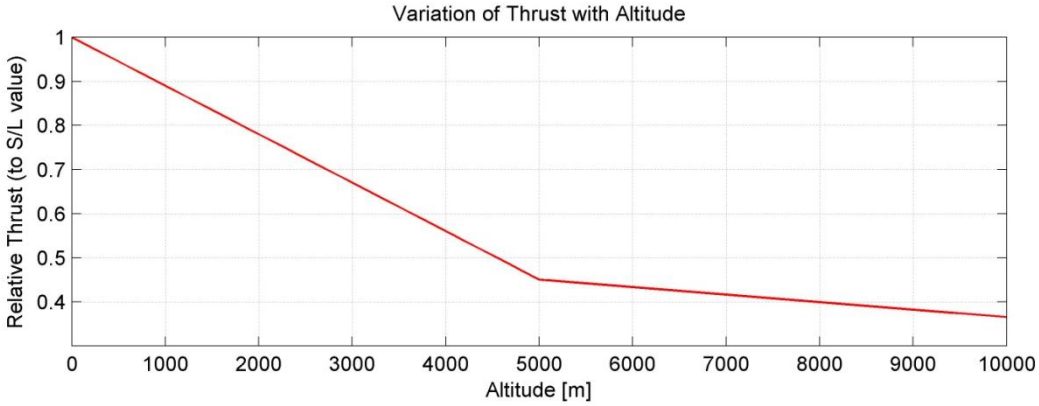

FIGURE 5.17: RELATIVE THRUST VARIATION WITH ALTITUDE

5.4.2.1.4 FLIGHT ENVELOPE

The flight envelope established from the simulator data is shown in Figure 5.18 in relation to the known limits for the A320 dictated by the maximum operating speed and altitude of 11,918 [m] and 350 [KTAS] (EASA, 2009), where KTAS is the unit of Knots True Airspeed. The stall limits are calculated from the specification values using the definition of the lift coefficient and assigning the lift equal to weight for the limiting condition.

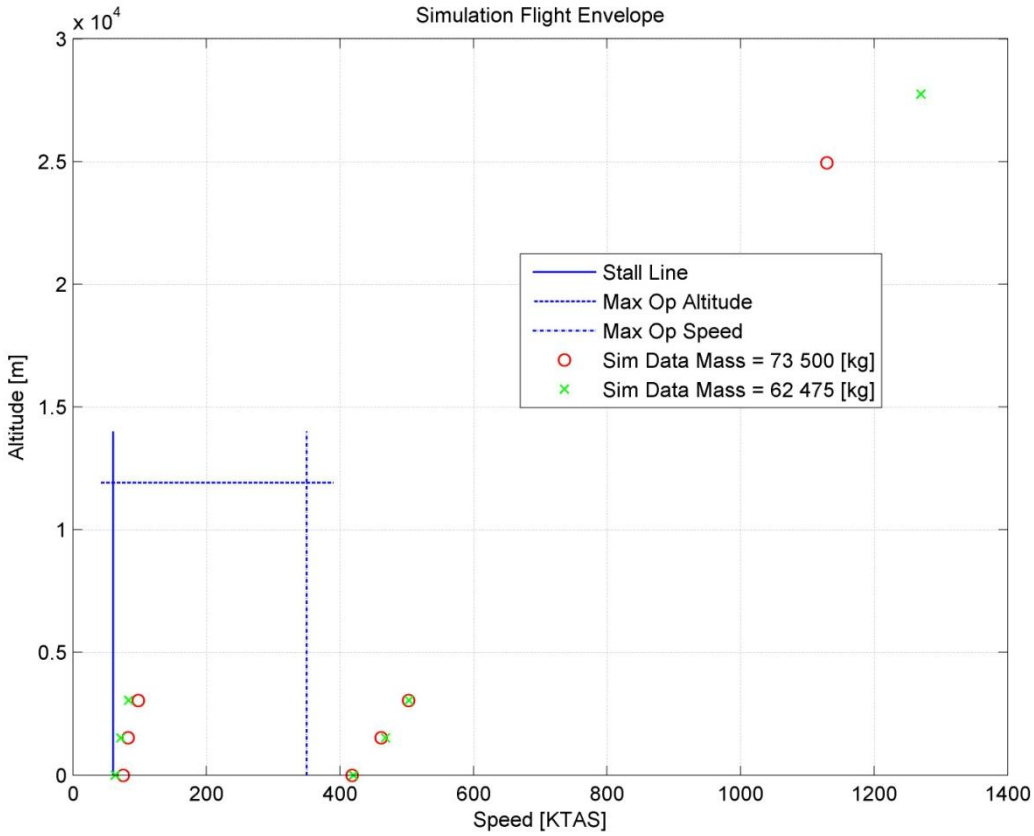

FIGURE 5.18: SIMULATION FLIGHT ENVELOPE

It is clear as suspected that the simulator is incapable of modelling the physical effects which limit the flight envelope in reality. In particular the operational ceiling is significantly exceeded. Even neglecting the relatively small discrepancy between the cabin-pressure-limited operational ceiling and the thrust-limited absolute ceiling, the limit for simulation is expected to lie within a suitable range. An explanation for this centres on the excess of lift force at the operational ceiling and is related to the previous point regarding thrust lapse. Clearly in order to achieve such altitudes and speeds there must be an imbalance in the equilibrium forces visualised as acting as in Figure 4.6. In accordance with Equation 4.5 and Equation 4.6 the drag and lift forces both increase with speed but through the density decrease with altitude for a constant lift coefficient as lift and drag are related through Equation 4.15. The incorporation of thrust lapse should serve to limit the excess thrust to drag and prevent excessive acceleration due to thrust. In conclusion, therefore, it can be assumed that the lack of thrust lapse inclusion into the model is one possible explanation for the excessive acceleration and hence climb performance.

Examining the distribution of data points collected at lower altitudes, the simulator stalls at speeds higher than the predicted limit even with full flaps extended. This may be caused by inaccuracies in the aerofoil data file or the flap specification, although a reduction in mass of the aircraft can extend the envelope as indicated by the simulator data. Furthermore, the general trend of the data suggests an increased value of stall speed with altitude which is consistent with a decrease in density and the shape of the generic envelope of Figure 5.5.

Other than stall, the extension of the top left of the envelope may be limited by engine surge. This phenomenon is related to the thermodynamic performance of the axial compressor of the jet engine. A reduction in the free stream velocity, through a reduction in the aircraft speed, reduces the mass flow rate of air through the compressor. When the mass flow rate decreases below a critical value related to the stability of the compressor operation the air flow over the compressor blades separates and the blades stall. The compressor loses the ability to work on the flow and ceases to increase the pressure. The air flow reverses through the engine resulting in a complete loss of thrust and potentially irreparable damage to the engine.

Aerodynamic heating, transonic drag rise and wing flutter are typical limitations to velocity

increases beyond the maximum operating speed – the right hand limit to the diagram. Aerodynamic heating is the consequence of a stagnation temperature rise of incoming flow brought to a halt by the aircraft obstructing the flow. The flow energy is dissipated in the form of heat when heats the airframe. At large speeds, the temperature can exceed the melting point of the airframe structure resulting in failure. The transonic drag rise is a divergence of drag from the typical subsonic value due to the introduction of supersonic regions of the flow. The associated phenomena, including shockwaves manifest themselves as a drag increase. This is likely to contribute to limiting the speed. Finally, wing flutter is the amplified, aeroelastic oscillation of thin structures such as the wing, tail and fin induced by vortex shedding from the trailing edge of the surface. The complexity of these phenomena is not to be underestimated and modelling in any capacity would be incredibly involved.

Other than the thrust lapse, all the limitations discussed above are not able to be modelled to any extent in the current capabilities of the Merlin software. However, in the absence of these models, it is suggested that the simulation should cease or issue a warning when its validity is called seriously into question as is true for other commercially available flight simulators such as Microsoft Flight Simulator where crash triggers detect speeds beyond the overspeed limit of the aircraft.

5.4.2.1.5 BALANCED FIELD LENGTH

The balanced field length curves are computed using quadratic fits as an approximation to the expected trend of the data. Establishment of the decision speed is taken from the time of engine failure plus 2 additional seconds of pilot reaction time; establishment of the required distances for landing abortion considers the runway length traversed up until stop; establishment of the continued take-off distance requires examination of the data file to determine the horizontal distance at which the aircraft climbs out past 35[ft] – the critical value given in the Airworthiness Standards (FAA, 2009) for take-off performance OEI. The resulting graph is shown in Figure 5.19 where the crosses indicate the data points recorded in the simulator. The critical decision speed is recorded as being 141 [kts] with a Balanced Field Length of 2235 [m].
The values agree with those predicted in line (15) of the performance summary. Although this appears to validate the simulator take-off performance, Figure 5.19 is deceptive. The distance from brake-release is measured in a direction parallel to the runway centreline. In reality, during the test, due to the yaw induced due to a thrust imbalance between the right-hand and left-hand sides, the aircraft veered off the runway. This is not acceptable practice in the real world and occurred in the simulator despite the best attempts of the pilot to apply full corrective rudder through the pedals. Therefore, the curves in Figure 5.19 should be higher up the chart increasing the balanced field length of the aircraft, potentially out of the acceptable range.
The inability of the aircraft to correct the adverse yaw induced by the OEI scenario raises questions about either the modelling of the rudder or the control mapping in the simulator mathematical model. In aircraft design, the rudder is sized to provide enough corrective aerodynamic force in the event of an engine failure at the critical decision speed. If the specification data is inappropriate for the A320 fin and rudder then this may explain the lack of rudder effectiveness. Alternatively, as the simulator directional control hardware is limited to pedals only, it can be assumed that the software governing the transition between nose wheel control and rudder control is preventing adequate directional manoeuvrability.

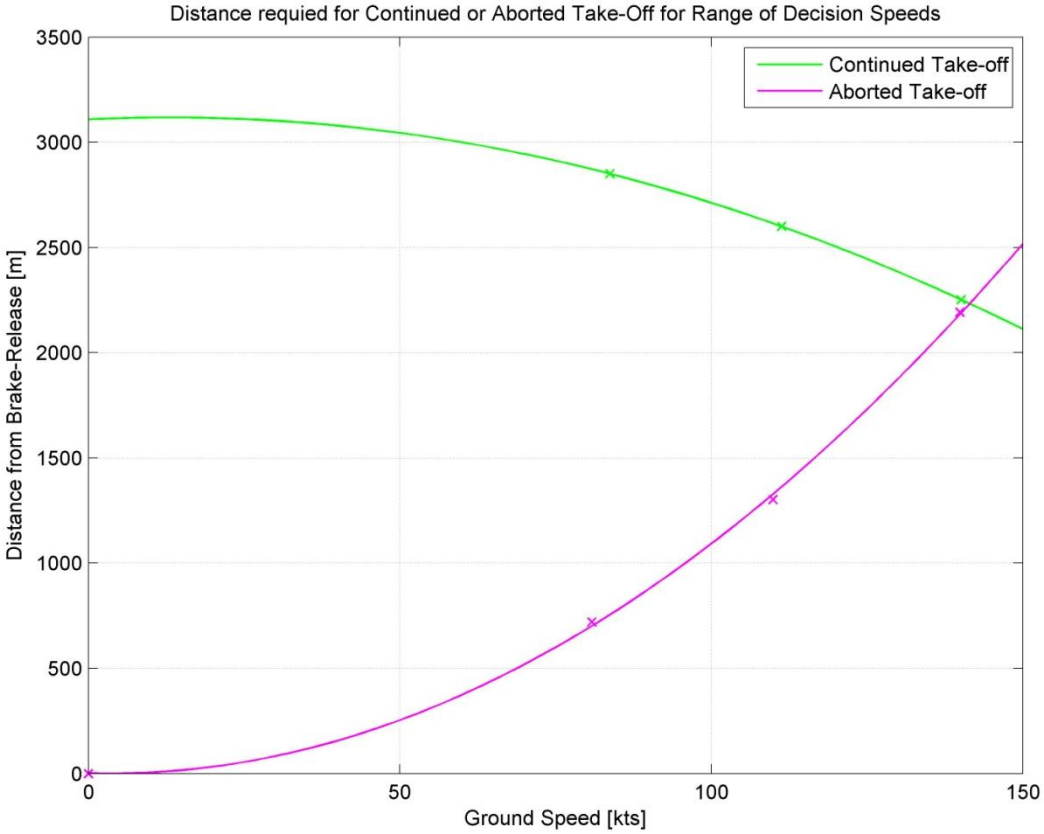

FIGURE 5.19: SIMULATED BALANCED FIELD LENGTH

5.4.2.1.6 SPECIFIC AIR RANGE & SPECIFIC ENDURANCE

The simulator data, processed using the code of Appendix N.2 generates the plots shown in Figure 5.20 and Figure 5.21. As expected, a heavier aircraft does not fly as far or for as long due to the increased thrust required to maintain the given cruise altitude. However, the ranges of values over which the data is distributed are low for both the SAR and the Endurance. This suggests that the simulator, assuming the fuel consumption has been correctly modelled, requires a higher thrust setting than anticipated at a given speed. In addition, the trend of the data for the SAR is in the opposite sense to that expected. According to the recorded data, the range of the aircraft decreases with increasing flight Mach number. Literature data suggests that the specific range for a given cruise altitude peaks at a minimum drag cruise speed. This speed is generally a design speed for the aircraft at cruise. The trends in the simulator data suggest therefore that the minimum drag of the aircraft at the given cruise altitude is less than the limit of the scale of the chart (currently Mach 0.7) which is unrealistic as the known cruise speed of the A320 is approximately Mach 0.85. Inconsistencies in the drag modelling of the aircraft are likely to produce inaccuracies as through manipulation of the original definition given the summary table, the SAR is in fact inversely proportional to the drag. For proof of this interpretation of the SAR expression, see (Filippone, 2006).
Finally, an anomalous test is identified. This data is duplicated from an earlier test (A1a – see Appendix H.1) which mimics the cruise speed and weight configuration required for the endurance and range test (E1a). Closer examination of the data shows a difference in incidence and a gradual climb throughout the test with significantly different thrust settings. These differences serve to upset the conditions required for the endurance tests and may be the cause of inaccuracies in the range data of line (1) of the performance summary as well as in these tests.

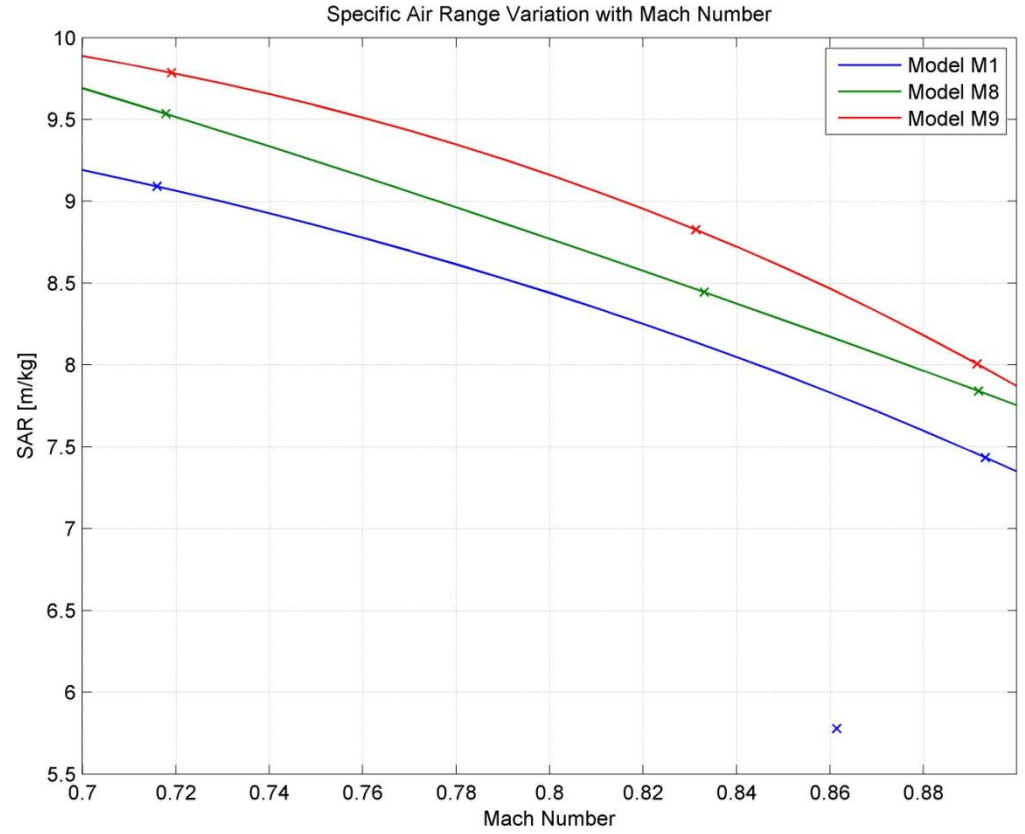

FIGURE 5.20: SIMULATED SPECIFIC AIR RANGE VARIATION WITH CRUISE MACH NUMBER

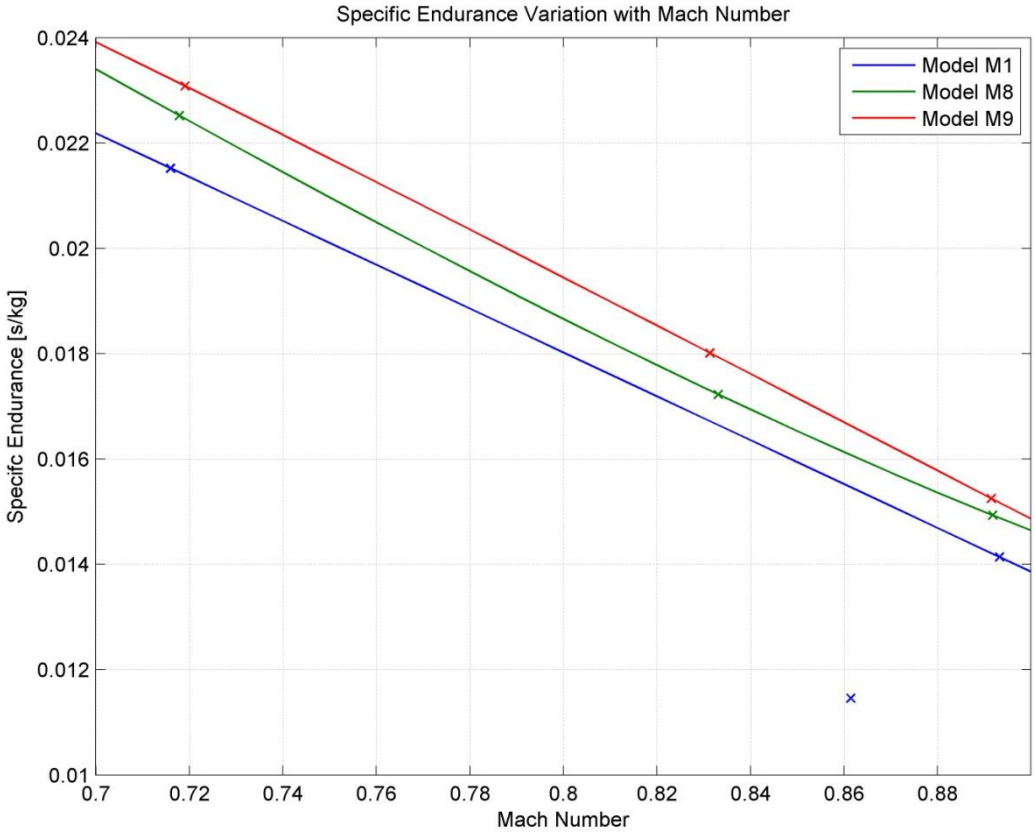

FIGURE 5.21: SIMULATED SPECIFIC ENDURANCE VARIATION WITH CRUISE MACH NUMBER

5.4.2.1.7 LONGITUDINAL STABILITY

The final performance area of focus is the longitudinal stability response. The tests performed collected response data corresponding to a selection of weight configurations. As indicated by Equation 5.2, the longitudinal response is described in full by the four state variables. Retaining this convention, the data from the simulations are consolidated (Figure 5.22).

The first thing that is apparent from Figure 5.22 is the fact that the data is difficult to read at the beginning of the test. This is due to both the relatively small magnitude of the short period response in comparison to the phugoid as well as the relatively large magnitude of the elevator displacement impact. It should be noted that due to limitations associated with ensuring replication of the response inducing input, the magnitude and duration of the elevator itself varies between 7 and 17 [deg] over 4 to 5 [s].
The short period mode is barely distinguishable. Although this seems appropriate to the scale of the plots, the short period data only consists of a small number of data points joined linearly. This is a deficiency of the flight test data logging. The E1 tool allows data capture at three different rates; 1 [Hz], 5 [Hz] and 25 [Hz]. The default setting is 1 [Hz], or one data point captured every second. The dynamics of the short period oscillation are in general faster than this rate and hence in order to obtain data to allow effective visualisation of the mode, the data capture rate needs configuring appropriately. This is an oversight at the planning stage of the flight test programme and will cost accuracy when the data is cross examined against other sources later.
Another potential impact on the accuracy of the response is the presence of a specification setting known as ‘dynamic actuation’. During the specification, in the E1 specification editor, of the control systems present in the aircraft, the tool provides an option of whether to activate the dynamic actuation system. Dynamic actuators are the result of a model within the simulator which mimics the behaviour of an electronic control system attached to the actuation system for the control surfaces. The control system attempts to smooth out sudden perturbations by inducing small control surface movements as appropriate. This has the effect of reducing the impact of elevator input and further reduces the magnitude of the short period oscillation. Once more, in hindsight, this setting could have been disabled. The simulator data used for the comparison in the case study however, did have this function disabled.
The overall magnitude of the quantities on the plots varies from those theoretical values found in Appendix J.6.1. This is explained by the difference in measured quantities. The theoretical calculations pay no heed to the initial trimmed conditions but consider perturbation quantities; the disturbance from trim is the value given. When considering Figure 5.22, the quantities used are the absolute values, taken from the simulator output file.
Finally, the period of the phugoid varies with the aircraft mass. This on first glance appears confusing as the Lanchester approximation given by Equation 5.9 does not contain a mass or weight term. However, when considering the trim conditions at the beginning of the test, it is possible to see that the values of free stream velocity are different. This is directly due to the mass as a larger mass results in a larger weight force needing to be balanced by a lift force that is proportional to the square of the free stream. Specifically, the effect of this trim velocity on the period of the phugoid according to the simulator data is illustrated by Table 5.5.

Trimmed Velocity [m/s]	Phugoid Period Time [s]
158.4	71.7
129.0	58.4
123.4	55.9

TABLE 5.5: FLIGHT TEST TRIM VELOCITY AND PHUGOID PERIOD TIME

Validation of the physical model developed in 4.5 Physical Modelling of an Aircraft is possible in parallel to validation of the simulator performance by considering the mode frequency and damping ratios. These calculations make use of Equation 5.6 to Equation 5.8 inclusive and incorporate the data from Table 5.2 also. The resulting values are summarised in Table 5.6.

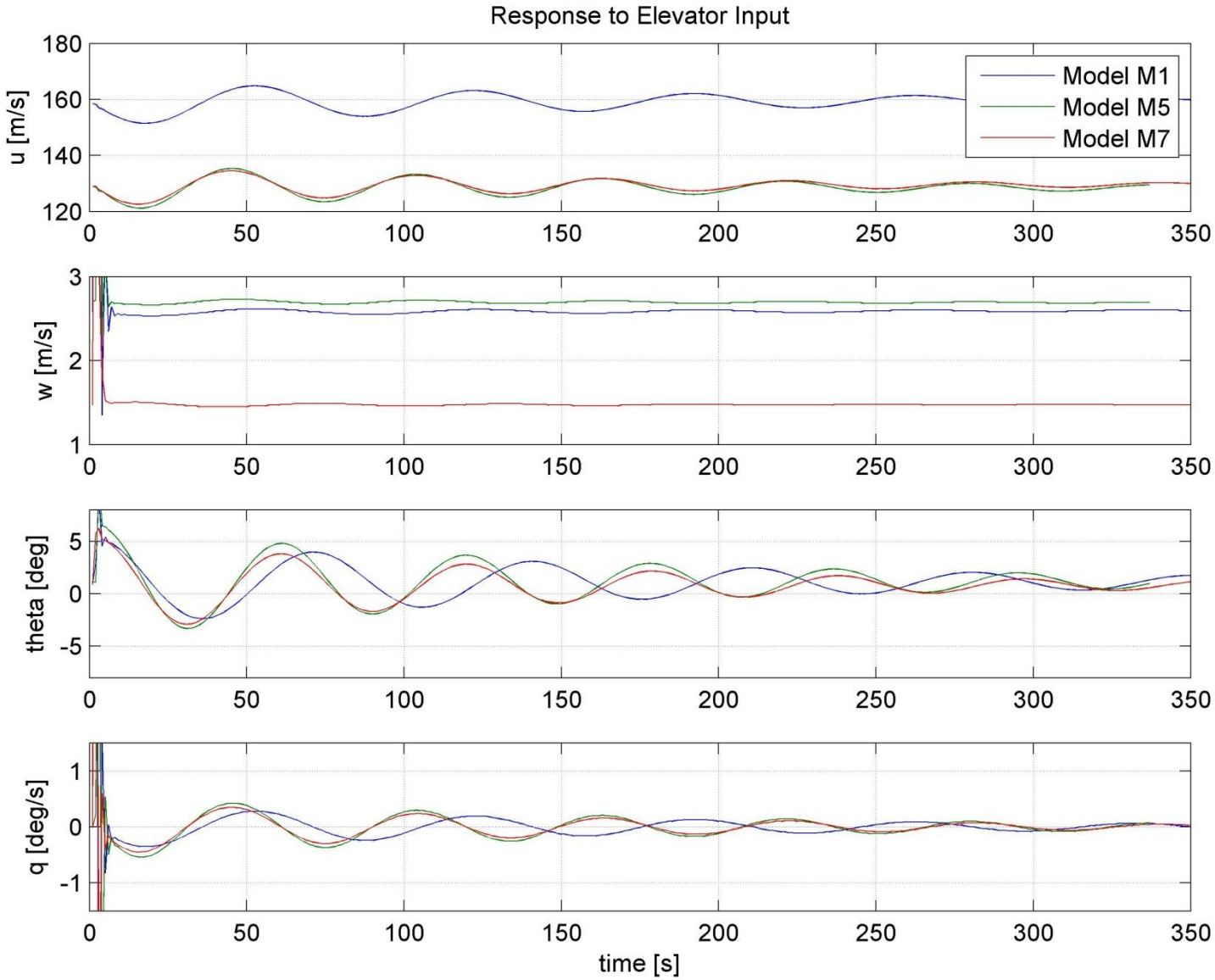

FIGURE 5.22: LONGITUNDINAL RESPONSE FROM SIMULATION

Source	Short Period Mode		Phugoid Mode	
	Frequency [rad/s]	Damping Ratio	Frequency [rad/s]	Damping Ratio
Sim Data Model M1	3.142	0.3077	0.0911	0.0404
Sim Data Model M5	3.142	0.3969	0.1083	0.0427
Sim Data Model M7	3.142	0.2850	0.1083	0.0478
Physical Model	3.396	0.2025	0.0614	0.0227
Theoretical Calculation	3.861	0.3360	0.1076	0.0511
Sim Data Alt Spec	3.142	0.3623	0.0722	0.0510

TABLE 5.6: LONGITUDINAL VALIDATION SUMMARY

With regards to the values in Table 5.6, the frequencies of the short period mode for the simulation data are identical owing to the lack of precision of the data points due to the coarse logging rate of only 1 [Hz]. Also when comparing the phugoid mode, the physical model shows signs of inaccuracy, most likely due to the approximations made during its construction. Admittedly, more work is required to diagnose and repair the model. Otherwise, the simulator data appears to agree with the other longitudinal studies adequately. Low damping ratios for the flight tests on the existing specification do not corroborate with the testing performed on the alternative specification and hence this suggests that the source of the under-damping originates in the model specification as opposed to the simulator software.

The success of the performance analysis is limited primarily by the quality of the data extracted from tests and the details of the real world data obtained from research. There are naturally inadequacies generated through the specification and execution of the test programme.

5.4.3 IDENTIFIED SIMULATION LIMITATIONS

It can be speculated that any unexpected results of the performance analysis may be attributed to a combination of erroneous simulator behaviour as well as model specification errors. Some flight tests give the impression that the simulator possesses a number of inadequacies. These arise in various forms from hardware limitations to software approximations. It is recommended that future, more focussed analysis be undertaken to provide a definitive assessment of the simulator based on the conclusions derived by this investigation. Limitations identified by this study include:

- Lift & Drag Modelling:
  The modelling of lift and drag is currently within reasonable limits according to the performance summary but when considering the format of the parametric specification the lift and drag integration is far from accurate. In E1, the wing is modelled as having a constant cross-section and zero washout. These options are key characteristics of the wing and prevent generalisation of the wing performance over the span which furthermore is not governed by the span loading (Oswald efficiency) factor e which would allow some control to be exercised over the three dimensional effects. Granted, the factor is intrinsic to a number of specified parameters such as the lift induced drag factor but external control would be preferable to ensure a more accurate specification of the lift and drag force application locations as well as the estimation of the downwash of the wing through vortex consideration.
  Noticeable was the lack of excess thrust on encroachment into transonic Mach numbers. This suggests that the mathematical model within the simulator does not acknowledge, or does not correctly model, the impact of the transonic drag rise. Drag seems to be calculated from the summation of specified dimensionless coefficients for landing gear, fuselage, wing, tail and fin. This is a reasonable drag estimate. However, at transonic speeds or higher, further drag factors are introduced due to the presence of shockwaves. This ‘wave drag’ is responsible for the drag divergence at large Mach numbers and

serves as a barrier to supersonic flight. The drag force is not recorded by the simulator output file and hence in order to investigate the variation in drag over a variety of speeds, further testing is required.
Finally, directly related to drag is the thrust and hence the fuel burn. Performance criteria tests designed to extrapolate fuel burn data for given cruise conditions were necessary to compute aircraft range. It was noted that the fuel burnt recorded within the first two minutes of flight responded in a step change in fuel quantity recorded by the output file. This is attributed to the restriction of the data recorder precision to only a single decimal place. However, once a linear fit had been preformed the gradient of the fuel burn lines collected from the tests was not as expected. The only variables intended for the range of tests performed were mass and as a direct consequence, the angle of attack. Therefore a direct relationship between mass and fuel burn was expected but data analysis showed that the relationship was not so. This may be a fault in the calculation of the drag but may also be attributed to the simulator initialisation discussed later.

- Known Structural Limits:
  In addition to weakness of the barrier to supersonic flight, the flight envelope of the aircraft suffers at most of its boundaries from an absence of reality. The complexities of the flight envelope limiting factors are discussed in the further clarification of the performance criteria assessment. Structural limits can be included through the integration of 'never exceed' forces or speeds into the crash simulation termination logic.

- Control Systems:
  The simulator links a movement of the control stick (including thrust levers) with proportional response of the machine being controlled be it a control surface or an engine. More intelligent relationships between the pilot controls and the actuating device mimics reality more closely. For example, the roll control of the model specification tested in the flight test programme is seen as being too responsive, particularly at high speed. This is due to the roll control being provided by outboard ailerons at all speeds – something which in reality is avoided due to the high stresses on the wing. In the absence of structural limitations being included, as referred to by the previous bullet, this behaviour is allowed. In reality, the control system locks out outboard ailerons above a speed threshold and roll control is reverted to inboard ailerons. Furthermore the engine control is simplified to a time delayed response, which, inferred through existing knowledge of engine control systems, is inaccurate.
  Although these issues seem like technicalities, the behaviour of the aircraft's control systems has a large bearing on its performance and the impact should not underestimated.

- Simulation Initialisation:
  The process of initialising the simulator requires the specification of altitude, heading and speed. The simulation then calculates the approximate values of elevator trim necessary to maintain these conditions in equilibrium. It was observed that in numerous cases, the trim value established at the beginning of the simulation was outside the valid range for the trim tab travel; if trim is changed by the pilot from the initial value, the condition can no longer be replicated as that value of trim could not be selected by the pilot. This suggests a software malfunction on initialisation and may harm the validity of the flight tests.

- Flaps, Spoilers, Brakes & Reverse Thrust:
  Systems responsible for a controlled increase in lift or drag are critical, primarily for the achievement of landing or aborted take-offs. It follows that simulator limitations in these areas impact the performance of the aircraft being modelled.
  Firstly, the cockpit hardware comprises a 3 way switch for flap control. Not only is this

inappropriate since the E1 editor allows specification of 4 flap stages (part of the model specification is rendered redundant by the cockpit hardware) but also many larger aircraft have more than 3 stages. Including the flaps being completely retracted, the A320 has 5 flap stages. All previous flight tests involving the flaps therefore can be regarded as being inaccurate as the flap modelling is limited by the simulator.
Furthermore, the flaps are limited to consideration of all devices as a single entity and as a result all information provided in the specification requires prior averaging which reduces the ability to specify an accurate model.
The simulator hardware that controls thrust input consists of two throttle levers. These levers are non-detachable and hence the throttle unit is limited to sending only two signals to the mathematical model – thrust for a right and left engine. There are throttle devices in existence which are accompanied by alternative lever configuration hardware and are programmable by the user to allow the replication of most combinations of throttle and engine control levers and their functions. Installation of such a device would remove the restriction on configuration imposed by the current simulator.
Reverse thrust is a notable absentee amongst the decelerating devices on the ground. The existing throttle levers are mapped to allow positive thrust only. This limits the deceleration performance of the aircraft and affects such criteria as the landing distance and balanced field length. Reverse thrust is a capability which could be provided by shifting the throttle lever mappings in the input file specification to allow a reverse trigger region at the lowest extent of the lever position. Whether the mathematical model would accept such a modification has not been investigated. However faithful modelling of the function is a much more complex task. Engine control systems provide reverse thrust by considering a number of sensed parameters to ensure safe deployment. One known case of reverser actuation requires a thrust lever interlock to be employed to prevent reverser door damage through hasty deployment by the pilot. The lock prevents lever movement which would increase thrust until the doors are clear. Such a function would not be possible to replicate using the current hardware.

- Directional Control:
  Dangerous behaviour is observed when simulating an engine failure during take-off. The Excalibur software allows the triggering of an engine malfunction at any given time. Testing has shown that even with realistic rudder and engine specifications, the adverse yaw resulting from an engine failure is not correctable by full rudder. It is speculated that software controlling the exchange of rudder control for nose wheel steering control through the cockpit pedals is not configured in a manner that replicates reality. This issue may come down to a weakness in the input file specification but increased clarity and sophistication when considering the transition between the two allows an improvement in the validity of degraded take-off tests.

- Data Logging:
  Finally, the output file compiled by the simulation data acquisition software acts as a flight data recorder and records a significant number of dynamic parameters over the simulation duration. It is restricting, however, when the choice of recorded parameters does not include the status of all cockpit hardware. Brake application and engine malfunction are not recorded which prevents the complete capture of ground test behaviour. Moreover, the precision of the recorded parameters varies, reducing some to a single decimal place which is not always appropriate for accuracy.

The above list documents those limitations that became apparent during the use of the flight simulation equipment. Others are likely to exist. As observed when constructing the earlier development models as part of this project, the statement of a model's purpose and limitations is paramount to the user. Clear definition is necessary to ensure the most efficient and effective use of the facility can be made.

5.4.3.1 E2 MODEL DEFINITION

During the project, an update to the software tool was released referred to henceforth as ‘E2’. Alterations to the software of interest to the project include modifications of the mathematical model in the simulator and hence the editor tool. Due to the immaturity of the new software, no project work is undertaken using its capabilities. However, a number of benefits may be gained by the future use of the software.

One of the primary features of the new software is the redefinition of the wing, tail and fin representation. Represented by prefabricated surfaces in E1 customisable to a limited extent by the parameter specification, the E2 tool allows full customisation of fewer or more arbitrary surfaces and does not fix the aircraft configuration in this respect. Fins and wings are specified by the user through declaration of the location and geometry of vertical or horizontal panels. A complete component such as a wing may be specified by more than one panel with each panel allowing the definition of leading edge, trailing edge or upper surface devices such as slats, flaps and spoilers. This method therefore allows the option to vary the aerofoil section over the span as the aerofoil data is specific to a panel.

In addition to high lift or lift dump devices, the panel may also be equipped with additional control surfaces, for example ailerons. Complimenting such an option is the added functionality of control surface speed scheduling. This allows the locking-out of certain control surfaces at higher speeds as is common in practice. For instance, once the aircraft accelerates beyond a set limit, the roll stick inputs will revert to actuation of the inboard ailerons with the outboard ailerons being inert.

One final item to highlight is the advancement of control system behaviour. There is provision for trim tab control as well as customisable parametric polynomials to allow definition of non-linear relationships between control stick displacement and control force. Additionally, the control inputs may be mapped directly onto movable surfaces on individual panels giving greater control over the control system architecture. A visual tool is available to allow the simulation of surface movements with stick displacement without the need for initialisation of a full scenario.

There is also an additional placeholder in the specification to allow the definition of a rotor, enabling the possibility of helicopter specifications.

These modifications increase the flexibility of the specification as well as going some way to addressing the many geometrical approximations made in existing E1 specifications as identified previously.

6 CONCLUDING REMARKS

The project work has allowed the formulation of conclusions throughout which are based on the technical knowledge acquired. However, in order for the project to be deemed an academic success, the learning objectives set out in the original proposal need to have been met in full as these are essentially the agreed minimum requirements. Appendix O returns to the learning objectives and assesses their status. In reality, as a result of hidden project merits, the learning exceeds that covered by the learning objectives.

This project has produced a functional 3-degree-of-freedom mathematical model which has been replicated in lower level software code. A physical model has been completed and interpreted to allow three-dimensional visualisation of the aircraft it represents. Data has been captured from these models and their execution and validated through comparison of their responses with a specified longitudinal dynamic scenario. The mathematical model has been compiled and executed in real-time with data in agreement with non-real time execution. The strengths, weakness and limitations of the models have been recognised and discussed during development. The application of current and new knowledge on the subject of aircraft dynamics through modelling has served to cement the vast amount of learning necessary to carry out the activities.
The existing flight simulation capability at the University of Manchester has been explored and assessed and speculation has been made regarding its limitations in a summary of validation activities. The resources have been used as intended to generate flight data which served to supply alternative sources of validation data as well as to assist in self validation of the equipment.
Prior to project commencement, it was recognised that the knowledge required to carry out the project work was not yet in place. Although the physical results have so far been mentioned, perhaps the largest product of this project is that which is intangible. The continuous acquisition of knowledge from beginning to end has resulted in an understanding of flight dynamics, modelling and simulation that has already been recognised as being highly transferrable; the familiarisation with topical resources such as reference books and software already seeing application in parallel projects. Ultimately, the project has allowed the realisation of the role of all programme areas of study in aerospace engineering and has highlighted the importance of general understanding.

6.1 LESSONS LEARNT

Using the tools developed during the project, it is expected that enough of the flight simulator structure (Figure 1.2) has been covered in sufficient depth to allow the construction of a flight simulator core. However, as well as technical experience, other lessons have been learnt from the execution of this project such that if the development of a flight simulator is undertaken in the future, planning and risk management may benefit. The identified lessons are summarised in Table 6.1.

Lesson	Description
When using the simulator, cursory checks of the extracted data should be performed to ensure consistency **during** the session.	One of the main inadequacies in conducting the performance assessment was the inconsistency in the flight test data. Had the data been checked for consistency during the flight test, any retesting could be conducted instantly as necessary. In fact the data was checked several weeks after the flight tests were conducted and as a result any flight tests which were inadequate could not be repeated due to time constraints. Further to this lesson, erroneous flight test data should be added to the risk register in future projects.
All software requirements for future activities should be explored prior to detailed work being performed.	On some occasions, particularly when exploring the real-time simulation work package, the true software demands were not fully realised until the work was performed to such an extent that early exit was not possible without sacrificing the chance of meaningful results.
Tool compatibility should be explored as a research activity before tools are acquired.	Further to the previous issue, any incompatibility between software tools was also realised at too late a stage in the work to exit. As a result, software was acquired and installed only to find the version was incompatible with other core software. Hence a great deal of time and energy was spent in patching or updating software in order to ensure compatibility. All software related risks due to the lessons raised should be documented in the risk register for subsequent projects.
Construction of Simulink models should be undertaken maintaining visibility of their full potential.	The modular approach to assembling Simulink models, in particular the physical model, limited the flexibility of the model in the long term. As the model grew in size and complexity, further alterations became more costly in terms of time that was necessary. Time could have been saved by considering the expandability of the model and leaving placeholders for additional degrees of freedom signals for instance.
During development work, a permanent record of progress including new ideas should be kept.	More of a 'worked well' than a lesson learnt; throughout the project, brief notes were kept under appropriate headings in documentation to ensure capture of all information. This eased the burden on final documentation. Periodically, it is recommended that these notes are transformed into prose to further assist the process.
All Simulink models should be initialised using a descriptive MATLAB script file.	During mathematical model development, the specification of the model was determined by a large number of blocks which held a mathematical constant. These were sometimes hard to locate in the multi-layered myriad of the block diagrams. It is therefore recommended that the constants be referred to a variable on creation. These variables can then be initialised by a single script file which also allows ease of modification.

The applicability of the model should be investigated and clearly stated.	As the models developed, the applicability of the models changed. When using results to support theory, the behaviour of the model version used was not known due to a lack of any record. The applicability investigation had to be performed again which cost time. If the applicability of all models is recorded then any use of older models is ensured to be in the correct manner.
The model structure should ensure clear traceability.	When simulations were performed using the Simulink models, any unexpected behaviour required investigation. The process of tracing the cause of the behaviour through the block diagram in order to diagnose problems was very convoluted. Logical structuring of the block diagram helps in simplifying this process.
Where time and accuracy are factors, modelling tools with built-in solvers such as Simulink should be used over software simulations.	Having studied both sides of the coin with both the production of Simulink models and the writing of simulation software code, it was learned that although software allows a greater flexibility, the time required to generate code to allow accurate integration with little prior knowledge is significantly larger than the time taken to arrange functional blocks in the Simulink interface. It is recommended that in the future a combination of the two be used; the flight simulator core should be built in a modelling environment which is then supported by software code which allows the flexibility and customisation.
When building complex, interoperable Simulink models, memory store blocks should be used where appropriate.	Signal routing can be simplified and block diagram clarity and simulation execution speed improved by replacing circular links with memory store blocks. These blocks allow the reading and writing of data to memory locations on the host PC and can also help in ensuring a structure which aids traceability.
A physical (SimMechanics) flight simulator core should be chosen over a pure Simulink core.	The physical representation not only replicates reality more successfully by easily describing physical relationships between components but also adheres to the software/block diagram allied structure described by an early lesson. The mechanics are simplified through use of different frames of reference without the need for transformation.

TABLE 6.1: LESSONS LEARNT SUMMARY

REFERENCES

Airbus. (2009). *A320 Family Technical Appendices*. Retrieved October 2009, from Airbus Corporate Website: http://www.airbus.com

Airbus. (n.d.). Getting to Grips with Weight and Balance. *Flight Operations Support & Line Assistance* .

Anderson, J. D. (2005). *Introduction to Flight.* Irwin: McGraw-Hill.

Banks, S. P. (1986). *Control Systems Engineering.* Prentice-Hall International (UK) Ltd.

Berndt, J. S. (n.d.). *JSBSim Flight Dynamics Model in C++.* Retrieved October 2009, from http://www.jsbsim.com/

BFF Design Limited. (2008). *BFF 3 Degrees of Freedom Cockpit Motion Driver User Manual.* Retrieved March 2010, from DIY 3 DOF Flight Simulator Motion Platforms: http://buggies.builtforfun.co.uk/Sim/

Budd, T. A. (1996). *An Introduction to Object Oriented Programming.* Addison Wesley.

Childs, S. (2006). *N.A.C.A. Aerofoils.* Retrieved October 2009, from Flightplan Calculators: http://www.flightplan.za.net/nacaAerofoils.php

Conway, H. G. (1958). *Landing Gear Design.* London: Chapman & Hall.

Cook, M. V. (1997). *Flight Dynamics Principles.* Oxford: Butterworth-Heinemann.

Dabney, J. B., & Harman, T. L. (2001). *Mastering Simulink 4.* New Jersey: Prentice-Hall.

Dassault Aviation. (2008, January). *HISAC: Project Perspectives.* Retrieved from KATNET: http://www.kat-net.net/publications/

Dingle, B. M. (2004). Rigid Body Motion An Introduction. Texas A&M University.

Diston, D. J. (2009). 1.4 Models. In D. J. Diston, *Computational Modelling and Simulation of Aircraft and the Environment* (pp. 10-11). Chichester: Wiley.

Diston, D. J. (2009). 2.1.4.5 Euler Angles. In D. J. Diston, *Computational Modelling and Simulation of Aircraft and the Environment* (pp. 37-39). Chichester: Wiley.

Diston, D. J. (2009). 2.5 Line of Sight. In D. J. Diston, *Computational Modelling and Simulation of Aircraft and the Environment* (pp. 56-62). Chichester: Wiley.

EASA. (2003). *CS-25.105-.121.* European Aviation Safety Agency.

EASA. (2007). *CS-E 50 a) 2).* European Aviation Safety Agency.

EASA. (2009, May). TCDS A.064. *Type Certification Data Sheet A318-A319-A320-A321* . European Aviation Safety Agency.

ESDU. (1996). Aerodyamic Centre of Wing-Fuselage Combinations. Item 76015. *Engineering Sciences Data* .

ESDU. (2003). Introduction to Aerodynamic Derivatives, Equations of Motion and Stability. Item 86021. *Engineering Sciences Data* .

ESDU. (2009). Introduction to Damping. Item 09005. *Engineering Sciences Data* .

FAA. (1995). *121 CFR Appendix H.* Federal Aviation Administration.

FAA. (2009). *23 & 25 CFR Airworthiness Standards.* Federal Aviation Administration.

Filippone, A. (2006). *Flight Performance of Fixed and Rotary Wing Aircraft .* Oxford: Butterworth-Heinemann.

Hoerner, S. F. (1965). *Fluid-Dynamic Drag: Practical Information on Aero-Dynamic Drag and Hydro-Dynamic Resistance. .* Midland Park, N. J.: The Author.

Houghton, E. L., & Carpenter, P. W. (2003). *Aerodynamics for Engineering Students.* Oxford: Butterworth-Heinemann.

Jackson, P., Munson, K., & Peacock, L. (2008). *Jane's All The World's Aircraft 2008-2009.* Coulsdon: Jane's.

Jenkinson, L. R., Simpkin, P., & Rhodes, D. (1999). *Civil Jet Aircraft Design.* London: Arnold.

Katz, J., & Plotkin, A. (2001). *Low-Speed Aerodynamics.* Cambridge: Cambridge University Press.

Kroo, I., & Shevell, R. (2006). *Aircraft Design: Synthesis and Analysis.* Stanford: Desktop Aeronautics Inc.

Mair, W. A., & Birdsall, D. L. (1996). *Aircraft Performance.* Cambridge: Cambridge University Press.

MTU Aero Engines. (n.d.). *Product Leaflet V2500.* Retrieved December 2009, from V2500 - MTU Aero Engines: http://www.mtu.de/en/products_services/commercial_mro/programs/v2500/index.html

Murphy, G. J. (1957). *Basic Automatic Control Theory.* Princeton: Van Nostrand.

Nakayama, Y., & Boucher, B. F. (1999). *Introduction to Fluid Mechanics.* London: Arnold.

Phoenix Simulation Software. (2002). A320 Operations Manual.

Project Airbus. (n.d.). Retrieved October 2009, from http://www.pairbus.com

Raymer, D. P. (1992). *Aircraft Design: A Conceptual Approach.* Washington D.C.: American Institute of Aeronautics and Astronautics.

Rolfe, J. M., & Staples, K. J. (1986). *Flight Simulation.* Cambridge: Cambridge University Press.

Scans, N. S., & Barns, A. G. (1979). *Fifty Years of Success and Failure in Flight Simulation.* London: Royal Aeronautical Society.

School of MACE. (2009). *Marking Scheme and Guidelines for Individual Projects 2009-2010.* Manchester: Univeristy of Manchester.

Shannon, R. E. (1975). *Systems Simulation: The Art and Science.* Englewood Cliffs: Prentice-Hall.

Shevell, R. S. (1989). *Fundamentals of Flight.* Englewood Cliffs: Prentice Hall.

Silberschatz, A., & Galvin, P. B. (1994). *Operating System Concepts.* Reading, U.S.A.: Addison Wesley.

Swedish Defence Research Agency. (n.d.). *ADMIRE.* Retrieved October 2009, from Swedish Defence Research Agency: www.foi.se

The Mathworks Inc. (2004). *Getting Started with xPC Target.*

The Mathworks Inc. (2003). *xPC Target User Guide.*

University of Sydney Aeromechanical Department. (2003). National Design Build Fly Competition 2003 Draft Concept. Sydney, Australia.

Weilkiens, T. (2008). *Systems Engineering with SysML/UML Modeling, Analysis, Design.* Morgan Kaufmann Press.

Weisstein, E. W. (2010). *Root-Mean-Square.* Retrieved March 2010, from Mathworld--A Wolfram Web Resource: http://mathworld.wolfram.com/Root-Mean-Square.html

White, F. M. (1999). *Fluid Mechanics.* London: McGraw-Hill.

White, F. M. (2006). *Viscous Fluid Flow.* London: McGraw-Hill.

Whittaker, E. T., & Robinson, G. (1944). The Newton-Cotes Formulae of Integration. In *The Calculus of Observations: A Treatise on Numerical Mathematics.* London: Blackie.

Zagoren, M. (2009). *Airbus A320-232 Performance (IAE V2527-A5).* Retrieved from Grupo SATA Virtual : http://www.satavirtual.org

This Page is Left Intentionally Blank

A WORK BREAKDOWN STRUCTURE

A.1 INITIAL WORK BREAKDOWN STRUCTURE

ID	Task Name	Start	Finish
0	**A320 Simulation Flight Test**	**05/10/09**	**24/03/10**
1	*Project Start*	*05/10/09*	*05/10/09*
2	**Planning**	**06/10/09**	**08/10/09**
3	Establish Objectives	07/10/09	08/10/09
4	Establish Methods	07/10/09	08/10/09
5	Establish Learning Outcomes	07/10/09	08/10/09
6	Generate Schedule of Work	06/10/09	08/10/09
7	Generate Provisional Plan	06/10/09	08/10/09
8	*Issue Draft Proposal & Plan*	*08/10/09*	*08/10/09*
9	**Initial Report**	**05/10/09**	**16/11/09**
10	Rework Proposal & Plan	22/10/09	23/10/09
11	Write Summary	13/11/09	16/11/09
12	Write Introduction	13/11/09	16/11/09
13	Conduct Literature Review	05/10/09	27/10/09
14	Write Literature Summary	09/10/09	29/10/09
15	Write Summary of Detailed Methodology	08/10/09	09/10/09
16	Update and Insert Plan	12/10/09	13/10/09
17	Complete & Include Risk Assessment	12/10/09	13/10/09
18	*Issue Initial Report*	*16/11/09*	*16/11/09*
19	**Mathematical Model Development**	**20/10/09**	**16/12/09**
20	Generate Initial Model for Vehicle Flight	20/10/09	17/11/09
21	Document Model Progress	22/10/09	30/11/09
22	Improve and Refine Model	17/11/09	15/12/09
23	*Model Freeze for Reporting*	*15/12/09*	*16/12/09*
24	*Issue Model Development Document*	*30/11/09*	*01/12/09*
25	**Parameter Model Pre-Test**	**08/10/09**	**15/12/09**
26	Agree List of Performance Criteria to be Satisfied	09/10/09	28/10/09
27	Generate List of Model Parameters by Inspection of Current Model	08/10/09	12/10/09
28	Populate Model Parameters with Expected Values	12/10/09	20/10/09
29	Populate Criteria with Expected Values	28/10/09	17/11/09
30	Define Test Procedures for Each Criteria	17/11/09	04/12/09
31	Document Agreed Strategy for Test Programme	04/12/09	15/12/09
32	*Issue Test Strategy Document*	*15/12/09*	*15/12/09*
33	**Parameter Model Test**	**15/12/09**	**29/12/09**
34	Run Test Programme for Model	15/12/09	23/12/09
35	Export Data	23/12/09	29/12/09
36	**Parameter Model Post-Test**	**29/12/09**	**10/02/10**
37	Manipulate Data to Obtain Appropriate Quantities	29/12/09	13/01/10
38	Compare Data with Expected Values & Document Findings	13/01/10	18/01/10
39	Suggest Sources of any Inconsistencies	18/01/10	01/02/10
40	Agree Improvement Strategies for Inconsistencies	01/02/10	10/02/10
41	*Issue Model Assessment & Planned Improvements Document*	*10/02/10*	*10/02/10*
42	**Parameter Model Improvements**	**10/02/10**	**18/03/10**
43	Perform Model Improvement Work	10/02/10	04/03/10
44	Summarise Work Completed	04/03/10	18/03/10
45	*Issue Model Improvements Document*	*18/03/10*	*18/03/10*
46	**Poster Presentation**	**01/02/10**	**24/02/10**
47	Plan Poster Layout	01/02/10	04/02/10
48	Draft Poster Material	04/02/10	18/02/10
49	Review and Rework Poster	18/02/10	24/02/10
50	Retain Copies of Supporting Documents	24/02/10	24/02/10
51	*Issue Poster*	*24/02/10*	*24/02/10*
52	**Final Report**	**16/11/09**	**24/03/10**
53	Update Plan	24/02/10	25/02/10
54	Write Summary	16/11/09	17/11/09
55	Write Introduction	16/11/09	17/11/09
56	Write Literature Summary	16/11/09	17/11/09
57	Write Detailed Summary of Work Performed	18/03/10	19/03/10
58	Write Discussion/Conclusions/Recommendations	18/03/10	22/03/10
59	Insert Plan	25/02/10	25/02/10
60	*Issue Final Report Draft*	*22/03/10*	*22/03/10*
61	Rework Final Report	22/03/10	24/03/10
62	*Issue Final Report*	*24/03/10*	*24/03/10*

Part 1 of 2

ID	Task Name	Baseline Start	Baseline Finish
0	**A320 Simulation Investigation**	**05/10/09**	**12/04/10**
1	*Project Start*	*05/10/09*	*05/10/09*
2	**Planning**	**06/10/09**	**08/10/09**
3	Establish Objectives	07/10/09	08/10/09
4	Establish Methods	07/10/09	08/10/09
5	Establish Learning Outcomes	07/10/09	08/10/09
6	Generate Schedule of Work	06/10/09	08/10/09
7	Generate Provisional Plan	06/10/09	08/10/09
8	*Issue Draft Proposal & Plan*	*08/10/09*	*08/10/09*
9	**Initial Report**	**05/10/09**	**15/12/09**
10	Plan Report Structure and Content	02/11/09	02/11/09
11	Write Abstract	12/11/09	12/11/09
12	Write Introduction	13/11/09	16/11/09
13	Conduct Literature Review	05/10/09	22/10/09
14	Summarise Current Activity	08/10/09	09/10/09
15	Summarise Future Activity	12/10/09	12/10/09
16	Update and Integrate Plan	13/10/09	14/10/09
17	Complete & Include Risk Assessment	12/10/09	13/10/09
18	*Issue Draft Initial Report*	*13/10/09*	*13/10/09*
19	Rework Initial Report	13/10/09	14/10/09
20	*Issue Initial Report*	*15/12/09*	*15/12/09*
21	**Mathematical Model Development**	**11/10/09**	**01/04/10**
22	Plan Generation of Vehicle Flight Model	11/10/09	14/10/09
23	**Phase One Dev**	**20/10/09**	**20/11/09**
24	Establish Environment	20/10/09	23/10/09
25	**2 DOF Model**	**24/10/09**	**02/11/09**
26	Weight Model	24/10/09	26/10/09
27	Aerodynamic Forces	27/10/09	27/10/09
28	Thrust Modelling	28/10/09	29/10/09
29	2-D Equations of Motion	02/11/09	02/11/09
30	**3 DOF Model**	**03/11/09**	**19/11/09**
31	Lift Investigation	03/11/09	17/11/09
32	Drag Investigation	18/11/09	19/11/09
33	Landing Gear Model	03/11/09	11/11/09
34	2-D Equations of Motion Modification	12/11/09	19/11/09
35	*Model Freeze for Reporting*	*20/11/09*	*20/11/09*
36	*Issue Model Development Document Issue 1*	*20/11/09*	*20/11/09*

Part 2 of 2

ID	Task Name	Baseline Start	Baseline Finish
37	**Phase Two Dev**	**29/01/10**	**01/04/10**
38	Development of Software Solution	29/01/10	29/01/10
39	Exploration of Real-Time Model	11/02/10	22/02/10
40	Mechanical Investigation	22/02/10	11/03/10
41	Longitudinal Stability Solutions	12/03/10	31/03/10
42	*Model Development Freeze*	*31/03/10*	*31/03/10*
43	Document Progress	01/03/10	10/03/10
44	*Issue Model Development Document Issue 2*	*01/04/10*	*01/04/10*
45	**Parameter Model Pre-Test**	**08/10/09**	**25/02/10**
46	Agree List of Performance Criteria to be Satisfied	09/10/09	23/10/09
47	Generate List of Model Parameters by Inspection of Current Model	08/10/09	12/10/09
48	Populate Lists with Expected Values	01/02/10	04/02/10
49	Populate Criteria with Expected Values	04/02/10	15/02/10
50	Agree Test Procedures & Finalise E1 Model for Test	15/02/10	24/02/10
51	*Issue Model Improvement Strategies Document*	*24/02/10*	*25/02/10*
52	**Parameter Model Analysis**	**25/02/10**	**08/04/10**
53	Adjust E1 Model	04/03/10	29/03/10
54	**Parameter Model Test**	**19/03/10**	**30/03/10**
55	Run Test Programme for Models	19/03/10	29/03/10
56	Export Data	29/03/10	30/03/10
57	Post Test Data Analysis	30/03/10	08/04/10
58	*Issue Model Improvements Document*	*08/04/10*	*08/04/10*
59	**Poster Presentation**	**08/02/10**	**04/03/10**
60	Plan Poster Layout	08/02/10	11/02/10
61	Draft Poster Material	25/02/10	02/03/10
62	Review and Rework Poster	02/03/10	04/03/10
63	*Issue Poster*	*04/03/10*	*04/03/10*
64	**Final Report**	**04/03/10**	**12/04/10**
65	Update Plan	04/03/10	04/03/10
66	Rework Summary	11/03/10	11/03/10
67	Rework Introduction	11/03/10	11/03/10
68	Extended Literature Summary	11/03/10	11/03/10
69	Write Detailed Summary of Work Performed	08/04/10	09/04/10
70	Write Discussion/Conclusions/Recommendations	08/04/10	12/04/10
71	Insert Plan	04/03/10	04/03/10
72	*Issue Final Report Draft*	*12/04/10*	*12/04/10*
73	Rework Final Report	12/04/10	12/04/10
74	*Issue Final Report*	*12/04/10*	*12/04/10*

Part 1 of 2

ID	Task Name	Baseline Start	Actual Start	Baseline Finish	Actual Finish
0	**A320 Simulation Investigation**	**05/10/09**	**05/10/09**	**12/04/10**	**19/04/10**
1	*Project Start*	*05/10/09*	*05/10/09*	*05/10/09*	*05/10/09*
2	**Planning**	**06/10/09**	**06/10/09**	**08/10/09**	**08/10/09**
3	Establish Objectives	07/10/09	07/10/09	08/10/09	08/10/09
4	Establish Methods	07/10/09	07/10/09	08/10/09	08/10/09
5	Establish Learning Outcomes	07/10/09	07/10/09	08/10/09	08/10/09
6	Generate Schedule of Work	06/10/09	06/10/09	08/10/09	08/10/09
7	Generate Provisional Plan	06/10/09	06/10/09	08/10/09	08/10/09
8	*Issue Draft Proposal & Plan*	*08/10/09*	*08/10/09*	*08/10/09*	*08/10/09*
9	**Initial Report**	**05/10/09**	**05/10/09**	**15/12/09**	**15/12/09**
10	Plan Report Structure and Content	02/11/09	02/11/09	02/11/09	02/11/09
11	Write Abstract	12/11/09	12/11/09	12/11/09	12/11/09
12	Write Introduction	13/11/09	13/11/09	16/11/09	16/11/09
13	Conduct Literature Review	05/10/09	05/10/09	22/10/09	22/10/09
14	Summarise Current Activity	08/10/09	08/10/09	09/10/09	09/10/09
15	Summarise Future Activity	12/10/09	12/10/09	12/10/09	12/10/09
16	Update and Integrate Plan	13/10/09	13/10/09	14/10/09	14/10/09
17	Complete & Include Risk Assessment	12/10/09	12/10/09	13/10/09	13/10/09
18	*Issue Draft Initial Report*	*13/10/09*	*13/10/09*	*13/10/09*	*13/10/09*
19	Rework Initial Report	13/10/09	13/10/09	14/10/09	14/10/09
20	*Issue Initial Report*	*15/12/09*	*15/12/09*	*15/12/09*	*15/12/09*
21	**Mathematical Model Development**	**11/10/09**	**11/10/09**	**01/04/10**	**29/03/10**
22	Plan Generation of Vehicle Flight Model	11/10/09	11/10/09	14/10/09	14/10/09
23	**Phase One Dev**	**20/10/09**	**20/10/09**	**20/11/09**	**20/11/09**
24	Establish Environment	20/10/09	20/10/09	23/10/09	23/10/09
25	**2 DOF Model**	**24/10/09**	**24/10/09**	**02/11/09**	**02/11/09**
26	Weight Model	24/10/09	24/10/09	26/10/09	26/10/09
27	Aerodynamic Forces	27/10/09	27/10/09	27/10/09	27/10/09
28	Thrust Modelling	28/10/09	28/10/09	29/10/09	29/10/09
29	2-D Equations of Motion	02/11/09	02/11/09	02/11/09	02/11/09
30	**3 DOF Model**	**03/11/09**	**03/11/09**	**19/11/09**	**19/11/09**
31	Lift Investigation	03/11/09	03/11/09	17/11/09	17/11/09
32	Drag Investigation	18/11/09	18/11/09	19/11/09	19/11/09
33	Landing Gear Model	03/11/09	03/11/09	11/11/09	11/11/09
34	2-D Equations of Motion Modification	12/11/09	12/11/09	19/11/09	19/11/09
35	*Model Freeze for Reporting*	*20/11/09*	*20/11/09*	*20/11/09*	*20/11/09*
36	*Issue Model Development Document Issue 1*	*20/11/09*	*20/11/09*	*20/11/09*	*20/11/09*
45	**Parameter Model Pre-Test**	**08/10/09**	**08/10/09**	**25/02/10**	**24/02/10**
46	Agree List of Performance Criteria to be Satisfied	09/10/09	09/10/09	23/10/09	23/10/09
47	Generate List of Model Parameters by Inspection of Current Model	08/10/09	08/10/09	12/10/09	12/10/09

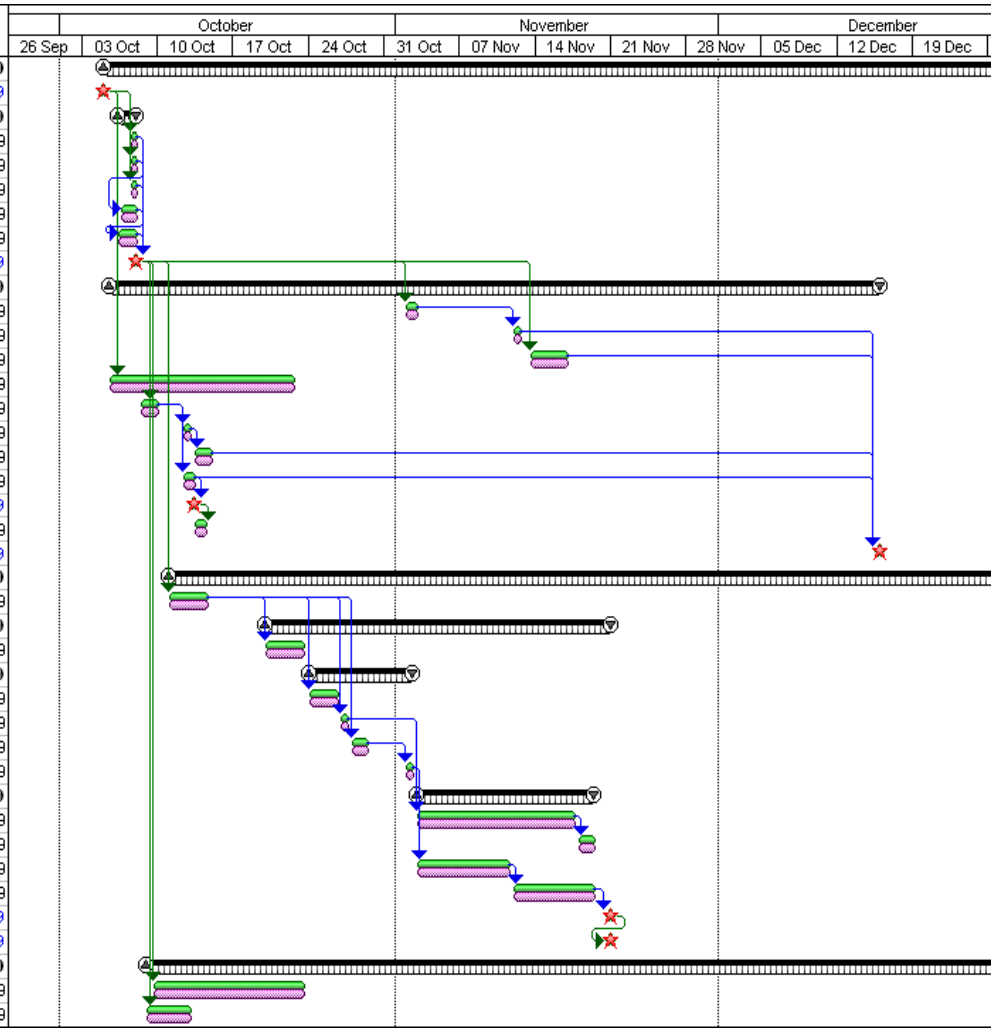

ID	Task Name	Baseline Start	Actual Start	Baseline Finish	Actual Finish
0	**A320 Simulation Investigation**	**05/10/09**	**05/10/09**	**12/04/10**	**19/04/10**
21	**Mathematical Model Development**	**11/10/09**	**11/10/09**	**01/04/10**	**29/03/10**
37	**Phase Two Dev**	**29/01/10**	**01/02/10**	**01/04/10**	**29/03/10**
38	Development of Software Solution	29/01/10	01/02/10	29/01/10	02/02/10
39	Exploration of Real-Time Model	11/02/10	11/02/10	22/02/10	22/02/10
40	Mechanical Investigation	22/02/10	22/02/10	11/03/10	11/03/10
41	Longitudinal Stability Solutions	12/03/10	10/03/10	31/03/10	29/03/10
42	*Model Development Freeze*	*31/03/10*	*29/03/10*	*31/03/10*	*29/03/10*
43	Document Progress	01/03/10	17/03/10	10/03/10	29/03/10
44	*Issue Model Development Document Issue 2*	*01/04/10*	*29/03/10*	*01/04/10*	*29/03/10*
45	**Parameter Model Pre-Test**	**08/10/09**	**08/10/09**	**25/02/10**	**24/02/10**
48	Populate Lists with Expected Values	01/02/10	01/02/10	04/02/10	04/02/10
49	Populate Criteria with Expected Values	04/02/10	04/02/10	15/02/10	15/02/10
50	Agree Test Procedures & Finalise E1 Model for Test	15/02/10	15/02/10	24/02/10	24/02/10
51	*Issue Model Improvement Strategies Document*	*24/02/10*	*24/02/10*	*25/02/10*	*24/02/10*
52	**Parameter Model Analysis**	**25/02/10**	**24/02/10**	**08/04/10**	**16/03/10**
53	Adjust E1 Model	04/03/10	26/02/10	29/03/10	08/03/10
54	**Parameter Model Test**	**19/03/10**	**24/02/10**	**30/03/10**	**09/03/10**
55	Run Test Programme for Models	19/03/10	24/02/10	29/03/10	08/03/10
56	Export Data	29/03/10	08/03/10	30/03/10	09/03/10
57	Post Test Data Analysis	30/03/10	09/03/10	08/04/10	16/03/10
58	*Issue Model Improvements Document*	*08/04/10*	*16/03/10*	*08/04/10*	*16/03/10*
59	**Poster Presentation**	**08/02/10**	**18/02/10**	**04/03/10**	**03/03/10**
60	Plan Poster Layout	08/02/10	18/02/10	11/02/10	23/02/10
61	Draft Poster Material	25/02/10	24/02/10	02/03/10	01/03/10
62	Review and Rework Poster	02/03/10	01/03/10	04/03/10	03/03/10
63	*Issue Poster*	*04/03/10*	*03/03/10*	*04/03/10*	*03/03/10*
64	**Final Report**	**04/03/10**	**29/03/10**	**12/04/10**	**19/04/10**
65	Update Plan	04/03/10	29/03/10	04/03/10	29/03/10
66	Rework Summary	11/03/10	29/03/10	11/03/10	29/03/10
67	Rework Introduction	11/03/10	29/03/10	11/03/10	29/03/10
68	Extended Literature Summary	11/03/10	29/03/10	11/03/10	29/03/10
69	Write Detailed Summary of Work Performed	08/04/10	30/03/10	09/04/10	08/04/10
70	Write Discussion/Conclusions/Recommendations	08/04/10	08/04/10	12/04/10	09/04/10
71	Insert Plan	04/03/10	09/04/10	04/03/10	12/04/10
72	*Issue Final Report Draft*	*12/04/10*	*12/04/10*	*12/04/10*	*12/04/10*
73	Rework Final Report	12/04/10	15/04/10	12/04/10	19/04/10
74	*Issue Final Report*	*12/04/10*	*19/04/10*	*12/04/10*	*19/04/10*

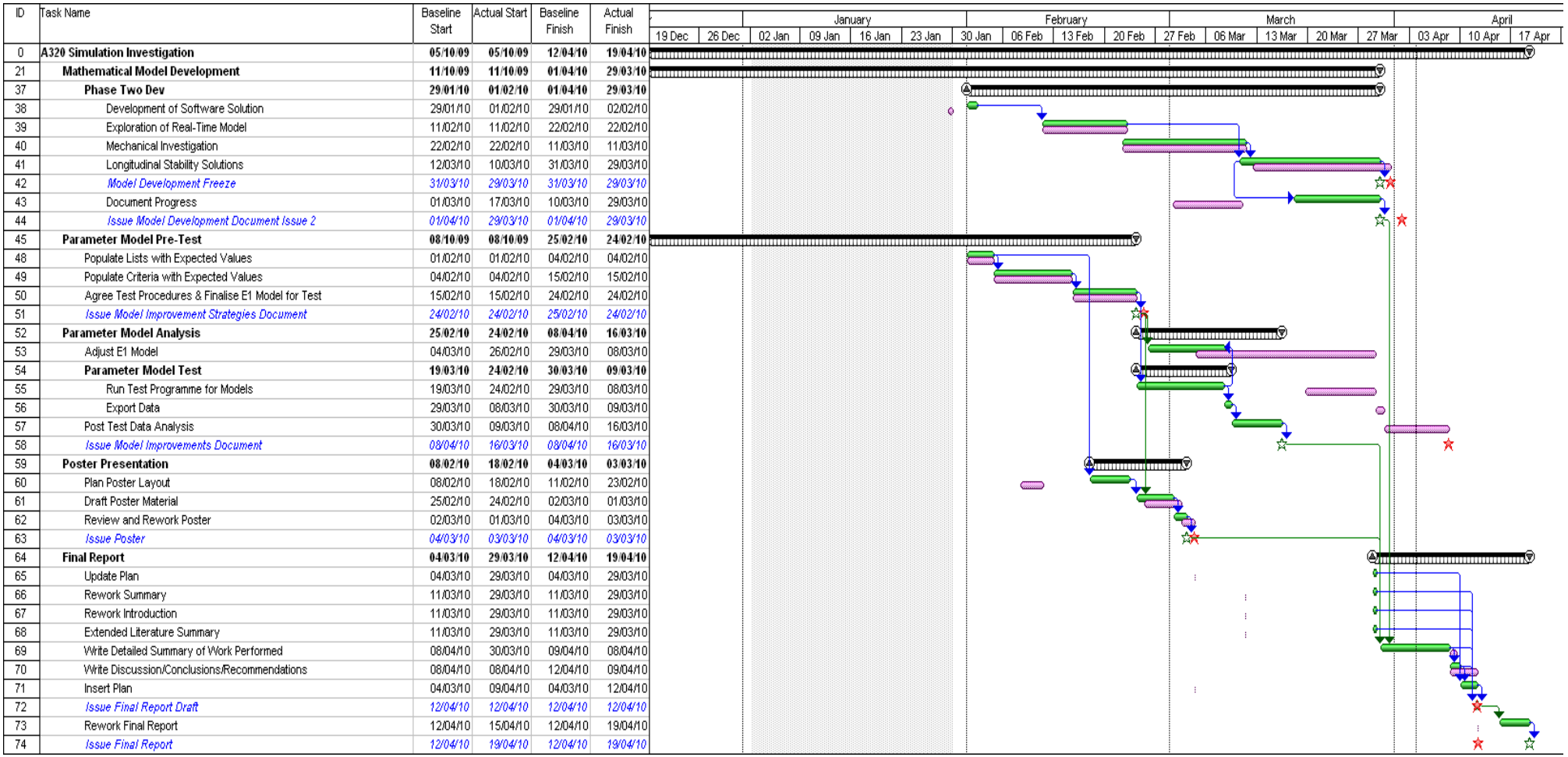

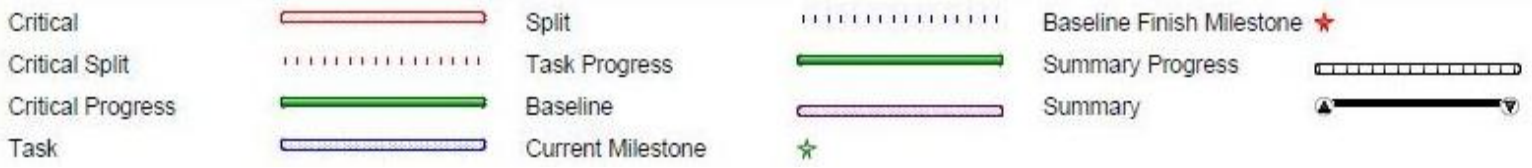

B.1 INITIAL RISK REGISTER

					Initial					Residual		
Risk No.	**If...**	**Then..**	**Status**	**Work Package**	**P**	**I**	**PI**	**Specific Impact**	**Mitigation Action**	**P**	**I**	**PI**
1	academic staff unavailable for consultation	delay in problem resolution	Active	All	H	M	HM	missed milestones / stress / progress limitation	1) Seek alternative sponsor 2) Plan parallel activities to ensure progress in delay of others	H	L	HL
2	mode of transport unavailable	unable to travel to site	Active	All	L	H	LH	missed hand-in or use of university software/hardware or resources	1) Arrange alternative modes of transport 2) Early planning of hand-in 3) Research electronic resources 4) Have personal copies of software	L	L	LL
3	communicatio n with university server from home impossible	work and associated resources inaccessible	Active	All	L	H	LH	Latest work inaccessible - time lost	1) Work backed up regular and to more than one source 2) Allow for non-server related communication methods	L	L	LL
4	laptop malfunctions	data unavailable and software unavailable	Active	All	L	H	LH	missed milestones / stress / progress limitation	1) Regular backups to external memory 2) Hard copies of software for install elsewhere	L	L	LL
5	library resources unavailable when required	research delayed	Active	All	M	H	MH	progress limitation / limits potential for higher quality activities	1) Plan ahead with resource selection 2) Seek other libraries	L	M	LM
6	there is a human resource shortfall	progress hampered	Active	All	M	H	MH	missed milestones / stress / progress limitation	1) Effective time management 2) Task delegation	L	H	LH
7	human resource not available	progress halted	Active	All	L	H	LH	missed milestones / project quality reduction / time cost	1) Healthy lifestyle options	L	H	LH

8	university IT resources unavailable	unable to use desktop resources	Active	All	M	H	MH	missed milestones / progress / access to materials	1) Find alternative reliable computer resources on site 2) VPN capability	M	M	MM
9	milestones are brought forward	loss of project quality or content	Active	All	L	H	LH	revised scope of work	1) Confirm of deliverable dates 2) Modular planning	L	M	LM
10	project scope changed with little notice	loss of project quality and reduction in low priority content	Active	All	M	H	MH	revised scope of work	1) Modular planning 2) Task priorities agreed	M	M	MM
11	work packages exceed scheduled time	project time overruns	Active	All	H	M	HM	revised project scope / increased documentation	1) Pessimistic work estimates	M	M	MM
12	project data to date is lost	latest material lost	Active	All	L	H	LH	reversion to last back up	1) Back up to multiple sources 2) Configuration control	L	L	LL
13	intellectual property leaked to 3rd parties	competitive advantage lost	Active	All	M	H	MH	originality of work damaged	1) Password Documents 2) Supervisor informed of research	L	M	LM
14	project scope creeps	loss of direction	Active	All	H	M	HM	hard to recognise / reduction in quality / personally imposed time constraints	1) Regular plan revisits 2) Scope limitation recognition	M	M	MM

					Current					Residual				Initial			
Risk No.	**If...**	**Then..**	**Status**	**Work Package**	**P**	**I**	**PI**	**Specific Impact**	**Mitigation Action**	**P**	**I**	**PI**		**P**	**I**	**PI**	**Specific Impact**
1	academic staff unavailable for consultation	delay in problem resolution	Active	All	H	L	HL	missed milestones / stress / progress limitation	1) Seek alternative sponsor 2) Plan parallel activities to ensure progress in delay of others	H	L	HL		H	M	HM	missed milestones / stress / progress limitation
2	mode of transport unavailable	unable to travel to site	Active	All	L	L	LL	missed hand-in or use of university software/hardware or resources	1) Arrange alternative modes of transport 2) Early planning of hand-in 3) Research electronic resources 4) Have personal copies of software	L	L	LL		L	H	LH	missed hand-in or use of university software/hardware or resources
3	communication with university server from home impossible	work and associated resources inaccessible	Active	All	L	L	LL	Latest work inaccessible - time lost	1) Work backed up regular and to more than one source 2) Allow for non-server related communication methods	L	L	LL		L	H	LH	Latest work inaccessible - time lost
4	laptop malfunctions	data unavailable and software unavailable	Active	All	L	L	LL	missed milestones / stress / progress limitation	1) Regular backups to external memory 2) Hard copies of software for install elsewhere	L	L	LL		L	H	LH	missed milestones / stress / progress limitation
5	library resources unavailable when required	research delayed	Active	All	L	M	LM	progress limitation / limits potential for higher quality activities	1) Plan ahead with resource selection 2) Seek other libraries	L	M	LM		M	H	MH	progress limitation / limits potential for higher quality activities
6	there is a human resource shortfall	progress hampered	Active	All	L	H	LH	missed milestones / stress / progress limitation	1) Effective time management 2) Task delegation	L	H	LH		M	H	MH	missed milestones / stress / progress limitation
7	human resource not available	progress halted	Active	All	L	H	LH	missed milestones / project quality reduction / time cost	1) Healthy lifestyle options	L	H	LH		L	H	LH	missed milestones / project quality reduction / time cost

8	university IT resources unavailable	unable to use desktop resources	Active	All	M	M	MM	missed milestones / progress / access to materials	1) Find alternative reliable computer resources on site 2) VPN capability ***Added*** 3) Use personal software 4) Travel home	M	L	ML		M	H	MH	missed milestones / progress / access to materials
9	milestones are brought forward	loss of project quality or content	Active	All	L	M	LM	revised scope of work	1) Confirm of deliverable dates 2) Modular planning	L	M	LM		L	H	LH	revised scope of work
10	project scope changed with little notice	loss of project quality and reduction in low priority content	Active	All	M	M	MM	revised scope of work	1) Modular planning 2) Task priorities agreed ***Added*** 3) Content Control Retained	L	M	LM		M	H	MH	revised scope of work
11	work packages exceed scheduled time	project time overruns	Active	All	M	M	MM	revised project scope / increased documentation	1) Pessimistic work estimates	M	M	M M		H	M	HM	revised project scope / increased documentation
12	project data to date is lost	latest material lost	Active	All	L	L	LL	reversion to last back up	1) Back up to multiple sources 2) Config control	L	L	LL		L	H	LH	reversion to last back up
13	intellectual property leaked to 3rd parties	competitive advantage lost	Active	All	L	M	LM	originality of work damaged	1) Password Documents 2) Supervisor informed of research	L	M	LM		M	H	MH	originality of work damaged
14	project scope creeps	loss of direction	**Closed**	All	M	M	MM	hard to recognise / reduction in quality / personally imposed time constraints	1) Regular plan revisits 2) Scope limitation recognition ***Added*** **3) Scope fix closes risk**					H	M	HM	hard to recognise / reduction in quality / personally imposed time constraints
15	flight simulator unavailable during test programme	use of critical resource is restricted	Active	Flight Test	M	H	MH	flight test programme becomes delayed resulting in loss of continuity and schedule slippage	1) Enquire as to availability 2) Plan flight test around availability	L	H	LH		New Risk			

16	other university demands such as exams encroach into project time	progress hampered or halted	Active	All	H	H	HH	exams require revision and hence large amount of time available is lost	1) Plan around inevitable encroachment of exams plus revision	H	L	HL	New Risk
17	modelling work demands more time than scheduled	other project areas are assigned less time by default	Active	Modelling Activities	H	M	HM	the work packages suffer in depth and quality	1) Package work to allow rescope if necessary 2) Allows development plan slack to incorporate slippage	M	L	ML	New Risk
18	reviewers are preoccupied when schedule demands report review	schedule hold ups	Active	All	M	H	MH	Rework may be delayed / errors (technical or otherwise) not spotted until too late	1) Plan to send to more than one reviewer 2) Engage reviewer early to ensure knowledge of time available	L	M	LM	New Risk
19	references are difficult to cite	time and quality of work suffers	Active	All	H	L	HL	Time is consumed in locating reference information such as dates and authors / uncited facts and figures degrade work quality	1) Ration time spent searching for lost reference details 2) Note references immediately when used to avoid loss of information	M	L	ML	New Risk
20	diverted from current project activities for long duration	technical reorientation necessary	Active	All	M	M	MM	time taken for familiarisation / potential loss of momentum & mental acuity	1) Ensure activities recorded in detail to time of interruption	M	L	ML	New Risk
21	parallel project demands reduce resource scheduled time	efficiency of human resources reduced	Active	All	H	M	HM	less time to increase quality of work performed / schedule slips / increased stress	1) Allow plan to drive only necessary weekly activities to control time consumption 2) Micro-management intra-week schedule	H	L	HL	New Risk
22	analysis and documentation under estimated in terms in work required	the project encounters time overruns	Active	All	H	H	HH	increased time spent on documentation activities / delivery of reports late	1) Sufficient lag planned for up to final deadline 2) Maintain detailed documentation throughout project	H	L	HL	New Risk

23	model performance grossly misaligned with expected result	the development work encounters significant time overruns	Active	Modelling Activities	M	M	MM	Models require alignment to main stream project work / diagnosis & debugging very time consuming	1) Package work to allow rescope if necessary 2) Allows development plan slack to incorporate slippage	M	L	ML		New Risk
24	flight test data is unexpected	the quality of the results is degraded	Active	Flight Test Data Analysis	M	M	MM	test results are inconsistent and results are misaligned with expectations / difficult to retest	1) Allow time for investigation into source	M	L	ML		New Risk
25	further software required than initially surmised	project schedule suffers	Active	All	M	M	MM	time consumed in downloading, installing, and learning new software	1) Ensure software requirements known in advance 2) Source software before required	L	L	LL		New Risk

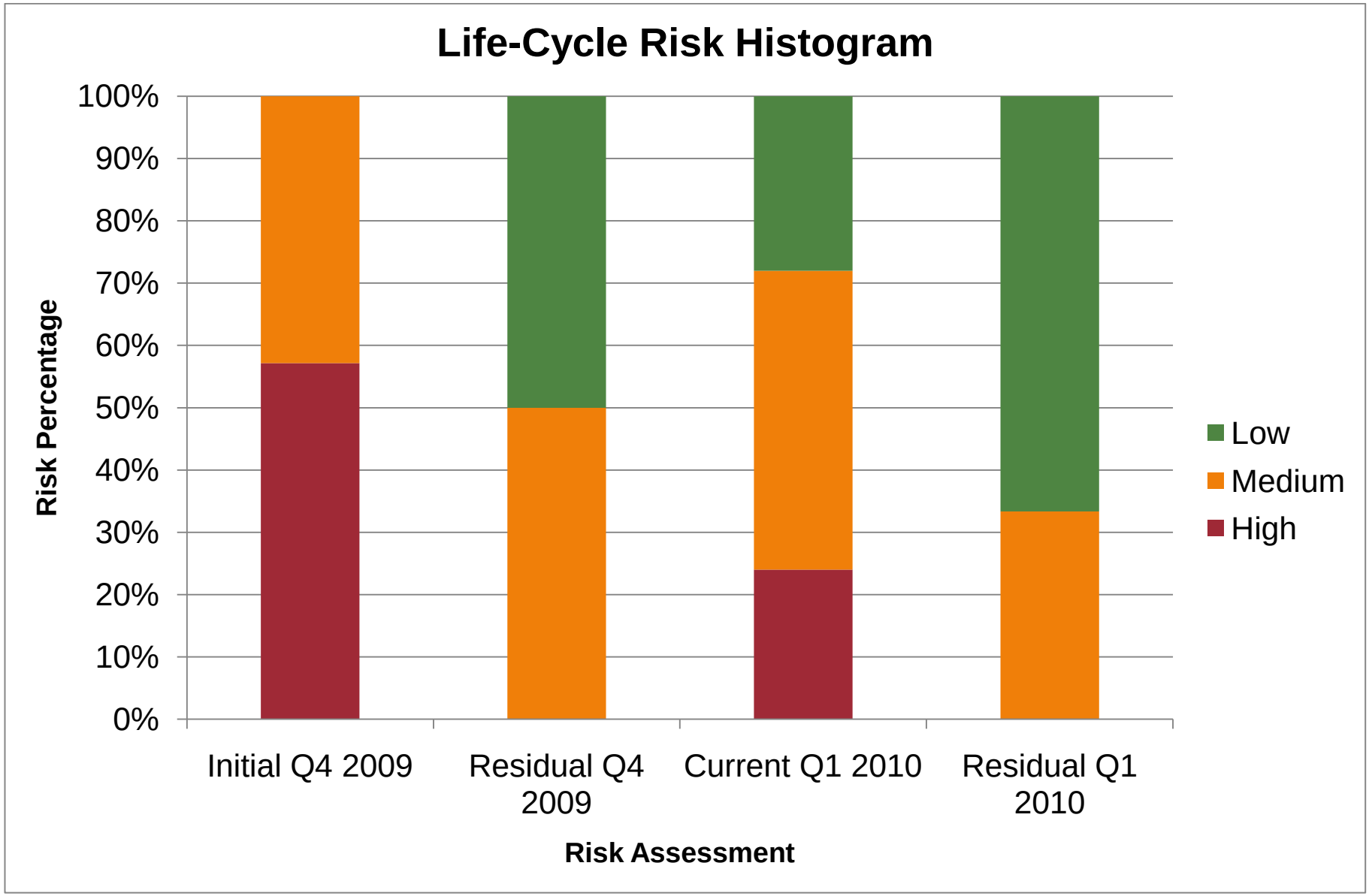
Life-Cycle Risk Histogram
100%
90%
80%
70%
60%
50%
40%
30%
20%
10%
0%
Risk Percentage
Initial Q4 2009
Residual Q4 2009
Current Q1 2010
Residual Q1 2010
Risk Assessment
Low
Medium
High

C.1 NACA AEROFOIL NOTATION

NACA 4-Digit Aerofoil

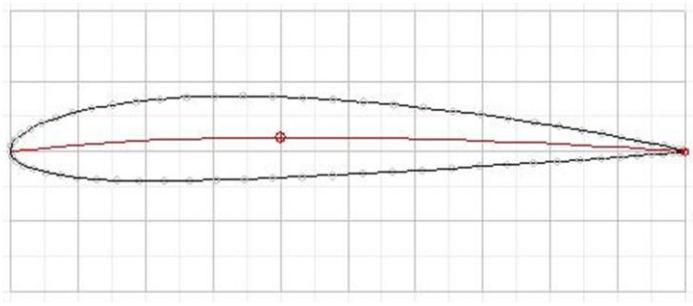

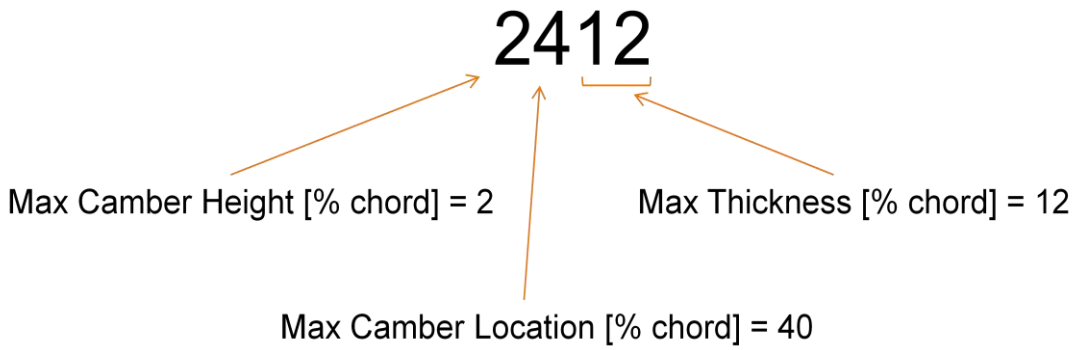

NACA 6-Series Aerofoil

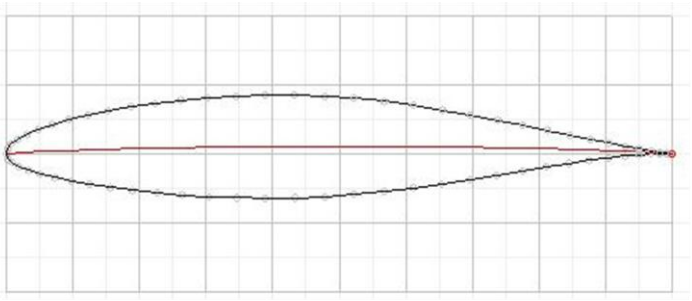

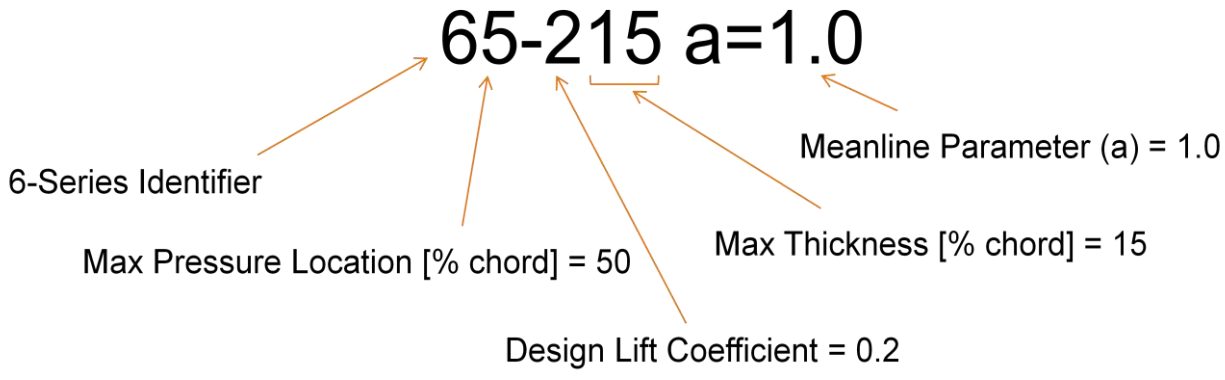

The 6A-series aerofoil uses a fixed Meanline Parameter (related to the camber location) equal to 0.8 and is identified by notation of the form 65A215.

```
function[CL,CM]=Naca(digits,alpha)
%
% Naca function returns the lift coefficient (CL) and moment about the
% quarter location (CM) for a given NACA 4-digit aerofoil (digits) and an
% angle of attack (alpha) in degrees
%
naca=num2str(digits);
alphar=alpha*pi/180;
%
% Find coordinates of maximum camber
m=str2num(naca(1))/100;
p=str2num(naca(2))/10;
thetap=acos(1-(2*p));
%
% Calculate Mathematical Coefficients for General Equation
A0=(m/(pi*(p^2)))*((((2*p)-1)*thetap)+(sin(thetap)))+(m/(pi*((1-p)^2)))*((((2*p)-
1)*(pi-thetap))-sin(thetap));
%
A1=((2*m)/(pi*(p^2)))*((((2*p)-1)*sin(thetap))+(0.25*sin(2*thetap))+(thetap/2))-
((2*m)/(pi*((1-p)^2)))*((((2*p)-1)*sin(thetap))+(0.25*sin(2*thetap))-(0.5*(pi-
thetap)));
%
A2=(((2*m)/(pi*(p^2)))*((((2*p)-
1)*((0.25*sin(2*thetap))+(0.5*thetap)))+(sin(thetap))-(((sin(thetap))^3)/3)))-
(((2*m)/(pi*((1-p)^2)))*((((2*p)-1)*((0.25*sin(2*thetap))-(0.5*(pi-
thetap))))+(sin(thetap))-(((sin(thetap))^3)/3)));
%
% Calculate Aerodynamic Coefficients
CL=(pi*(A1-(2*A0)))+(2*pi*alphar);
CM=((-pi/4)*(A1-A2));
```

D MATHEMATICAL MODEL SUMMARY

The following diagram illustrates the functions and sub-system hierarchy of the mathematical model.

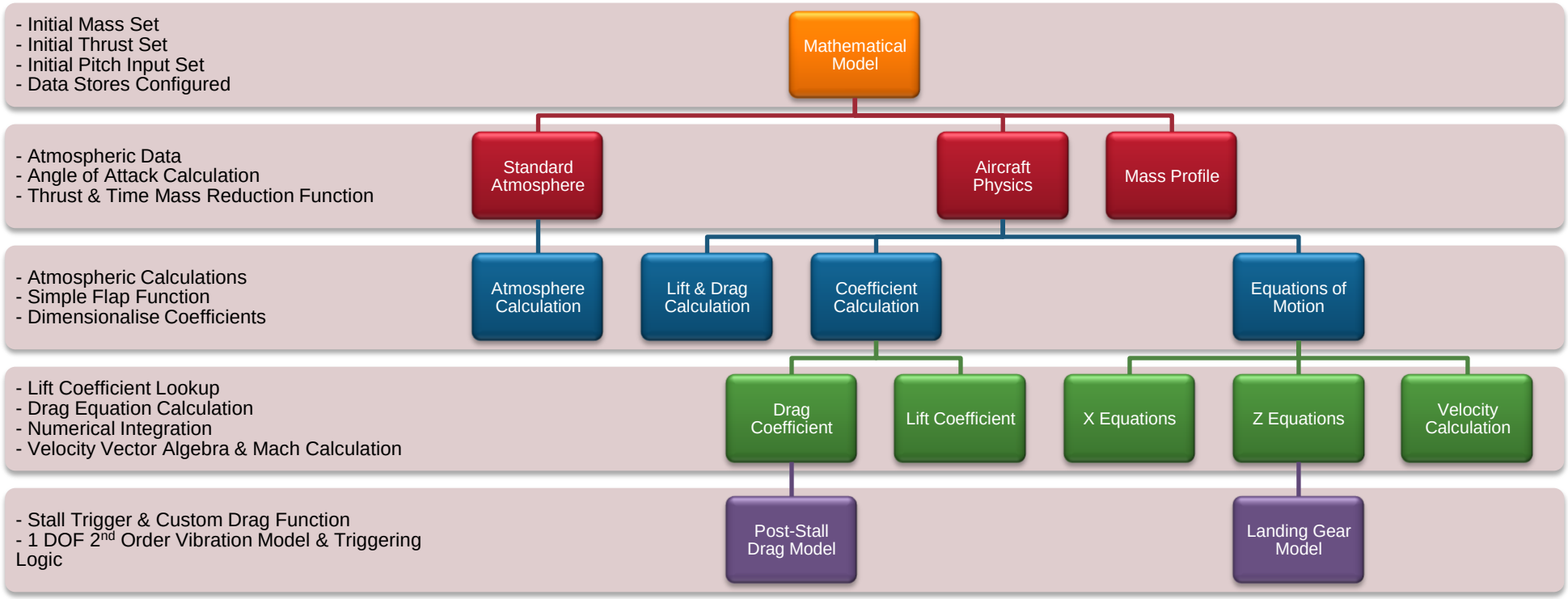

E SIMULATION SOFTWARE DATA

E.1 SIMULATION SOFTWARE GOVERNING EQUATIONS

Gravitational Model:

$$g = g_0 \left(\frac{R_E}{z + R_E} \right)^2$$

Atmospheric Model:

$$T = T_0 - \lambda z$$

$$p = p_0 \left(\frac{T}{T_0} \right)^{-g_0/\lambda R}$$

$$\rho = \rho_0 \left(\frac{T}{T_0} \right)^{-\left[\left(g_0/\lambda R\right)+1\right]}$$

$$a = \sqrt{\gamma R T}$$

Thrust Model:

$$\tau_{z \geq 5000} = \tau_{z=SL}.\left[0.45 - 0.17 \times 10^{-4}(z - 5000)\right]$$

$$\tau_{z<5000} = \left[\frac{(\tau_{max} - \tau_{z=SL})z}{5000} \right].\tau_{z=SL}$$

Mass & Weight Reduction Profile:

$$m_n = m_{n-1} - (\xi.\tau_n)$$

$$W = mg$$

Angle of Attack:

$$\alpha = \theta - \mu$$

Coefficient Calculation:

$$C_L = C_{L0} + C_{L\alpha}\alpha$$

$$C_D = C_{D_0} + k{C_L}^2$$

X Equations of Motion:

$$F_X = T\cos(\theta) - L\sin(\mu) - D\cos(\mu)$$

$$\ddot{x} = \frac{F_X}{m}$$

$$\dot{x}_n = \dot{x}_{n-1} + \ddot{x}.dt$$

$$x_n = x_{n-1} + \dot{x}.dt$$

Landing Gear Equation (as applicable):

$$F_{LG} = c\dot{z} - kz$$

Z Equations of Motion:

$$F_Z = Tsin(\theta) + Lcos(\mu) - Dsin(\mu) - W + F_{LG}$$

$$\ddot{z} = \frac{F_Z}{m}$$

$$\dot{z}_n = \dot{z}_{n-1} + \ddot{z}.dt$$

$$z_n = z_{n-1} + \dot{z}.dt$$

Velocity Vector Equations:

$$V_\infty = \sqrt{\dot{x}^2 + \dot{z}^2}$$

$$\mu = \arctan\left(\frac{\dot{z}}{\dot{x}}\right)$$

$$M = \frac{V_\infty}{a}$$

Lift and Drag Forces:

$$L = \frac{1}{2}\rho S_w C_L {V_\infty}^2$$

$$D = \frac{1}{2}\rho S_w C_D {V_\infty}^2$$

```
%% Code Start
%
% 3 DOF Simulation Software for Flight Simulation Model
% Adrian Harwood Individual Project 2009-2010
%
clear
close all
clc
%
%
%% Setting of Fundamental Parameters (A320-200 Where Applicable)
%
Texit=150;          % Exit Condition Time s
dt=0.1;             % Iteration Time Step s
%
p0=1013.2;          % SL Pressure Pa
r0=1.225;           % SL Density kg/m^2
T0=288.15;          % SL Temperature K
a0=340.26;          % SL Speed of Sound
gam=1.4;            % Ratio of Specific Heats
lam=6.5e-3;         % Temperature Reduction Factor K/m
R=287;              % Difference in Specific Heats
frc=2e-4;           % Mass Reduction Constant kg/s.N
mass0=70000;        % Initial Mass kg
g0=9.8;             % SL Acceleration Due To Gravity m/s^2
Cd0=0.04;           % Profile Drag Factor
Cdk=0.02;           % Lift Induced Drag Factor
LGk=1e5;            % LG Stiffness N/m
LGc=2e5;            % LG Damping Ns/m
S=122.4;            % Wing Area m^2
Cl0=1.0569;         % Zero AoA Lift Coefficient (inc. Flap Contribution)
Cla=0.115;          % Lift Curve Slope /deg
RadE=6.368e6;       % Average Radius of the Earth m
%
%
%% Preallocation of Variables
%
Th=zeros(1,((Texit*(1/dt))+1));
Tlim=zeros(1,((Texit*(1/dt))+1));
AoA=zeros(1,((Texit*(1/dt))+1));
Cl=zeros(1,((Texit*(1/dt))+1));
Cd=zeros(1,((Texit*(1/dt))+1));
Fx=zeros(1,((Texit*(1/dt))+1));
Fz=zeros(1,((Texit*(1/dt))+1));
LGF=zeros(1,((Texit*(1/dt))+1));
M=zeros(1,((Texit*(1/dt))+1));
%
%
%% Initialisation of Variables
%
% Iteration Counter Initialisation (m=1 == Initial Conditions)
m=1;
%
%
% Initial Conditions m=1
t(m)=0;             % Time
T(m)=T0;            % Temperature
p(m)=p0;            % Pressure
r(m)=r0;            % Density
a(m)=a0;            % Speed of Sound
x(m)=0;             % Horizontal Displacement
xdot(m)=0;          % Horizontal Velocity
```

```
xddot(m)=0;          % Horizontal Acceleration
z(m)=0;              % Vertical Displacement
zdot(m)=0;           % Vertical Velocity
zddot(m)=0;          % Vertical Acceleration
mass(m)=mass0;       % Mass
W(m)=mass0*g0;       % Weight
pit=0;               % Pitch Angle
vva(m)=0;            % Velocity Vector Angle
Vinf(m)=0;           % Freestream Velocity
L(m)=0;              % Lift
D(m)=0;              % Drag
g(m)=g0;             % Acceleration Due to Gravity
Tset(m)=100000;      % Desired Thrust
%
%
%% Iteration Procedure
%
% Waitbar Startup
wb=waitbar((m/((1/dt)*Texit)),'Calculating...');
%
%
while t(m)<Texit
    % Iteration Count
    m=m+1;
    t(m)=t(m-1)+dt;
    %
    waitbar(m/((1/dt)*Texit));
    %
    %
    % Gravity Model
    g(m)=g0*((RadE/(RadE+z(m-1)))^2);
    %
    %
    % ISA Model Data
    T(m)=T0-(lam*z(m-1));
    p(m)=p0*((T(m)/T0)^(g(m)/(lam*R)));
    r(m)=r0*(p(m)/p0)*(T0/T(m));
    a(m)=sqrt(gam*R*T(m));
    %
    %
    % Thrust and Thrust Lapse
    Tset(m)=100000;
    Tlim(m)=Tset(m)*(0.45-0.17e-4);
    if z(m-1)>=5000
        Th(m)=Tset(m).*(0.45-0.17e-4.*(z(m-1)-5000));
    else
        Th(m)=(((Tlim(m)-Tset(m))/5000)*z(m-1))+Tset(m);
    end
    %
    %
    % Mass Reduction
    mass(m)=mass(m-1)-frc*Th(m);
    W(m)=mass(m)*g(m);
    %
    % Coefficient Calculation
    AoA(m)=pit-vva(m-1);
    Cl(m)=Cl0+Cla*(AoA(m)*180/pi);
    Cd(m)=Cd0+(Cdk*(Cl(m)^2));
    %
    %
    % X Equations of Motion - Rectangular Integration
    Fx(m)=(Th(m)*cos(pit))-(L(m-1)*sin(vva(m-1)))-(D(m-1)*cos(vva(m-1)));
    xddot(m)=Fx(m)/mass(m);
    xdot(m)=xdot(m-1)+(xddot(m)*dt);
```

```
    x(m)=x(m-1)+(xdot(m)*dt);
    %
    %
    % Z Equations of Motion - Rectangular Integration
    % Landing Gear Logic
    if z(m-1)<=0
        LGF(m)=-((LGk*z(m-1))+(LGc*zdot(m-1)));
    else
        LGF(m)=0;
    end
    % Equations
    Fz(m)=(Th(m)*sin(pit))+(L(m-1)*cos(vva(m-1)))-(D(m-1)*sin(vva(m-1)))-
W(m)+LGF(m);
    zddot(m)=Fz(m)/mass(m);
    zdot(m)=zdot(m-1)+(zddot(m)*dt);
    z(m)=z(m-1)+(zdot(m)*dt);
    %
    %
    % Velocity Vector
    Vinf(m)=sqrt((xdot(m)^2)+(zdot(m)^2));
    vva(m)=atan(zdot(m)/xdot(m));
    M(m)=Vinf(m)*a(m);
    %
    %
    % Lift and Drag Forces
    L(m)=Cl(m)*0.5*r(m)*S*(Vinf(m)^2);
    D(m)=Cd(m)*0.5*r(m)*S*(Vinf(m)^2);
end
%
close(wb)
%
%% Post Processing of Data
%
% File to Simply Plot Graphs
postprocessor_0
```

F XPC TARGET DATA

F.1 XPC TARGET SOFTWARE CONFIGURATIONS

Software	Version
Operating System	Windows XP SP3
MATLAB	Version 7.9
Simulink	Version 7.4
Real Time Workshop	Version 7.4
C Language Compiler	Microsoft Visual C/C++ Version 9.0
xPC Target	Version 4.2

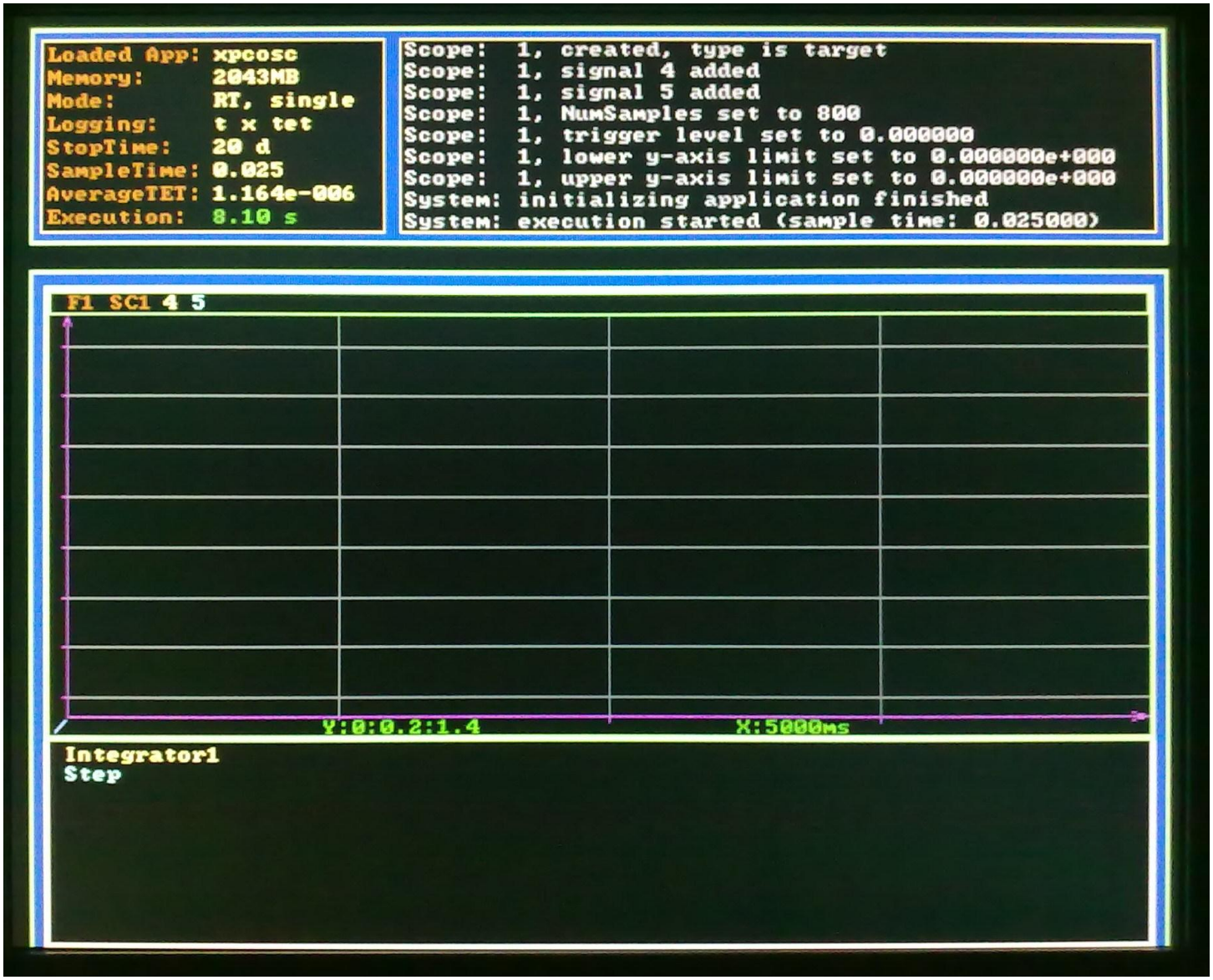
Loaded App: xpcosc
Memory: 2043MB
Mode: RT, single
Logging: t x tet
StopTime: 20 d
SampleTime: 0.025
AverageTET: 1.164e-006
Execution: 8.10 s
Scope: 1, created, type is target
Scope: 1, signal 4 added
Scope: 1, signal 5 added
Scope: 1, NumSamples set to 800
Scope: 1, trigger level set to 0.000000
Scope: 1, lower y-axis limit set to 0.000000e+000
Scope: 1, upper y-axis limit set to 0.000000e+000
System: initializing application finished
System: execution started (sample time: 0.025000)
F1 SC1 4 5
Y:0:0.2:1.4
X:5000ms
Integrator1
Step

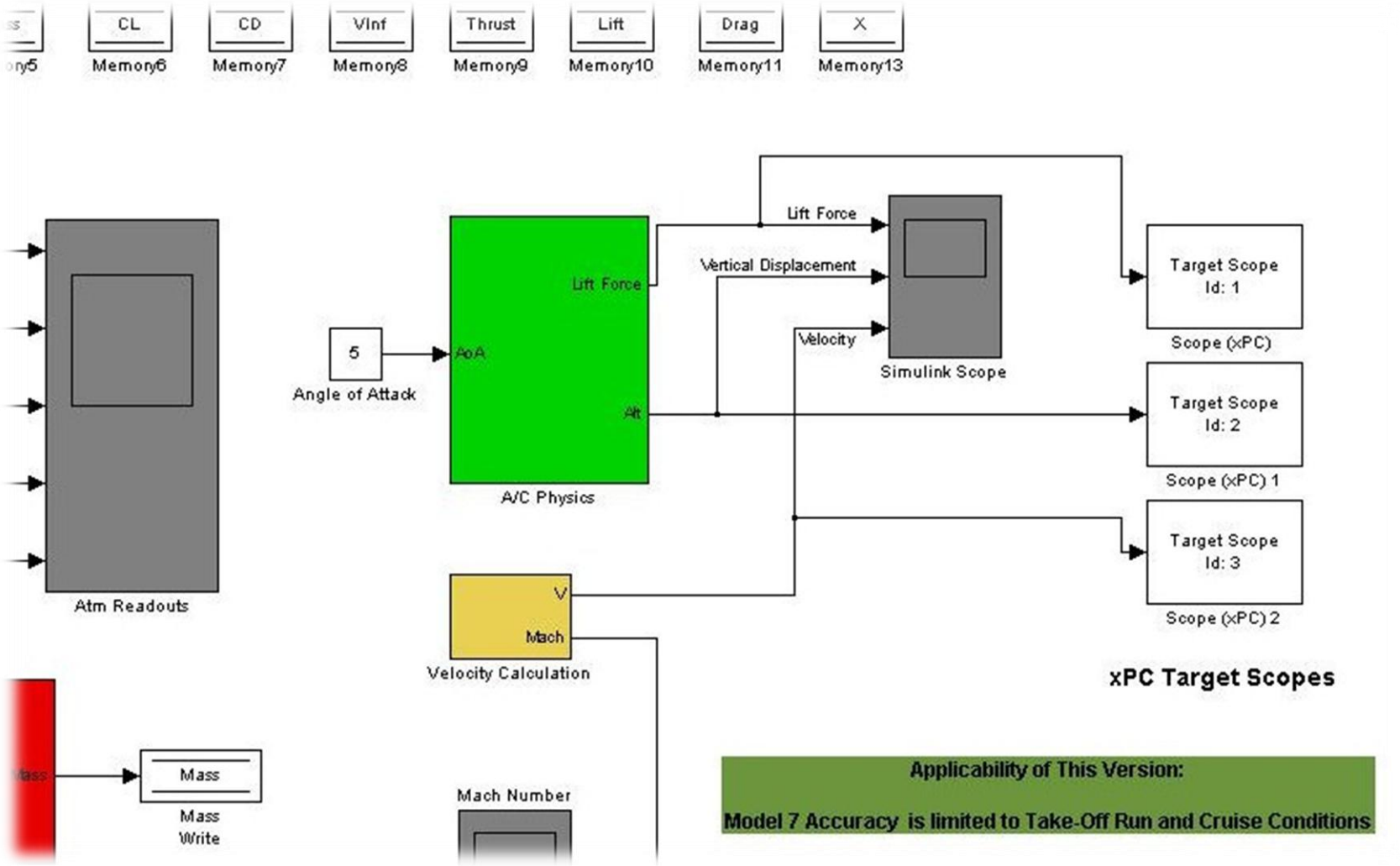
CL
CD
Vinf
Thrust
Lift
Drag
X
Memory6
Memory7
Memory8
Memory9
Memory10
Memory11
Memory13
Lift Force
Vertical Displacement
Velocity
Simulink Scope
Target Scope Id: 1
Scope (xPC)
Target Scope Id: 2
Scope (xPC) 1
Target Scope Id: 3
Scope (xPC) 2
5
Angle of Attack
AoA
Lift Force
Alt
A/C Physics
Atm Readouts
V
Mach
Velocity Calculation
xPC Target Scopes
Mass
Mass Write
Mach Number
Applicability of This Version:
Model 7 Accuracy is limited to Take-Off Run and Cruise Conditions

G.1 PHYSICAL MODEL INITIALISATION SCRIPT

```
%% SimMechanics Model Initialisation
% Adrian Harwood Individual Project 2009-2010
% This file specifies the data required to define the physical model
% construction and initial simulation conditions.
% Axes defined as: X (tail to nose), Y (left to right), Z (bottom to top)
% Axis rotations are Euler.
clear
%
%% Basic Data
FLen=37.57;          % Fuselage Length [m]
%
% Full Fuel Inertia [kg.m^2] - as computed by E1 Tool
FIxx=1901628;
FIyy=3210118;
FIzz=4750479;
FIxz=475048;
FMass=73500;         % Full Fuel Mass [kg] -MTOW
WSpan=34.09;         % Wing Span [m]
WSweep=25;           % Wing Sweep [deg]
TPSpan=12.7;         % Tail Plane Span [m]
TPSweep=25;          % Tail Plane Sweep [deg]
TMax=45000;          % Max Thrust [N] - one engine
CruiseU=270;         % Cruise Velocity [m/s]
%
% Aerodynamic Data Wing
Wdi=3;               % Dihedral Angle [deg]
WArea=122.4;         % Wing Area [m^2]
WingSet=0;           % Wing Setting Angle [deg]
Cd0=0.01;            % Profile Drag Factor
Cdk=0.01534;         % Lift Induced Drag Factor
Cla=0.115;           % Lift Curve Slope [1/deg]
Cl0=0.36734;         % Zero AoA Lift Coefficient
%
% Aerodynamic Data Tail
TPDi=6;              % Tailplane Dihedral [deg] - Graphical Estimate
TPArea=31;           % Tail Plane Area [m^2]
TPSet=0;             % Tail Plane Setting Angle [deg]
Cd0t=0.04;           % Profile Drag Factor (Tail)
Cdkt=0.04;           % Lift Induced Drag Factor (Tail)
Clat=0.105;          % Lift Curve Slope [1/deg] (Tail)
Cl0t=0.3;            % Zero AoA Lift Coefficient (Tail)
%
% General Aero Data
ClMax=1.2;           % Maximum Lift Coefficient (Wing and Tail - no HLDs)
FArea=13;            % Fuselage Reference Area [m^2]
FClMax=0.2;          % Fuselage Max Lift Coefficient
FCdMax=0.54;         % Fuselage Max Drag Coefficient
%
%% Fuselage
% CG Location from Model Estimate [m]
Fcg=[-15.7 0 -1];
%
% Back End of Fuselage
FEnd=[-FLen 0 0];
%
% Inertia Tensor
FMoi=[FIxx 0 FIxz; 0 FIyy 0; FIxz 0 FIzz];
%
```

```
% Wing Connection Location and Orientation
FWing=[-14.4 0 -0.6];
FWingO=[WingSet Wdi 0];
%
% Tail Connection Location and Orientation
FTail=[-34.4 0 1.12];
FTailO=[TPSet TPDi 0];
%
%% Wing Left
% Wing Tip Location
LWTip=[-((WSpan/2)*tand(WSweep)) -WSpan/2 0];
%
% Engine Location
LWEng=[-12.95 -5.71 -1.5];
%
% Aero Centre Location - Assumed to lie on the MAC
LWAero=[-14.4 -8 0.5];
%
%% Wing Right
% Wing Tip Location
RWTip=[-((WSpan/2)*tand(WSweep)) WSpan/2 0];
%
% Engine Location
RWEng=[-12.95 5.71 -1.5];
%
% Aero Centre Location - Assumed to lie on the MAC
RWAero=[-14.4 8 0.5];
%
%% Tail Left
% Tail Plane Tip Location
LTPTip=[-((TPSpan/2)*tand(TPSweep)) -TPSpan/2 0];
%
% Tail Plane Aero Centre - Assumed to lie on the MAC
LTPAero=[-33.4 -3.1 2.2];
%
%% Tail Right
% Tail Plane Tip Location
RTPTip=[-((TPSpan/2)*tand(TPSweep)) TPSpan/2 0];
%
% Tail Plane Aero Centre - Assumed to lie on the MAC
RTPAero=[-33.4 3.1 2.2];
%
```

The following diagram illustrates the arrangement and functionality of the physical model.

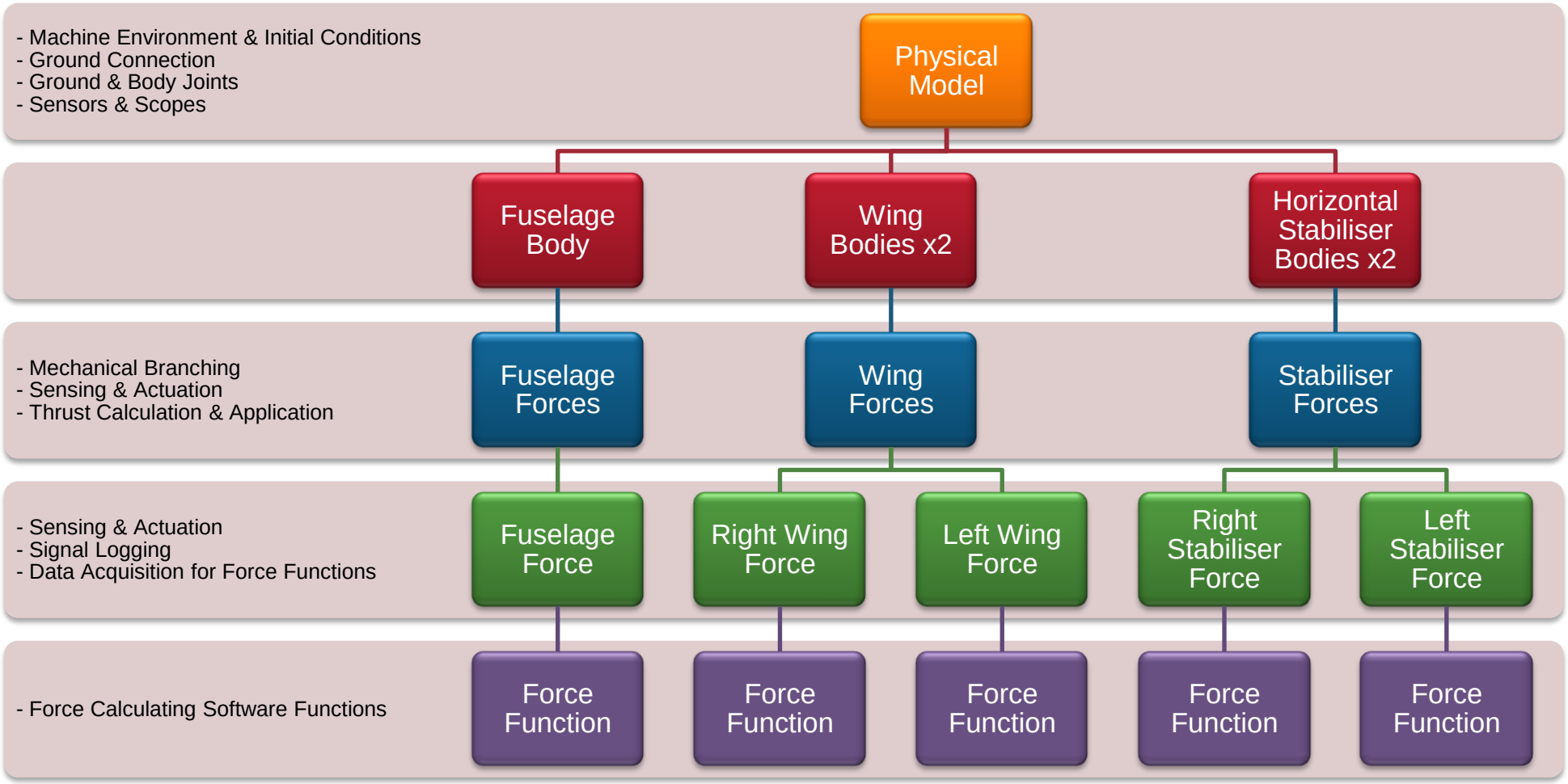

H.1 FLIGHT TEST PLAN

Test Phase Designator	Test Procedure	Models Required
A1a	1. Set flaps to up for TO, as early as possible with fixed trim.	M1
A1b	2. Climb Out and rate of 2000 ft/min to 30,000 ft, trimmed flight at 340 kts IAS. 3. Fly for 2 Minutes straight and level for data capture.	M1
A2a	1. Set flaps to Stage One for TO, as early as possible with fixed trim.	M2
A2b	2. Climb Out and rate of 2000 ft/min to 30,000 ft, trimmed flight at 340 kts IAS. 3. Fly for 2 Minutes straight and level for data capture.	M2
A3a	1. Set Flaps to Stage Two for TO, as early as possible with fixed trim.	M3
A3b	2. Climb Out and rate of 2000 ft/min to 30,000 ft, trimmed flight at 340 kts IAS. 3. Fly for 2 Minutes straight and level for data capture.	M3
B1, B2, B3	1. TO and downwind leg at 3000 ft for 8 nm approach at 120 kts IAS. 2. Trimmed ILS approach.	M4, M5, M6 *Conducted using 50% Fuel Load*
C1a, C2a, C3a	1. Execute TO run and abort at V1 braking to a stop with Reverse and Spoilers. Note: $V1_{C1}$= 80 kts; $V1_{C2}$= 110 kts; $V1_{C3}$= 140 kts	M1
C1b, C2b, C3b	2. Execute TO run and continue with OEI @ V1. Note: $V1_{C1}$= 80 kts; $V1_{C2}$= 110 kts; $V1_{C3}$= 140 kts	M1
D1a, D2a, D3a	1. TO with maximum nose up trim, and Climb at Maximum possible rate with Flaps and Gear Retracted at 200 ft.	M1, M5, M7
D1b, D2b, D3b	2. Trim at 5,000 ft in Straight and Level flight. 3. Insert Control Input and Release controls to generate Short Period & Phugoid.	M1, M5, M7
E1a, E2a, E3a	1. Climb Out and rate of 2000 ft/min to 30,000 ft, trimmed flight at 340 kts IAS. 2. Fly for 2 Minutes straight and level for data capture.	M1, M8, M9
E1b, E2b, E3b	3. Trim at 300 kts IAS and fly for 2 minutes straight and level.	M1, M8, M9
E1c, E2c, E3c	4. Trim at 380 kts IAS and fly for 2 minutes straight and level.	M1, M8, M9
E1d, E2d	5. Climb to Ceiling for Maximum Thrust. 6. Trim at Ceiling and maintain Maximum Thrust to terminal velocity. 7. Reduce speed and Maintain Altitude until Stall. 8. Descend to 10,000 ft and repeat step 6 and 7. 9. Descend to 5,000 ft and repeat steps 6 and 7. 10. Trim at 5,000 ft in straight and level flight. 11. Repeat step 7 with Flap Stage One.	M1, M8

Model Designator	Weight Variable Details
M1	Max Payload + Fuel = MTOW
M2	Max Fuel + Payload = MTOW
M3	Zero Payload + Max Fuel < MTOW
M4	Zero Payload + Fuel = MLW
M5	Zero Payload + Fuel = 0.95 * MLW
M6	Zero Payload + Fuel = 0.9 * MLW
M7	Zero Payload + Fuel = 0.85 * MLW
M8	Payload + Max Fuel = 0.85 * MTOW
M9	Payload + Fuel = 0.75 * MTOW

Source: (Diston, 2.1.4.5 Euler Angles, 2009)

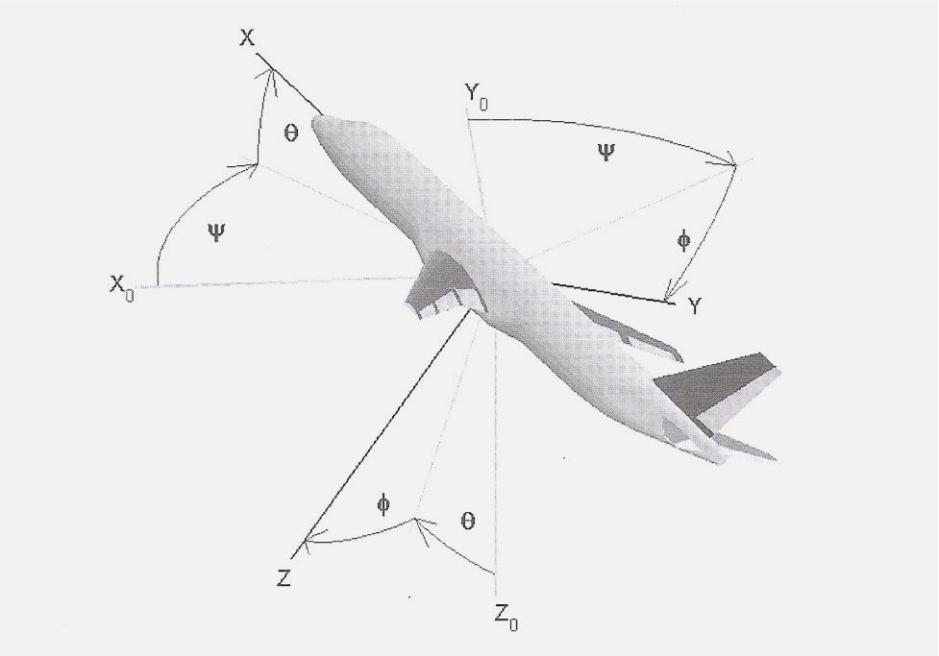

The convention of the above diagram is given in the table below.

Quantity	Description
$[X_0 \quad Y_0 \quad Z_0]$	Datum Axes
$[X \quad Y \quad Z]$	Aircraft Body Axes
$[\theta \quad \phi \quad \psi]$	Euler Angles [Pitch Roll Yaw]

J.1 SIMPLE STATIC STABILITY DEFINITION

Source: (Cook, 1997)

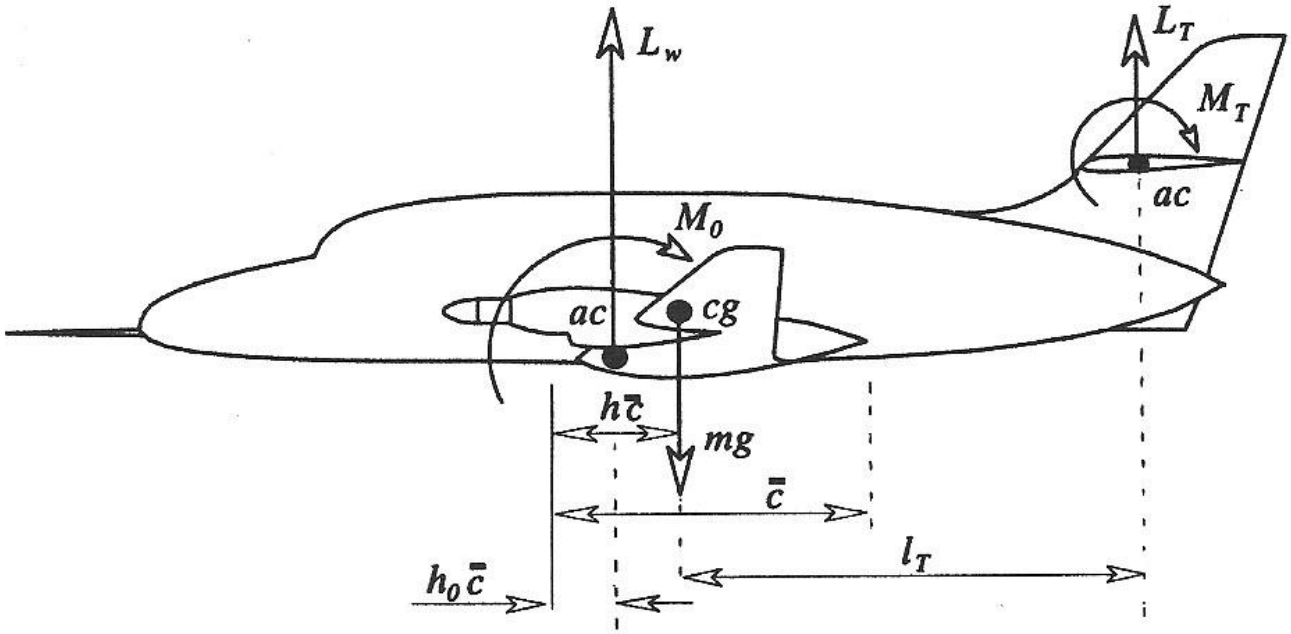

Applying equilibrium conditions:

$$M = M_0 + L_w(h - h_0)\bar{\bar{c}} - L_T l_T + M_T$$

J.2 MASS, INERTIA, AERODYNAMIC STABILITY & CONTROL DERIVATIVES

$$m' = \frac{m}{\frac{1}{2}\rho V_0 S}$$

$$I'_x = \frac{I_x}{\frac{1}{2}\rho V_0 S b}$$

$$I'_y = \frac{I_y}{\frac{1}{2}\rho V_0 S \bar{\bar{c}}}$$

$$I'_z = \frac{I_z}{\frac{1}{2}\rho V_0 S b}$$

$$I'_{xz} = \frac{I_{xz}}{\frac{1}{2}\rho V_0 S b}$$

$$X_u = -2C_D - V_0\frac{\partial C_D}{\partial V} + \frac{1}{\frac{1}{2}\rho V_0 Z}\frac{\partial \tau}{\partial V}$$

$$X_w = C_L - \frac{\partial C_D}{\partial V}$$

$$X_q = -\bar{V}_T \frac{\partial C_{D_T}}{\partial \alpha_T}$$

$$X_{\dot{w}} = -\bar{V}_T \frac{\partial C_{D_T}}{\partial \alpha_T} \frac{d\varepsilon}{d\alpha} \equiv X_q \frac{d\varepsilon}{d\alpha}$$

$$Z_u = -2C_L - V_0 \frac{\partial C_L}{\partial V}$$

$$Z_w = -C_D - \frac{\partial C_L}{\partial \alpha}$$

$$Z_q = -\bar{V}_T a_1$$

$$Z_{\dot{w}} = -\bar{V}_T a_1 \frac{d\varepsilon}{d\alpha} \equiv Z_q \frac{d\varepsilon}{d\alpha}$$

$$M_u = V_0 \frac{\partial C_m}{\partial V}$$

$$M_w = \frac{dC_m}{d\alpha} = -aK_n$$

$$M_q = \bar{V}_T a_1 \frac{l_T}{\tilde{c}} \equiv Z_q \frac{l_T}{\tilde{c}}$$

$$M_{\dot{w}} = \bar{V}_T a_1 \frac{l_T}{\tilde{c}} \frac{d\varepsilon}{d\alpha} \equiv M_q \frac{d\varepsilon}{d\alpha}$$

$$X_\eta = -2 \frac{S_T}{S} k_T C_{L_T} a_2$$

$$Z_\eta = -\frac{S_T}{S} a_2$$

$$M_\eta = -\bar{V}_T a_2$$

$$x_u = \frac{X_u}{m'} + \frac{\frac{\tilde{c}}{V_0} X_{\dot{w}} Z_u}{m'\left(m' - \frac{\tilde{c}}{V_0} Z_{\dot{w}}\right)}$$

$$z_u = \frac{Z_u}{m' - \frac{\tilde{c}}{V_0} Z_{\dot{w}}}$$

$$m_u = \frac{M_u}{I'_y} + \frac{\frac{\tilde{c}}{V_0} M_{\dot{w}} Z_u}{I'_y\left(m' - \frac{\tilde{c}}{V_0} Z_{\dot{w}}\right)}$$

$$x_w = \frac{X_w}{m'} + \frac{\frac{\tilde{c}}{V_0} X_{\dot{w}} Z_w}{m'\left(m' - \frac{\tilde{c}}{V_0} Z_{\dot{w}}\right)}$$

$$z_w = \frac{Z_w}{m' - \frac{\tilde{c}}{V_0} Z_{\dot{w}}}$$

$$m_w = \frac{M_w}{I'_y} + \frac{\frac{\tilde{c}}{V_0} M_{\dot{w}} Z_w}{I'_y\left(m' - \frac{\tilde{c}}{V_0} Z_{\dot{w}}\right)}$$

$$x_q = \frac{\tilde{c} X_q - m' W_e}{m'} + \frac{\left(\tilde{c} Z_q + m' U_e\right)\frac{\tilde{c}}{V_0} X_{\dot{w}}}{m'\left(m' - \frac{\tilde{c}}{V_0} Z_{\dot{w}}\right)}$$

$$z_q = \frac{\tilde{c} Z_q + m' U_e}{m' - \frac{\tilde{c}}{V_0} Z_{\dot{w}}}$$

$$m_q = \frac{\tilde{c} M_q}{I'_y} + \frac{\left(\tilde{c} Z_q + m' U_e\right)\frac{\tilde{c}}{V_0} M_{\dot{w}}}{I'_y\left(m' - \frac{\tilde{c}}{V_0} Z_{\dot{w}}\right)}$$

$$x_\theta = -g\cos\theta_e - \frac{\frac{\tilde{c}}{V_0} X_{\dot{w}} g \sin\theta_e}{m' - \frac{\tilde{c}}{V_0} Z_{\dot{w}}}$$

$$z_\theta = -\frac{m' g \sin\theta_e}{m' - \frac{\tilde{c}}{V_0} Z_{\dot{w}}}$$

$$m_\theta = -\frac{\frac{\tilde{c}}{V_0} M_{\dot{w}} m' g \sin\theta_e}{I'_y\left(m' - \frac{\tilde{c}}{V_0} Z_{\dot{w}}\right)}$$

$$x_\eta = \frac{V_0 X_\eta}{m'} + \frac{\frac{\tilde{c}}{V_0} X_{\dot{w}} Z_\eta}{m'\left(m' - \frac{\tilde{c}}{V_0} Z_{\dot{w}}\right)}$$

$$z_\eta = \frac{V_0 Z_\eta}{m' - \frac{\tilde{c}}{V_0} Z_{\dot{w}}}$$

$$m_\eta = \frac{V_0 M_\eta}{I'_y} + \frac{\tilde{c} M_{\dot{w}} Z_\eta}{I'_y\left(m' - \frac{\tilde{c}}{V_0} Z_{\dot{w}}\right)}$$

J.4 SIMPLE FLAP (ELEVATOR) SIMULATION ILLUSTRATION

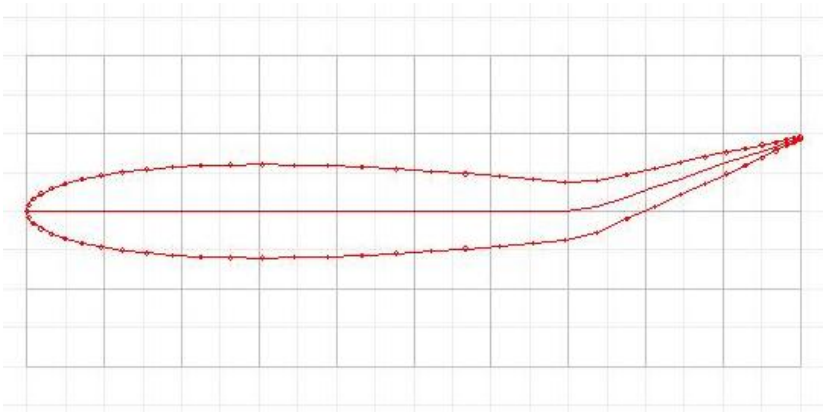

J.5 STATE SPACE ASSEMBLY CODE

```
%% State Space Assembly and Solution
% Adrian Harwood Individual Project 2009-2010
% This script produces and solves the state space for the modelled
% A320-200.
%
%% Population of Parameters
%
close all
%
g=9.81;                 % Acceleration Due to Gravity [m/s^2]
m=73500;                % Mass
                        % Full Fuel Inertia [kg.m^2] - as computed by E1 Tool
Ixx=1901628;
Iyy=3210118;
Izz=4750479;
Ixz=475048;
%
% Wing Data
b=34.09;                % Wing Span [m]
cbar=3.36;              % MAC [m]
Sw=122.4;               % Wing Area [m^2]
Cd0=5.18e-3;            % Profile Drag Factor
kt=5.93e-2;             % Lift Induced Drag Factor
Cla=4.026;              % Lift Curve Slope [1/rad]
Clc=0.7;                % Cruise Lift Coefficient
Cl=Clc;                 % Lift Coefficient
Cda=2*kt*Cl*Cla;        % Derivative of Drag Equation [1/rad]
Cd=Cd0+(kt*(Cl^2));     % Drag Equation
Cma=-6.711;             % Moment Curve Slope [1/rad]
%
% Tail Data
St=31;                  % Tail Plane Area [m^2]
lt=18.7;                % Tail Arm [m]
Vbart=1.405;            % Tail Volume Ratio
Cdta=0;                 % Tail Drag Equation Derivative [1/rad]
epa=0.5;                % Downwash Increment with Incidence
Clta=3.87;              % Tail Lift Curve Slope
Clteta=-4.469;          % Cl vs Elevator Deflection Slope [1/rad]
Clt=Clta;               % Tail Lift Coefficient
%
% Initial Conditions - From Simulator Data
V0=188.43;          % Body Velocity [m/s]
```

```
Rho=1.0556;          % Density
Ue=V0;               % Forward Body Component of Velocity - assume body axes
coincident with Earth axes.
We=0;                % Vertical Body Component of Velocity - assume body axes
coincident with Earth axes.
the=0;               % Inclination of Forward Body Axis to Earth - assume body axes
coincident with Earth axes.
%
%% Dimensionless Mass and Inertia
mdash=m/(0.5*Rho*V0*Sw);
Idashx=Ixx/(0.5*Rho*V0*Sw*b);
Idashy=Iyy/(0.5*Rho*V0*Sw*cbar);
Idashz=Izz/(0.5*Rho*V0*Sw*b);
Idashxz=Ixz/(0.5*Rho*V0*Sw*b);
%
%% Calculation of Non-Zero Derivatives
disp('Assumed that d*/dV = 0')
disp('Xq = Xwdot = Mu = 0 due to above approximation')
% Stability Derivatives
Xu=(-2*Cd);          % Terms that are zero have been omitted from the definition.
Xw=(Cl-Cda);
Xq=0;                % See Earlier Approximation.
Xwdot=0;             % See Earlier Approximation.
%
Zu=(-2*Cl);          % Terms that are zero have been omitted from the definition.
Zw=(-Cd-Cla);
Zq=(-Vbart*Clta);
Zwdot=(Zq*epa);
%
Mu=0;                % See Earlier Approximation.
Mw=Cma;
Mq=(Zq*(lt/cbar));
Mwdot=(Mq*epa);
% Control Derivatives
Xeta=(-2*(St/Sw)*kt*Clt*Clteta);
Zeta=(-(St/Sw)*Clteta);
Meta=(-Vbart*Clteta);
%
%% Concise Derivatives
xu=(Xu/mdash)+((Xwdot*Zu*(cbar/V0))/(mdash*(mdash-((cbar/V0)*Zwdot))));
zu=(Zu/(mdash-((cbar/V0)*Zwdot)));
mu=(Mu/Idashy)+((Mwdot*Zu*(cbar/V0))/(Idashy*(mdash-((cbar/V0)*Zwdot))));
%
xw=(Xw/mdash)+((Xwdot*Zw*(cbar/V0))/(mdash*(mdash-((cbar/V0)*Zwdot))));
zw=(Zw/(mdash-((cbar/V0)*Zwdot)));
mw=(Mw/Idashy)+((Mwdot*Zw*(cbar/V0))/(Idashy*(mdash-((cbar/V0)*Zwdot))));
%
xq=(((cbar*Xq)-
(mdash*We))/mdash)+((((cbar*Zq)+(mdash*Ue))*(cbar/V0)*Xwdot)/(mdash*(mdash-
((cbar/V0)*Zwdot))));
zq=((cbar*Zq)+(mdash*Ue))/(mdash-((cbar/V0)*Zwdot));
mq=((cbar*Mq)/Idashy)+((((cbar*Zq)+(mdash*Ue))*(cbar/V0)*Mwdot)/(Idashy*(mdash-
((cbar/V0)*Zwdot))));
%
xth=(-g*cos(the))-(((cbar/V0)*Xwdot*g*sin(the))/(mdash-((cbar/V0)*Zwdot)));
zth=(-mdash*g*sin(the))/(mdash-((cbar/V0)*Zwdot));
mth=(-(cbar/V0)*Mwdot*mdash*g*sin(the))/(Idashy*(mdash-((cbar/V0)*Zwdot)));
%
xeta=((V0*Xeta)/mdash)+(((cbar/V0)*Xwdot*Zeta)/(mdash*(mdash-((cbar/V0)*Zwdot))));
zeta=(V0*Zeta)/(mdash-((cbar/V0)*Zwdot));
meta=((V0*Meta)/Idashy)+((cbar*Mwdot*Zeta)/(Idashy*(mdash-((cbar/V0)*Zwdot))));
%
%% Generate State Space Matrices of Concise Derivatives
%
```

```
AA=[xu xw xq xth; zu zw zq zth; mu mw mq mth; 0 0 1 0];
BB=[xeta; zeta; meta; 0];
CC=eye(4);
DD=zeros(4,1);
%
%% Generate LTI Model Object
%
% Generate Labels for Charts
states={'u' 'w' 'q' 'theta'};
inputs = {'elevator'};
outputs = {'u' 'w' 'q' 'th'};
notes={'Created by Adrian Harwood, March 2010'};
%
A320LTI=ss(AA,BB,CC,DD,'statename',states,'inputname',inputs,'outputname',outputs,
'notes',notes);
%
disp('Script Complete')
%
ltiview(A320LTI)
```

J.6.1 STATE VARIABLE PLOTS

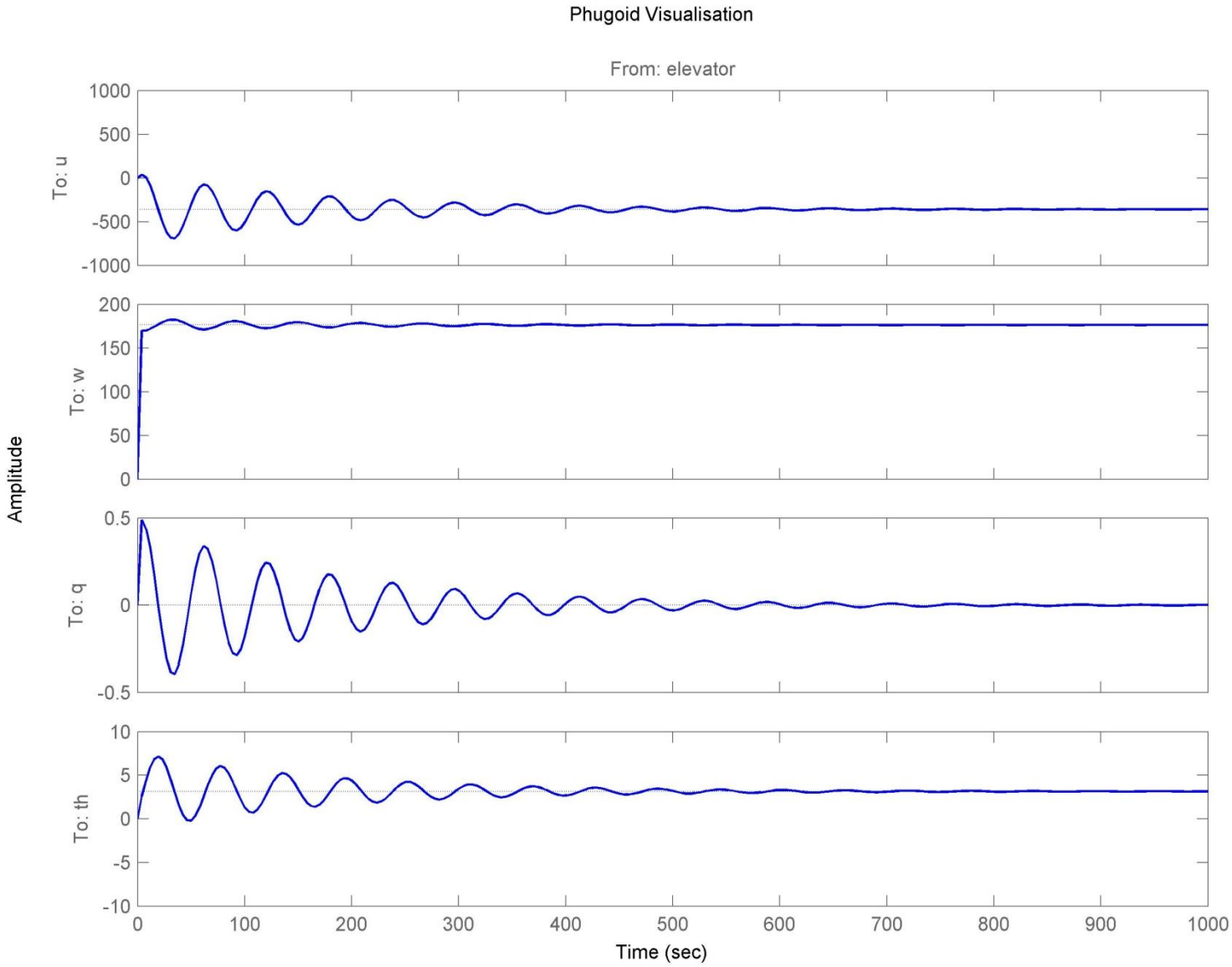

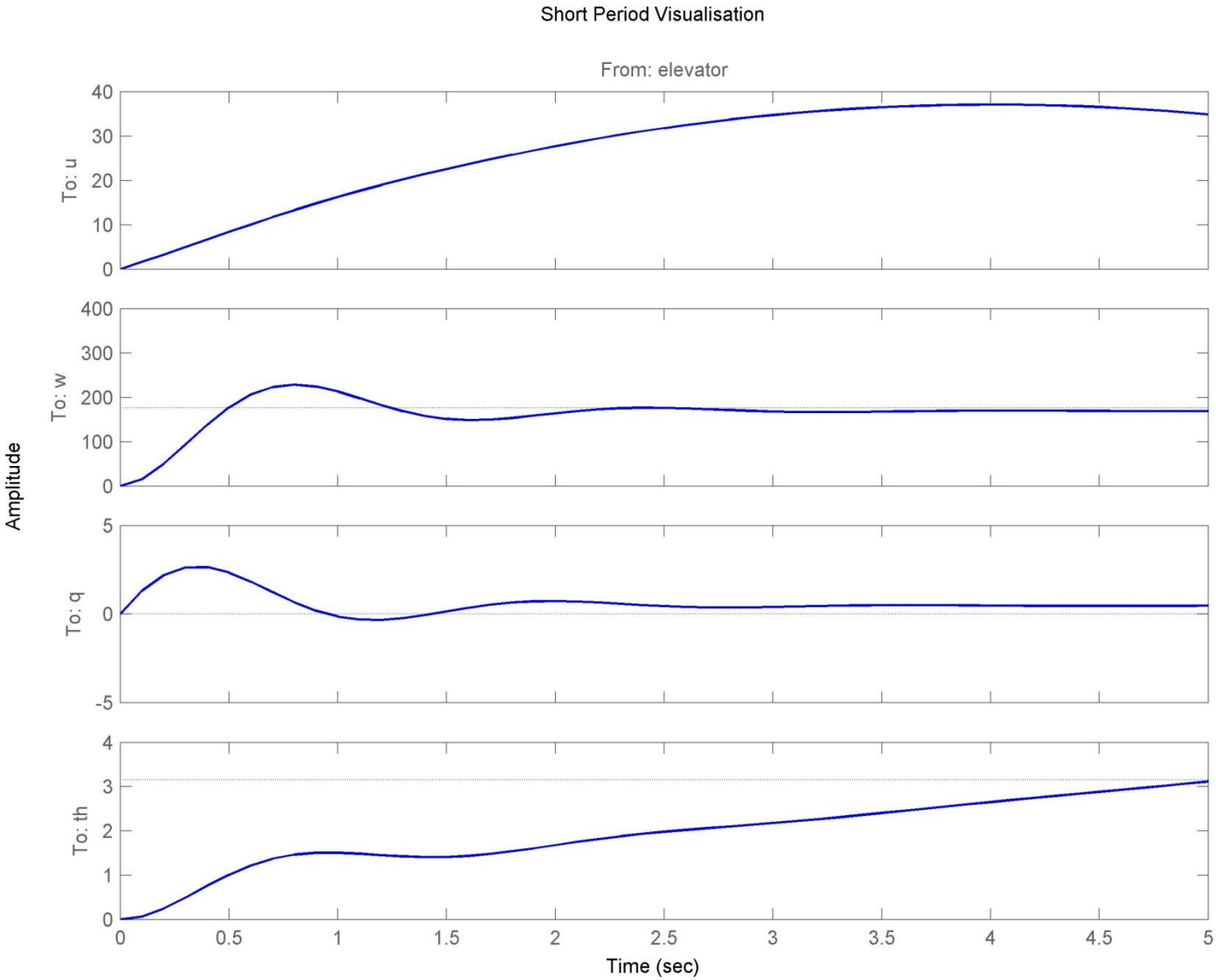
Short Period Visualisation
From: elevator
To: u
To: w
To: q
To: th
Amplitude
Time (sec)

J.6.2 EIGENVALUE PROBLEM SOLUTION

State Space Matrix:

$$[A'] = \begin{bmatrix} -0.0027 & 0.1104 & 0 & -9.8100 \\ -0.2300 & -0.6626 & 183.7544 & 0 \\ 0.0008 & -0.0831 & -2.0019 & 0 \\ 0 & 0 & 1 & 0 \end{bmatrix}$$

Eigenvector Matrix:

$$[V] = \begin{bmatrix} 0.0012 - j0.0030 & 0.0012 + j0.0030 & 0.9998 & 0.9998 \\ 0.9998 & 0.9998 & -0.0179 - j0.0012 & -0.0179 + j0.0012 \\ -0.0034 + j0.0210 & -0.0034 - j0.0210 & 0.0012 - j0.000 & 0.0012 + j0.000 \\ 0.0052 - j0.0008 & 0.0052 + j0.0008 & -0.0007 - j0.0110 & -0.0007 + j0.0110 \end{bmatrix}$$

Eigenvalue Matrix:

$$[\Lambda] = \begin{bmatrix} -1.2976 + j3.8614 & 0 & 0 & 0 \\ 0 & -1.2976 - j3.8614 & 0 & 0 \\ 0 & 0 & -0.0055 + j0.1077 & 0 \\ 0 & 0 & 0 & -0.0055 - j0.1077 \end{bmatrix}$$

J.6.3 TIME DOMAIN STATE VARIABLE RESPONSE

Using the solutions to the eigenvalue problem given in J.6.2 the following time domain responses may be formulated:

$u(t)$:

$$\left.\begin{array}{c} (0.0012 - j0.0030)e^{-1.2976t}(\cos 3.8614 + j \sin 3.8614) \\ (0.0012 + j0.0030)e^{-1.2976t}(\cos 3.8614 - j \sin 3.8614) \\ (0.9998)e^{-0.0055t}(\cos 0.1077 + j \sin 0.1077) \\ (0.9998)e^{-0.0055t}(\cos 0.1077 - j \sin 0.1077) \end{array}\right\}$$

$w(t)$:

$$\left.\begin{matrix}(0.9998)e^{-1.2976t}(\cos 3.8614 + j\sin 3.8614)\\(0.9998)e^{-1.2976t}(\cos 3.8614 - j\sin 3.8614)\\(-0.0179 - j0.0012)e^{-0.0055t}(\cos 0.1077 + j\sin 0.1077)\\(-0.0179 + j0.0012)e^{-0.0055t}(\cos 0.1077 - j\sin 0.1077)\end{matrix}\right\}$$

$q(t)$:

$$\left.\begin{matrix}(-0.0034 + j0.0210)e^{-1.2976t}(\cos 3.8614 + j\sin 3.8614)\\(-0.0034 - j0.0210)e^{-1.2976t}(\cos 3.8614 - j\sin 3.8614)\\(0.0012 - j0.000)e^{-0.0055t}(\cos 0.1077 + j\sin 0.1077)\\(0.0012 + j0.000)e^{-0.0055t}(\cos 0.1077 - j\sin 0.1077)\end{matrix}\right\}$$

$\theta(t)$:

$$\left.\begin{matrix}(0.0052 - j0.0008)e^{-1.2976t}(\cos 3.8614 + j\sin 3.8614)\\(0.0052 + j0.0008)e^{-1.2976t}(\cos 3.8614 - j\sin 3.8614)\\(-0.0007 - j0.0110)e^{-0.0055t}(\cos 0.1077 + j\sin 0.1077)\\(-0.0007 + j0.0110)e^{-0.0055t}(\cos 0.1077 - j\sin 0.1077)\end{matrix}\right\}$$

Where the actual time domain response is a summation of these contributory mode shapes.

J.6.4 STATE VARIABLE TRANSFER FUNCTIONS

$$\frac{u(s)}{\eta(s)} = \frac{16.21s^3 + 44.19s^2 + 293s - 69.26}{s^4 + 2.606s^3 + 16.63s^2 + 0.214s + 0.1929}$$

$$\frac{w(s)}{\eta(s)} = \frac{35.04s^3 + 2815s^2 + 27.13s + 34.02}{s^4 + 2.606s^3 + 16.63s^2 + 0.214s + 0.1929}$$

$$\frac{q(s)}{\eta(s)} = \frac{14.95s^3 + 7.243s^2 + 0.609s - 4.06 \times 10^{-17}}{s^4 + 2.606s^3 + 16.63s^2 + 0.214s + 0.1929}$$

$$\frac{\theta(s)}{\eta(s)} = \frac{14.95s^2 + 7.243s + 0.609}{s^4 + 2.606s^3 + 16.63s^2 + 0.214s + 0.1929}$$

K FLIGHT SIMULATOR DATA

K.1 MACE FLIGHT SIMULATOR EXPORTED DATA

System Variables

Description	Units
Simulation elapsed time	seconds
Event marker, zero for no event being recorded, incremental positive integer to flag events	

Rigid Body Variables

Description	Units
North position (from simulation start)	m
East position (from simulation start)	m
Altitude above sea level	m
Latitude	deg
Longitude	deg
Body axis forward speed	m/s
Body axis lateral speed	m/s
Body axis vertical (down) speed	m/s
Body axis forward acceleration	m/s^2
Body axis lateral acceleration	m/s^2
Body axis normal acceleration	m/s^2
Euler roll attitude	deg
Euler pitch attitude	deg
Euler heading angle	deg
Body axis roll rate	deg/s
Body axis pitch rate	deg/s
Body axis yaw rate	deg/s
Body axis roll acceleration	deg/s^2
Body axis pitch acceleration	deg/s^2
Body axis yaw acceleration	deg/s^2

Speed & Flight Path Variables

Description	Units
Incidence angle	deg
Sideslip angle	deg
Flight path angle	deg
True (inertial) speed	kts
True air speed	kts
Indicated air speed	kts
Equivalent air speed	kts
Ground speed	kts
Ground track angle	deg
Rate of change of altitude	m/s
Mach number	
Load factor (g)	
Height above terrain (radio altitude)	m

Aircraft Control Deflections

Description	Units
Elevator deflection	deg
Aileron deflection	deg
Rudder deflection	deg
Airbrake (spoiler) deflection	0.0 = retracted 1.0 = deployed
Flap deflection	0.0 = retracted n.0 = flap stage
Undercarriage deflection	0.0 = retracted 1.0 = deployed
Roll spoiler deflection	deg
Left engine thrust	N
Right engine thrust	N

Cockpit Control Deflections

Description	Units
Longitudinal stick position	+/- 1.0
Lateral stick position	+/- 1.0
Pedal position	+/- 1.0
Left throttle position	0.0 ->1.0
Right throttle position	0.0 ->1.0
Flap switch position	0.0 ->1.0
Gear switch position	0.0 ->1.0
Airbrake (spoiler) switch position	0.0 ->1.0

Aircraft Parameters

Description	Units
Aircraft total mass	kg
Moment of inertia	$kg.m^2$
Moment of inertia	$kg.m^2$
Moment of inertia	$kg.m^2$
Moment of inertia	$kg.m^2$
Fuel state	0.0 = full 1.0 = empty
Current CG position	m
Current CG position	m
Current CG position	m

Empty Mass	Aileron Cl Increment	Engine 3 Yaw Mounting Angle	Roll Control Surface Travel Up
Fuel Capacity	Aileron Cd Increment	Engine 3 Pitch Mounting Angle	Roll Control Surface Travel Down
Payload	Aileron Span Fraction	Engine 4 Yaw Mounting Angle	Pitch Control Dead Band
Full Fuel Mass	Aileron Y Moment Arm	Engine 4 Pitch Mounting Angle	Pitch Control Stick Shaping
Zero Fuel Mass	Fuselage Minimum Cd	Engine 1 Mounting Position X	Pitch Control Rate Limit
Ixx Zero Fuel	Fuselage Maximum Cd	Engine 1 Mounting Position Y	Pitch Control Surface Travel Up
Iyy Zero Fuel	Fuselage Aero Centre X Coordinate	Engine 1 Mounting Position Z	Pitch Control Surface Travel Down
Izz Zero Fuel	Fuselage Aero Centre Z Coordinate	Engine 2 Mounting Position X	Yaw Control Dead Band
Ixz Zero Fuel	Fuselage Reference Area	Engine 2 Mounting Position Y	Yaw Control Stick Shaping
Ixx Full Fuel	Fuselage Length	Engine 2 Mounting Position Z	Yaw Control Rate Limit
Iyy Full Fuel	Spoiler Cd Increment	Engine 3 Mounting Position X	Yaw Control Surface Travel Up
Izz Full Fuel	Spoiler Cl Increment (wrt Wing Area)	Engine 3 Mounting Position Y	Throttle Mapping Lever Position Low
Ixz Full Fuel	Spoiler Reference Area	Engine 3 Mounting Position Z	Throttle Mapping Lever Position Mid
CG x Zero Fuel	Spoiler Aero Centre X Coordinate	Engine 4 Mounting Position X	Throttle Mapping Lever Position High
CG y Zero Fuel	Spoiler Aero Centre Z Coordinate	Engine 4 Mounting Position Y	Throttle Mapping Power Selection Low
CG z Zero Fuel	Tailplane Setting Angle	Engine 4 Mounting Position Z	Throttle Mapping Power Selection Mid
CG x Full Fuel	Tailplane Downwash Immersion	Thrust Lapse 1,1 (Air Density Ratio vs Mach)	Throttle Mapping Power Selection High
CG y Full Fuel	Tailplane Aero Centre X	Thrust Lapse 2,1 (Air Density Ratio vs Mach)	Flap Transit Time (per Stage)
CG z Full Fuel	Tailplane Aero Centre Z	Thrust Lapse 3,1 (Air Density Ratio vs Mach)	Spoiler Transit Time
Pilot Eye Position x	Tailplane Lift Curve Slope	Thrust Lapse 1,2 (Air Density Ratio vs Mach)	Gear Transit Time
Pilot Eye Position y	Tailplane Profile Drag Factor	Thrust Lapse 2,2 (Air Density Ratio vs Mach)	Pitch Trim Rate
Pilot Eye Position z	Tailplane Induced Drag Factor	Thrust Lapse 3,2 (Air Density Ratio vs Mach)	Roll Trim Rate
Wing Area	Tailplane Area	Thrust Lapse 1,3 (Air Density Ratio vs Mach)	Yaw Trim Rate
Wing Setting Angle	Elevator Cl Increment	Thrust Lapse 2,3 (Air Density Ratio vs Mach)	Roll Trim Authority
Wing Span	Elevator Cd Increment	Thrust Lapse 3,3 (Air Density Ratio vs Mach)	Yaw Trim Authority
Wing MAC	Fin Aero Centre X	Main Gear Track	Q Feel Max Q Speed
Wing Taper Ratio	Fin Aero Centre Z	Main Gear X Coordinate	Q Feel Min Q Speed
Wing Aspect Ratio	Fin Lift Curve Slope	Main Gear Z Coordinate (Extended)	Q Feel Min Q
Wing Dihedral Angle	Fin Profile Drag Factor	Main Gear Stiffness	Wing Area Check
Wing Sweep Angle	Fin Induced Drag Factor	Main Gear Damping	Aspect Ratio Check
Wing Aero Centre X Coordinate	Fin Area	Main Gear Preload	Tail Volume Ratio
Wing Aero Centre Z Coordinate	Rudder Cl Increment	Nose Gear X Coordinate	Fin Volume Ratio

Wing Stall Warning Angle	Rudder Cd Increment	Nose Gear Z Coordinate (Extended)	Thrust/Weight Ratio
Wing Panel Span Fraction	Engine Type	Nose Gear Stiffness	Wing Loading
Wing Mount Dihedral Scale	Number of Engines	Nose Gear Damping	Cruise Speed
Stage 1 Flap Cl Increment	Engine Time Constant	Nose Gear Preload	Thrust Loading
Stage 1 Flap Cd Increment	Engine 1 Throttle Assignment	Brakes Max Friction Coefficient	Power Loading
Stage 1 Flap Cm Increment	Engine 2 Throttle Assignment	Brakes Actuator Time Constant	Undercarriage Natural Frequency
Stage 2 Flap Cl Increment	Piston Engine Power	Brakes Low Speed Friction Gradient	Undercarriage Damping Ratio
Stage 2 Flap Cd Increment	Piston Prop Diameter	Brakes Rolling Friction Coefficient	Undercarriage Gear Balance
Stage 2 Flap Cm Increment	Piston Max Prop Efficiency	Nosewheel Steering Travel	Undercarriage Static Deflection
Stage 3 Flap Cl Increment	Piston Prop Design Speed	Nosewheel Steering Washout Speed (low)	Tuning Lp
Stage 3 Flap Cd Increment	Piston SFC	Nosewheel Steering Washout Speed (high)	Tuning Lr
Stage 3 Flap Cm Increment	Jet Max SSL Thrust	Gear Drag Coefficient	Tuning Nr
Stage 4 Flap Cl Increment	Jet SFC	Gear Drag Reference Area	Tuning Lv (Lbeta)
Stage 4 Flap Cd Increment	Engine 1 Yaw Mounting Angle	Gear Drag Z Coordinate	Tuning Nv (Nbeta)
Stage 4 Flap Cm Increment	Engine 1 Pitch Mounting Angle	Roll Control Dead Band	Tuning Mq
Flap Span Fraction	Engine 2 Yaw Mounting Angle	Roll Control Stick Shaping	Tuning Mw (Malpha)
Empty Mass	Engine 2 Pitch Mounting Angle	Roll Control Rate Limit	

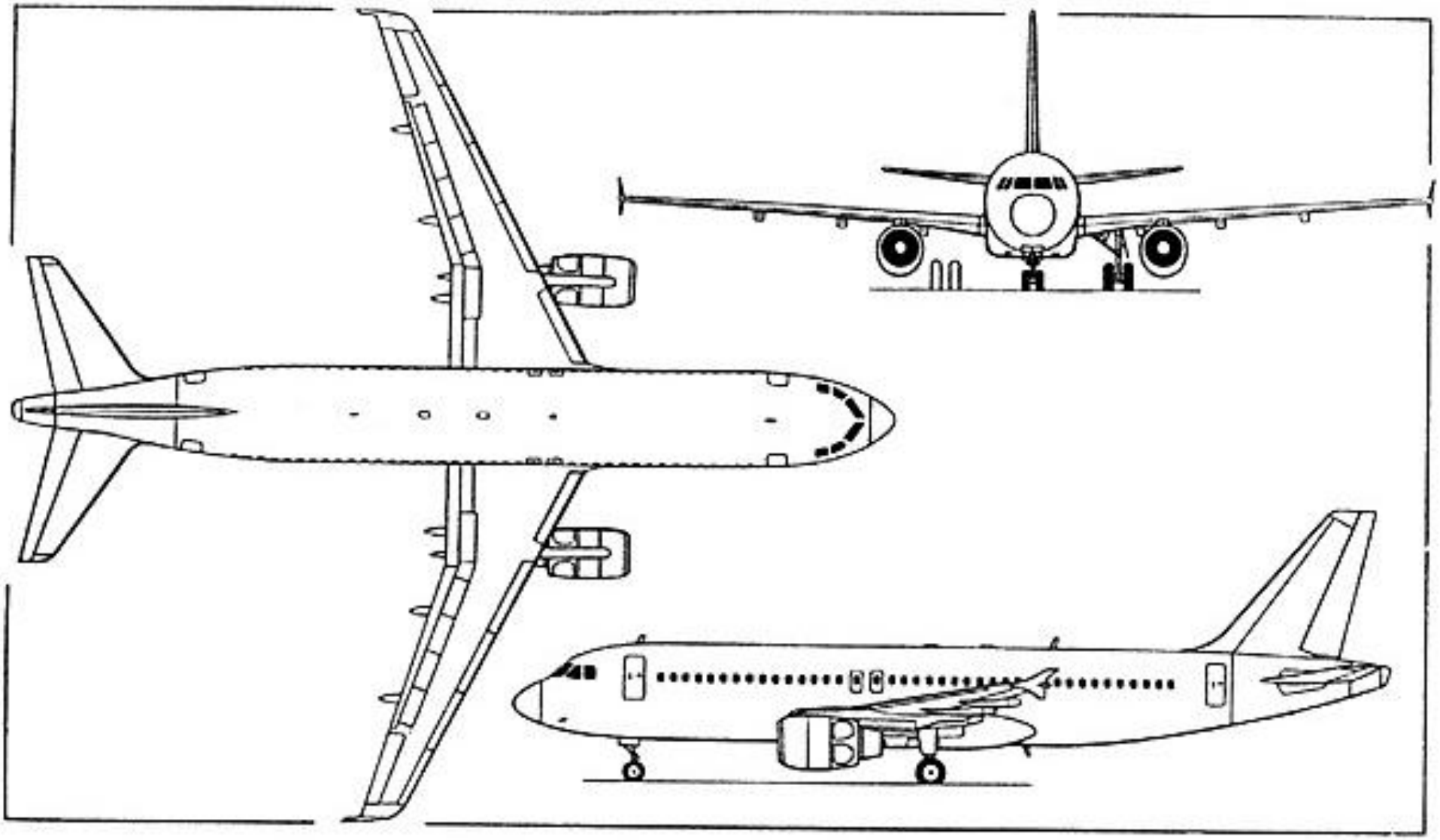

M.1 INPUT VALUE ASSESSMENT

Following this assessment are a number of supplementary notes that serve to clarify elements of the following table. Those values chosen to formulate an alternative model specification as referred to in the main body of the report are highlighted in green.

ID	Parameter	Units	Current	Source of Information				Notes:
				Research (Airbus, 2009)	**Research** (Jackson, Munson, & Peacock, 2008)	**3rd Party Model** (Project Airbus)	**Estimation or Simulation** (Jenkinson, Simpkin, & Rhodes, 1999)	***(Assumed A322,V2500, Fully Loaded) Datum (X,Y,Z) = (Wing Leading Edge @ Root, Fuselage Centreline, Centre Fuselage)***
1	Empty Mass	kg	40150	42600	42482	43727		Weights vary based on configurations and customisations. Basic Configuration used for source data.
2	Fuel Capacity	kg	3510	19464	19159	19185		Density of fuel 804 kg/m3 (Jet A-1 Source: BP) 6303.8 USG = 23862 Litres Fuel capacity in litres or gallons can then be used to obtain a mass estimate.
3	Payload	kg	2340	18143	18518	13002		Airbus Data estimated from Payload Range Chart in specifications.
4	Full Fuel Mass	kg	46000	80207	80159	75914	**73500**	Computed Value by E1 Tool. Note: MTOW = 73.5t (Airbus) - Hence Max Combination Fuel + Payload Impossible but red values take into account the maximum payload configuration.
5	Zero Fuel Mass	kg	42490	60743	61000	56729	**61000**	Computed Value by E1 Tool. Values shown here in red correspond to the alternative model specification.
6	Ixx Zero Fuel	kg.m^2	1099322	1571572	1578222	1467720	**1595021**	
7	Iyy Zero Fuel	kg.m^2	1855754	2652955	2664180	2477643	**2664180**	
8	Izz Zero Fuel	kg.m^2	2746229	3925964	3942574	3666530	**396171**	
9	Ixz Zero Fuel	kg.m^2	274623	392596	394257	366653	**358606**	
10	Ixx Full Fuel	kg.m^2	1190134	2075154	2073912	1964084	**1921869**	
11	Iyy Full Fuel	kg.m^2	2009054	3503047	3500950	3315550	**3210118**	

12	Izz Full Fuel	kg.m^2	2973089	5183968	5180866	4906502	**4773531**	
13	Ixz Full Fuel	kg.m^2	297309	518397	518087	490650	**477353**	
14	CG x Zero Fuel	m	-0.15			-2.76	-3.44	3rd Party model says 0.63ft forward of half MAC. Estimated as 15% forward limit of MAC mapped to centreline **See Note 1.**
15	CG y Zero Fuel	m	0				0	Assumed symmetric so on centreline
16	CG z Zero Fuel	m	2.032					Difficult to obtain estimate without precise knowledge of fuel distribution. Expected that it is lower than centre fuselage but inside fuselage limits.
17	CG x Full Fuel	m	-0.15			-2.76	-3.44	CG in reality likely to move but main fuel tank located near the expected CG position so fuel assumed to be of minimal effect on location for full payload.
18	CG y Full Fuel	m	0				0	Assumed symmetric so on centreline
19	CG z Full Fuel	m	2.032					Difficult to obtain estimate without precise knowledge of fuel distribution. Expected that it is lower than centre fuselage but inside fuselage limits. Left unchanged.
20	Pilot Eye Position x	m	0				10.81	Graphical estimate of seat location.
21	Pilot Eye Position y	m	0				-0.61	Taken to be the left hand seat (Captain). Graphical estimate.
22	Pilot Eye Position z	m	0			-1.33	-0.82	Graphical estimate using the defined datum with down being taken as positive. 3rd party data converted from [ft].
23	Wing Area	m^2	122.4	122.6	122.4	122.4		Well documented quantity. Includes within-fuselage area as is the convention. Majority vote on the value for the alternative specification.
24	Wing Setting Angle	deg	2			-0.5	3.5	3rd Party reference and graphical estimate vary. In reality the incidence of the wing varies along the half span (known as 'washout').
25	Wing Span	m	33.91		34.09	37.3	34.09	Graphically estimated from drawing as well as 3rd party data converted from [ft].
26	Wing MAC	m	3.33				3.36	Graphically Estimated from drawing
27	Wing Taper Ratio		0.3				0.26	Graphically Estimated from drawing

28	Wing Aspect Ratio		9.48		9.5	9.49		Widely available formula Aspect Ratio = [b^2 /A]
29	Wing Dihedral Angle	deg	5.11			3.298901	5	Graphically estimated from drawing. Suspected that this is the initial dihedral value at the wing root and not the average over the half span.
30	Wing Sweep Angle	deg	24.696			25	29	Graphically estimated from drawing
31	Wing Aero Centre X Coordinate	m	-0.58				-1.49	Assume Quarter Chord Location as is common for subsonic aerofoils.
32	Wing Aero Centre Z Coordinate	m	2.102				0.6	Graphical estimate of vertical MAC location.
33	Wing Stall Warning Angle	deg	13				15	Warning at maximum lift coefficient from lift curve slope data. Realistically it will be earlier than this value but the stall warning in the simulator is based on angle only and not flow behaviour.
34	Wing Panel Span Fraction		0.6				0.65	Estimate within-fuselage wing section from planform. What percentage of wing area is then available as a lift surface?
35	Wing Mount Dihedral Scale	deg/m	-2				-0.91	Graphically estimated from drawing. How does the dihedral change from the initial value at the root to the final value at the tip.
36	Stage 1 Flap Cl Increment		0.9			0.20875	1.1462	One dimensional, lookup values for flap deployment. Assumed that slats play no part, and stages are arbitrary. In reality the increments will relate to the precise amount of deflection of the flap. 3rd Party data considers linear distribution of increments. The estimated data is derived from simulated flap data in Design Foil. Due to the limited range of the software simulations, the data is first processed using a polynomial fit to obtain charts for lift, drag and moment coefficients against deployment angle and then increments are calculated from extrapolation of the data for the appropriate flap angles taken from 3rd party data up to the maximum known deflection of 35 [deg]. The aerofoil section used is equivalent to that of the wing. Due to the potential error associated with
37	Stage 1 Flap Cd Increment		0.1			0.051	0.0031	
38	Stage 1 Flap Cm Increment		-0.06			-0.0075	-0.1809	
39	Stage 2 Flap Cl Increment		1.4			0.4175	1.4931	
40	Stage 2 Flap Cd Increment		0.3			0.102	0.0067	
41	Stage 2 Flap Cm Increment		-0.1			-0.015	-0.02350	
42	Stage 3 Flap Cl Increment		1.4			0.62625	1.8862	
43	Stage 3 Flap Cd Increment		0.3			0.153	0.0127	
44	Stage 3 Flap Cm Increment		-0.1			-0.0225	-0.2958	

45	Stage 4 Flap Cl Increment		1.4			0.835	2.4284	extrapolation, the 3rd party data is preferred for the alternative specification.
46	Stage 4 Flap Cd Increment		0.3			0.204	0.0252	
47	Stage 4 Flap Cm Increment		-0.1			-0.03	-0.3784	
48	Flap Span Fraction		0.8				0.66	How much of the half span is flap? Graphical estimate approximated as rectangular surfaces.
49	Aileron Cl Increment	/deg	0.05				0.0321	3rd Party Data difficult to interpret. Design Foil flap simulation data used as for the flaps. Modelled using aerofoil section equivalent to that of the wing for graphically estimated surface width.
50	Aileron Cd Increment	/deg	0				0.0001	See previous.
51	Aileron Span Fraction		0.15				0.16	How much of the half span is aileron? Graphical Estimate.
52	Aileron Y Moment Arm	m	14				15.17	Graphical estimate from the datum to the centre of the outboard aileron.
53	Fuselage Minimum Cd		0.1				0.08	Considering the Skin Friction Drag only, this is approximated to the Drag of a cylinder in a 'face on' orientation. It also includes a factor representing the wing body interference amongst other drag inducing phenomena.
54	Fuselage Maximum Cd		0.4				0.52	Considering the Skin Friction Drag only, this is approximated to the Drag of a cylinder in a 'side on' orientation. It also includes a factor representing the wing body interference amongst other drag inducing phenomena. **See Note 2**
55	Fuselage Aero Centre X Coordinate	m	7.8				3.88	Estimated at quarter length location. Appropriate method for combination is available. **See Note 3**
56	Fuselage Aero Centre Z Coordinate	m	0				0	Assumed Centre fuselage which is equal to the datum location
57	Fuselage Reference Area	m^2	12.25				13.07	Assumed to be frontal area from the order of magnitude of the current value. A graphically estimated average cross sectional area is used.

58	Fuselage Length	m	37.57	37.57	37.57		36.72	Graphical estimate is used but most sources corroborate the original value – this may provide an insight into the accuracy of the graphical methods used so far.
59	Spoiler Cd Increment		1.5				0.2305	3rd Party Data difficult to interpret. Design Foil flap simulation data used as for the flaps. Modelled using aerofoil section equivalent to that of the wing for wing area.
60	Spoiler Cl Increment (wrt Wing Area)		-0.5				-1.02	See previous.
61	Spoiler Reference Area	m^2	8.64		8.64		8.82	Graphical estimate of spoiler planform.
62	Spoiler Aero Centre X Coordinate	m	-1.44				-6.01	Average location of spoilers with respect to the datum. Realistically the spoiler location varies with sweep as they lie along the trailing edge of the wing.
63	Spoiler Aero Centre Z Coordinate	m	-0.07				0.2	Graphical estimate of average spoiler vertical location.
64	Tailplane Setting Angle	deg	-3				-5	Graphical estimate from drawing assuming zero washout (change in twist over half span).
65	Tailplane Downwash Immersion	%	50					No precise data available for comparison but in general for subsonic airliners with the tailplane positioned higher than the wing, 50 [%] may be a suitable estimate used for example calculations in literature (Cook, 1997).
66	Tailplane Aero Centre X	m	-16.68				-21.4	Assumed quarter chord of a graphical estimate of the tailplane MAC.
67	Tailplane Aero Centre Z	m	-1.55				-1.12	Graphical estimate of vertical location of tailplane MAC.
68	Tailplane Lift Curve Slope	/rad	3.87				6.805	No data available for comparison but in general, the tailplane is a symmetric aerofoil. Design Foil data produced for simple NACA 0012 symmetric section.
69	Tailplane Profile Drag Factor		0.05				0.0068	Interpolation of Design Foil data allows estimate of drag equation which yields this value.
70	Tailplane Induced Drag Factor		0.02				0.00385	See previous.
71	Tailplane Area	m^2	31		31	30.9	29.2	3rd Party data converted from [ft^2]. Graphically modelled as a trapezium for estimate of area from

								drawing.
72	Elevator Cl Increment	/deg	0.03				0.081	3rd Party Data difficult to interpret. Design Foil flap simulation data use. Modelled using aerofoil section equivalent to that of the wing for graphically estimated surface width.
73	Elevator Cd Increment	/deg	0				0.0002	See previous.
74	Fin Aero Centre X	m	-19.64				-17.2	Modelled as a wing of symmetric section mounted vertically, the aero centre location is assumed to be at the quarter chord of a graphical estimate of the fin MAC.
75	Fin Aero Centre Z	m	4.07				-4.7	Graphical estimate of vertical location of fin MAC.
76	Fin Lift Curve Slope	/rad	3.79				6.805	Modelled and simulated as per the tailplane.
77	Fin Profile Drag Factor		0.05				0.0068	Modelled and simulated as per the tailplane.
78	Fin Induced Drag Factor		0.02				0.00385	See previous.
79	Fin Area	m^2	21.5		21.5	21.59	25.6	3rd Party data converted from [ft^2]. Graphically modelled as a trapezium for estimate of area from drawing.
80	Rudder Cl Increment	/deg	0.03				0.081	3rd Party Data difficult to interpret. Design Foil flap simulation data use. Modelled using aerofoil section equivalent to that of the wing for graphically estimated surface width.
81	Rudder Cd Increment	/deg	0				0.0002	See previous.
82	Engine Type		Turbofan					Selected from a drop down list. Indisputable choice.
83	Number of Engines		2					Agreed.
84	Engine Time Constant	sec	0.5					This is the engine response delay to the pilot lever control input. There is no better data available as in reality it is a complex figure based on numerous electronic and mechanical factors related to the engine control system. Airworthiness Regulations (EASA, 2007) state that the response should be within 1 [s].
85	Engine 1 Throttle Assignment		Left Throttle					Agreed.

86	Engine 2 Throttle Assignment		Right Throttle					Agreed.
87	Piston Engine Power	BHP	160					Check Box Controlled by E1 Tool. Relevant only to piston powered aircraft specifications.
88	Piston Prop Diameter	m	1.9					
89	Piston Max Prop Efficiency		0.75					
90	Piston Prop Design Speed	m/s	35					
91	Piston SFC	kg/BHP.h	0.2					
92	Jet Max SSL Thrust	N	111250	117877.83			106000	This value is for the entire aircraft (2 engines). Realistically, it is expected that engine achieves 90% of rated value due to mechanical wear and limitations imposed by the control system and other real world phenomena.
93	Jet SFC	kg/N.h	0.0554				0.05537	This value is for the entire aircraft (2 engines). **See Note 4**
94	Engine 1 Yaw Mounting Angle	deg	0					Graphically estimated yaw is minimal so neglected.
95	Engine 1 Pitch Mounting Angle	deg	0					Graphically estimated pitch is zero.
96	Engine 2 Yaw Mounting Angle	deg	0					Graphically estimated yaw is minimal so neglected.
97	Engine 2 Pitch Mounting Angle	deg	0					Graphically estimated pitch is zero.
98	Engine 3 Yaw Mounting Angle	deg	0					N/A
99	Engine 3 Pitch Mounting Angle	deg	0					
100	Engine 4 Yaw Mounting Angle	deg	0					
101	Engine 4 Pitch Mounting Angle	deg	0					
102	Engine 1 Mounting Position X	m	4.23				0	Graphically estimated from drawing.
103	Engine 1 Mounting Position Y	m	-5.74				-5.71	See previous.

104	Engine 1 Mounting Position Z	m	1.41				1.84	
105	Engine 2 Mounting Position X	m	4.23				0	
106	Engine 2 Mounting Position Y	m	5.74				5.71	
107	Engine 2 Mounting Position Z	m	1.41				1.84	
108	Engine 3 Mounting Position X	m	0					N/A
109	Engine 3 Mounting Position Y	m	0					
110	Engine 3 Mounting Position Z	m	0					
111	Engine 4 Mounting Position X	m	0					
112	Engine 4 Mounting Position Y	m	0					
113	Engine 4 Mounting Position Z	m	0					
114	Thrust Lapse 1,1 (Air Density Ratio vs Mach)		1				0.39	Relates the variation of thrust due to altitude (density) and speed. Empirical relationships as used in the development of the simulation software (4.3 Simulation Software) are used to a limited extent here to compute the lookup table. **See Note 5**
115	Thrust Lapse 2,1 (Air Density Ratio vs Mach)		1				0.61	
116	Thrust Lapse 3,1 (Air Density Ratio vs Mach)		1				1.0	
117	Thrust Lapse 1,2 (Air Density Ratio vs Mach)		1				0.39	
118	Thrust Lapse 2,2 (Air Density Ratio vs Mach)		1				0.61	
119	Thrust Lapse 3,2 (Air Density Ratio vs Mach)		1				1.0	

120	Thrust Lapse 1,3 (Air Density Ratio vs Mach)		1				0.39	
121	Thrust Lapse 2,3 (Air Density Ratio vs Mach)		1				0.61	
122	Thrust Lapse 3,3 (Air Density Ratio vs Mach)		1				1.0	
123	Main Gear Track	m	7.59		7.59		7.446	Graphical estimate from drawing.
124	Main Gear X Coordinate	m	-0.76				-1.15	Coordinates are taken from the centre of gravity (CG) location unusually. This is taken into consideration when estimating the location from the drawing.
125	Main Gear Z Coordinate (Extended)	m	3.26					CG vertical location is unknown so value is left unchanged.
126	Main Gear Stiffness	N/m	350000			825144		3rd Party data unit conversion required. Alternatively, an empirical estimate could be derived as in the mathematical modelling procedure (4.2.3.5 Landing Gear Model).
127	Main Gear Damping	Ns/m	300000			605646		See previous.
128	Main Gear Preload	N	0					Relevance of this quantity is unknown. The preload on the landing gear would be any load on the gear in absence of the aircraft weight. Experimental variation of this parameter showed no apparent difference in the simulator.
129	Nose Gear X Coordinate	m	12.01		12.65		11.4	Coordinates are taken from the centre of gravity (CG) location unusually. This is taken into consideration when estimating the location from the drawing.
130	Nose Gear Z Coordinate (Extended)	m	3.26					CG vertical location is unknown so value is left unchanged.
131	Nose Gear Stiffness	N/m	150000			513769		3rd Party data unit conversion required. Alternatively, an empirical estimate could be derived as in the mathematical modelling procedure (4.2.3.5 Landing Gear Model).

132	Nose Gear Damping	Ns/m	80000			66400		See previous.
133	Nose Gear Preload	N	0					Relevance of this quantity is unknown. The preload on the landing gear would be any load on the gear in absence of the aircraft weight. Experimental variation of this parameter showed no apparent difference in the simulator.
134	Brakes Max Friction Coefficient		0.7					Defined by FAR 25.109 (FAA, 2009).
135	Brakes Actuator Time Constant		0.5					Control system delay between pilot input and brake force introduction. Similar to engine time constant – no better data available.
136	Brakes Low Speed Friction Gradient		10					Variation in friction with speed (assumed here linear for low speed applications). Braking performance of the aircraft is critical and may be deduced from landing performance flight tests. However, no data is available from the aircraft manufacturer but data may be reverse engineered from typical decision speeds and deceleration performance in accordance with the balanced field length.
137	Brakes Rolling Friction Coefficient		0.05					Related to the resistance associated with brake components in situ. Order of magnitude agrees with rolling friction associated with the surface as given in 4.2.3.5 Landing Gear Model so no change.
138	Nosewheel Steering Travel	deg	20					No data available for comparison. Value left unchanged.
139	Nosewheel Steering Washout Speed (low)	kts	0					Research suggests that washout in terms of steering may relate to either the motion system reaction to steering or to the limits at which the nose wheel loses effectiveness. Uncertainty has driven no change on this parameter.
140	Nosewheel Steering Washout Speed (high)	kts	20					See previous.
141	Gear Drag Coefficient		1				0.92	3rd Party Data not defined well for comparison as the order of magnitude appears inconsistent with the expected dimensionless drag coefficient. **See Note 6**
142	Gear Drag Reference Area	m^2	0				6.9	Approximated by a graphical estimate of the frontal gear area and doors.

143	Gear Drag Z Coordinate	m	2				2.04	Located at the centre of a graphical estimate of the average gear frontal area.
144	Roll Control Dead Band	%	4					This corresponds to the area around the control stick in the cockpit in which any movement will not result in control surface deflection. It is a parameter defined by the control system in use hence there is no data available for comparison.
145	Roll Control Stick Shaping	%	4					Control system specific quantity defined by the manufacturer. Details are unlikely to be available in the public domain for comparison.
146	Roll Control Rate Limit	deg/sec	100					See previous.
147	Roll Control Surface Travel Up	deg	30			25		Maximum travel of the surface in reality does not necessarily govern the maximum allowable roll angle as fly by wire technology generally restricts these for safety. Therefore, real-world data on travel is neglected for data on allowable roll limits. Therefore there is 3rd Party data only.
148	Roll Control Surface Travel Down	deg	30			15		See previous
149	Pitch Control Dead Band	%	4					This corresponds to the area around the control stick in the cockpit in which any movement will not result in control surface deflection. It is a parameter defined by the control system in use hence there is no data available for comparison.
150	Pitch Control Stick Shaping	%	4					Control system specific quantity defined by the manufacturer. Details are unlikely to be available in the public domain for comparison.
151	Pitch Control Rate Limit	deg/sec	100					See previous.
152	Pitch Control Surface Travel Up	deg	30			25		Maximum travel of the surface in reality does not necessarily govern the maximum allowable pitch angle as fly by wire technology generally restricts these for safety. Therefore, real-world data on travel is neglected for data on allowable pitch limits. Therefore there is 3rd Party data only.
153	Pitch Control Surface Travel Down	deg	30			15		See previous

154	Yaw Control Dead Band	%	4					This corresponds to the area around the control stick in the cockpit in which any movement will not result in control surface deflection. It is a parameter defined by the control system in use hence there is no data available for comparison.
155	Yaw Control Stick Shaping	%	4					Control system specific quantity defined by the manufacturer. Details are unlikely to be available in the public domain for comparison.
156	Yaw Control Rate Limit	deg/sec	70					See previous.
157	Yaw Control Surface Travel Up	deg	20			25		Maximum travel of the surface in reality does not necessarily govern the maximum allowable yaw angle as fly by wire technology generally restricts these for safety. Therefore, real-world data on travel is neglected for data on allowable yaw limits. Therefore there is 3rd Party data only.
158	Throttle Mapping Lever Position Low		0					In absence of Electronic Engine Controller (EEC), this like for like value is agreed. However, in reality, the EEC will adjust output power based on a number of environmental factors including flight conditions.
159	Throttle Mapping Lever Position Mid		0.5					
160	Throttle Mapping Lever Position High		1					
161	Throttle Mapping Power Selection Low		0					
162	Throttle Mapping Power Selection Mid		0.5					
163	Throttle Mapping Power Selection High		1					
164	Flap Transit Time (per Stage)	sec	5			4		Based on 3rd Party data, the average transition time for the deployment of the full flaps from the retracted state is 20 seconds. Since there are 5 stages for an A320, it is approximated as 4 [s] per stage.
165	Spoiler Transit Time	sec	1			1.5		Available data consists of 3rd Party data only.
166	Gear Transit Time	sec	5			12		See previous.

167	Pitch Trim Rate	%/sec	10					The rate of trim and authority of the trim tab are control system specific quantities and are not available in the public domain.
168	Roll Trim Rate	%/sec	10					
169	Yaw Trim Rate	%/sec	10					
170	Roll Trim Authority	%	20					
171	Yaw Trim Authority	%	20					
172	Q Feel Max Q Speed	kts	600					The 'Q feel' is the force feedback felt on the control stick due to the dynamic pressure on the control surface. For a fly by wire system, these values are technically zero but can be simulated for pilot 'comfort'. These parameters relate to the applicability and magnitude of the artificial force.
173	Q Feel Min Q Speed	kts	50					
174	Q Feel Min Q	%	25					
175	Wing Area Check		0.923				**0.936**	Software Diagnostic from the E1 Tool. It is suspected that the check values are related to the approximations within the simulator's mathematical model and a value of 1 suggests maximum accuracy. Values not equal to one may suggest inaccuracies in the specification although with the opinion of the manufacturer it is difficult to say. Most other diagnostics are the result of mechanical calculations. Values shown here in red correspond to those calculated for the alternative model specification.
176	Aspect Ratio Check		1.074				**1.068**	
177	Tail Volume Ratio		1.257				**1.405**	
178	Fin Volume Ratio		1.028				**0.755**	
179	Thrust/Weight Ratio		0.527				**0.373**	
180	Wing Loading	N/m^2	3452.3				**4647.8**	
181	Cruise Speed	kts	326				**379**	
182	Thrust Loading	kg/kN	387.2				**547.1**	
183	Power Loading	kg/BHP						
184	Undercarriage Natural Frequency	rad/s	4.4				**6.1**	
185	Undercarriage Damping Ratio		1.78				**1.80**	
186	Undercarriage Gear Balance		4.27				**2.07**	
187	Undercarriage Static Deflection	m	0.5				**0.26**	
188	Tuning Lp		1				1	Multiplication factor of the derivative of the Rolling Moment with respect to Roll Rate as calculated by the simulation. These values ought not to be treated as a 'fudge factor' for the simulation hence there is no reason to alter them.
189	Tuning Lr		1				1	Multiplication factor of the derivative of the Rolling

								Moment with respect to Yaw Rate as calculated by the simulation. These values ought not to be treated as a 'fudge factor' for the simulation hence there is no reason to alter them.
190	Tuning Nr		2				1	Multiplication factor of the derivative of the Yawing Moment with respect to Yaw Rate as calculated by the simulation. These values ought not to be treated as a 'fudge factor' for the simulation hence there is no reason to alter them.
191	Tuning Lv (Lbeta)		3				1	Multiplication factor of the derivative of the Rolling Moment with respect to the Sideslip Angle as calculated by the simulation. These values ought not to be treated as a 'fudge factor' for the simulation hence there is no reason to alter them.
192	Tuning Nv (Nbeta)		1				1	Multiplication factor of the derivative of the Yawing Moment with respect to the Sideslip Angle as calculated by the simulation. These values ought not to be treated as a 'fudge factor' for the simulation hence there is no reason to alter them.
193	Tuning Mq		1				1	Multiplication factor of the derivative of the Pitching Moment with respect to the Pitch Rate as calculated by the simulation. These values ought not to be treated as a 'fudge factor' for the simulation hence there is no reason to alter them.
194	Tuning Mw (Malpha)		1				1	Multiplication factor of the derivative of the Pitching Moment with respect to the Incidence Angle as calculated by the simulation. These values ought not to be treated as a 'fudge factor' for the simulation hence there is no reason to alter them.

Additional Notes

1. "Center of Gravity Limits
   The A320 has two certified CG envelopes. One is a curtailed (normal) envelope with a forward limit of 25%. The other is a full envelope with a forward limit of 15%. Most airplane combinations of fuel and passenger loading will operate in the curtailed envelope. When load planning identifies an aircraft as having a forward CG use the Forward Center of Gravity procedure in the takeoff section"
   Source: (Phoenix Simulation Software, 2002)

2. Table of Drag of Bodies for different reference areas and lengths. High Reynolds Number assumed and data extrapolated.
   Source: (Nakayama & Boucher, 1999)

3. Method to calculate influence of presence of fuselage on the Aero Centre.
   Source: (ESDU, 1996)

4. V2500 Engine Specifications:

Engine Variant	V2522-A5	V2524-A5	V2527-A5	V2530-A5	V2533-A5
Application	A319-100	A319-100	A320-200	A321-100	A321-200
Entry Into Service	October97	June97	December93	March94	April97
Take-off thrust (lbf)	22,000	24,000	27,000	31,400	33,000
Fan diameter (in)	63.5	63.5	63.5	63.5	63.5
Air flow rate (lbs/s)	770	781	811	858	872
Bypass ratio	4.9	4.9	4.8	4.6	4.5
Cruise SFC (lbs/hr/lbf)	0.543	0.543	0.543	0.543	0.543

   Conversion between (lb/hr.lbf) to (kg/h.N) is necessary for the model specification.
   Source: (MTU Aero Engines)

5. Thrust lapse due to Mach ignored, but thrust lapse due to density ratio included using empirical relationship derived for software model.

Density Ratio / Mach Number	0	0.4	0.8
0.4	0.39	0.39	0.39
0.7	0.61	0.61	0.61
1.0	1.0	1.0	1.0

6. Taken from an online report written by staff at the University of Sydney Engineering Department about model landing gear:

   “Drag on gear is mainly due to pressure drag. The frontal area of struts... comes from detailed drawings.... The struts have a diameter of 12.7mm, and length of 137mm, the wheels have a diameter of approximately 80mm and thickness of 25.4mm, which is found in (White, Fluid Mechanics, 1999) to have [drag coefficient of] 0.82 based on frontal area for laminar flow at Reynolds numbers above 10000. From (Hoerner,

1965) the wheels could be approximated as supercritical sphere for their drag coefficient. This coefficient had a value of...0.1."
Source: (University of Sydney Aeromechanical Department, 2003)

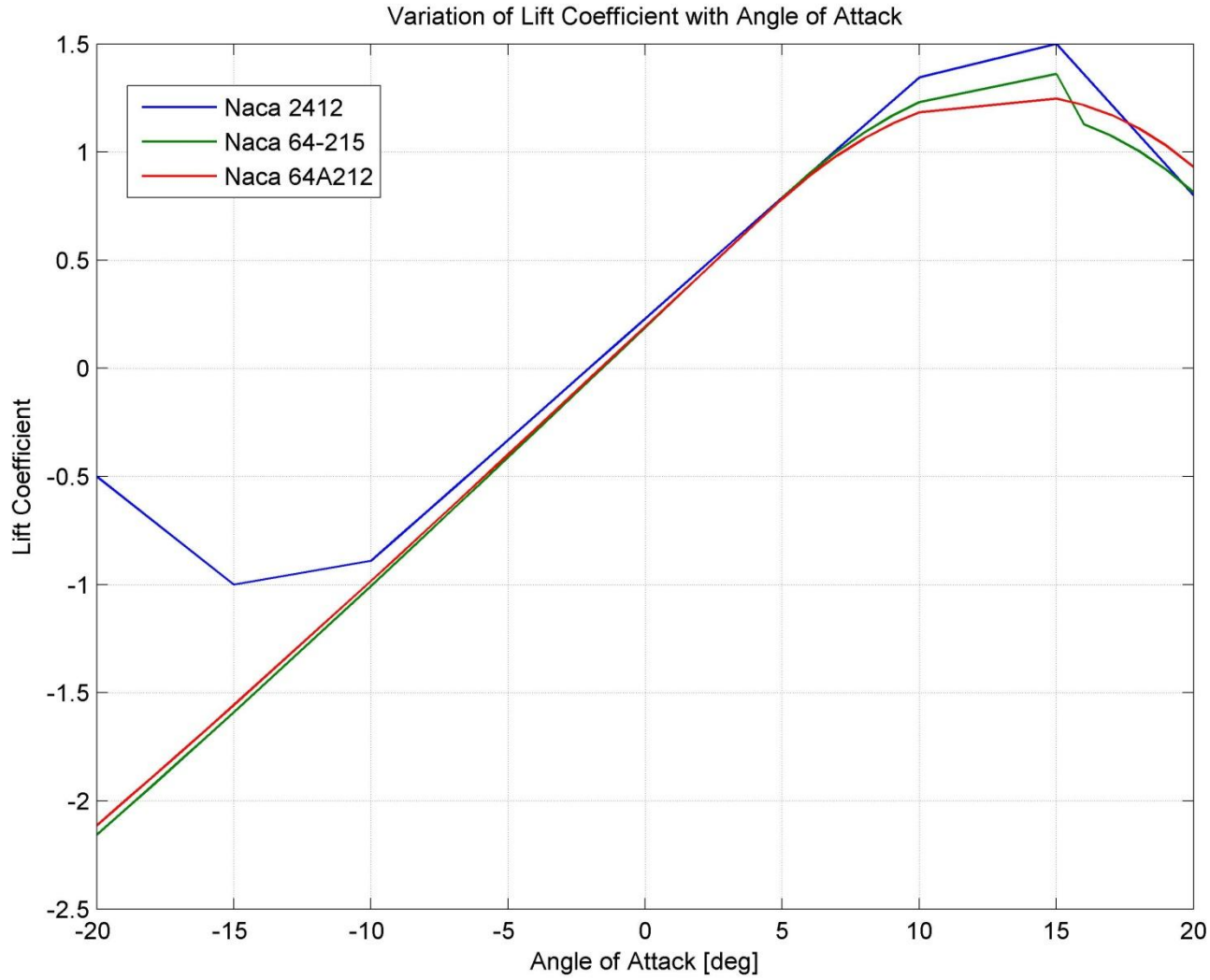
Variation of Lift Coefficient with Angle of Attack
Naca 2412
Naca 64-215
Naca 64A212
Lift Coefficient
Angle of Attack [deg]
1.5
1
0.5
0
-0.5
-1
-1.5
-2
-2.5
-20
-15
-10
-5
0
5
10
15
20

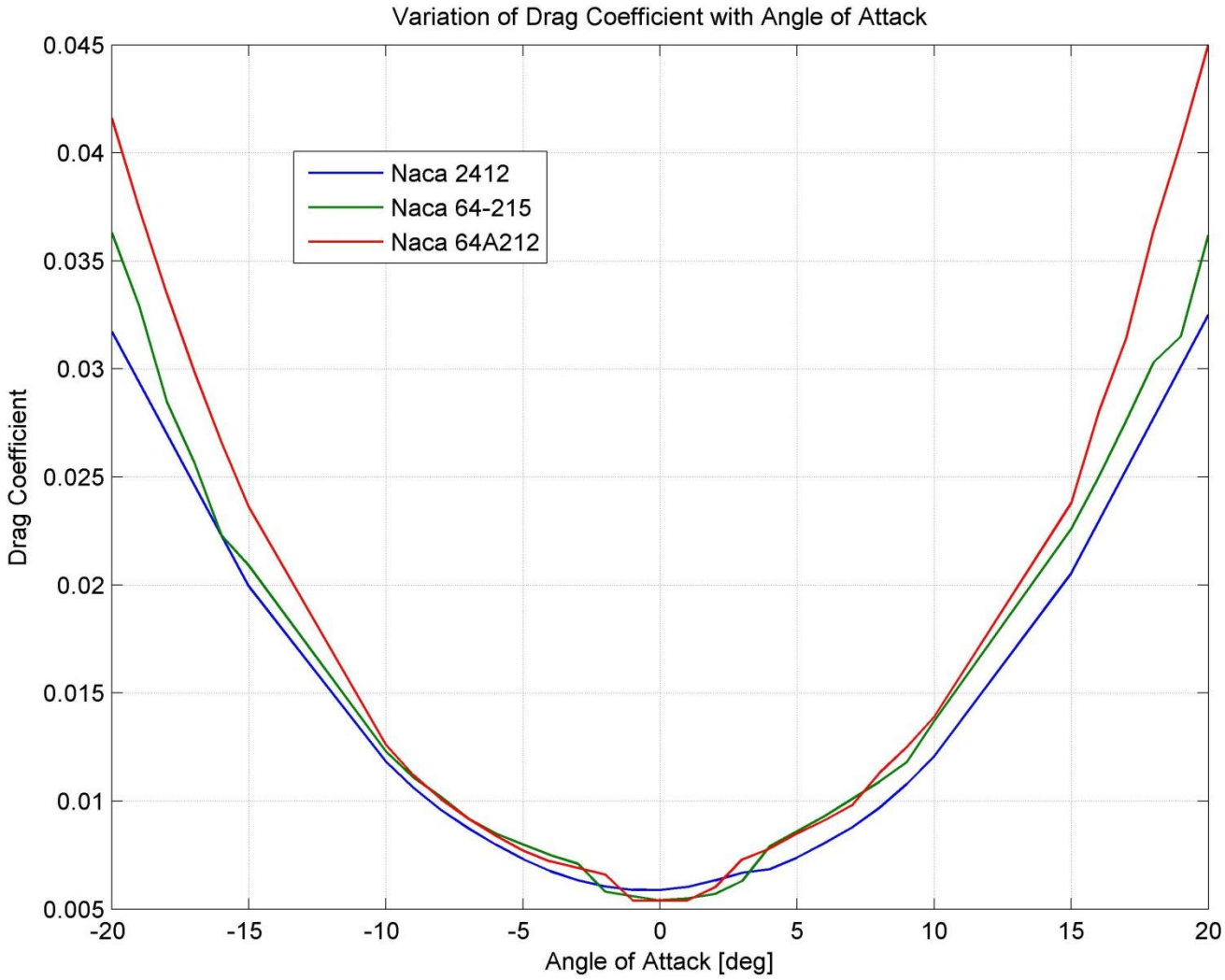
Variation of Drag Coefficient with Angle of Attack
Naca 2412
Naca 64-215
Naca 64A212
Drag Coefficient
Angle of Attack [deg]
0.045
0.04
0.035
0.03
0.025
0.02
0.015
0.01
0.005
-20
-15
-10
-5
0
5
10
15
20

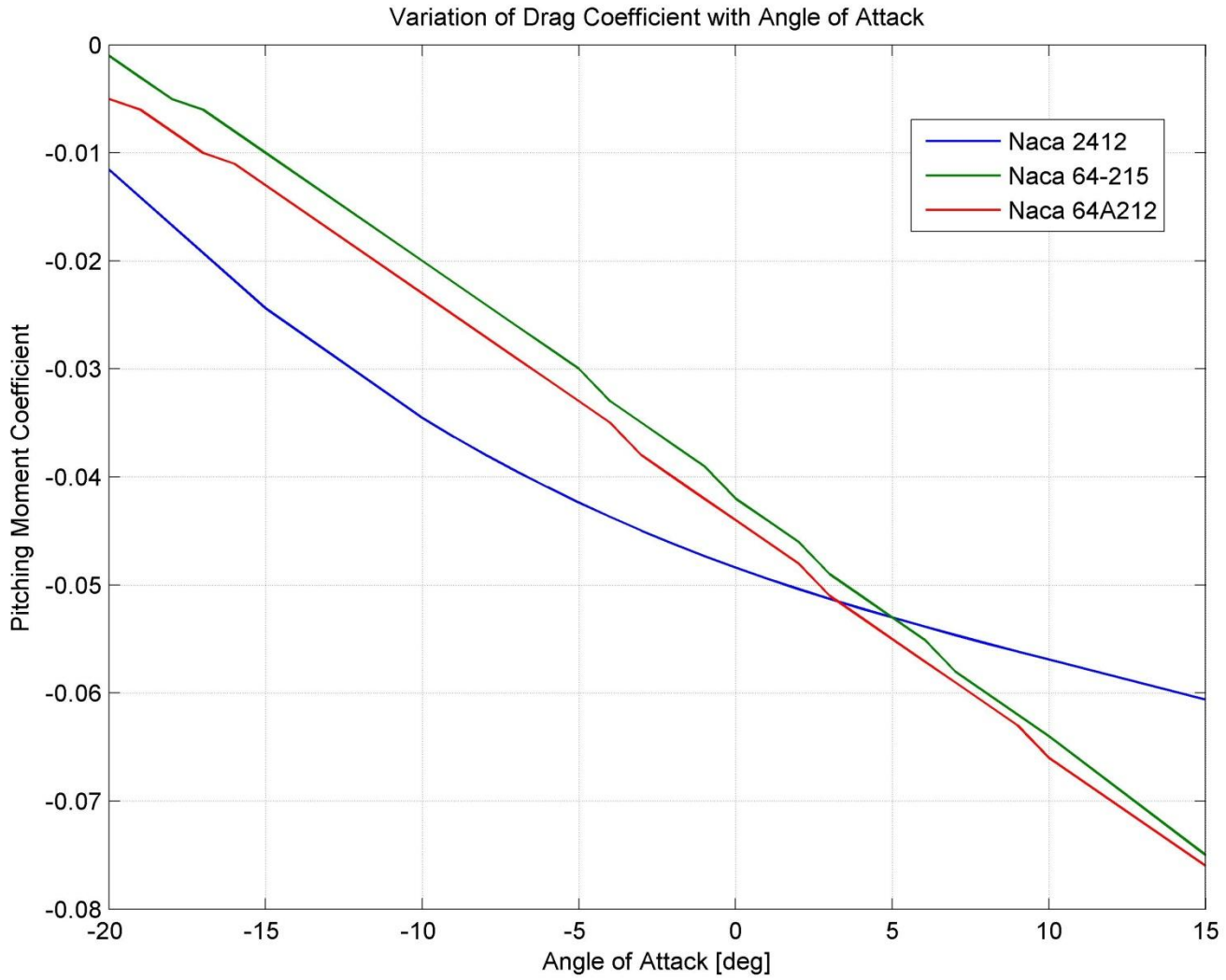
Variation of Drag Coefficient with Angle of Attack
Pitching Moment Coefficient
Angle of Attack [deg]
Naca 2412
Naca 64-215
Naca 64A212
0
-0.01
-0.02
-0.03
-0.04
-0.05
-0.06
-0.07
-0.08
-20
-15
-10
-5
0
5
10
15

N.1 PAYLOAD RANGE CODE

```
%% Fuel Extrapolation
% Code to extrapolate fuel data to produce a range
% Column 1 is time; Column 58 is fuel state;
%
% To allow reuse on other data files
M=input('What is the name of the data matrix for fuel extrapolation? ');
Lim=input('How much fuel does the flight start with [kg]? ');
%
% Create Fuel Vector
F=M(:,58).*Lim;
%
%% Poly Fit
% Obtain coefficients for polynomial of order 5:
% p=polyfit(M(:,58),M(:,1),5);
%
% Obtain values of polynomial corresponding to input values of fuel state:
% q=polyval(p, M(:,58));
%
% Plot results to examine accuracy of fit:
% plot(M(:,58),M(:,1),M(:,58),q)
%
% Experiment shows that a polynomial fit does not extrapolate in the manner
% desired.
%
%% Linear Fit
% Takes the last value of the data range and the first value as two
% distinct data points and fits a line through the points of the form:
% time = k + (j * fuel)
% Find the reference to the last line of data:
L=length (M(:,1));
% Find Linear Coefficients:
j=(M(L,1)-M(1,1))/(F(L,1)-F(1,1));
k=M(1,1)-(j*F(1,1));
% Evaluate time at extrapolated location of fuel=0:
f=0;
t=k+(j*f);
% Create a test plot for visual verification:
t1=k+(j*F(:,1));
plot(F(:,1),M(:,1),F(:,1),t1)
title('Linear Fit Checking Plot');
%
%% Average Ground Speed
% Column 30 contains the Ground Speed;
% Setup a loop to sum the elements of the column vector:
n=0;
dump=0;
for n=1:length(M(:,30))
    dump=dump+M(n,30);
end
% Calculate average velocity:
verge=dump/n;
%
%% Breguet Range Equation
% This equation requires the Velocity, the SFC [1/s], L/D approximated as
% average (W/T), Initial and Final Weight for the cruise mission segment.
%
% Average velocity is computed in the Previous Cell = verge
% Initial and Final Weights, neglecting other mission segments can be
```

```
% approximated as Full Model Weight and Zero Fuel Weight respectively.
% Average Weight and Thrust can be computed from Columns 53, 43 and 44.
%
% Average Weight
n=0;
dump=0;
for n=1:length(M(:,53))
    dump=dump+M(n,53);
end
Wav=9.81*dump/n;
%
% Average Thrust
n=0;
dump=0;
for n=1:length(M(:,43))
    dump=dump+(M(n,43)+M(n,44));
end
Tav=dump/n;
%
% Obtain model data through input
C=9.81*input('Model SFC [kg/N.h]? ');
Wi=9.81*input('Model Initial Mass [kg]? ');
We=9.81*input('Model Zero Fuel Mass [kg]? ');
%
%% Range Calculation
% Use Linear Fit endurance to calculate range estimate:
range=verge*t/3600;
%
% Use Breguet Range Equation
rangeBRE=(verge/C)*(Wav/Tav)*log(Wi/We);
% Display Answer
disp(['Linear ' num2str(range) '[nm]'])
disp(['BRE ' num2str(rangeBRE) '[nm]'])
```

N.2 SPECIFIC RANGE AND ENDURANCE CODE

```
%% SAR and Specific Endurance Processor
% Known Quantity
TSFC=0.0554;          % in [kg/N.h]
%
% Find Matrices
M=input('What is the name of the data matrix for SAR and Specific Endurance? ');
%
%% Find Average Thrust
n=0;
dump=0;
for n=1:length(M(:,43))
    dump=dump+(M(n,43)+M(n,44));
end
% Calculate average thrust:
Tav=dump/n;
%
%% Find Average Speed
n=0;
dump=0;
for n=1:length(M(:,30))
    dump=dump+M(n,30);
end
% Calculate average velocity:
Vav=dump/n;
%
n=0;
```

```
dump=0;
for n=1:length(M(:,33))
    dump=dump+M(n,33);
end
% Calculate average velocity:
Mav=dump/n;
%
%% Convert TSFC
%
TSFCmods=TSFC/60;
%
%% Print Coordinates
% SAR
disp(['(SAR/Vel) ' num2str(Vav/(TSFCmods*Tav)) ' / ' num2str(Mav) ')'])
%
% Endurance
disp(['(End/Vel) ' num2str(1/(TSFCmods*Tav)) ' / ' num2str(Mav) ')'])
%
%% Compose Vectors From Displayed Values
%
M1Mach=[0.86143 0.71598 0.89325];
M1SAR=[5.7776   9.0908  7.4343];
M1End=[0.011456 0.02152 0.014139];
%
M8Mach=[0.83308 0.71786 0.89182];
M8SAR=[8.4452   9.5347  7.8405];
M8End[0.017226  0.022522    0.014932];
%
M9Mach=[0.83131 0.71906 0.89148];
M9SAR=[8.8265   9.7857  8.0065];
M9End=[0.018015 0.023082    0.015252];
%
%% Plotter
Mrge=0.7:0.01:0.9;      % Sampled Mach Number Range
%
f=2;                    % Polynomial Order
%
ps1=polyfit(M1Mach(:,2:3),M1End(:,2:3),2);      % Remove the anomalous values from
the fit
M1Endf=polyval(ps1,Mrge);
%
ps8=polyfit(M8Mach,M8End,f);
M8Endf=polyval(ps8,Mrge);
%
ps9=polyfit(M9Mach,M9End,f);
M9Endf=polyval(ps9,Mrge);
%
plot(Mrge,M1Endf,Mrge,M8Endf,Mrge,M9Endf,'LineWidth',1)
hold on
plot(M1Mach,M1End,'x',M8Mach,M8End,'x',M9Mach,M9End,'x','LineWidth',1)
%
% ...Repeat for SAR data.
```

Learning Objective Review			
Objective Review Outcome:	**Passed with Qualification**	***Owner:*** *Adrian Harwood*	
Number of Reds (Objective not Met - Further Work Required)	**0**		
Number of Ambers (Objective not Met - Work Planned)	**0**		
Number of Green (Objective Met)	**11**		
To be completed as part of regular review sessions or on project completion			
Learning Objective	**RAG**	**Comments**	**Reference**
To be familiar with aircraft performance parameters and make decisions on their relevance to a variety of specific applications.	G	Performance criteria research and suitability assessed. Selection process encouraged decisions on relevance and related test procedures applied to both existing and alternative model specifications.	Section 5.2
To explore a method for flight dynamic model verification and validation, an integral part of aircraft development programmes.	G	Theoretical methods to verify flight dynamic output behaviour of variety of models. Flight testing to validate model specifications for appropriate dynamic behaviour.	Section 4 & Section 5.2/4
To develop data mining skills through literature reviews.	G	Continuous research necessary for knowledge on flight simulation, software, modelling, methods, comparative data for parametric assessment.	All
To develop communication and informational skills in report writing and presentation delivery.	G	Delivery of reports, poster and presentation on schedule. Presentation required preparation making use of prompt cards and useful figures in anticipation of questions.	None
To learn project management techniques through planning, control and risk management.	G	Planning and initial risk management activities undertaken prior to project start followed by updates and tracking to baseline as appropriate.	Section 3

To gain a firm understanding of flight dynamics and related knowledge areas and develop an appreciation of their roles in the mathematical modelling of flight.	G	Flight dynamics essential in developing the models. Specific mathematical involvement required further research on the subject which serve to cement the understanding.	Section 5.3
To appreciate and manage the inevitable challenges of accurately modelling vehicle flight.	G	All modelling regularly encountered issues and hence continuous mitigation and planning necessary. Appreciation of the issues developed first hand through experience.	Section 4
To cultivate cognitive skills such as critical thinking and decision making by working on a multi-disciplinary, unbound problem within boundaries and certain constraints.	G	Most of the activities in the project required a degree of decision making and critical thinking. In particular, knowing where to draw the line on lines of investigation, how best to tackle the model construction and best use flight simulation capabilities	All
To develop an appreciation of skills required to solve engineering problems.	G	The problem which drives the project, is the need to understand flight simulation to an appropriate level. From an engineering perspective, specialist is learnt and applied to achieve the goal.	All
To become familiar with product research and development activities	G	The research of current industry machines took the project into analysis of the university's flight simulator and the modelling and simulation used to develop the project models is an integral part of product development in terms of life-cycle verification and validation.	Section 4/5
To be educated on technology and software tools in current use in the field of interest	G	Other than the familiarisation with the E1 editor, the use of numerical programs and modelling tools is evident throughout.	All

MANCHESTER 1824

The University of Manchester

Adrian Harwood
adrian.harwood@student.manchester.ac.uk
Aerospace Engineering (MEng)
Tutor: Dr I Dupère
Project Supervisor: Dr D Diston

Aerospace Vehicle Simulation

Flight Simulation as an Engineering Discipline

Modelling Techniques for Flight Simulation Applications

Capability Analysis and Improvement Delivery

Primary Learning Outcomes

- ✓ Familiarisation with aircraft performance parameters.
- ✓ Exploration of methods for flight dynamic model verification.
- ✓ Development of data mining skills through literature reviews.
- ✓ Development of communication skills in report writing and presentation delivery.
- ✓ Development of PM techniques through planning, control and risk management.
- ✓ Gain a firm understanding of flight dynamics and related knowledge areas and recognise their roles in the mathematical modelling of flight.
- ✓ Appreciation and management of the inevitable challenges of accurately modelling vehicle flight.
- ✓ Development education of technology and software tools in current use in the field of interest.

Introduction to Flight Simulation

- ➔ Research into the role and historical development of flight simulation
- ➔ Determination of requirements for flight simulation
- ➔ Identification of skills, tools and techniques for further research, replication or acquisition

Mathematical Modelling

- ➔ Fundamental approach to modelling and simulation process
- ➔ Representation of system in terms of functional elements and physical laws
- ➔ Visual representation of responses compliment other work areas

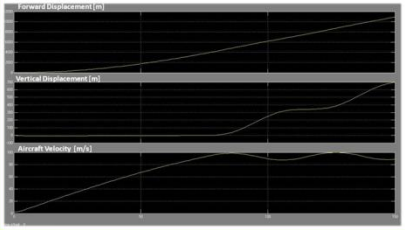

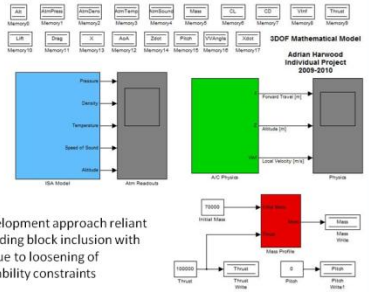

➔ Development approach reliant on building block inclusion with time due to loosening of applicability constraints

Model Specification & Assessment

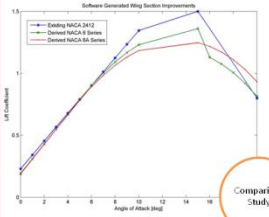

➔ Use of variety of tools and sources to obtain information necessary to verify accuracy of existing model (*Below*)

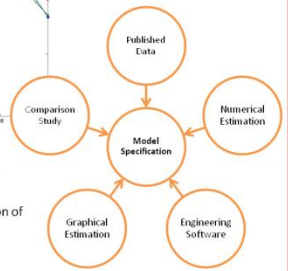

➔ Identification of limitations of current capabilities
➔ Suggestion and implementation of some improvements (*Above*)
➔ Alternate Model Formulation

Modelling & Simulation Performance

- ➔ Using existing simulation resources, assess existing aircraft model and simulation software for fidelity
- ➔ Determination of sources of error and suggestion of magnitude
- ➔ Understanding of aircraft performance and definition of appropriate flight test procedures to produce relevant data

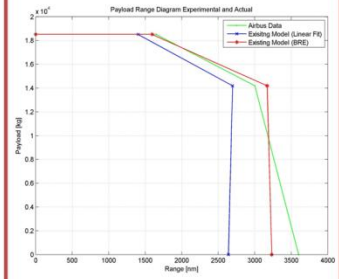

➔ Validation of existing and alternate model definition (*Above*)
➔ Visualisation of flight dynamics and stability through analysis of test results (*Below*)
➔ Application of flight dynamics mathematical theory through problem solution using matrix algebra (state space representation) as well as control theory

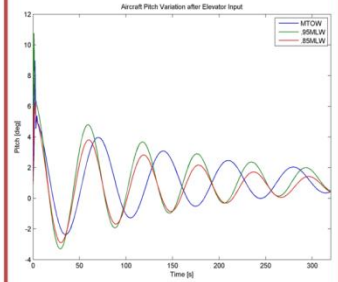

Simulation Software

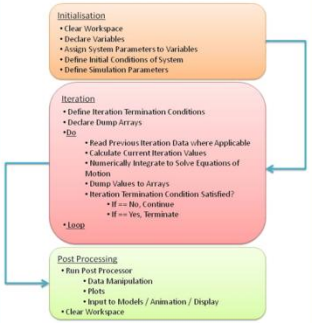

➔ Examination of solution procedures at a lower level of abstraction
➔ Assemble well structured code for efficient simulation
➔ Education of coding structure and numerical methods

Physical Modelling

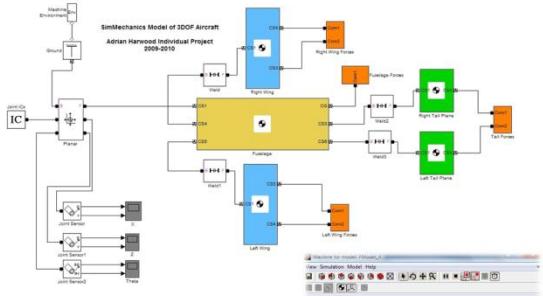

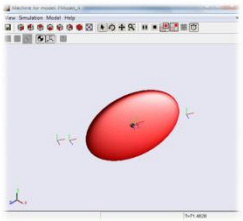

➔ Incorporation of component properties and related behaviour into model and simulation (*Above*)
➔ Visualisation capability (*Right*) and improved compatibility with 3D graphical environment and potential for input to motion system
➔ Exploration of software capabilities
➔ Parameterised approach mimicking existing capabilities

Real-Time Execution

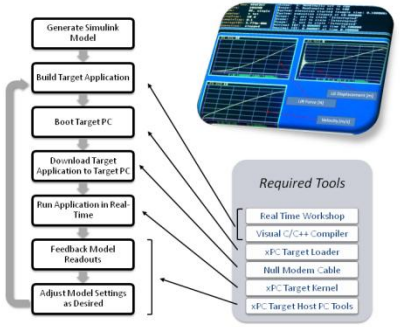

➔ Realisation of core flight simulation capability
➔ Investigation of one particular method of achieving Real-Time execution (*Bottom*)
➔ Generation of Real-Time results for flight simulation model (*Top*) allows comparison to non-Real-Time data as well as supply to graphical sink for Real-Time animation